University of Reading

Impact of Toll-like receptor 4 biased signalling on the behaviours of glioma stem cells

School of Chemistry, Food and Pharmacy

Department of Pharmacy

Yiming Meng

September 2022

Acknowledgement

I would like to thank Dr. Darius Widera and Dr. Graeme Cottrell for their great help as my supervisors, I fully appreciate their supports and professional guidance, it has been a great honour to be their PhD student. I learnt a lot, not just knowledges, but also some qualities that I could benefit for my whole life. From them, I understand how to maintain passion for science, commit oneself to something he/she loves, to see things objectively and to think logically. I always admire them and appreciate them and my life teachers.

I also thank Dr. Tom Vallance, Dr. Jonathan Sheard as great colleagues and co-authors of my publications, the lab atmosphere could not been as warm if there weren't them around. I also would like to thank Dr. Hisham- Al- Obaidi for inviting me to collaborate in one of my side projects. I would like to extend my thanks to my examiners, Dr. Sam Boateng and Dr. Thamil Selvee Ramasamy for their suggestions to my thesis and their time contributed for my viva. I would like to thank my friends, for being around and be so supportive during the past few years. Last but not least, I would like to thank my parents, Prof. Qingyun Meng and Ms. Jingshuang Wu for their selfless love and supports during my PhD journey.

Abstract

Glioblastoma cancer stem cells (CSCs) are a subpopulation of cells that play important roles in tumour metastasis, tumour recurrence and anticancer therapy resistance. Toll-like receptors (TLRs) are type I integral membrane proteins found on glioblastoma CSCs, which are also essential pathogen recognition receptors within the innate immune system. MyD88-dependent pathway and MyD88-independent pathway are two major signalling pathways triggered by TLRs, and Toll-like receptor 4 (TLR4) is the only member of TLRs that can trigger both in a biased manner. Depending on the ligand, signalling via TLR4 can either activate the pro-inflammatory transcription factor 'Kappa-light-chain-enhancer' of activated B cells (NF-κB) or the anti-viral and anti-inflammatory interferon regulatory factor 3 (IRF3). Currently, TLR4 in cancer was widely studied. However, the TLR4 and inflammation in glioblastoma, especially how the biased signalling is impacting the glioblastoma CSCs behaviours is a gap of the field.

In this study, using 2D and 3D cell cultivation, I demonstrated that TLR4 mediated NF-κB and IRF3 have opposing effects on U251 cells. The activation of TLR4- NF-κB pathway is able to increase the tumourigenicity, migration, and the overall percentage of CSCs. Activation of TLR4-IRF3 pathway is able to increase the differentiation of CSCs, decrease the stemness and suppress tumourigenicity of glioblastoma. In addition, I demonstrated that in 3D, U251 cells showed significant increase of tumourigenesis and stemness. Also, 3D cultivated U251 cells proliferated quicker than 2D cultivated cells, and had higher resistance to Temozolomide. I have also demonstrated that curcumin is an efficient anti-inflammatory compound and showed that a novel curcumin microemulsion increases its anti-inflammatory potential. Lastly, I have developed an IRF3 reporter system that can be used to generate a quad-reporter cell line, which in the future could be a very useful tool to study the biased signalling downstream of TLR4. In general, my research has clinical

application potential. By developing drugs to regulate TLR4 downstream pathways, it could offer new treatment options for glioblastoma either alone or in combination with conventional treatment options. In addition, 3D cell culture and curcumin also have great prospects in anti-cancer drug development.

Declaration

I confirm that this is my own work and the use of all material from other sources has been properly and fully acknowledged.

Yiming Meng

Publications

Sheard JJ, Bicer M, **Meng Y**, Frigo A, Aguilar RM, Vallance TM, Iandolo D, Widera D. ***Optically Transparent Anionic Nanofibrillar Cellulose Is Cytocompatible with Human Adipose Tissue-Derived Stem Cells and Allows Simple Imaging in 3D***. Stem Cells Int. 2019 Oct 7; 2019:3106929. doi: 10.1155/2019/3106929. PMID: 31687032; PMCID: PMC6800951.

Sanduk, F., **Meng, Y**., Widera, D., Kowalczyk, R.M., Michael, N., Kaur, A., Yip, V., Zulu, S., Zavrou, I., Hana, L., Yaqoob, M., & Al-Obaidi, H. (2020). ***Enhanced anti-inflammatory potential of degradation resistant curcumin/ferulic acid eutectics embedded in triglyceride-based microemulsions***. Journal of Drug Delivery Science and Technology.

Vallance TM, Sheard JJ, **Meng Y**, Torre EC, Patel K, Widera D, Vaiyapuri S. ***Development and characterization of a novel, megakaryocyte NF-κB reporter cell line for investigating inflammatory responses.*** J Thromb Haemost. 2021 Jan; 19(1):107-120. doi: 10.1111/jth.15118. Epub 2020 Nov 5.

Meng Y, Sheard JJ, Bashford A***. High-content quantitation of cancer stem cells from a glioblastoma cell line cultured in 3D using GrowDex®-T hydrogel.*** 2021. (Application Note 10 of GrowDex-T®). Retrieved from website upmbiomedicals.com at *https://www.upmbiomedicals.com/resource-center/application-notes/high-content-quantitation-of-cancer-stem-cells-from-a-glioblastoma-cell-line-cultured-in-3d-using-growdex-t-hydrogel/ .*

Table of contents

Abbreviations

Abbreviation	Acceptation
2D	Two dimensional
3D	Three dimensional
aNFC	Anionic nanofibrillar cellulose
AP1	Activator protein 1
BSA	Bovine serum albumin
CD	Cluster of differentiation
CSC	Cancer stem cell
DAMP	Damage-associated molecular pattern
DMEM	Dulbecco's Modified Eagle's Medium
DMSO	Dimethyl sulfoxide
ECACC	European Collection of Authenticated Cell Cultures
EDTA	ethylenediamineteraacetic acid
EGF	Epidermal growth factor
EGFR	Epidermal growth factor receptor
ERK	Extracellular signal-regulated protein kinase
EV	Extracellular vesicle
FBS	Fetal bovine serum
FGF	Fibreblast growth factor
GBM	Glioblastoma multiforme
GCSC	Glioblastoma cancer stem cell
GFAP	Glial fibrillary acidic protein

IRF3	Interferon regular factor 3
IFNβ	Interferon β
IκB	Inhibitor of κB protein
IKK	Inhibitor of κB protein kinase
IL	Interleukin
IRAK	IL-1R-associated kinase
IRF3	Interferon regulatory factor
JNK	c-Jun amino-terminal kinase
LBP	Llipopolysaccharide binding protein
LPS	Lipopolysaccharide
LRR	Leucine-rich repeat
MACS	Magnetic-activated cell sort
mCMV	Minimal cytomegalovirus
MyD88	Myeloid differentiation primary response 88
NFC	Nanofibrillar cellulose
NF-κB	Nuclear factor κ light chain enhancer of activated B
PAMP	Pathogen-associated molecular patterns
PBS	Phosphate Buffered Saline
PKD-1	Protein kinase D 1
PRR	Pattern recognition receptor
RLuc	Renilla Luciferase
ROS	Reactive oxygen species
TANK	TRAF family member-associated NF-κB activator
TAK1	TRAF-activated kinase 1

TBK	TANK binding kinase
TIR	Toll-/interleukin-1 receptor
TIRAP	TIR domain-containing adapter protein
TLR	Toll-like receptor
TME	Tumour microenvironment
TMZ	Temozolomide
TRAF	tumour necrosis factor receptor-associated factor
TRAM	TRIF-related adaptor molecule
TRIF	Toll/interleukin-1 (IL-1) receptor-domain-containing adapter-inducing interferon-β
TNF-α	Tumour necrosis factor alpha
U251	Human glioblastoma astrocytoma grade IV cell line

Chapter 1. Introduction

1.1. Cancer stem cells

1.1.1. CSC model

Research into drugs capable of targeting specific cancer cells is currently of great importance and significance, as the tumour recurrence and metastasis were proved to have strong links to those cells which named cancer stem cells (CSCs) [1]. The classic cancer stem cell (CSC) theory was proposed in the last century. CSCs were first discovered in 1987, and were identified in human leukaemia in the late 1990s [2]. They were defined as a small group of cancer cells with tumorigenesis and self-renewal capabilities and differentiation potential as well as limited proliferation potential [3, 4]. In the CSC model, the heterogenetic tumour cells can be divided into CSCs and non-cancer stem cells (non-CSCs). CSCs, according to Singh et al. 2004, are tumour initiating cells, capable of tumour initiation in NOD-SCID (non-obese diabetic, severe combined immune-deficient) mice, while non- CSCs are not capable of generating xenografts [5]. In CSC studies, those cells could be identified by using a range of CSC markers. The CSC model is believed to be the most likely carcinogenesis model, and CSCs are suggested to be the key of cancer progression which could be a very important cellular target in cancer therapies [6].

In oncology, tumours are recognized and defined as a complex group of aberrant cells which form one or multiple lumps [7, 8]. Tumours can be in benign, premalignant, and malignant stages. From the clinical point of view, malignant tumours are aggressive and are defined as cancer. The CSC model explains clonality and heterogeneity in tumours. A fundamental theory of tumour development claims that tumours are frequently formed as an evolutionary process starting from a single cell of origin [9], which explains the clonality of

cancer cells. The first abnormal cells are defined as `neoplastic` and are the ancestors of malignant tumours [9]. Clonality in tumours has been defined as the relationship between cells that result from a single somatic cell's mitotic division [10]. It has been demonstrated in multiple cancer types including myeloma, lymphoma, breast cancer, prostate cancer, head and neck cancer, and brain cancer [11-16]. Maley et al. suggested that, in early cancer development, clonal expansion and clonal diversity are the fundamentals of establishing genetic risk factors in tumours [17], but clonality in human cancer cells is dynamic. With cancer cells' fast cell division rate , mutations in DNA sequence level could be caused by mutational drivers and could accumulate as the tumour progresses [18]. In addition, the cancer clone dynamics could also be dramatically changed by 'artificial selection', chemotherapy or radiotherapy [18]. The clonality of cancer cell groups can thus be quite complex. In the context of cancer clonality, malignant cells, especially highly aggressive tumours, appear to be heterogeneous at the same time [19]. Heterogeneity in cancer can be defined in two aspects: one is intra-tumour heterogeneity, a series of hierarchical differentiation stages passed through by cancer cells in a tumour; the second is heterogeneity among tumours, which shows as chromosomal differences. Those could be cause by DNA mutations. For example, the genomic imbalance within glioblastoma multiform (GBM) was reported by Nobusawa et al. [20]. The authors referred to the existence of numerous tumour area-specific genomic imbalances in GBM [20]. In the CSC model, CSCs, with their property of cancer-initiating and self-renewal, can divide symmetrically or asymmetrically to either sustain the tumour growth or contribute to the tumour's heterogeneous and phenotypical diversity [4]. Therefore, CSCs contribute to both the clonality and the heterogeneity of malignant tumours.

1.1.2 Cancer stem cell markers

CSCs have been identified in human acute myeloid leukaemia, breast cancer, brain cancer, colorectal cancer etc. using so called cell surface markers. To demonstrate CSC markers in those tumour types, xenograft assay could be used. In this assay, NOD/SCID mice were transplanted with tumour cells with or without certain markers. If cancer cells with certain markers can transfer disease after transplanting, then the cancer cells with that marker are highly likely to be CSCs. Specifically, leukemic stem cells or leukaemia initiating cells were defined as $CD34^{+}CD38^{-}$, or $CD34^{+}CD38^{-}CD19^{+}$ [21, 22]. Similarly, $CD44^{+}/CD24^{-/low}$ cells were recognized as breast cancer tumorigenic cells or breast CSCs [23]. Within the central nervous system (CNS), glioblastoma multiforme cancer initiating cells or CSCs were defined by the expression of $CD133^{+}$ [24]. In addition, CD133 has been reported as a CSC marker in other cancer types including colorectal, bladder, liver, and ovarian cancer, justified by the finding that $CD133^{+}$ cells are able to initiate new tumours in immunodeficient mice after tumour spheroid cultivation [25]. Therefore, CD133 is now widely used to isolate and characterize CSCs in general. CD133 is now known as a glycoprotein on cell surface, also called prominin. It is also expressed on some somatic stem cells, including neural stem cells, hematopoietic stem cells, endothelial progenitor cells, etc. [26-28]. The role of CD133 is not yet fully known, but it has been suggested that it contributes to stem cell-fate decision, maintenance and expansion [29]. Apart from those markers, there are CSC markers which are specific to different cancer types. For instance, in glioblastoma multiforme (GBM), proteins like SOX2, NANOG, and nestin [30-32], are known as CSC markers. The suggested CSC markers of different cancer types are listed below in table 1.1.

Type of cancer	CSC markers	CSC percentage	Ref.
Breast cancer	ESA^+CD44^+ $CD24^{-/low}$ ALDH1/ α6-integrin	2%	[33] [34]
Human AML	$CD34^{++}$ $CD38^-$	<0.2%	[35]
Colon cancer	$CD133^+CD44^+CD24^+$	2.5%[36]	[36-38]
Pancreatic cancer	$CD133^+$ $CXCR4^+$ $CD44^+$ $CD24^+$ ESA^+ $ALDH1^+$ $nestin^+$ $ABCG2^+$	0.2%-0.8%	[39] [40] [41]
Prostate cancer	$CD44^+$ / $\alpha_2\beta_1^{hi}$/$CD133^+$	0.1%0.3%	[42]
Glioblastoma	$CD133^+$/$CD44^+$/$nestin^+$ $CD15^+$/SSEA-1^+	19%-29%[5]	[24, 30] [43]
Medulloblastoma	$CD133^+$	6%-21%[5]	[5, 30]
Melanoma	$CD133^+$ /$CD20^+$ /$CD166^+$ $nestin^+$ /$CD271^+$	20%-56%	[44, 45]
Ovarian cancer	CD133+/ALDH1 $CD44^+$/$CD24^-$/$CK19^+CD117^+$ EpCAM/$LGR5^+$/LY6A	31%-49.1%	[46, 47]
Liver cancer	$CD133^+CD90^+CD44^+CD49f^+$	0.04%-2.34%[48] 3.5%-4%[49]	[48-50]
Lung cancer	$CD133^+$ $ALDH1^+CD90^+$	<1.5%[51]	[51, 52]
Head and neck cancer	$CD44^+$ $CD133^+$ $ALDH^+CD98^+$		[53-55]
Renal cancer	$CD105^+$,CD44	0.03-93.9%	[56]

Table 1.1. CSC markers in different cancer types, calculated CSC percentage in relative type of cancer using listed CSC markers.

1.1.3 CSC Niche

CSCs reside in niches that are unique phenotypic states which contribute to CSCs' stemness, heterogeneity and plasticity [57]. CSC niches are complex tumour microenvironments (TME) that are able to provide cell-cell interactions and regulate CSC characteristics. This includes non-CSCs, epithelial cells, endothelial cells, fibroblastic cells, perivascular cells, immune cells and extracellular matrix components; signalling pathways involve cytokines and growth factors etc. [58]. It has been postulated that CSC niches produce factors that stimulate CSC self-renewal properties and stemness, and facilitate metastasis of the tumour. The niche of CSCs is very important in cancer cell studies, as, when the CSC's TME changes, both the phenotype and the gene expression at transcriptional and translation level can be altered [59] [60]. In addition, Bissell et al. suggested in a breast cancer study that the TME-caused genetic alterations play a very important role in maintaining cell functions and during tumour progression [61].

In TME, astrocytes derived extracellular vesicles (EVs) can mediate the cell-cell communication in cancer progression [62], and contributes to neuroinflammatory response through TLR4 activation [63]. EVs are the confluence of cell specific cargo molecules: proteins, RNA, DNA wrapped by lipid bound structures [64]. Among the EV cargo categories, microRNA (miRNA), which are short (20-22 nucleotides) non-coding RNA molecules are those mostly studied and are believed to be strongly associated with cancer progression.

Bursting extracellularly of EVs outside cells contributes to the format to the growth factor rich extracellular environment [65]. EVs' direct fusion and endocytosis are intracellular methods of direct cellular information exchange [66, 67]. Several reports have indicated that the majority of the miRNAs genes from in those EVs from TME are either locate in cancer-associated regions of human genome, or at those genomic sites which are more fragile than others,

hence could contributes in the tumour progression [68, 69]. In many types of cancers, the miRNAs from EVs have been reported to involve and play important roles during cancer progression [70]. Mechanisms of miRNA regulated cancer progression vary. Mouse models featuring miRNA overexpression or ablation have demonstrated causal links between miRNAs and cancer development by bringing resistance to growth factor inhibitors [71]. The miRNA is also reported to promote drug resistance capability in cancer cells [72]. Si et al. suggested the drug resistance-related genes could be targeted by miRNAs and also the genes related to cell proliferation, cell cycle and apoptosis could be regulated by miRNAs [72]. In addition, Ibáñez et al. demonstrated that EVs derived from glial cells has a role as an intercellular mediator between inflammatory responses and TLR4, but the mechanism stayed unknown [63]. Moreover, Al- Nedawi et al. showed that growth factors in EVs could activate the growth and survival proteins in U373 glioma cells [73]. It could also activate the growth proteins and Akt and ERK, as well as enhance the ability of cell growth in soft agar. Those results suggested that EVs and influence the behaviours of cancer cells [73]. Therefore, mimicking the TME, especially mimicking the cell-cell interactions, is very important in cancer research.

In CSC niches, CSCs are regulated by complex signalling pathways intrinsic to and extrinsic of tumour microenvironment. CSCs share multiple stemness maintenance pathways with somatic stem cells, such as Notch, Hedgehog, NF-κB, Wnt, PI3K/AKT/mTOR, JAK/STAT [74-78] and TLR4 down-stream pathways [79]. Those key signalling pathways in CSCs respond in regulating cell activities regarding self-renewal capability, cell survival, proliferation and differentiation. By switching on the cell transcription factors and regulating signal transducer and activator of transcription [80, 81], signalling pathways network together to regulate genes in CSCs and maintain the CSC cell properties.

1.1.4. Clinical implication of CSC

The choice of anti-cancer therapies is at present limited. Surgery, chemotherapy and radiotherapy are the most commonly used [82]. A small population of CSCs are reported to resist chemotherapy and/or radiotherapy. The resistance of CSCs to chemo- and radio-therapy are believed to be due to the CSC niche and properties. Firstly, the stem cell niche and the cross talk between CSCs play important roles in cell regeneration, maintenance, homeostasis, and cell repair [83]. In addition, the hypoxic tumour TME also promotes the survival of CSCs. It has been suggested that the hypoxia-inducible factors 1α induce the DNA repair of CSCs [84]. It is also able to help keep the stemness properties of CSCs by preventing cellular differentiation and controlling cellular apoptosis [84]. CSCs and TME together have been proposed by Mannio and Chalmers as ‘microenvironment- stem cell units’ in glioma cells, able to affect the radio-resistance of CSCs [85]. In GBM, the activated DNA damage checkpoint response and high DNA repair capacity are the main causes of CSCs’ radio-resistance [86].

Secondly, CSCs tend to stay quiescent in solid tumours. Some CSCs remain in a reversible G0 phase of the cell cycle, and therefore escape anti-cancer drugs [87]. As Temozolomide (TMZ), the traditional alkyl chemotherapy reagent of GBM is known to induce cell cycle arrest at G2/M phase to induce apoptosis of cells [88]. In other words, anti-cancer drugs target the cells that are in a cell cycle and cannot target those which stay in G0.

Thirdly, CSCs have multiple mechanisms in chemo-resistance. The slow cycling of CSCs stops the drugs targeting CSC DNA. Also, CSCs have developed mechanisms of removing anti-cancer drugs. High numbers of adenosine triphosphate-biding cassette (ABC) transporter proteins can be found in CSCs. ABC transporters can mediate the transport of drugs out of the cell plasma and membranes against the drug concentration gradient [89]. This

mechanism promotes the survival of CSCs and induces chemo-resistance of CSCs.

In addition, some intracellular survival pathways also contribute to anti-cancer drug resistance. In hepatocellular carcinomas, the development of CD133 CSCs chemo-resistance is reported to be established by expressing survival proteins through Akt/PKB and Bcl-2 survival pathways [90]. Moreover, in a study of breast cancer, $CD44^{+}/CD24^{-/low}$ cells (CSCs) were reported to survive and proliferate under radiation [91].

Apart from the above aspects, CSCs are able to escape from immune responses. The quiescent CSCs acquire immune tolerance by reducing antigenicity in T-cells and cause a break down in the immune system [84, 92].

The survival of CSCs against both chemo- and radiation therapy explains the relapse of cancers, as the cancer cells in patients are not eradicated via chemo- or radio-therapy [93]. CSCs with self-renewal and proliferation potential can enter cell cycle, and then proliferate and differentiate to normal cancer cells. In a worst-case scenario, those CSCs can also migrate and cause metastasis and develop secondary tumours. Therefore, if CSCs can be eradicated, the prognosis for malignant tumours will be superior to what we have today. However, targeting and eliminating CSCs is a challenge. This is not only because CSCs stay quiescent and have resistance to anti-cancer treatments. CSCs share similar biological characteristics with somatic stem cells, such as essential survival pathways like Wnt/β-catenin, Hedgehog and Notch. Therefore, it is difficult to target CSCs without harming normal cells [94]. Previous research in our lab demonstrated that CSCs express Toll-like receptor 4 (TLR4) and have biased signalling via TLR4 [79]. In Chapter 3 & 4, the behaviour of U251 CSC s were studied. I demonstrated that TLR4 signalling can affect the differentiation and proliferation of CSCs, as well as the stemness of GBM. By decreasing the stemness of the whole cancer cell population, and by regulating the CSCs' proliferation and differentiation balance, CSCs

differentiation from non-CSCs can be targeted, and this may be used as a new future treatment option for GBM.

1.2. Glioblastoma multiform (GBM)

1.2.1 Definition and pathology

Brain tumours in humans are classified by the cells of origin. There are astrocytic tumours, oligodendrogliomas, ependymomas and mixed gliomas [95]. According to the World Health Organization's international standard of gliomas, GBM is grade IV of astrocytoma [96]. It is the most aggressive and most common type of brain tumour in humans. Within brain cancer patients, 60% of all malignant primary brain tumours in adults are diagnosed as GBM [97]. GBMs are very difficult to eradicate, and patients have a very low long-term survival rate. Even with treatment, the GBM prognosis is extremely poor as the patients have a very low median survival time after diagnosis (12-15 months [98, 99]).

GBM pathology can be complex. Primary tumours and secondary tumours can have slightly different pathology. Mutation of p53, a tumour suppressor gene, is one of the most common causes of cancers. In GBM, around 25%-40% patients have a deleted or altered p53 gene [100]. In addition, mutation of genes encoding for the epidermal growth factor receptor (EGFR) has also been found in nearly half of GBM tumours. As EGFR is essential for cell proliferation, GBM usually develops quickly [101]. Also, mutation of phosphatase and tensin homolog (PTEN), over expression of mouse double minute 2 (MDM2), deletion of cyclin-dependent kinase inhibitor 2A/B (CDKN2A/B) and CDKN2C also cause an increase in Nuclear factor kappa B (NF-κB) activation and translocation in GBM. All of these play a role in GBM development [95, 100-102].

1.2.2 GBM CSC

CD133 was first used to isolate human neural stem and progenitor cells in 2000 [103], and was first identified as GBM CSC marker in 2003 [24]. In the following, further studies proved that CD133 is one of the crucial markers for glioma cancer stem cells [24, 30], as CD133+ cells are able to generate new tumours in vivo, but CD133- cells cannot [5]. Since CSCs were first identified, other molecular markers apart from CD133 have also been described for glioma CSCs. Those markers are: SOX2, nestin, *bmi-1*, musashi-1, *melk*, NANOG, SALL4. [30, 32, 104, 105].

GBM CSCs are CD133 positive cells and have self-renewal and differentiation potential. *In vivo*, regulation factors of GBM CSC including genetics, epigenetics, metabolism, niche, TME, and the immune system etc. [106]. GBM is a particularly useful type of cancer to focus on when studying CSC because it has clear cell markers and enrichment methods and the GBM CSCs are thus easier to identify and study. Like in other tumours, CSC in GBM to tumour initiation and treatment resistance [106]. Despite the critical cellular microenvironment in GBM, CSCs are able to survive and maintain differentiation and self-renewal capability in the necrotic, acidic and hypoxic microenvironment. Stemness of CSCs and many signalling pathways have been proved to contributes to the CSC survival and maintenance in this stressful condition and as well contribute to tumour progression [106], including Notch, Hedgehog, NF-κB, and Wnt signalling [107-109]. However, it is still not quite clear how the GBM CSCs begin: whether they are from normal stem cells or are transferred from stromal abnormal cells. Furthermore, many signalling pathways and how the signalling pathways regulate GBM CSC behaviour remained partially known.

In GBM CSCs, oncogenic signalling pathways like Hedgehog, Notch, Bmi1, Wnt/β catenin, NF-κB etc. are involved in cell self-renewal and cell differentiation mechanisms [79, 108, 109]. Those pathways take charge of CSC

life maintenance and affect the CSC behaviours. Wnt/β signalling pathway, for example, can impede CSC differentiation in GBM [110]. Notch pathway is also reported to have an important role in maintaining CSCs' un-differentiated state, as the inhibiting Notch pathway promotes GBM differentiation to astrocytes [111]. Bm1 protein, which is known to be highly enriched in CSCs, silences p16 and p19Arf locus. The latter are genes that suppress cell proliferation [112]. Wnt pathway controls the cell- renew and cellular fate development of CSCs [113]. Hedgehog and Notch pathways promote cell proliferation and differentiation, and prevent apoptosis [114]. NF-κB pathway in CSC is crucial for cell survival and is reported to promote GBM cell radiation resistance via transcriptional programme [115]. Many of those signals have been suggested to have links to the GBM progressions, especially maintaining the stemness of cells. CSCs have *in vivo* quiescence and have radio- and chemo-therapies resistance [116]. Those properties of CSCs are proved to link to the stemness of CSCs [117]. It is predictable that by reducing the stemness and promoting the differentiation of CSCs, it would increase the efficiency of anti-cancer treatments. Therefore, studying the behaviours of glioma CSCs is one of the crucial tasks that need to be achieved. Knowing how TLR4 would change the CSC properties is one of the main aims of my project.

1.2.3 Current GBM therapy options and limitations

The treatment of glioblastomas is palliative and includes surgery, radiotherapy, and chemotherapy using an alkylating agent like Temozolomide (TMZ) [95]. GBM treatment today is still very challenging in clinical oncology. As an aggressive type of cancer, the complex character of a GBM tumour itself, the heterogeneous biology of the tumour, and the diffuse nature of the tumour cells makes it very difficult to treat the disease by therapeutic intervention [118]. GBM is not only hard to cure, but also has a high tumour recurrence rate [119].

1.3. Toll-like receptor

1.3.1 Toll-like receptor family

The Toll receptor protein was first discovered in 1985 in the larvae of the fruit fly *Drosophila melanogaster*. The toll protein binds to its endogenous ligand and plays a role in *Drosophila* larvae development, and the signalling of the Toll protein involves an immune response in *Drosophila* adults. Its ligand, a cytokine called spätzle, controls the expression of antifungal protein drosomycin in *Drosophila* [120, 121]. In mammals, the immune system is much more complex than that of an insect. Our innate adaptive immunity ensures that we are defended well in a world with varies types of pathogens. In mammals, the homologue of the Toll protein, Toll-like receptor (TLR), has a similar function to Toll and plays an essential role in our innate immune system.

TLRs are type I integral membrane proteins, belong to Toll-/interleukin-1 receptor (TIR) super family, and form a group of highly conserved receptors that function as microbial pattern recognition receptors (PRR). As type I integral membrane receptor, TLR form of dimers and have conserved structures. They share an N-terminal ligand recognition domain, a single transmembrane helix, and a C-terminal cytoplasmic signalling domain [122]. TLRs contains conservative 3-4 turns, 27-29 amino acid long of leucine-rich repeat (LRR), which form an extended β-sheet to interact with PAMPs, with or without an accessory molecule, such as myeloid differentiation factor 2 (MD-2) [122, 123].

In humans, ten types of functional TLRs have been identified. The activation of these TLRs requires adaptor proteins. Two downstream pathways of TLRs were identified in mammalian cells: the myeloid differentiation primary response 88 (MyD88) dependent pathway and the MyD88-independent/TRIF dependent pathway [124]. According to a study by Zeuner et al., they can respectively be regarded as pro- and anti-inflammatory pathways [79]. Adapter proteins for TLRs include MyD88, MyD88 adapter like protein (Mal) (also named as TIR

domain containing adapter protein, TIRAP), TIR-domain containing adapter inducing interferon (TRIF) (also known as TIR-domain-containing molecule1, TICAM1), and TRIF-related adapter molecule (TRAM) (also known as TIR-domain-containing molecule2, TICAM2). Adaptor protein MyD88, has a N-terminal death domain (DD), which is crucial for the subsequent signalling cascade as it enables the construction “myddosome” (a large multimeric complex), and is playing an essential role in the production of inflammatory cytokines such as TNFα, Interleukin 1β, interleukin 8. TRIF in TLR3 and TLR4 driven MyD88-independent pathways is crucial for the expression of type I interferons (IFN), while TRAM is TLR4 specific and helps TRIF in MyD88-independent pathway [124].

TLRs recognize and bind a series of damage/danger-associated molecular patterns (DAMPs) and pathogen associated molecular patterns (PAMPs) and initiate downstream pathways to regulate immune responses [125, 126]. A summary of the TLR family in humans is shown in Table 1.2, which lists the TLR ligands, ligand origins, the intracellular adaptor, and the interaction proteins [123, 124]. Among all the TLRs, TLR1, TLR2 and TLR4 are believed to be located on cell surface to respond to extracellular patterns (in Golgi apparatus, too [127]), and are able to form phagosomes after activation, while TLR3, TLR7 which recognize RNA, and TLR9 which recognizes DNA, are located in the endoplasmic reticulum, but not in the cell membrane [124].

Receptor	Ligand	Origin of Ligand	Intracellular adaptor	Interaction with	Reference
TLR1	Triacyl lipopeptides peptidoglycan	Bacteria and mycobacteria	MyD88	Cluster of differentiation-14 (CD14) TLR2	[128] [129]
TLR2	Lipoprotein/lipopeptides Peptidoglycan Zymosan Heat-shock protein 70	Various pathogens Gram-positive bacteria Fungi Host	MyD88	TLR1 TLR6 TLR10 CD14	[130] [131] [132] [129]
TLR3	Double-stranded RNA	Viruses	TRIF	NA	[133]
TLR4	Lipopolysaccharide Heat-shock protein 22, 60 & 70, CD138, fibrinectin, hyaluronan etc.	Gram-negative bacteria *Chlamydia pneumoniae* Host	MyD88 TRIF	MD2 CD14	[126] [134] [135, 136]
TLR5	Flagellin	Bacteria	MyD88	NA	[137]
TLR6	Diacyl lipopeptides Lipoteichoic acid Zymosan	*Mycoplasma* Gram-positive bacteria Fungi	MyD88	TLR2	[138] [139] [132]
TLR7	Single strand RNA	virus	MyD88	CD14	[140, 141]
TLR8	Single strand RNA	Host, viruses	MyD88	NA	[140]
TLR9	Non-methylated CpG-contained DNA	Virus, bacterium	MyD88	CD14	[141, 142]
TLR10	Remained unclear, might	Bacteria, virus	MyD88	TLR2	[136, 143-145]

	be PAMP same to TLR1/2, HIV glycoprotein, diacylated lipopeptides				

Table 1.2: Summary of TLR family in humans is shown [123, 124]. TLRs have different ligands, which are from varies of origins. The intracellular adaptor proteins of the TLRs are MyD88 and TRIF. Some TLRs need interaction proteins for the downstream pathways.

1.3.2 TLR4 and its ligands

TLR4, also known as cluster of differentiation 284 (CD284), is one of the essential receptors in the innate immune responses. In the TLR family, TLR4 is the only TLR that has two intracellular adaptors, MyD88 and TRIF. This means that TLR4 is the only TLR that can activate both MyD88-dependent and TRIF-dependent pathways depending on the ligand, while other TLRs only signal through one pathway. The activation of the two downstream pathways could be triggered by different TLR4 ligands and biased activation of the two downstream pathways was observed [79].

One type of TLR4 ligands are lipopolysaccharide (LPS) from gram-negative bacteria. When LPS binds to TLR4, it first binds to LPS binding protein (LBP) to form a complex. Continuing with the help of CD14, LBP and LPS then bind to TLR4 at the LRR area of TLR4-MD2 complex and form oligomeric structures [146]. MD-2 as an indispensable co-receptor molecule binds to LPS and the extracellular domain of TLR4 [127]. Fig. 1.1 shows an overall structure of TLR4-MD-2-LPS complex, and the binding of LPS to TLR4 triggers the homo-dimerization of TLR4-MD-2. It is worth mentioning that a recent study found that CD14 is not always necessary for TLR4 signalling via MyD88 dependent pathway in response to high concentrations of LPS [147].

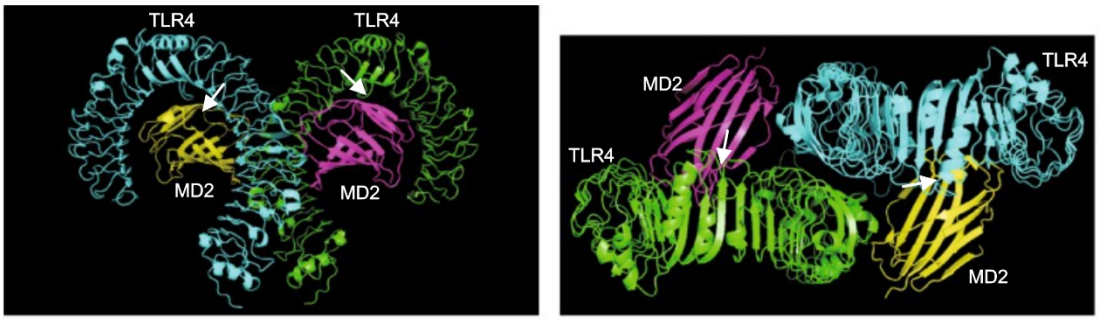

Figure 1.1. Overall structure of TLR4-MD-2 dimer [146]. TLR4 has LRR strands which forms β-strand and β-sheet to interact with its ligand LPS under the help of MD-2. MD-2 as a co-receptor molecule, binds to LPS and the extracellular domain of TLR4. Arrows are the biding site of LPS. Figure from Kim H.M. & Vallance T.[146, 148].

Apart from the pathogen-associated molecular pattern (PAMP) LPS, TLR4 has wide varieties of their corresponding ligands, which are endogenous damage-associated molecular patterns (DAMPs). The release of those DAMPs is often associated with infections and cell injury [136]. Those DAMPs that recognised by TLR4 are: biglycan [149], CD138 [150], fibrinogen[151], fibronectin [152], HMGB1 [153], Heat shock protein (HSP) Gp96 [154], HSP22 [155], HSP 60 [134], HSP70 [156], hyaluronan [157], surfactant protein A [158] etc.

1.3.3 TLR4 biased signalling

Biased signalling of TLR4 has been reported [79]. TLR4 is expressed on the surface of multiple cell types including hematopoietic cells, endothelial cells, central neural system cells, and some cancer cells including GBM cells [159-161]. This biased signalling might be ligand dependent, as this feature was observed when stimulating TLR4 with ligands of different chemo types. One ligand of TLR4 is lipopolysaccharides (LPS). Taking LPS as an example, it is composed of an O-antigen, outer and inner core and multiple chains of lipid A [162]. LPS from different bacterial species have conserved structured lipid A,

but the number of lipid A chains may vary. Therefore, LPS from different bacteria species may give various strengths for modulating the host immune response [163]. Biased signalling of TLR4 in GBM was reported after stimulating the receptor using *Salmonella minnesota* LPS and *Escherichia coli* LPS [161]. The variation of lipid A may lead to different signalling activation and this might explain the biased signalling of TLR4.

MyD88-dependent pathway

Taking LPS as an example, when LPS binds to TLR4 and triggers MyD88-dependent pathway, LPS-TLR4-MD2 forms. The TIRAP is recruited by the TIR domain of LPS-TLR4-MD2 complex on the membrane, followed by recruitment of MyD88 and interleukin-1 receptor-associated kinases (IRAK). Six units of MyD88, four IRAK and four IRAK1/2 form the 'Myddosome' and trigger the interaction between tumour necrosis factor receptor-associated factor (TRAF) 6 and TRAF-activated kinase 1 (TAK1). Under normal circumstances, pro-inflammatory transcription factor NF-κB is suppressed by inhibitors of NF-κB (IκBs), which is an ubiquitination enzyme that can be phosphorylated The double phosphorylation is catalysed by a kinase complex called IκB kinase (IKK). IKK complex includes active kinases IKKα, IKKβ and regulatory subunit IKKγ/ NF-κB essential modulator (NEMO). Activation of IKK complex leads to the phosphorylation and degradation of IκB, freeing NF-κB and allowing NF-κB nuclear translocation. Activated NF-κB can translocate into the nucleus and is able to promote expression of proinflammatory cytokines including TNFα and interleukin-1β [148]. TAK1 can at the same time target extracellular signal-regulated kinases (ERK), c-Jun amino-terminal kinases (JNKs) and p38 mitogen activated protein kinases and lead to the activation of the transcription factor activator protein 1 (AP-1). Also, the AP-1 combined with activated NF-κB increases the expression level of pro-inflammatory cytokines [148, 164-166] (Fig. 1.2).

MyD88-independent/TRIF dependent pathway

In the TRIF-dependent pathway, TRIF-related adaptor molecule (TRAM) recruits TRIF and promotes the CD-14 dependent internalisation of TLR4 to endosomes via a clathrin- or caveolin-dependent mechanism forming the TLR4-TRAM-TRIF complex. TRAF3 is then recruited to the complex by TRIF and is subsequently poly-ubiquitinated. This leads to the activation of TRAF family member-associated NF-κB activator-(TANK-) binding kinase-(TBK-) 1 and IKK ε, followed by the phosphorylation and activation of interferon regular factor 3 (IRF3) and regulation of the expression levels of type one interferon β (IFNβ) [148, 167, 168].

Apart from IRF3 activation, NF-κB activation is also reported in MyD88-independent pathway, but the responses are delayed compared to IRF3 activation [124]. This NF-κB activation is recognized as “late phase NF-κB activation” compared to the early “NF-κB activation” in the MyD88-dependent pathway. For this case, IRIF is essential for NF-κB activation, suggesting that interferon beta (IFN-β) production can be modulated by TRIF-mediated late phase NF-κB activation alone [124, 169].

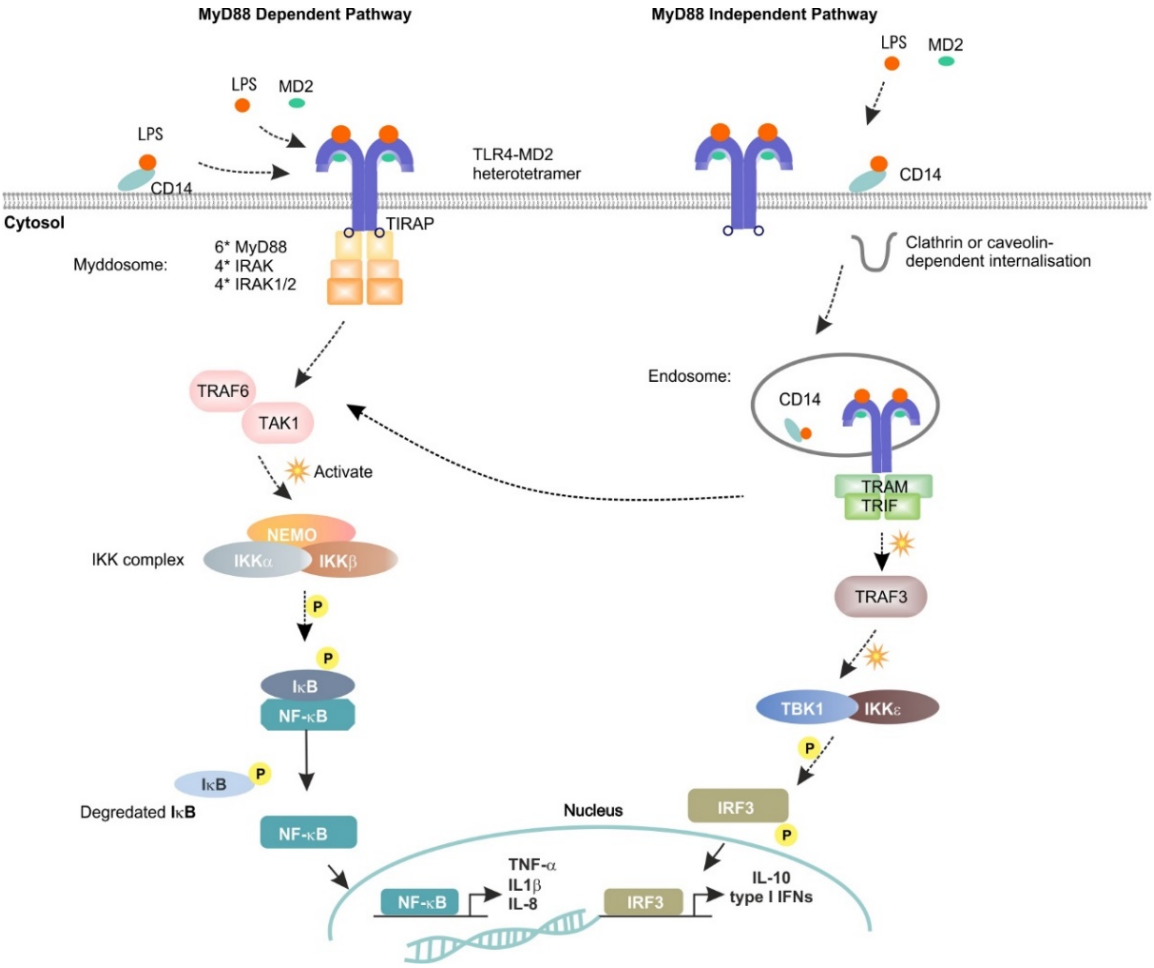

Figure 1.2. Schematic graph of two major intracellular TLR4 signalling pathways: MyD88-dependent and MyD88-independent pathways. LPS is transferred to CD14, which acts as a co-receptor and transfer LPS to TLR4-MD2 to form heterotetramer. In MyD88 independent pathway, internalisation of the heterotetramer occurs and transcription factor IRF3 which stimulates the transcription of anti-inflammatory cytokines is activated as the result of the signalling flow. In MyD88 dependent pathway, nuclear translocation of NF-κB and AP-1 will be triggered, pro-inflammatory cytokines expression will be increased as a result[148]. Abbreviations: MD-2: myeloid differentiation factor 2. TIRAP: Toll-interleukin 1 receptor (TIR) domain-containing adaptor protein. TRAF: TNF receptor-associated factor. TAK1: TRAF-activated kinase 1. IRAK: Interleukin receptor-associated kinase. NEMO: NF-κB essential modulator. IKK: IκB kinase. TRIF: TIR domain-containing adaptor- inducing interferon- β. TRAM:

TRIF – related adaptor molecule. TBK: TRAF family member-associated NF-κB activator- binding kinase.

1.4. TLR4 in cancer

1.4.1. MyD-88 dependent pathway and the transcription factor NF-κB

The transcription factor NF-κB is activated by the MyD88-dependent downstream pathway of TLR4. It has been studied for decades and plays an important role in the mammalian immune system. NF-κB protein family consists of five subunits: p50, p52, Rel A (p65), Rel B and c-Rel [170]. As a transcription factor, NF-κB recognises the DNA sequences which match the following consensus sequence: 5'-GGRNYYYCC-3', where R stands for a purine, Y stands for a pyrimidine, and N could be any nucleotide [171]. In neuroinflammation, the cytokine TNFα activates NF-κB. In addition, in TNFα signalling, NF-κB p65 protects cells from apoptosis by modulating transcription of c-IAP, bcl-2, and bcl-xL genes [170, 172, 173]. At the same time, NF-κB does have a pro-apoptotic function in cancer development, depending on the co-stimulation of other signalling pathways [174]. Moreover, TNF-induced NF-κB activity is suggested to increase the proliferation of neural cancer stem cells via up-regulation of cyclin-D1 and c-myc [173, 175, 176]. In cancer development, it has been suggested that tumour progression is hugely affected by NF-κB. As an important transcription factor, it not only promotes cancer cell proliferation and modulates cell survival and cell metastasis but also contributes in cancer cell chemotherapeutic resistance. With various cross talks between NF-κB and other signalling pathways such as p53, IRF, STAT3 etc. [177], NF-κB could be regarded as a key death or survival factor in tumour cells [178].

1.4.2 MyD88-independent pathway and the transcription factor IRF3

The IRF family was first identified in 1988, when IRF-1 was found to specifically bind the regulatory element of IFNβ gene acting as a transcription regulatory element [179]. IRF family (IRF1-IRF9) is believed to have essential regulatory functions in immunity and oncogenesis by contributing to governing the inflammation. The IRFs activated by TLR4 are IRF3 and IRF5. IRF3 has anti-inflammatory effects on tumour tissue and is activated by MyD88-independent pathway (TRIF associated TLR4 activation pathway. A series of anti-inflammatory cytokines genes was then targeted and regulated by IRF3 including type I interferon (IFN), IL-15, IL-12p35 etc. [180].

IRF3 is expressed constitutively in many cell types and plays an important role in the innate immune system by activating the interferon-stimulated genes and mediating

anti- viral and anti-inflammatory effects in human tissue [181]. Tian et al. suggested that IRF3 could inhibit the translocation of β-catenin and therefore suppress colorectal tumorigenesis [182]. Recently, IRF3 has been reported to have the ability to inhibit the migratory potential of GBM cells [183]. In chapter 3, my results also suggested that IRF3 has the function of driving cell differentiation in GBM.

There is evidence that different pro-inflammatory cytokines and IFN are main regulators of downstream TLR4 signalling [184, 185]. Apart from IRF3, different ubiquitin ligase proteins are involved in regulating pro-inflammatory cytokines and IFN. TRAF3, for example, interacts with both MyD88 and TRIF and has differential ubiquitination to select the production of type 1 IFNs versus proinflammatory cytokines [186]. TRAF3 is able to process self-ubiquitination and activate IFN response, as well as TAK1 response, and when it binds to TAK1, NF-κB and JNK pathways will be enhanced [187]. Another E3 ubiquitin ligase, NRDP1, is also a regulator of the pro- and anti-inflammatory pathways of TLR4. By binding and ubiquitinating MyD88 and TBK1, it is able to reduce the inflammatory cytokine production and induce the preferential type I IFN production [188]

1.4.3 TLR4 in cancer

With its important role in the immune system, TLR4 is also crucial in the cancer defence system. First, activation of TLR4 by DAMPs (HSP70, HMGB1 etc.) is able to trigger immune response of dendritic cells and further enhance the induction of anti-tumour T-cell immune response [189]. This is the mechanisms to recognise abnormal cells and chemically stressed cancer cells to reduce cancer progression [189]. Some studies in human melanoma, lung cancer and ovarian cancer have suggested that in tumours, the inflammation microenvironment and activation of TLR4 can downregulate the anti-tumour activities in immune cells and promote tumour growth to some extent [190-192]. Second, TLR4 in cancer cells has pro- and anti-cancer effects. In TME, the MyD88-dependent pathway of TLR4 could be switched on by PAMPs and increase the inflammation as well as suppress the immune activities. This induces cell proliferation and cell invasion and can promote chemo-resistance to tumour cells [193]. In addition, the TLR4 pro-inflammatory pathway is also proved to increase the stemness of the CSCs in hepatoma cells [194]. In contrast, the MyD88-independent pathway is able to promote the expression of anti-inflammatory cytokines in the TME.

Therefore, it is very important to understand the biased signalling of TLR4 and understand the cell behaviours impacted by the biased signalling.

1.4.4 TLR4 in Glioblastoma (GBM) CSCs

Evidence showed that TLRs are expressed in GBM cells, and also within GBM CSCs [79]. TLR4 has been reported to express in GBM tumour samples and GBM cell line u251, U87 [79, 195, 196]. However, evidence demonstrated by Alvarado et al. showed that TLR4 expression level has been reported to be lower in GBM CSCs than in surrounding cells, suggesting that this could be a mechanism CSCs use to escape from inhibitory innate immune signalling [197]. The mechanism suggested that, in GBM, reducing retinoblastoma binding protein 5 (RBBP5) is highly expressed in CSC compared to non-CSCs. RBBP5 is known to be one of the regulators in GBM CSCs, via tank-binding kinase 1 (TBK-1) downstream of TRIF-dependent TLR4 signalling pathway, to maintain the stemness of GBM CSCs [197]. There is also evidence that TLR4 is upregulated when glioma CSC goes into cycle. During this procedure, glioma CSCs have a MyD88-dependent pathway activated to keep differentiation and proliferation properties [198].

Therefore, in GBM, or even other cancer types, CSCs and non-CSCs undertake different roles and share different properties. Non-CSCs as the main population of GBM are very proliferative, but CSCs mainly stay outside the cell cycle and remain quiescent. When CSCs enter the cell cycle, begin to differentiate to non-CSCs and start proliferation, TLR4 starts to express and MyD-88 dependent signalling pathway activates. The mechanism of why the CSCs enter the cell cycle has been poorly studied. In general, TLR4 has different expression levels in GBM cells and shows opposite effects to GBM CSCs and GBM non-CSCs. TLR4 in non-CSCs has been known to be involved within inflammation microenvironments in solid tumours and tumour expanding activities such as cell proliferation, as well as being metastatic via MyD88 dependent pathway [199, 200]. Besides, TLR4 has also been suggested relative to epidermal growth factor receptor (EGFR) to promote cell migration in GBM cell lines [201]. It seems that in GBM CSCs, if TLR4 is activated, then TRIF-dependent pathway is predicted to be the dominant signalling pathway and to have functions of suppressing stemness as well as proliferation.

1.5. Project background, aims of study and hypothesis

It has been demonstrated by our lab that TLR4 is a subject of biased signalling that could be activated by *E. coli* LPS and *S. minnesota* LPS. Our lab generated an U251 NF-κB reporter cell line, and used it as a tool to demonstrate that the MyD-88 dependent pathway is a pro-inflammatory pathway and MyD-88 independent pathway is an anti-inflammatory pathway.

In this study, the overall aim is to better understand how the TLR4 biased signalling impacts glioma cell behaviour. Specifically, I aimed to use both 2D and 3D cell culture techniques to address the impact of TLR4 mediated biased signalling on the stemness, proliferation, migration, differentiation and survival of GBM CSCs. The overall hypothesis is that different chemotypes of LPS differentially impact the behaviour of CSCs in glioblastoma, while 3D cell culture should bring changes to cell behaviour in comparison to 2D.

In detail, the first aim of my study is to test the chemotypes of LPS, and see how they differently impact the U251 cell behaviours by acting as NF-κB or IRF3 biased TLR4 ligands. The hypothesis here is the IRF3-biased TLR4 agonists will reduce the stemness and proliferation whereas NF-κB-biased agonists will have the opposite effect.

Second, I wanted to address the different impacts of the biased signalling to GBM cells in 2D and 3D. I wanted to understand how 3D cell culture changes the CSC behaviours. The hypothesis here is that in 3D cell culture, GBM cells show different characteristics and react differently in comparison to 2D, and react differently to the biased TLR4 signalling. This would be very helpful for me to understand the features and the biased signalling in clinical tumours. My hypothesis is that,

Third, in order to quantify the activation level of the two downstream pathways of TLR4, I aimed to generate a novel dual reporter cell line using U251 cells. This would be a robust tool for future research in this area. Quantifying the activation level of the biased signalling would be a great help in understanding the mechanism of the bias.

Last, I used curcumin, the most pharmacologically active component in turmeric, as TLR4-NF-κB inhibitor. Curcumin was proved to have high anti-inflammatory effect to

GBM [202]. An efficient curcumin delivery system was proposed and was suggested to have great potential in GMB treatment.

Chapter 2. Materials and methods

2.1. Cell culture

Cell line

U-251 MG (ATCC) is a human glioblastoma astrocytoma cell line. (Formerly known as U-373 MG) (European Collection of Authenticated Cell Cultures catalogue number 09063001). It was derived from a malignant glioblastoma tumour by explant technique. According to the UK Health Security Agency.org.uk, the background of this cell line was described as: *'The American Type Culture Collection (ATCC) reported that their stock of U-373 MG had been shown to have differing genetic properties to stock from the originator's laboratory, and to share similarities with another glioblastoma cell line, U-251. The U-373 MG cell line listed under catalogue number 89081403 has been re-named as 'U-251 MG and has the new ECACC catalogue number 09063001*. '[203]

Adherent cell culture

U251 cells (ATCC) were cultivated in Dulbecco's Modified Eagle's Medium (DMEM) High Glucose (Sigma-Aldrich Company Ltd., Dorset, UK) comprising 1% L-glutamine (200 mM, Sigma-Aldrich), 10% heat-inactivated foetal calf serum (FCS, lot:126K3398, Sigma-Aldrich)) in absence of antibiotics and antimycotics (referred to as 'normal cultivation media') in a humidified incubator (Thermo Fisher Scientific, Loughborough, UK) at 37°C and 5% CO_2 unless stated otherwise. Cells were early passage cells (<20 passage) and were provided with fresh medium every 2-3 days and passaged at 80-90% confluency. U251-NF-κB-GFP-Luc reporter cells were used which have been previously developed and characterised [204]. Normal cultivation media for the reporter cells contained 5 µg/ml Puromycin (Apollo Scientific).

Passaging of cells

To assist the resuspension of cells, Trypsin-ethylenediamineteraacetic acid (EDTA) solution was used to detach the cells from the adherent flask. U251 cells in the flask were first washed with 10ml of (phosphate-buffered saline) PBS solution, followed with

4ml of Trypsin-EDTA solution. Cells in Trypsin-EDTA solution were incubated in the 37º C incubator for 2-3 mins until all the cells were detached from the bottom of flask. 4-6 ml of growth media were added to the flask to form cell suspension. Cell suspension were then placed into a 15ml falcon tube. Centrifuge (Eppendorf, 5810R) were used to centrifuge down the cells at 300g. Cells were then re-suspended from the bottom pellet of the falcon tube. The cells were split at a ratio between ratios of 1:4 to 1:6 into new flasks.

Cell counting

To determine the number of cells in cell suspension, a small volume of sample (20µl) was taken into a 0.2ml PCR tube. Cell suspension were mixed 1:1 with Trypan blue (T6146, Sigma-Aldrich Company Ltd.). Haemocytometer with a clean coverslip were placed under the EVOS cell imaging system (EVOS XL core, ThermoFisher). Cell suspension + Trypan blue mixture were added to the edge between the coverslip and the haemocytometer. The number of viable cells were counted within the defined four 1mm^2 squares area. The equation of determine the cell concentration, the following equation was used:

$$\boldsymbol{Cell\ concentration} = \frac{\boldsymbol{Number\ of\ cell\ counted\ in\ total}}{\boldsymbol{Number\ of\ squares}} \times \boldsymbol{10^4} \times \boldsymbol{dilution\ factor}$$

And the total cell number was determined as:

$$\boldsymbol{Cell\ number = cell\ concentration \times volume\ of\ cell\ suspension}$$

Cell cultivation in Growdex® - a nonofibrillar cellulose (NFC)

Early passage of U251 cells (passage 6-12)(ATCC) were first cultivated in Dulbecco's Modified Eagle's Medium (DMEM) High Glucose (D5671, Sigma-Aldrich Company Ltd., Dorset, UK) comprising 1% L-glutamine (200mM, Sigma-Aldrich), 10% heat-inactivated foetal calf serum (FCS, lot:126K3398, Sigma-Aldrich), 1 % B27 50x (Thermo Fisher Scientific) as well as 1 % L-Glutamine, 20ng/ml FGF-2 (Promega) and 20 ng/ml EGF (Promega) in absence of antibiotics (referred to as 'growth media') in a humidified incubator (Thermo Fisher Scientific, Loughborough, UK) at 37°C and 5% CO_2. Before transferring cells to Growdex® NFC (UPM Biomedicals), cells were detached using Trypsin EDTA solution (T3924, Sigma-Aldrich) to single cell suspension.

NFC or an anionic nanofibrillar cellulose (aNFC) was mixed well with growth media (as above) without FCS as 0.1%, 0.2% to form NFC/aNFC media hydrogel as final working solution. U251 cells were mixed well with the final solution before seeding, as 500 cells/ µl and 1000cells/µl seeding density. To cultivate cells, 100µl of cells and working solution mix was embedded in each well of 96 well plate. 100µl of growth media was gently added on top of cells in each well without disturbing the bottom 100µl of cell-NFC/aNFC working solution mixture. The top 100µl of media was carefully changed every 48 hours.

Tumourispheres formation

Adherent early passage (passage 3-6 of the cells got from supplier which was passage 51) U251 or early passage U251-NF-κB-GFP-Luc cells were cultivated as described above. Adherent cells were dislodged using Trypsin-EDTA (Sigma-Aldrich Company Ltd.) after a 5 ml PBS (Sigma-Aldrich Company Ltd.) wash. Cell pellet was resuspended in DMEM/F12 medium (Sigma-Aldrich Company Ltd.) containing 1% B27 50x (Thermo Fisher Scientific) as well as 1% L-Glutamine, 20 ng/ml FGF-2 (Promega) and 20 ng/ml EGF (Promega) and cultivated as suspension culture at 37°C and 10% CO_2 and used at passage 3-6 until tumourispheres were formed.

Stimulation of adherent U251 and U251 tumourispheres

Cells were cultivated as tumourispheres and used at passages 3-10. Trypsin-EDTA and mechanical disruption was used to singularize cells, before they were cultivated under adherent conditions using normal cultivation media comprising the respective treatments. Treatment consisted of 1 µg/ml ultrapure LPS derived from either *Salmonella minnesota* (ultrapure *S. minnesota* R595 in endotoxin-free water, InvivoGen, Toulouse, France) or *Escherichia coli* (ultrapure *E. coli* LPS in endotoxin-free water, InvivoGen) for 7 days. For co-stimulation with antagonists or inhibitors, 10 µg/ml *Rhodobacter sphaeroides* LPS (*R. sphaeroides* LPS in endotoxin free water, InvivoGen) or 10 µM IMD0354 (Sigma-Aldrich, in DMSO) were present. Medium was changed every day to maintain constant conditions. All the treatment concentration were suggested by Zeuner et al. [79], following with cytotoxicity test using U251 cells (data not shown).

Treatment to U251 cells in GrowDex®

Cells were cultivated in GrowDex® NFC hydrogel for 24 hours before adding respective treatments. Treatment consisted of 10µg/ml TNFα (Peprotech), 1 µg/ml ultrapure LPS derived from either *Salmonella minnesota* (ultrapure *S. minnesota* R595 in endotoxin-free water, InvivoGen, Toulouse, France) or *Escherichia coli* (ultrapure *E. coli* LPS in endotoxin-free water, InvivoGen) for 7 days. 50 µl of hydrogel and cells were seeded in the 96 well plate wells, treatments were added to the 100µl of growth media in the 96 well plate on top of the hydrogel.

2.2. Cellular experiments

Magnetic cell sorting

U251 cells were cultivated as spheres and were used directly or were further stimulated with LPS as described above for 7 days. $2x10^6$ cells were labelled using a PE-conjugated anti-CD133 antibody (Miltenyi biotec Ltd., Woking, UK) followed by incubation with an anti-PE Antibody conjugated to a microbead as recommended by the manufacturer (Miltenyi Biotec Ltd.). LS column and MACS separator (Miltenyi Biotec Ltd.) were used. MACS buffer were made with: PBS (Sigma-Aldrich Company Ltd.), PH7.2, 0.5% BSA (A3733, Sigma-Aldrich Company Ltd.), 2 mM EDTA (Sigma-Aldrich Company Ltd.), keep buffer cold (2-8 degrees).

Quantitative PCR

After sphere formation 10^4 cells per well (6-well) were singularized and cultivated adherent for 7 days in normal cultivation media in presence of either 1 µg/ml *E. coli* LPS (InvivoGen), 1 µg/ml *S. minnesota* LPS (InvivoGen) or left untreated (control) as described above. In case of the additional treatment with the inhibitors or antagonistic LPS, medium also contained 10 µM IMD0354 or 10 µg/ml *R. sphaeorides* LPS (InvivoGen) at all times, respectively. RNA was harvested after 7 days using the NucleoSpin RNA isolation kit (Macherey Nagel GmbH & Co KG, Düren, Germany). Remaining genomic DNA was digested using DNAse I digestion Kit (Thermo Fisher Scientific). cDNA was amplified using RevertAid RT Reverse Transcription Kit

(Thermo Fisher Scientific) and random hexamers according to manufacturer's guidelines. For quantitative PCR, 4 µl of cDNA (1:10 dilution) was mixed with 7.5 µl SYBR Green PCR Master Mix (Applied Biosystems, Thermo Fisher Scientific) and 0.25 µl of the respective primers (10 µM, Sigma-Aldrich, Table 2.1) before the solution was adjusted to 10 µl with DEPC-treated water. qPCR was performed using StepOne Plus Cycler (Applied Biosystems).

The primers used for qPCR were listed below, all primers were ordered from Sigma-Aldrich.

Target	Forward primer sequence (5'-3')	Reverse primer sequence (5'-3')
GAPDH	CATGAGAAGTATGACAACAGCCT	AGTCCTTCCACGATACCAAAGT
PPIA	CAAGCATGTGGTGTTTGGCA	TGGTCTTGCCATTCCTGGAC
CD133	GTCCTGGGGCTGCTGTTTAT	TCTGTCGCTGGTGCATTTCT
Nestin	GCGTTGGAACAGAGGTTGGA	GAGCGATCTGGCTCTGTAGG
β-III-tubulin	CACCGGACCCTGTCTTACAGC	CGATCAAGCTTCTGCTGCCTC
GFAP	TCGATCAACTCACCGCCAAC	ATAGGCAGCCAGGTTGTTCT

Table 2.1. Primer list for qPCR.

Immunocytochemistry of adherent U251 cells

For After sphere culture, $4x10^3$ cells were cultivated on cell culture-treated coverslips in 12-well plates (Sarstedt, Leicester, UK) and treated respectively as described above. For immunocytochemistry of spheres, cells were not dissociated but cultivated in normal cultivation medium for up to 1 h until spheres attached to the cover slip. After 20 min incubation with 4% paraformaldehyde (Sigma-Aldrich), cells were treated with PBS containing 0.02% Triton X-100 (PBT, Sigma-Aldrich; not used when stained for CD133) comprising 5% normal goat serum (Stratech Scientific Unit, Suffolk, UK) for 30 min. Stemness marker nestin, CD133, differentiation marker GFAP and β-III-tubulin expressions were checked. Cells were stained with mouse anti-human CD133 primary antibody (1:60 in PBS, Developmental Studies Hybridoma Bank (DSHB), University of Iowa, Iowa City, USA; Clone HB#7), mouse anti-nestin (1:500, RnD Systems, Clone MAB1259), mouse anti-GFAP (1:200, Sigma-Aldrich, Clone G-A-5), mouse anti-β-III-tubulin (1:500, Promega Corp, Southampton, UK) and mouse anti-nestin (1:500, RnD Systems, Clone MAB1259) for 1.5 h at room temperature. Followed by secondary goat anti-mouse IgG conjugated Alexa fluor™ 555 (1:300 in

PBS, Life Technologies Ltd., Paisley, UK) Alexa fluor™ 488 (1:300 in PBS, Life Technologies Ltd., Paisley, UK) for 1h at room temperature and DAPI (25mg/ml, 1:2000 in PBS, Sigma-Aldrich, Darmstadt, Germany) for 15 min at room temperature. Pictures were taken by Axio imager A1 microscope system (Carl Zeiss, Jena, Germany) and CQ1 spinning disc confocal microscope (Yokogawa) under the same conditions for acquisition. Image acquisition was performed using respective analysis software (Axiovision4 or CQ1 measurement software). Cells that express the protein of interest were counted, and the percentages were calculated using ImageJ by measuring pixel intensity. For pixel intensity measurement and additional image processing, Fiji software was used [205].

Immunocytochemistry for U251 in GrowDex-T®

U251 cells were cultivated in 0.2% of GrowDex-T® (aNFC) at 1000 cells/µl. Treated with 10µg/ml TNFα (Peprotech), TNFα+ 10 µM NF-κB inhibitor Bay11-7082. Untreated cells were used as control. After 72 hours of cultivation, spheroids were fixed in blocking buffer (1x Phosphate buffered saline, 0.02% Triton™X-100, 5% goat serum) for 30 mins followed by incubation with Nestin mouse monoclonal antibody (diluted 1:250 blocking buffer, R&D systems) for overnight at 4ºC. Spheroids were gently washed in PBS for 5 times and incubated with Goat anti-mouse Alexa Fluor 488 (diluted 1:300 blocking buffer, Invitrogen) for overnight at 4ºC. Spheroids were then washed with PBS 0.02% Triton™X-100 (PBT, Sigma-Aldrich) for 30 mins, PBS for 5 times and incubated over night at 4ºC. Nuclear counterstaining was achieved using DAPI (1:2000 in PBS, Sigma-Aldrich) for 2 hours. Phalloidin-Atto 550 diluted in PBS (0.2nM, 1:100, Sigma-Aldrich) were used for phalloidin filaments in the spheroids with overnight incubation. 96 well plates were imaged using the ImageXpress Micro Confocal high content imaging system. QuickID targeted acquisition was used on single field of view acquired at 4x magnification using DAPI channel. Spheroids were automatically selected based on size, shape and subsequently imaged at high magnification. Images were acquired in the DAPI, FITC, TRITC channels with Z-stack of 120µm (20 x 5 µm step size).

Immunocytochemistry for pLenti6.3IRF3mCMV-mCherry-P2A-Renilla luciferase and pcDNA3.1mCherry-P2A-Renilla luciferase transfected U251 cells

For testing pLenti6.3IRF3mCMV-mCherry-P2A-Renilla luciferase and pcDNA3.1mCherry-P2A-Renilla luciferase transfected U251 cells, cells were

transfected and cultivated with growth media on coverslips for 3 days. Cells were then washed with PBS and fixed using 4% paraformaldehyde (Sigma-Aldrich). cells were treated with PBS containing 0.02% Triton X-100 (PBT, Sigma-Aldrich) comprising 5% normal goat serum (Stratech Scientific Unit, Suffolk, UK) for 30 min. Cells were stained with mCherry antibody (1:200 in PBS, Stress marq, SPC-1268D, mouse, polyclonal) for 1.5h at room temperature. Followed by secondary goat anti-mouse conjugated with Alexa fluor ™ 488 (1:300 in PBS, Abacam) for 1h at room temperature. Pictures were taken by Axio imager A1 microscope system (Carl Zeiss, Jena, Germany).

Proliferation assay

For LPS treatment: cells were seeded in 6-well plates with at least 3 wells per plate after sphere culture and were exposed to LPS derived from *E. coli* or *S. minnesota* (1 µg/ml) or left untreated as described above. Cells were detached from one plate per condition every 24 hour for cell number determination. Cells were counted using haemocytometer under EVOS XL Core cell image system (Thermo Fisher scientific, Waltham, MA USA).

For U251 cells cultured in GrowDex®: cells were seeded and cultivated and treated as above in 0.2% GrowDex®. After 3 days, GrowDase™ were added to the well and incubated in 37ºC for overnight to digest the NFC. Recruited U251 cells were digested by Trypsin EDTA solution (T3924, Sigma-Aldrich) and counted using haemocytometer under EVOS XL Core cell image system (Thermo Fisher scientific, Waltham, MA USA) for cell number determination.

Cell viability assay (XTT assay)

For LPS treated U251 cells: U251 cells were seeded in at least seven 24-well plates with at least 9 wells per plate after sphere culture and were exposed to LPS derived from *E. coli* or *S. minnesota* (1 µg/ml) or left untreated as described above. Cell proliferation Kit II (Sigma-Aldrich, product No.11465015001) was prepared by mixing XTT labelling reagent and electron-coupling reagent at 50:1. The spectrophotometerical absorbance of the sample was measured at a excitation wavelength of 490nm and a reference wavelength of 650nm. Readout was carried out after 4h using Spectra Max 340PC plate reader (Molecular Devices, Wokingham, UK). XTT assay was performed for each plate every 24 hours after the seeding.

For curcumin (CUR) treated U251 cells: Cell viability assays were performed using the Cell Proliferation Kit II (Sigma-Aldrich) according to manufacturer's recommendations.

$5x10^3$ early passage (passage under 20) U251 cells per well were seeded in 96-well plates for 24 hours to reach 50% confluency before being treated with CUR. After reaching confluency in each well, the medium was changed to the cultivation medium with the CUR treatment, CUR+DMSO and CUR1 (Table. 6.1) in a concentration of 0μM to 10μM and 0μM to 200μM. XTT assay was performed after 48 hours of incubation using Cell proliferation Kit II (Sigma-Aldrich). Absorbance was measured using Spectra Max iD3 plate reader (Molecular Devices, Wokingham, United Kingdom) at an excitation wavelength of 490 nm and a reference wavelength of 650 nm.
For LPS treated U251 cells in GrowDex®, cells were seeded, cultivated and treated as described above. Viability assay was performed using Cell proliferation Kit II (11465015001, Sigma-Aldrich) (prepared according to the manufacturer's guidelines) after 7 days of cultivation. Readout was carried 4 hours after adding the XTT labelling mixture using SpectraMax® iD3 plate reader (Molecular Device).

Luciferase assay

For LPS and TNFα treatment, U251-NF-*κ*B-GFP-Luc cells were cultivated as spheres followed by 7 days of *E. coli* or *S. minnesota* ultrapure LPS (1 μg/ml) (InvivoGen), TNFα (10ng/ml), or left untreated as described above. After 7 days of cultivation, medium was removed and cells were rinsed with PBS. Cells were detached using Trypsin-EDTA solution (Sigma-Aldrich) and were collected using centrifugation. *Firefly* lucifase assay was performed using *firefly* Luciferase Assay System (Promega Crop., Southampton, United Kingdom). Cell lysis buffer (Promega Crop.) were used for preparing cell lysates. Luciferase Assay Reagent were added to cell lysates 10 seconds before the plate reading. *Firefly* luciferase signal was determined by detecting chemi-luminesce channel signal using Lucy 1 microplate reader (Anthos Labtec, Salzburg, Austria).
For curcumin (CUR) treatment, U251-NFκB-GFP-LUC cells were seeded in 24-well plates in normal cultivation medium prior to two hours starvation in FBS-free medium and subsequently exposed to 10μM of the respective curcumin formulation, 10 ng/mL tumour necrosis factor alpha (TNF-α) (PeproTech), TNF-α + curcumin, 1 μg/mL ultrapure *Escherichia coli* (*E. coli*)-derived lipopolysaccharide (LPS, *Escherichia coli* K12, InvivoGen), 1 μg/mL *E. coli* LPS +curcumin, 10ng/ml TNF-α + 2.5μM Bay-11-7082 (InvivoGen), and 1μg/mL *E. coli* LPS+ 2.5μM Bay-11-7082, respectively. Cells were lysed using Cell lysis buffer (PeproTech) after 48 hours of cultivation. Luciferase

Assay Reagent were added to cell lysates 10 seconds before the plate reading. Luciferase bioluminescence was assessed using *firefly* Luciferase Assay System (Promega Crop.) and a Spectra Max iD3 plate reader (Molecular Device) at chemi-luminesce channel.

Cell migration scratch assay

U251 cells were cultivated as described above. For LPS stimulation scratch assay, U251 cells were seeded at 30,000 cells per well in 24 well plates. After 24 hours of seeding, cells were starved with FCS free growth media for four hours before stimulation of LPS. After four hours of starvation, cells were treated with: 1 µg/ml *E. coli* LPS (InvivoGen), 1 µg/ml *S. minnesota* LPS (InvivoGen), 10 ng/ml TNFα (Peprotech) or left untreated (control). After 4 hours of stimulation, a line was scratched in the middle of each well using a P1000 pipette tip, while the treatment media has not been removed. Transfected U251 scratch assay: cells were co-transfected in two groups: vector 'pcDNA3.1 –IRF3' and GFP, vector 'prosa- IKK2-ca' and GFP separately by Amaxa Biosystems nucleofector™ II, using Amaxa™ cell line nucleofector™ kit V. For control cells, pmaxCloning™ Vector (GFP) was used. Cells were transfected 4 days before seeding, 30,000 cells were seeded per well in 24 well plates. After 24 hours of seeding, a line was scratched in the middle of each well using P1000 pipette tips. Images of cells were acquired 0 hour after scratch. Cells were then cultivated in 37ºC, 5%CO_2 incubator for 12 hours. Images of cells were acquired again. For images, 5 pictures per well (total 3 wells per condition each repeat) of cells in different area of wells were taken by EVOS fluorescence microscope (Thermo Fisher scientific, Waltham, MA USA) GFP channel. Cell wounds at both 0hr and 12hrs time point were determined using ImageJ. Mean closure rate was calculated for each well in the plate.

Soft agar assay

U251 cells passage 4 were cultivated as described above. Nobel agar (A5431, Sigma-Aldrich, Darmstadt, Germany) was used with growth media (FCS was added after gel powder was melted) to prepare 0.5% and 0.3% of agar. In a 6 well plate (Sarstedt, Nümbrecht, Germany), each well was filled by 1.5 ml 0.5% nobel agar gel mixed with 10,000 cells as bottom layer, and 1.5ml 0.3% nobel agar gel as top layer. Cells were mixed very well with gel before seeding. 1 ml of growth media was poured on the top to keep the gel moist. From the second day of seeding, the top growth media was

removed, and TLR4 ligands were added to the well in parallel with control growth media. The final concentration of the ligands are: 1 µg/ml *E. coli* LPS, 1 µg/ml *S. minnesota* LPS, 10 µg/ml TNFα. Treatment media was changed every 2 days and lasted for 21 days in total. Gels were stained by 0.1% crystal violet (0775, Sigma-Aldrich, Darmstadt, Germany) for 30 mins followed by several washes of water. 5 pictures per well of cells (3 wells per condition per repeat) at different area of wells and same horizontal level were taken by EVOS microscope (Thermo Fisher scientific, Waltham, MA USA). The number of colonies were counted in each picture and the diameter of the colonies were measured using ImageJ.

Electron Microscopy and analyse of GrowDex-T® - an anionic nanofibrillar cellulose (aNFC)

0.5% anionic form of NFC (aNFC) without cells was fixed, frozen and coated for electron microscope scanning. Samples were viewed in a FEI verios 460 scanning electron microscope at an accelerating voltage of 2.00 kV and a probe current of 50pA. Images were acquired in a secondary electron mode using either an Everhart-Thornley Detector (ETD). Image was analysed using Image J. Fibres and pores were picked randomly and measured.

Temozolomide killing curve assay

U251 cells were seeded as adherent cells and in 0.2% GrowDex® as 500 cells/µl in 96 well plates described as above. Temozolomide (TMZ) were dissolved in dimethyl sulfoxide (DMSO). 3 days after cell seeding, TMZ was added to cells following with 3 days of cell cultivation. Cells were incubated with various concentration of TMZ in 37ºC incubator, 5% CO_2. Cell viability was performed using Cell proliferation Kit II (Sigma-Aldrich) after 4 hours of cultivation with test reagent. 2D cells were cultured in parallel in 96 well plates for the same treatment. TMZ was added to 2D cells when they reached 90% confluency.

CUR microemultions' stability study using photo-spectroscopy

1 g of each CUR microemulsion was diluted by a factor of 5 using phosphate buffer (pH 7.5), and then 1 mL was transferred to three separate centrifuge tubes that contained CUR or eutectic mixtures. All the tubes with samples were placed onto a rotary mixer with fixed mixing speed for 24h and light protected using aluminium foil. Samples were then centrifuged for 5 min at 13,000 rpm (Sanyo MSE Micro Centaur, UK). 100 µl of the supernatant was taken and diluted to 25 mL with propan-2-ol.

Samples were placed under room temperature. Absorbance was determined at a wavelength of 429 nm using Varian Cary Bio (Agilent, USA). Degradation experiments were carried out via adding 30 µL of the CUR solution (methanol) to 3 mL of buffer (pH 7.5) in order to maintain the CUR concentration difference between initial concentrations of 4 mM to final concentration of 40 µM.

Cell transfection using Amexa Biosystems nucleofector™ II

U251 and U251-NF-κB-GFP-Luc reporter cells were cultivated as described above (section 2.1). Cells were detached from the flask using a Trypsin-EDTA solution and centrifuged at 300 *g* for 10 mins. The cell pellet was re-suspended in 100µl Nucleofector ™ Solution V in an aluminium cuvette. 1µg of vector was added to the cell suspension respectively along with or without 0.5 µg/µl pmaxGFP™ Vector. All cell transfections were performed by Amaxa Biosystems nucleofector™ II (Lonza), using Amexa™ cell line nucleofector™ kit V (VCA-1003, Lonza).

For immunocytochemistry, equal amount of U251 cells were transfected with constructed vectors pcDNA3.1-mcherry-P2A-RLuc and plenti6.3-IRF3Mcmv-mcherry-RLuc separately.

For *Renilla* luciferase assay and Western blot, equal amount of U251 cells were transfected separately to U251 cells with: 1) pcDNA5/FRT (control vector); 2) pcDNA3.1-mcherry-P2A-RLuc+pcDNA5/FRT; 3) pLenti6.3-IRF3mCMV-mCherry-RLuc + pcDNA5/FRT; 4) pLenti6.3-IRF3mCMV-mCherry-RLuc+pcDNA3.1-IRF3-FL (addgene); 5) untransfected.

For Dual luciferase assay, U251-NF-κB-GFP-Luc reporter cells were transfected with constructed vector pLenti6.3-IRF3mCMV-mcherry-P2A-RLuc along with 0.5 µg/µl pmaxGFP™ vector. Cells were cultivated for 3 days after transfection to perform Dual luciferase assay.

Treatment of cells for Dual Luciferase assay

Transfected U251-NF-κB-GFP-Luc reporter cells were cultivated as described above (Section 2.1) but with puromycin 5 µg/ml in 24 well plates. The cells were then seeded in 12 well plates at 40%-50% confluency for at least 1 day followed by 24 hours of cell starvation. Cells were starved with growth media but in absence of FCS for 24 hours before stimulation. Transfected U251-NF-κB-GFP-Luc cells were then stimulated by final concentration of TLR4 agonists TNFα (PeproTech EC Ltd., London, UK) in 0.1%

BSA (Sigma-Aldrich) in PBS 10 ng/µl, ultrapure *S. minnesota* LPS (in endotoxin free water, InvivoGen, Toulouse, France) 1 µg/µl, ultrapure *E. coli* LPS (in endotoxin free water, InvivoGen, Toulouse, France) 1 µg/µl, ultrapure LPS derived from *Pseudomonas aeruginosa* (in endotoxin free water, InvivoGen, Toulouse, France) 1µg/µl. Transfected U251-NF-κB-GFP-Luc cells were also stimulated with TLR3 agonist Human recombination Poly (I:C) (in endotoxin free water , InvivoGen, Toulouse, France) 10ng/µl for luciferase assay.

Western blot

U251-NF-κB-GFP-Luc reporter cells were transfected with five different combination of vectors with: 1) pcDNA5/FRT (control vector); 2) pcDNA3.1-mcherry-P2A-RLuc+pcDNA5/FRT; 3) pLenti6.3-IRF3mCMV-mCherry-RLuc + pcDNA5/FRT; 4) pLenti6.3-IRF3mCMV-mCherry-RLuc+pcDNA3.1-IRF3-FL (addgene); 5) untransfected. Cells were washed and lysed using Cell Lysis Buffer (Promega, UK) at a concentration of 1 x10^6 cells/ml. Cell lysates were shaken in a microcentrifuge tube for 30mins at 4ºC. Cell lysates were then centrifuged for 10mins at 13,000 rpm at 4ºC. Protein concentration were determined using BCA assay. Protein (20 µg) was run though the 10% polyacrylamide separating gel at 100V. 10% separating gel and 3% stacking gel for Western blot was prepared as below:

Separating gel	10ml	Stacking gel	5ml
1.5M Tris/HCl, ph8.8	2.5ml	0.5M Tris/HCl, pH6.8	1.25ml
10% SDS (Sigma-Aldrich)	100µl	10% SDS	50µl
40% Acrylamide	2.5ml	40% Acrylamide	0.375ml
10% APS (0.1g/ml) (Sigma-Aldrich)	100µl	10% APS (0.1g/ml)	100µl
DDW	4.8ml	DDW	3.2ml
Temed (T9281, Sigma Aldrich)	5µl	Temed	5µl

Table. 2.2. Separating gel and stacking gel for Western blot. Temed: N,N,N,N′-Tetramethyl ethylenediamine. APS: Ammonium Persulfate. SDS: Sodium dodecyl sulfate.

After gel electrophoresis, proteins were transferred to a low fluorescence methanol activated 0.2µm polyvinylidene difluoride (PVDF) membrane (22860, ThermoFisher

Scientific) using a Wet/Tank Transfer System (Bio-Rad) at 1 A for 1 h. The PVDF membranes were blocked in 1 %(w/v) Fish gelatin in PBS-Tween-20 [PBS-T, 0.1(v/v) (P7949 Sigma-Aldrich)] for 1 hour in room temperature.

Proteins were incubated with 1:1000 primary antibodies mouse-anti β-actin (monoclonal, Abacam) and rabbit anti-Renilla luciferase (ThermoFisher Scientific) at 4ºC on a shaker for overnight. Flurorescence secondary antibody donkey Alexa Fluor™ 800 conjugated anti-mouse IgG (Invitrogen) and donkey Alexa Fluor™ 680 conjugated anti-rabbit (Invitrogen) were used at 0.2 µg/ml in 1% (w/v) Fish gelatin in PBS-T. Proteins were visualised through fluorescence. 700nm and 800nm channel of *LI-COR* Odyssey® XF Imaging System (LI-COR Biosciences, Ltd, UK) were used.

Dual Luciferase assay

pLenti6.3-IRF3mCMV-mcherry-P2A-RLuc transfected U251-NF-κB-GFP-Luc cells were harvested. Plates were washed with PBS and cells were lysed using 100µl 1 x passive cell lysis buffer (Promega) per well. Cell lysates were kept on ice for luciferase signal determination. NF-κB-dependent *firefly* luciferase activity and IRF3-dependent *Renilla* luciferase activity were assessed using Dual-Luciferase ® Reporter Assay System (E1910, Promega Corporation, Madison, USA). Stop & Glo® reagent was prepared freshly before use. Stop & Glo® Substrate was mixed with Stop & Glo® Buffer 1:50 in a glass tube for *Renilla* luciferase signal measurements. Luciferase Assay Reagent II (LARII) were prepared by suspending the Luciferase Assay Substrate in the supplied Luciferase Assay Buffer II to measure the *Firefly* luciferase signal. The luciferase chemi-luminescence signals were measured using SpectraMax iD3 (Molecular Devices, California, United States). 20µl of cell lysate was used for each measurement. 50µl of LARII were added to the cell lysates 10 seconds before the reading started. Once the Firefly luciferase measurement finished, 50 µl of Stop & Glo® reagent were added to the cell lysates. Measurements of the *Renilla* lucifearase signal were carried out promptly after adding the Stop & Glo® reagent.

Statistical analysis

GraphPad Prism 5 (GraphPad, La Jolla, CA, USA) was used to perform statistical analysis. Student's t-test (two-tailed, 95% confidence interval) or one-way ANOVA with Bonferroni's Multiple Comparison Test (95% confidence interval) was applied as appropriate. In cell migration scratch assay, cell proliferation assay and soft agar

assay, the normalisation of the data was tested using the non-parametric statistical test. The data size was statistically significant, data from at least three independent experiments was collected. At least 3 repeats in each independent experiment were used. The data was presented as mean ± SEM. P value< 0.05 was considered as significant.

2.3. Molecular biology methods

Transformation of competent bacteria

Bacteria MACH1 [genotype: ΔrecA1398 endA1 tonA Φ80ΔlacM15 ΔlacX74 hsdR(rK-mK+)](Invitrogen, Thermo Fisher Scientific), GM2163 (genotype: *F - dam-13:Tn9(CamR) dcm-6*) (New England Biolabs, Herts, UK) or Stbl 3 (Invitrogen, genotype: F– mcrB mrr hsdS20 (rB–, mB–) recA13 supE44 ara-14 galK2 lacY1 proA2 rpsL20 (StrR) xyl-5 λ– leu mtl-1) were used as competent cells for transformation and DNA preparation. MACH1 cells were used as the default cells for cloning. This fast-growing type of *E. coli* is suitable for the propagation of cloned DNA for Plasmid Mini Prep [206]. GM2163 *E. coli* were used the prepare plasmid DNA when the restriction enzymes used for cloning required non-methylated DNA e.g., *Cla* I and *Xba* I. Stbl3 were used for the large-scale preparation of plasmid DNA as they have a reduced the propensity for homologous recombination of long terminal repeats, thus ensuring the integrity of the lentivirus plasmids [207]. For transformation, competent *E. coli* cells were taken out from -80ºC and thawed on ice for 30 mins before transformation. Microcentrifuge tubes were pre-chilled on ice. Fresh Super Optimal Broth (SOB)-agar plates were prepared and placed in an incubator at 37ºC. 50 µl of cell suspension were gently aliquoted to an Eppendorf tube using wide bore tips. 1µl of target vector (100 ng/µl) was added to the cell suspension. DNA and competent cells were mixed well by stirring. Cells were then rested on ice for another 30 mins. *E. coli* competent cells were then heat shocked at 42ºC for 30 seconds. Cells were then immediately put into an ice-water mixture for 5 mins. SOB (950 µl) with 20 mM glucose (SOC media) were added to the competent cells. Cells were then incubated in the shaker at 37ºC, 250 rpm for 1 h. Cells were then collected by centrifuging at 3500 *g* for 3 min. Under the flame, the lids of the tube of cells were opened and supernatant were discarded. Cells were seeded on to agar plates with ampicillin (100 µg/ml, Sigma Aldrich) and kept in

37ºC incubators overnight. *E. coli* were grown at 28ºC when cells were transformed with lentivirus vectors to reduce the chances of homologous recombination.

Plasmid Mini-Prep

Bacterial cells containing plasmids were grown on agar plates allowed to grow overnight. Under the flame, the bacteria from single colonies were collected using a pipette tip, and inoculated into 5ml SOB media to grow, under the condition of 250RPM, 37ºC or 28ºC overnight. QiAprep Spin Miniprep kit (Cat No. /ID: 27104, QIAGEN) (Spin column, DNA collection tube, buffers named P1, P2, N3 PB, and PE were included) was used to extract DNA from bacteria. To prepare for the Mini-Prep, cells were harvested by centrifugation at 4ºC for 15min at 3500 *g*, and suspended in 250µl resuspension buffer P1 which contained 0.1 mg/ml RNase A. After cells were fully suspended, 250µl lysis buffer P2 were added to the tube. The tube was inverted gently for 6 times for the buffer and cell lysates to mix. 350µl neutralization buffer N3 were then added to the tube followed by immediate gentle inverting of the tube. The tube was then centrifuged in room temperature for 10 mins at 13, 000 rpm. The suspension was then transferred to the QIAprep Spin Column and a 2 ml collection tube for DNA collection. DNA collection was done by centrifuging the column and the collection tube for 60 seconds at 13,000 rpm. PB buffer and PE buffer were used to wash the DNA in the column. DNA was collected in a fresh Eppendorf tube by adding 50µl of pure water followed with centrifugation at 13,000rpm under room temperature. NanoDrop™ 2000 Spectrophotometer (ThermoFisher Scientific) was used to determine the concentration of DNA.

Plasmid Maxi-Prep

Bacterial cells containing constructed reporter system DNA fragments were grown on agar plates allowed to grow overnight. Underthe flame, the Stbl 3 *E.coli* bacteria from single colonies were collected using a pipette tip, and inoculated into 200ml SOB media to grow, under 250RPM, 28ºC to avoid the formation of homologous recombination of the long terminal repeats. QIAGEN® Plasmid Maxi Kit (Cat No. /ID: 12165, QIAGEN) was used. Stbl3 bacteria were harvested by centrifugation at 6000 *g* for 15 min at 4ºC. The bacterial pellet was suspended in 20ml Buffer P1 until no cell clumps remain. Buffer P2 (10ml) was then added and gently mixed with the cell suspension for cell lysis, followed by 5 mins incubation in room temperature. After that, ice-chilled Buffer P3 (10ml) was added to the cell lysates. The tube was inverted 4-6

times and incubated on ice for 10 min. The cell protein- DNA mixture was centrifuged at ≥13,000 g for at least 30 min at 4ºC, and the supernatant was filtered through Buffer QBT equilibrated QIAGEN-tip. The QIAGEN-tip was the nwashed with 2 x 15 ml Buffer QC. DNA was eluted with 7.5ml Buffer QF and collected in a 50ml tube. Room-temperature isopropanol (0.7 volumes) was used to precipitate DNA from the eluted DNA. DNA pellet was collected using centrifugation at ≥15,000 *g* at 4 ºC for 1h. DNA was air-dried and re-dissolved in 0.5-1ml TE buffer (pH 8.0). NanoDrop™ 2000 Spectrophotometer (ThermoFisher Scientific) was used to determine the concentration of DNA.

Nucleic Acid Electrophoresis

1% or 2% agarose gels were prepared using agarose (A2929, Sigma Aldrich) and Tris-Acetate-EDTA (TAE) buffer, including SYBR Safe DNA Gel Stain (1:25,000, ThermoFisher Scientific). 2µl of DNA samples were mixed with 1µl DNA Gel Loading dye (R0611 ThermoFisher Scientific) and DDW. The sample mixture was then loaded into the wells of the agarose gel. 1 kb DNA ladder (N3232L, New England Biolabs® Inc.) and 100 bp DNA ladder (N3231L, New England Biolabs® Inc.) were used to determine the band size. Electrophoresis chamber Mini-Sub Cell GT Horizontal Electrophoresis System (Bio-Rad) and PowerPac HC 250V-3A-300W Electrophoresis Power Supply (Bio-Rad) were used.

Purification of DNA from agarose gels

DNA was purified from agarose gels using a QIAquick Gel Extraction Kit (Cat No. /ID: 28704, QIAGEN). To prepare the purification, a DNA band was excised from the agarose gel and weighed on an analytical balance. For 1% agarose gel, 3 volumes of Buffer QG were added to 1 volume of gel (1mg to 1µl). For 2% agarose gel, this volume needed to be doubled. Buffer QG and the excised gel were incubated at 50ºC for 10 mins or until the gel was completely dissolved. After that, 1 volume of isopropanol was added to the sample mix to help increase the yield of <500 bp or >4kb DNA fragments. The mixture was then transferred to QIAquick column, and centrifuged for 1 min. The flow-through was discarded. 0.75ml of Buffer PE were added to the column to wash the DNA by 1min centrifugation. The flow-through was discarded. An additional 1 min of the centrifugation was done after this to remove any remaining ethanol. DNA was eluted by adding 30-50µl of Buffer EB or H_2O to the centre of the column, followed with 1 min of standing and 1 min centrifugation.

PCR

DNA was amplified using Real-Time PCR System Bio-RAD PTC-1146 MJ mini (Cat No. /ID: 27104), with the primer sequence as below. All primers were provided by Sigma-Aldrich Co. LLc.

DNA sequence	primers	sequence (5'-3')
IRF3REmCMV promoter	ClaIIRF3REmCMV promfor	TATATAATCGATCTTCTGAGTCTTAGAGAAAAAGGAACTGGAGCCCCAGACCGCGCCCCATTGACGCAAATGG
	BGHrev	TAGAAGGCACAGTCGAGG
	(-20) M13for	GTAAAACGACGGCCAGT
	M13rev	CAGGAAACAGCTATGAC
mCherry	mCherryBamHIfor	TATATAGGATCCACCATGGTGAGCAAGGGCGAGGAG
	mCherryEcoRIrev	TATATAGAATTCCTTGTACAGCTCGTC
	CMVfor	CGCAAATGGGCGGTAGGCGTG
	mCherrynostopEcoRIrev	TATATAGAATTCCTTGTACAGCTCGTC
P2A template	EcoRI-P2Along for	TATATAGAATTCGGAAGCGGAGCTACTAACTTCAGCCTGCTGAAGCAGGCTGGAGACGTGGAGG
	P2Along-NheI-rev	TATATAGCTAGCCCAGGTCCAGGGTTCTCCTAACGTCTCCAGCCTGCTTCAGCAGGC
P2A	EcoRIP2A-shortfor	TATATAGAATTCGGAAGCGG
	P2Ashort-NheI-rev	TATATAGCTAGCCCAGGTCC

Table 2.3. Primers for the construction of 'Quad Fire' reporter system. The forward and reverse primers of the IRF3mCMV promoter, mCherry, P2A template and P2A.

The PCR cycle is designed as below:

98 ºC	3 min
98 ºC	30 s each for 25 cycles
55 ºC	
72 ºC	
72 ºC	10 min
10 ºC	∞ on hold

Table 2.4. General PCR cycle used systems used for generating 'Quad Fire' reporter system.

Two PCR reaction systems were composed as bellow:

10x buffer for KOD hot start polymerase	5µl
10mM dNTP (N0447S, New England Biolabs® Inc.)	1µl
Forward primer(1µmol/µl)	2µl
Reverse primer (1µmol/µl)	2µl
Template	10 ng
KOD DNA polymerase (Sigma-Aldrich)	1µl
50mM $MgSO_4$	2.5µl
Distilled and de-ionised water (DDW)	35.5µl
Total volume	50ul
10x Taq Buffer (For colony PCR)	2µl
10mM dNTP (N0447S, New England Biolabs® Inc.)	0.4µl
Forward primer(1µM)	1µl
Reverse primer (1µM)	1µl
Template	10ng
Taq polymerase	0.05µl
Distilled and de-ionised water (DDW)	13.55
Total volume	20µl

Table 2.5. General PCR reaction systems used for generating 'Quad Fire' reporter system.

DNA ligation.

DNA ligation was performed as indicated below (Table 5.4) in an Eppendorf tube and allowing 4 hours to overnight incubation at 14ºC. DNA ligation was run by MJ mini™ Gradient Thermal Cycler (#PTC-1148, Bio- RAD), with the system designed as:

	Vector only (as control)	Vector with insert
T4 DNA 10 x ligase buffer New England Biolabs® Inc.)	0.5µl	0.5µl
vector	0.5µl	0.5µl
DNA insert	-	2µl
T4 DNA Ligase (M0202M, New England Biolabs® Inc.)	0.25µl	0.25µl
DDW	3.75µl	1.75µl
Total	5µl	5µl

Table 2.6. General DNA ligation system used for generating 'Quad Fire' reporter system.

DNA restriction Digest

Restriction digest was done by mixing the above and incubating the mixture for 1-2 hours in a 37ºC incubator using the following reagents. The restriction digest buffers were NEBuffer (New England Biolabs® Inc.). All the restriction enzymes were provided by New England Biolabs® Inc.

10x Buffer (Buffer type varies)	2 µl
10x (Bovine Serum Albumin) BSA(1mg/ml)	2 µl
Restriction enzyme total volume	0.5 µl
DNA	4.5 µl
DDW	11 µl
Total	20 µl

Table 2.7. General restriction digest system systems used for generating 'Quad Fire' reporter system.

Chapter 3. NF-kB biased signalling via TLR4 increases stemness of glioma cancer stem cells

3.1. Introduction

TLR signalling has been suggested to be associated with cancer development and progression in many *in vitro* and *in vivo* studies [192, 208-212]. TLR activation is well known to cause the production of biological factors that drive inflammatory responses as well as activate the adaptive immune system [208]. Still, the relationship between TLRs and cancer is highly controversial, with contradictory datasets in the literature. On the one hand, TLRs inhibit cancer progression in some models [209-211]. On the other hand, they also have been linked to cancer progression [192, 212]. Therefore, a deeper understanding of the relationship between the TLRs, inflammation as well as cancer development and progression is still an important open question in cancer research.

Pathways downstream of TLR4 include the MyD88-independent IRF3 pathway, and the MyD88-dependent NF-κB pathway. The induction of transcription of numerous pro-inflammatory genes is one of the key events after NF-κB activation [213]. In mouse macrophages and human tumour cells, shifts to pro-inflammatory phenotypes were reported [214, 215]. Studies suggested that the pro-inflammatory responses are able to promote the tumour cell survival [216]. In this chapter, I hypothesised that MyD88-dependent signalling pathway is a risk factor in cancer progression. Specifically, a potential link between the two TLR4 downstream signalling pathways and glioma cancer stem cell (CSC) migration, proliferation, differentiation, and stemness would be studied. In a previous study from our group, it was demonstrated that *E. coli* LPS is a NF-κB-biased TLR4 ligand [79]. Moreover, this study showed that *S. minnesota* LPS results in an IRF3-biased, anti-inflammatory response. In this chapter, U251 cells were used and stimulated with the above ligands to study CSC behaviour after activation of TLR4. New evidence will be presented linking TLR4 signalling with the development of glioblastoma CSC.

3.1.1 Cancer cell proliferation

Activation of TLR4 has been shown to affect cancer cell proliferation. Tarassishin and Lee suggested the transcription factor IRF3, which is activated by TLR4/MyD88 independent pathway, can inhibit glioma proliferation [217]. LPSs, as one type of TLR4 ligand, are used widely in TLR4 research. It has been shown that activation of TLR4 with LPS (chemotype of which was not specified) results in increased proliferation of melanoma cells [218]. Moreover, TLR4/MyD88-dependent signalling was reported to increase proliferation of breast cancer cells [219]. In contrast, TLR4 mediated activation of NF-κB has been shown to inhibit the proliferation of prostate cancer cells [219, 220]. In the previous research from our lab, biased signalling via TLR4 was reported (see in introduction) [79]. Thus, the chemotype of LPS is crucial to determine the impact of TLR4 activation on cell proliferation.

In this chapter tumourispheres were generated, and NF-κB and IRF3-biased TLR4 ligands were used to stimulate the cells. Proliferation assays were used to directly evaluate the proliferation levels of glioblastoma cells under the stimulation of TLR4 ligands.

3.1.2 Cancer cell migration

Cancer cell migration has strong links to tumour metastasis. During the development of cancers, cancer cells may become migratory and obtain the ability to detach from the primary tumour. The cancer cells can then enter the bloodstream or lymphatic vessels and seed in distant organs to generate secondary tumours [221]. For this progress, the migration ability of tumour cells is the key determining factor. Su et al. suggested that the CD133/ β-catenin is promoting polarized cell migration [222], indicating that the CSCs may play important role in tumour metastasis.

Cell migration can be impacted by many factors including cell-cell adhesion, cell-cell communication, the epithelial-mesenchymal transition (EMT) etc [221]. In addition, chemokines, adhesion receptors, and other related stimuli in the microenvironment of tumours are also important [223]. The EMT process in cancer is regulated by many different factors and signalling pathways including TNF-a, Wnt, Notch, and several growth factors. EMT includes variety changes to cells, for example, the loss of apical-basal polarity, downregulation of cell–cell adhesion, adoption of a more fibroblast-like appearance, and, in some cases, acquisition of stem- or progenitor-cell phenotypes

and gene expression, etc [58]. During the development of cancer, those changed properties would enhance the ability of a cell to migrate, invade other tissues and initiate tumours at distant sites[224]. As a result, cancer cells detach from the primary tumour and migrate using different strategies. Migration can occur either as individual cells, using mesenchymal type movement or as cell sheets, or clusters using collective migration [221].

Previous studies reported that TLR4 can impact the migration of human cancer cells. Wang et al. showed that inhibiting the TLR4 pathway by down-regulating NF-κB could suppress the breast cancer migration [218, 220]. Another study carried out by Yang et al. suggested that LPS activates the MyD88-dependent pathway of TLR4. Although they did not specify the chemotype of LPS, this activation subsequently led to the upregulation of matrix metalloproteinase (MMP)-2, MMP-9, as well as IL-6 and IL-10 [225]. As result, MMP-2 and MMP-9 promoted the secretion of VEGF and pro-inflammatory cytokines leading to increased levels of inflammation within the tumour microenvironment. As a result, antitumor responses were inhibited, and the migration and invasion of tumour cells were promoted [226, 227]. To support this, Zkaria et al. suggested that inhibiting NF-κB could prevent the self-renewal and migration of lung CSCs [228]. In contrast, Takazawa et al. reported that LPS of undisclosed chemotype and its stimulation of TLR4 promotes the migration of melanoma cells via NF-κB pathway. In a glioblastoma invasion study, Pattwell and Holland indicated that IRF3 is a transcriptional suppressor for pro-invasive extracellular matrix and might have a function of suppressing the cancer cell migratory potential [183].

3.1.3 Cancer cell differentiation

The differentiation level of cancer cells in solid tumours can indicate how aggressive a tumour is. Therefore, it is a central factor in histopathological diagnosis in clinic. Also, the differentiation level of the tumour is directly linked to its cell behaviour. In general, more differentiated tumours are less aggressive in comparison to those less differentiated [229]. Neuroblastoma is an aggressive heterogenous solid tumour, and the differentiation level of the tumour may vary in clinics. In neuroblastoma, the differentiation stages vary and are classified into three levels: 1). The benign tumour contains only ganglion-like cells and stroma cells; 2). The tumour contains neuroblast-like immature cells (less differentiated) with small nuclei and less cytoplasm mixed with a proportion of more differentiated tumour cells with larger nuclei and more

cytoplasm content; 3) The tumour contains neuroblastoma-like cells but less tumour cells that show ganglionic differentiation [229].

The rapid and recent development of stem cell and cancer stem cell research has galvanised the study of cancer differentiation processes, providing insights into the cellular and molecular biological studies. The mechanisms of differentiation and dedifferentiation of tumour cells were studied. In neuroblastoma, retinoic acid inhibited the differentiation of cells *in vitro*, and at the same time, many neuroblastoma cell lines also retained the capacity of differentiation [230]. Researchers found that when inducing tumour cell differentiation, ubiquitination and proteolysis of Cyclin D1 could be observed. In other words, when cells differentiate and do not proliferate, the aggressiveness of tumour decreases [231]. These findings suggested that by inducing a differentiation, aggressive neuroblastomas might become less aggressive. Moreover, Cyclin D1 is an important transcriptional target of NF-κB, Guttridge et al. suggested NF-κB is involved in the early phase of cell passage and is a suppressor of cell differentiation [232]. However, IRF3 expression, is reported to be positively associated with cell differentiation [233]. Also, IRF3 has been suggested to be a depressor of pro-invasive factors, by targeting the ECM components related genes, it significantly reduces the invasive capacity of glioblastoma cells [234]. As both NF-κB and IRF3 are transcription factors that can be activated by TLR4 stimulation, it is very important investigate the impact of TLR4 signalling on cancer cell differentiation, as it could provide a novel target for cancer therapy.

3.1.4 Stemness

Stemness is a term used to describe the ability of stem cells to self-renew and to give rise to differentiated cell types. In adult tissue, stem cells/progenitor cells of self-renew, and contribute to regeneration processes via differentiation [235]. In cancer, a small population of CSCs retain their stemness [236]. CSCs have been shown to interact with their environment and to maintain a balance between a quiescent and proliferative state. From clinical point of view, CSCs contribute to tumour heterogeneity and cancer plasticity that leads to tumour relapse, and have high resistance to the chemo- and radiotherapy [87].

CSCs express defined set of markers that are not present in non-cancer stem cells or somatic cells in this respective combination. Hence, those markers are considered to

be related to the stemness characteristic of CSCs [237]. CD133 has been considered as a neural stem cell marker and as a marker of solid tumours CSC [237]. However, it was first identified as CSC marker by Singh et al. in 2003 in glioblastoma [24]. Singh identified $CD133^+$ cells to be those carcinogenic cells as only $CD133^+$ formed new tumours when transplanted into the brains of immune-compromised mice, [5]. In this chapter, I used nestin as another marker for glioblastoma CSC. Nestin was identified as a neuronal stem cell protein [238]. In cancer, co-expression of nestin with additional CSC markers such as CD133 was identified as a CSC characteristic. Importantly this was further confirmed using *in vitro* tumourigenicity assays [31].

3.1.5 Tumourigenicity

In cancer biology, tumourigenicity describes the ability of cells to form tumours. Highly tumourigenic cells tend to have high level of reactive oxygen species (ROS), high genetic instability (DNA damage), enhanced cell proliferation, high levels of cellular growth and survival, as well as low levels of apoptosis [239]. Genetic instability has significant clinical impact as it contributes to the resistance to chemotherapy and increased risk of relapse [240].

One of the most important molecular regulators of processes contributing to tumourigenicity is the pro-inflammatory transcription factor NF-κB. It is not only a central coordinator of immune responses, but also an important factor in cancer development and progression [241, 242]. NF-κB has specific involvement in oncogenesis, including regulation of proliferation, cell survival, cell cycle and resistance to therapies [232, 243]. Inoue et al. suggested that TLR-mediated-TRAF6-NF-kB pathway plays major roles in NF-κB activation in malignant and premalignant tumour cells [244]. This induces the production of inflammatory cytokines such as TNFα, IL-1 and IL-6, which constitute the inflammatory cancer microenvironment and play a key role in promoting the proliferation and survival of genetically altered cancer cells. The inflammatory microenvironment can also lead to additional genetic changes associated with tumourigenicity and interferes with the expression of anti-tumour genes, such as the IκB gene [244].

Furthermore, pro-survival phosphoinositide-3-kinase (PI3K)/Akt can up-regulate NF-κB by inducing phosphorylation of and subsequent degradation of the NF-κB inhibitor, IκB, which can increase of frequency of metastasis by inducing a feed forward loop

[245]. In this process, p65 phosphorylation and activation in response to TNFα and IL-1 are essential [246]. The up-regulation of NF-κB in microenvironment of cancer cells facilitates mitochondrial dysfunction and increases the mitochondrial ROS level, which leads to the DNA damage of the premalignant cells. This up-regulation also feed forward and activate NF-κB [247], which induces expression of anti-apoptotic genes and induce tumourigenicity. The increased level of ROS can also cause the activation of EGF receptor and protein kinase D (PKD)1 signalling [248], while the latter has been shown to promote cell survival through activating ERK1/2 and down-regulating the pro-apoptotic c-Jun N terminal protein kinase (JNK) pathway to enhance cancer cell survival [249, 250]. This activation of ERK1/2 signalling pathway has been reported to be the result of growth factor stimulation and NF-κB activation in many cancer types, including breast, leukaemia, ovarian cancer and melanoma [251-253]. Results of ERK1/2 signalling activation include increased and cell survival [252, 254]. In addition, PKD signalling pathways have been suggested to play important role in glioma growth. In particular, PKD2 has been found in $CD133^+$ glioma tumour initiating cells and was found to be able to mediate the activation of NF-κB [255, 256]. PKD2 has a function of inducing cyclin D1 expression in glioma cells and promote cell cycle G1/S progression and increase cell proliferation and further promote tumourigenicity of glioma [255].

In contrast, IRF3 was reported to be a negative regulator of the Wnt/β-catenin pathway and to prevent colorectal tumourigenesis [182]. However, the role of IRF3 in anti-tumourigenesis in GBM still needs further study.

In this chapter, soft agar colony formation assay has been used to assess tumourigenesis *in vitro*. This technique mimics the 3D cellular environment to that is seen in vivo closer than conventional 2D monolayer cultivation or 3D spheroid cultivation [257]. In soft agar, cells that considered to be carcinogenic can grow irrespective of their surroundings, proliferate and form colonies [258]. In contrast, non-tumourigenic cells tend to undergo apoptotic due to contact inhibition [259].

3.2. Results

More CSCs could be found in tumourispheres compared to cells cultured in monolayers.

CD133, a surface protein, was used as a marker of CSC in this project [5]. U251 cells were used and cultured in serum-free media in presence of FGF-2 & EGF. Tumourispheres were formed *in vitro* as early as 24 h after plating of the cells in serum-free medium (Fig. 3.1B). MACS was used to assess the percentage of CSCs. I found that the percentage of CD133 positive cells in spheroid U251 cells is 8.07 ±1.48 % after 14 days of spheroid formation (Fig. 3.1C), while in adherent cells, the percentage of CSCs was 4.88 ± 0.37% (Fig. 3.1C).

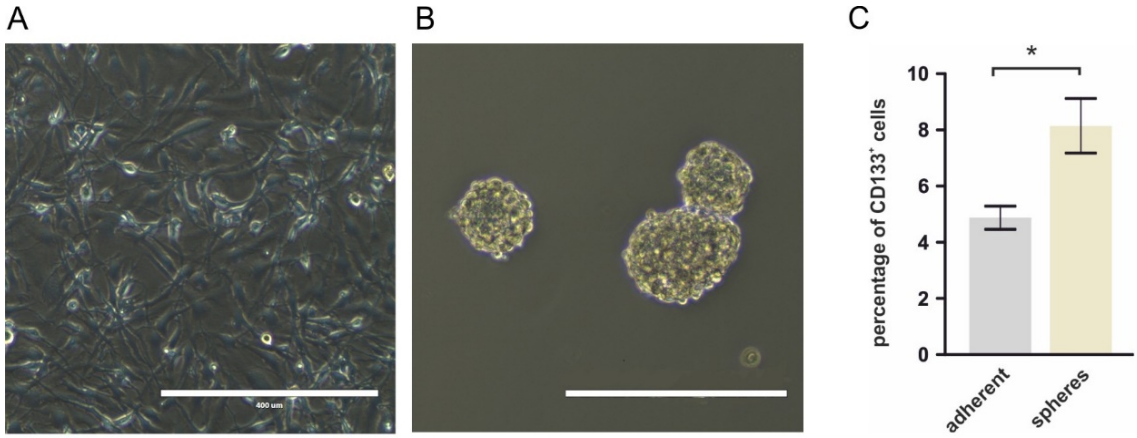

Figure 3.1. More CSCs could be found in U251 tumourispheres in comparison to adherent U251 cells. A. Adherent U251 cells (scale bar=400μm). B. U251 tumourispheres, (scale bar=400μm). **C.** Percentage of $CD133^{+}$ cells in U251 in adherent and spheroid culture. Data are presented as mean± SEM from 5 biological repeats of experiments, analysed using student t-test. * $p<0.05$.

Immunocytochemistry was used to determine expression of the stem cells marker nestin in U251 cells. Fig. 3.2 shows U251 pre-cultivated as tumourispheres and cultured as adherent cultures. Immunocytochemistry analysis revealed that the cells are heterogeneous with positive and negative cells within the cell population.

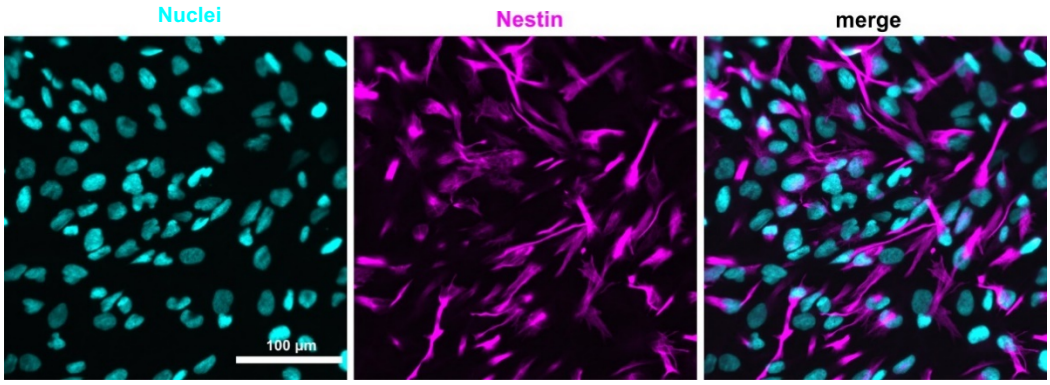

Figure 3.2. Tumourispheres pre-cultivated U251 cells show characteristic of CSC-like cells under adherent conditions. Adherent U251 cells express nestin. Scale bar: 100 µm. (

E. coli LPS promote tumourigenicity while *S. minnesota* LPS decreases it.

A soft agar assay was used to test the tumorigenicity of U251 cells after exposure to different TLR4 ligands.

U251 cells were seeded into soft noble agar and treated with TLR4 ligands *E. coli* LPS, and *S. minnesota* LPS. TNFα was used to as a positive control for NF-κB activation, and untreated cells were also seeded as negative control. After 21 days of cultivation, spheroids were stained by crystal violet and images acquired (Fig. 3.3 A-D).

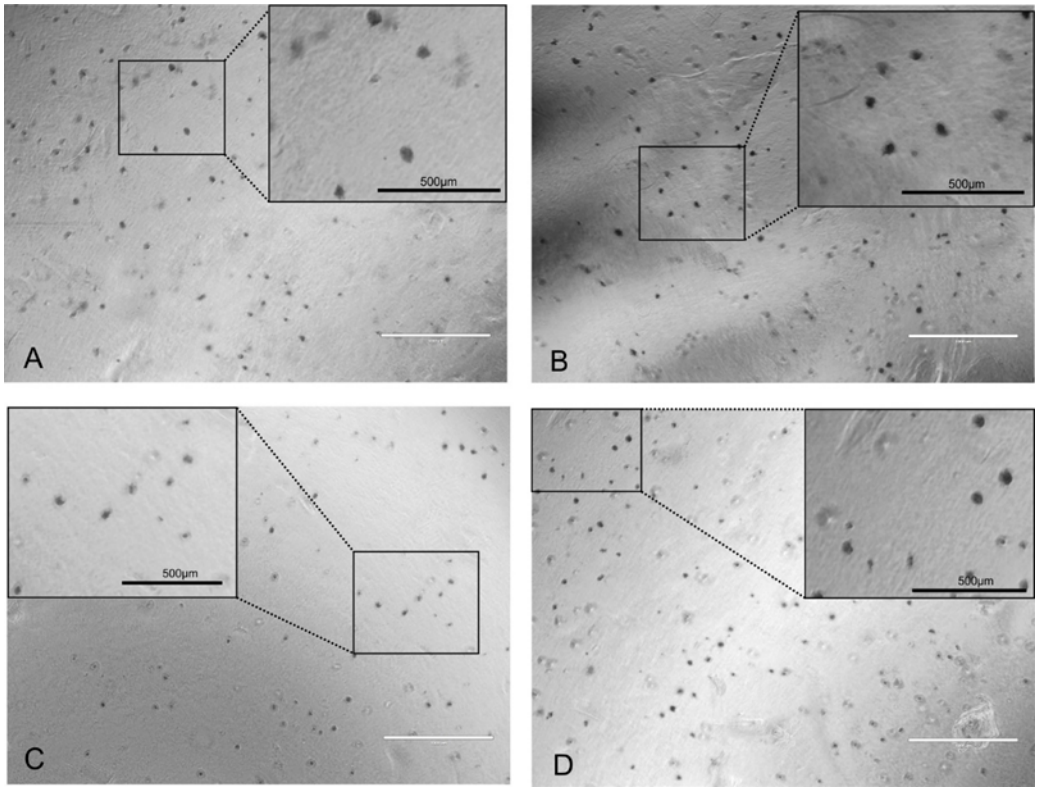

Figure 3.3. AVOS pictures of 21 Days soft agar assay of U251 cells treated with *E. coli* LPS, *S. minnesota* LPS and TNFα. Scare bar: 1000μm. Zoomed in scare bar: 500μm. **A.** U251 cells treated with growth media. **B.** U251 cells treated with *E.coli* LPS. **C.** U251 cells treated with *S. minnesota* LPS. **D.** U251 cells treated with TNFα.

U251 cell spheres treated with *E.coli* LPS and TNFα (Fig. 3.3B & 3.3D) showed with higher numbers when comparing to untreated U251 cells and *S. minnesota* LPS treated cells (Fig. 3.3A & 3.3C). To analyse, colony number and average diameter were determined. Results suggested that *E.coli* LPS and TNFα treated U251 cells formed more colonies, but *S. minnesota* LPS treated U251 cells did not show significant differences to untreated cells. The diameters of the spheres suggested that tumourispheres formed by *E.coli* LPS treated U251 cells had largest diameter comparing to other three groups. *S. minnesota* LPS treated U251 cells tumourispheres were significantly smaller than other groups (Fig 3.4 A&B).

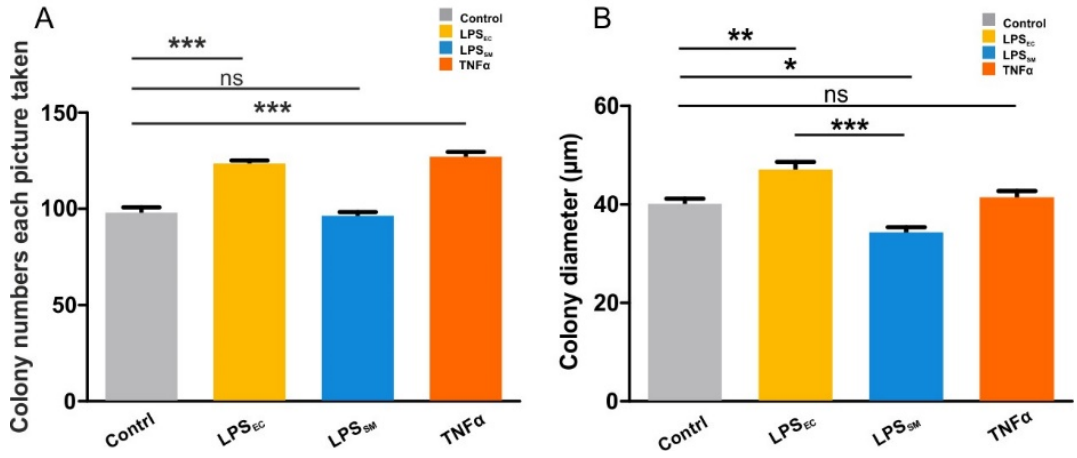

Figure 3.4. Effect of *E. coli* LPS in U251 increases the tumourigenicity of U251 cells, while *S. minnesota* LPS reduces size but not numbers of U251 tumourispheres. **A.** Colony numbers were counted in each condition of treatment. *E. coli* LPS and TNFα treated U251 cells generated more tumourispheres than the other two groups. **B.** Diameter of colonies were measured in each condition of treatment. *E. coli* LPS treated cells had significantly biggest spheres, while S. minnesota LPS treated cells had significantly smaller spheres than all other experimental groups. Mean ± SEM from 5 biological repeats experiments were analysed using ANOVA with Bonferroni correction (CI 95%); *p<0.05; **p<0.01; ***p<0.001.

LPS does not change viability and proliferation of whole population of U251 cells.

Tumourispheres pre-cultivated U251 cells were seeded in adherent plates and stimulated with TNFα and TLR4 ligands *E. coli* and *S. minnesota* LPS. There was no significant difference of cell viability or cell number among all the treatment groups (Fig. 3.5).

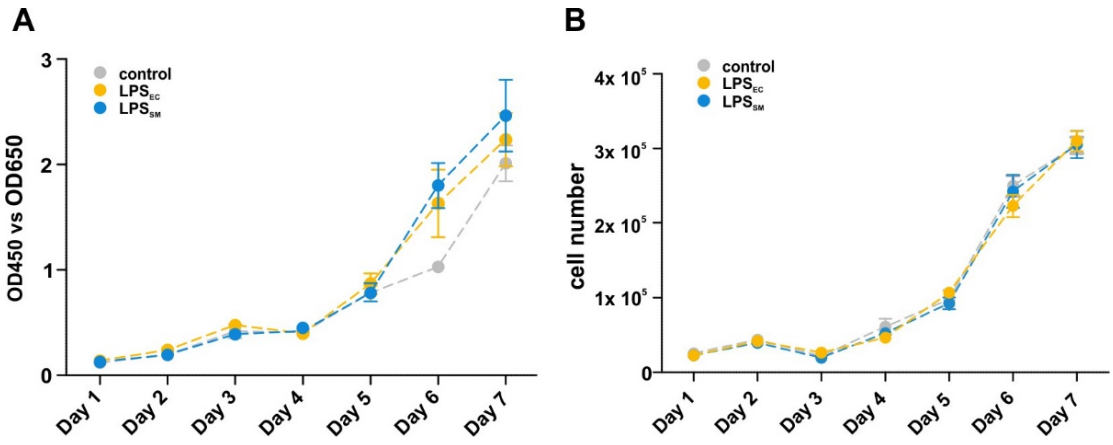

Figure 3.5. Both viability and cell number were not affected by treatment of U251 cell with *E. coli* LPS or *S. minnesota* LPS compared to untreated cells. A. XTT-determined cell viability in 7 days. **B.** Cell number was monitored over 7 days. Mean ± SEM from a minimum of 3 different experiments were analysed using ANOVA with Bonferroni correction (CI 95%) *p<0.05.

Stemness of U251 cells is promoted by the NF-κB biased TLR4 ligand *E. coli* LPS.

To study the impact of TLR4 ligands on the stemness of the CSC-enriched population of U251 cells, two TLR4 ligands, *E. coli* and *S. minnesota* LPS were used. U251 cells were cultivated as tumourispheres, then separated and seeded into adherent flask with either in presence of *E. coli* LPS, *S. minnesota* LPS or remained untreated for 7 days (Fig. 3.6). The expression level of CSC markers CD133 and nestin were analysed at mRNA and protein level using qPCR, ICC, and MACS.

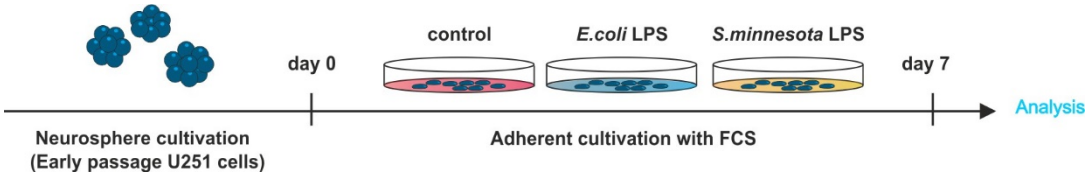

Figure 3.6. The process of U251 cultivation. U251 cells were cultivated into spheres, then adherently, followed with different analyses.

CD133 mRNA expression is promoted in the presence of *E. coli* LPS.

qPCR analysis results indicated that *E. coli* LPS increased the expression of CD133 at mRNA level about 4-fold compared to the control group. Exposure of the cells to *S. minnesota* LPS did not result in significant differences comparing to the control group (Fig.3.7). In parallel, nestin was also tested using qPCR. *E. coli* LPS had a trend of promoting nestin mRNA transcription, but there was no significant difference between the three conditions.

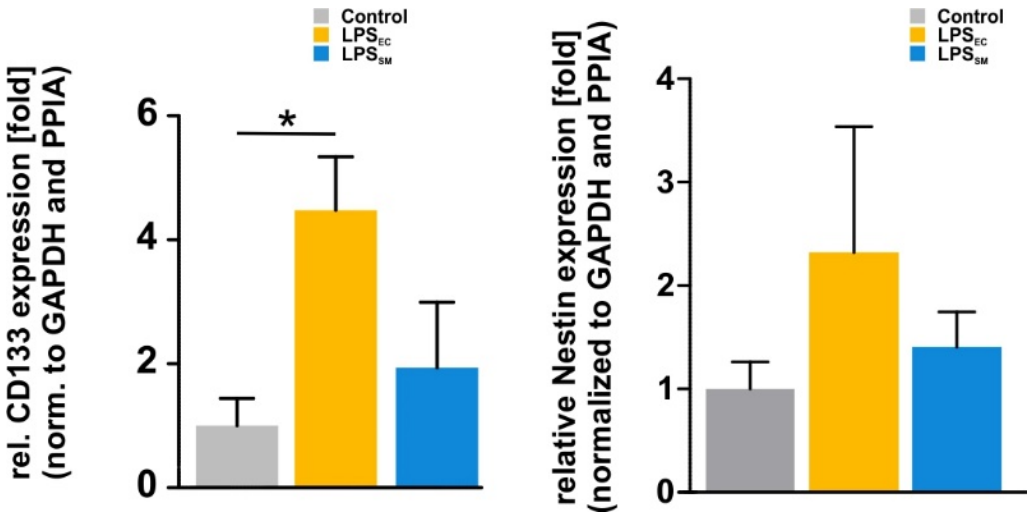

Figure 3.7. CD133 was increase in cells cultivated with *E. coli* LPS at mRNA level. No significant difference of nestin mRNA between all conditions. A. CD133 mRNA relative to GAPDH and PPIA was significantly elevated in cells cultivated with *E. coli* LPS compared to untreated cells or cells stimulated with *S. minnesota* LPS. **B.** No significant difference of nestin mRNA could be found among three groups. Mean ± SEM from 3 biological repeats were analysed using ANOVA with Bonferroni correction. *p<0.05.

CD133 expression is promoted in the presence of *E. coli* LPS at protein level.

U251 cells treated with *E. coli* and *S. minnesota* LPS and control group were stained with CD133 antibody and counterstained with DAPI (Fig. 3.8A). Images were taken with same exposure time for each channel. Image analysis showed highest expression of CD133 in *E. coli* LPS treated U251 cells. (Fig. 3.8A-B). Results indicated significantly higher levels of CD133 in *E. coli*-treated cells compared to both untreated

and *S. minnesota* LPS treated cells, suggesting that the expression of CD133 was promoted by *E. coli* LPS at protein level.

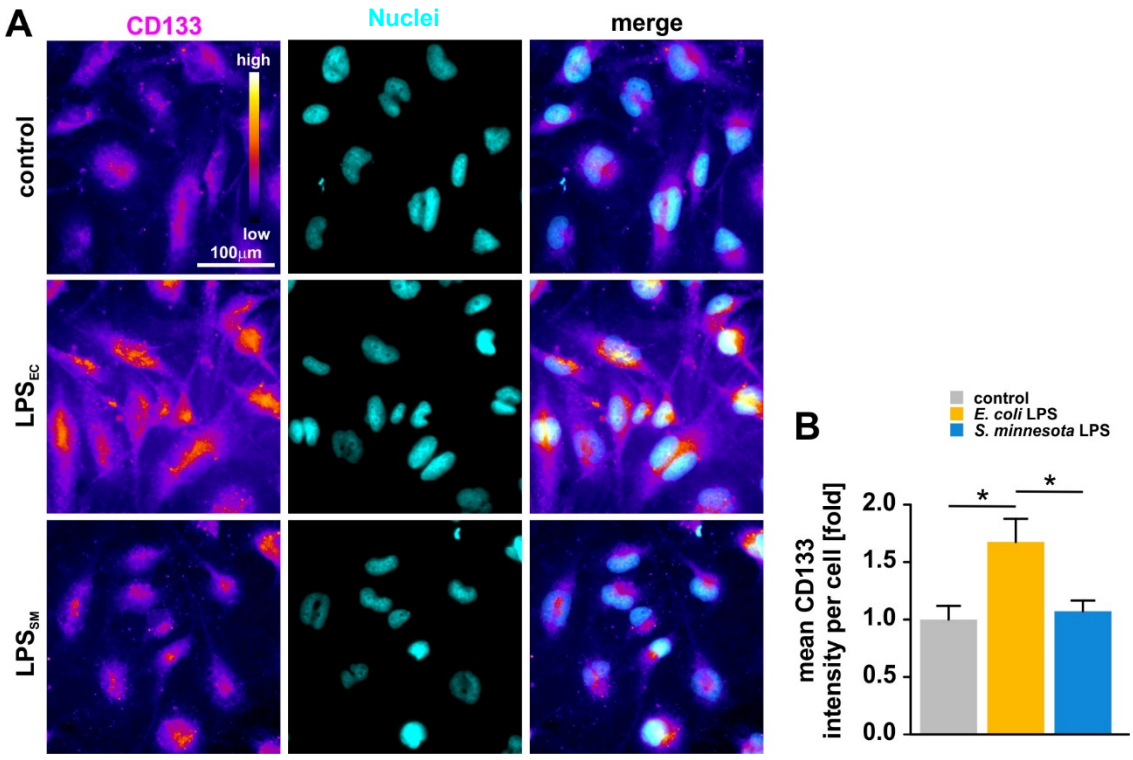

Figure 3.8. *E. coli* LPS increases expression of CD133 at protein level. A. ICC pictures of U251 cells treated with *E. coli* and *S. minnesota* LPS, cells were stained with CD133 antibody and DAPI. Scale bar 100 µm. **B.** Pixel intensity of CD133 in each cell of the images. Data are presented as mean ± SEM from 3 different experiments, analysed using ANOVA with Bonferroni correction (CI 95%) *p<0.05.

E. coli LPS increases the percentage of CD133$^+$ U251 cells

MACS was performed after pre-cultivating cells as indicated in Fig. 3.6 and CD133$^+$ cells were counted MACS of the cells for CD133 with subsequent counting revealed a significantly higher percentage of CD133$^+$ cells in the population cultivated with *E. coli* LPS compared to both *S. minnesota* LPS treated cells and untreated control cells (Fig. 3.9).

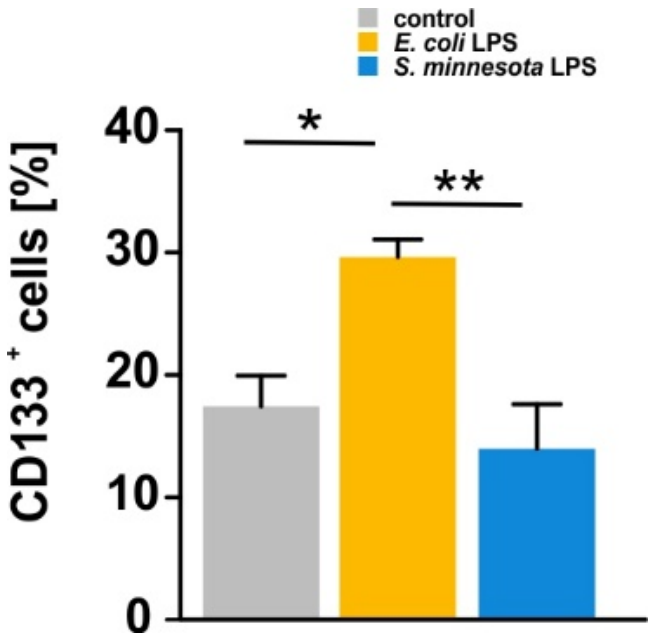

Figure 3.9. Percentage of CD133 + cells treated with *E. coli* LPS U251 is significantly higher than *S. minnesota* LPS treated U251 and control cells. Data are presented as mean ± SEM from 3 different experiments, analysed using ANOVA with Bonferroni correction (CI 95%), *p<0.05, **p<0.01.

E. coli LPS showed no significant impact but only a trend on promoting de-differentiation of CD133⁻ cells to CD133⁺ CSCs.

U251 cells after cultivated as tumourispheres followed with MACS. Sorted CD133 - cells were cultivated as adherent cultures. TLR4 ligands *E. coli* LPS and *S. minnesota* LPS were used to treat U251 cells. Subsequently, MACS was performed to determine the CD133 + cell population (Fig. 3.10A). Result of the second MACS suggested that *E.coli* LPS treated U251 cells had a trend to result in a higher percentage of CD133 + cells than the other two groups. However, the data is not significant when analysed with ANOVA (Fig. 3.10B).

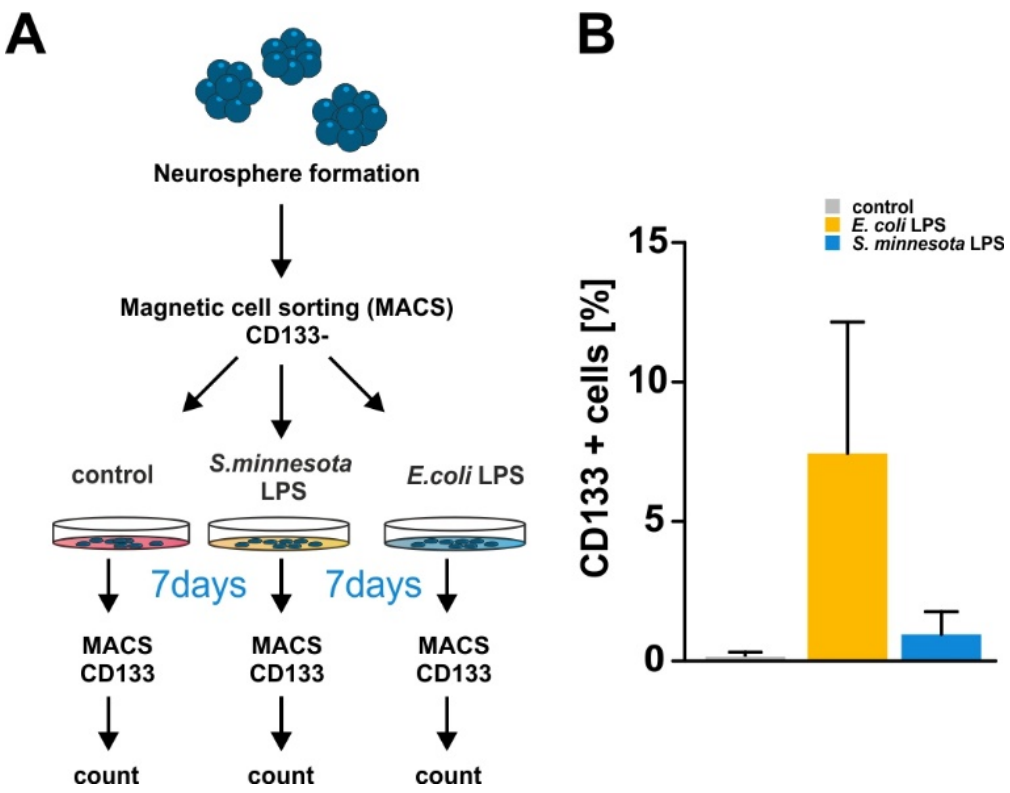

Figure 3.10. CD133 $^{-}$ cells cultivated with *E. coli* LPS has a trend of increasing the number of CD133 $^{+}$ cells. Data are presented as mean ± SEM from 3 different experiments, analysed using ANOVA with Bonferroni correction (CI 95%).

To further investigate this, same number of CD133^{-} cells were then cultivated with TLR4 ligands *E. coli* LPS and *S. minnesota* LPS for 7 days in growth media. CD133 $^{-}$ cell number were determined with MACS (Fig. 3.11). Results suggested that *S. minnesota* LPS stimulated U251 cells has a significantly higher number of CD133 $^{-}$ cells than untreated control and *E. coli* LPS treated cells. As all the groups of cells were seeded with same cell number and from the same population, it would seem logical to predict the opposite is true for the number of CD133^{+} cells. Those results suggested that *E.coli* LPS can promote the converting of CD133 $^{-}$ cells to CD133 $^{+}$ cells.

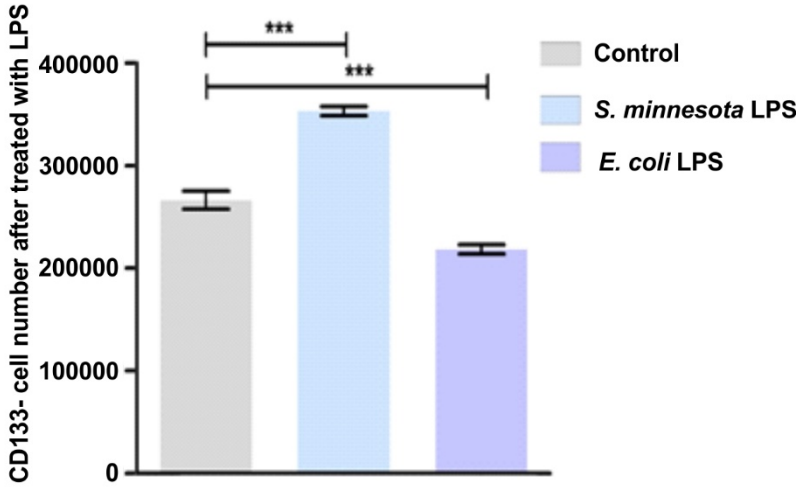

Figure 3.11. *S. minnesota* LPS significantly increased non-CSC number. *S. minnesota* LPS treated U251 cells showed highest level of non-CSCs. *E. coli* LPS treated U251 has the lowest number of non-CSCs. Mean ± SEM from 3 biological repeats were analysed using ANOVA with Bonferroni correction. **p<0.01, ***p<0.001.

TLR4 mediated MyD88 dependent pathway has a trend of increasing stemness of U251 cells.

To further understand the impact of the TLR-4 mediated TRIF pathway and MyD88 pathway on cell stemness, I transfected U251 cells with vectors coding for a constitutively active form of IRF3 and a constitutively active form of the MyD88 downstream kinase IKK2. Briefly, cells were transfected with pcDNA3.1 –IRF3 and pRosa- IKK2-ca vectors respectively to have the continue activation of transcription factor IRF3 and NF-κB. In the following, the expression of nestin was assessed using ICC and cell counting. Within the cell groups, nestin positive cells were counted. Even though there is higher number of cells expressing nestin in pRosa- IKK2-ca transfected cells, the difference is not significant (Fig .3.12).

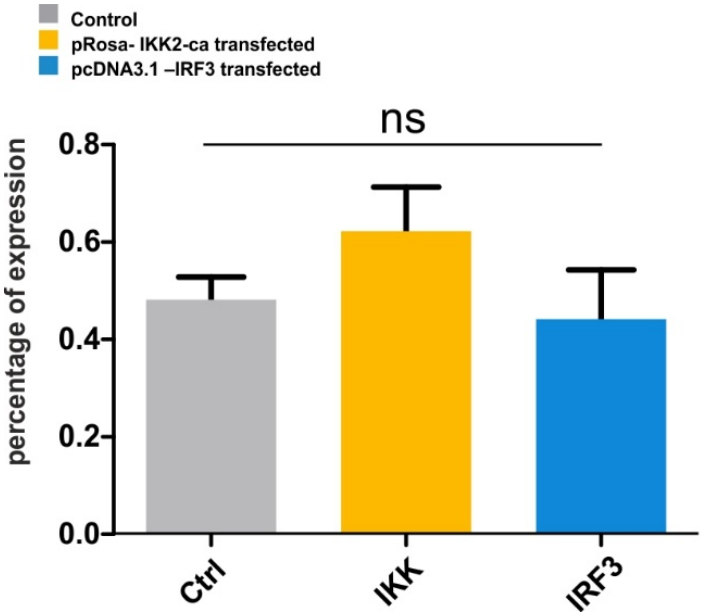

Figure 3.12. pRosa- IKK2-ca transfected group did not significantly impact but only has a trend of increasing the percentage of CSCs. Mean ± SEM from 5 biological repeats were analysed using ANOVA with Bonferroni correction (CI 95%).

U251 cell migration is promoted by TLR4-mediated NF-κB activation

U251 cells were stimulated with *E. coli* LPS, *S. minnesota* LPS and TNFα following with scratch assay. The closure distance of the three groups were measured, and the closure rate was calculated respectively. From results, it could be seen that the TNFα treated U251 has significantly high closure rate than other three groups. Although there is no significant difference on closure rate of LPS treated cells, the *E.coli* LPS treated U251 has a trend to migrate faster than control group and *S. minnesota* LPS treated group (Fig. 3.14A).

To test the impact of the TRIF and MyD88 pathway on cell migration, U251 cells were co-transfected in two groups: vector pcDNA3.1 –IRF3 and GFP, vector prosa- IKK2-ca and GFP separately. The transfection of two vectors would activate the IRF3 and NF-κB respectively, and GFP will be the marker of successfully transfected cells. Cell pictures were taken under fluorescent microscope (Fig. 3.13). The closure distances were measured and closure rate were calculated. It is clear to be seen that the U251 cells transfected with pRosa- IKK2-ca has the fastest closure rate in 12 hours after scratch (Fig. 3.13). pRosa- IKK2-ca transfected cells' scratch mark closure between

of 0h and 12h time point was significantly higher than cells transfected with pcDNA3.1 –IRF3 and control group (Fig. 3.14B).

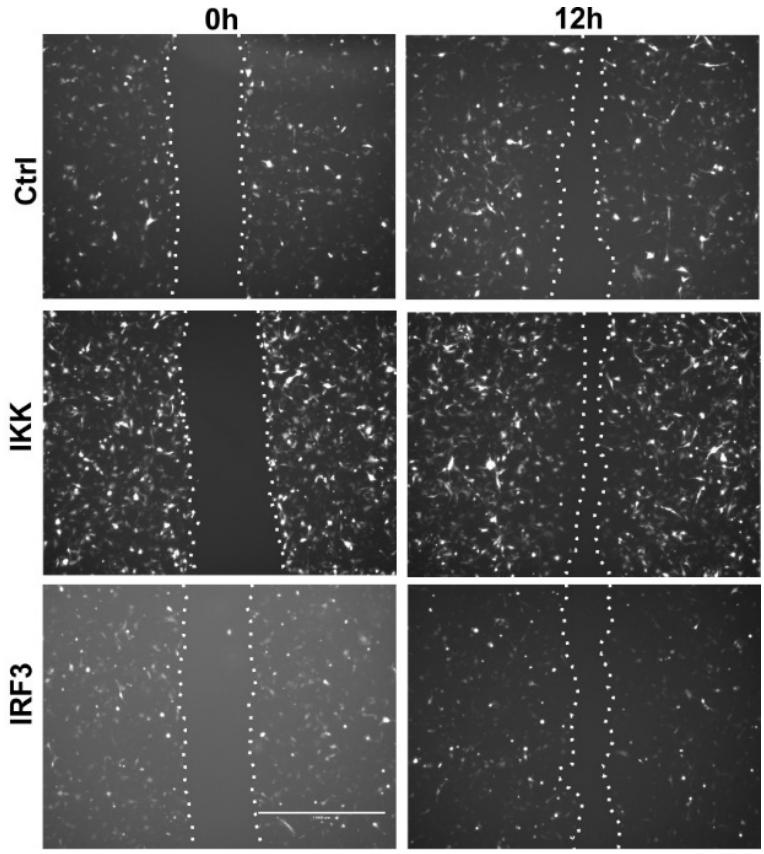

Figure 3.13. When NF-κB is activated by transfecting U251 cells with pRosa-IKK2-ca, cells has highest closure rate. Pictures were taken at 0h and 12h time point. Scale bar 400μm.

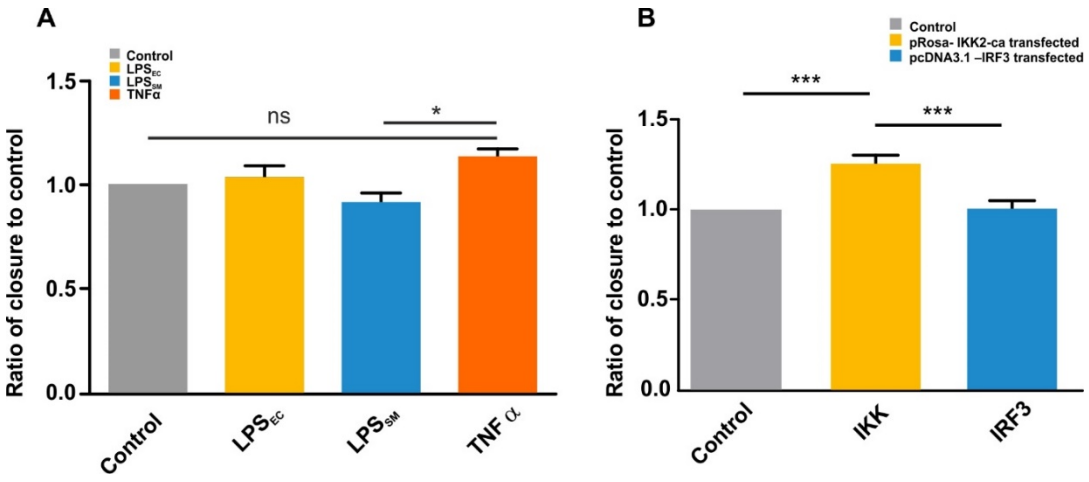

Figure 3.14. The TLR-mediated NF-κB activation significantly promoted the migration of U251 cells. A. TNFα treated U251 cells' migration rate was significantly higher than *S. minnesota* LPS treated U251 cells. **B.** pRosa- IKK2-ca transfected cells' migration rate was significantly higher than other two groups.

S. minnesota LPS and TLR4-mediated TRIF pathway increases differentiation of U251 cells.

Differentiation markers glial fibrillary acid protein (GFAP) and β-III-tubulin were used to test the differentiation level of U251 cells. Early passage U251 cells were cultivated in adherent plates for 7 days in the presence of *E. coli* or *S. minnesota* LPS separately. qPCR and immunocytochemistry were used to assess the expression levels of GFAP and β-III-tubulin. In comparison to untreated control group, both GFAP and β-III-tubulin were significantly upregulated at mRNA level in *S. minnesota* LPS treated U251 cells (Fig. 3.15). Results suggested that transcription of GFAP in *S. minnesota* LPS treated cells were promoted to 4 folds comparing to control group. *E.coli* LPS treated cells has lower but not significant decrease of GFAP at mRNA level compare to the control group (Fig. 3.15A). As for β-III-tubulin, *S. minnesota* LPS promoted the β-III-tubulin transcription to 7 folds compared to the control group at mRNA level (Fig. 3.15B).

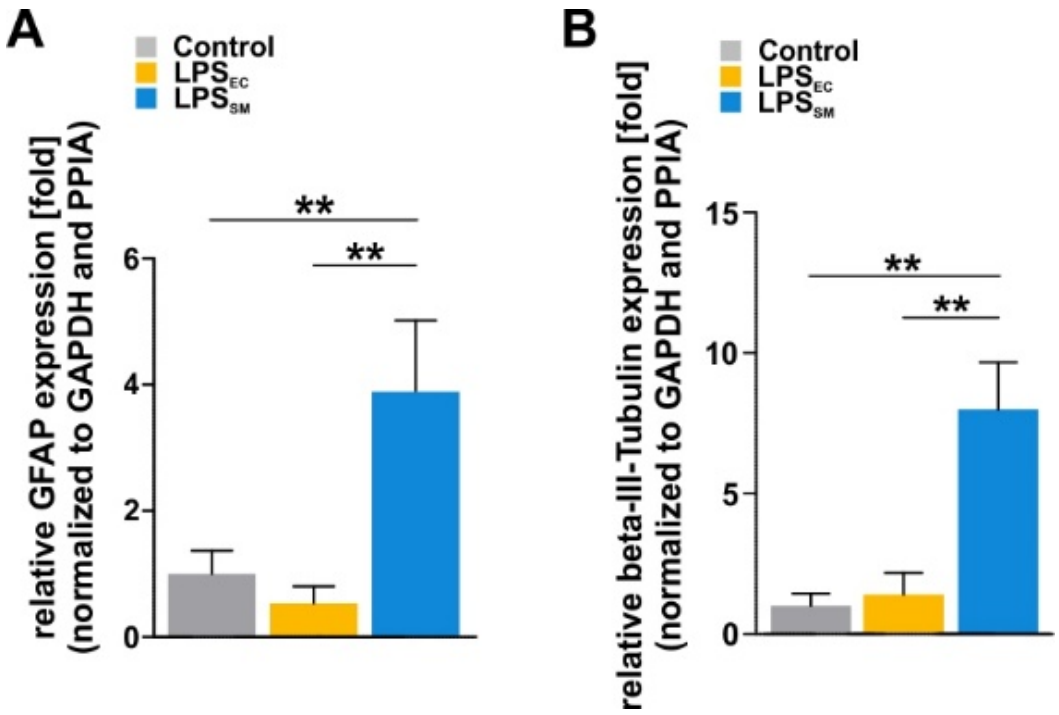

Figure 3.15. The GFAP and β-III-tubulin mRNA relative to GAPDH and PPIA was significantly higher in *S. minnesota* LPS treated U251 cells compared to both, control and *E. coli* treated cells. A. Relative GFAP expression [fold]. **B.** Relative β-III-tubulin expression [Fold]. Mean ± SEM from a minimum of three independent experiments were analysed using ANOVA with Bonferroni correction (CI 95%) *p<0.05; **p<0.01.

ICC was used to determine the expression of GFAP and β-III-tubulin at protein level. Cells were labelled and pixel intensity of cells were measured (Fig. 3.16). Results suggested that there is no significant difference of GFAP expression among three groups at protein level (Fig. 3.16 B). In *S. minnesota* LPS treated cells, only β-III-tubulin showed significant increase (Fig. 3.16D).

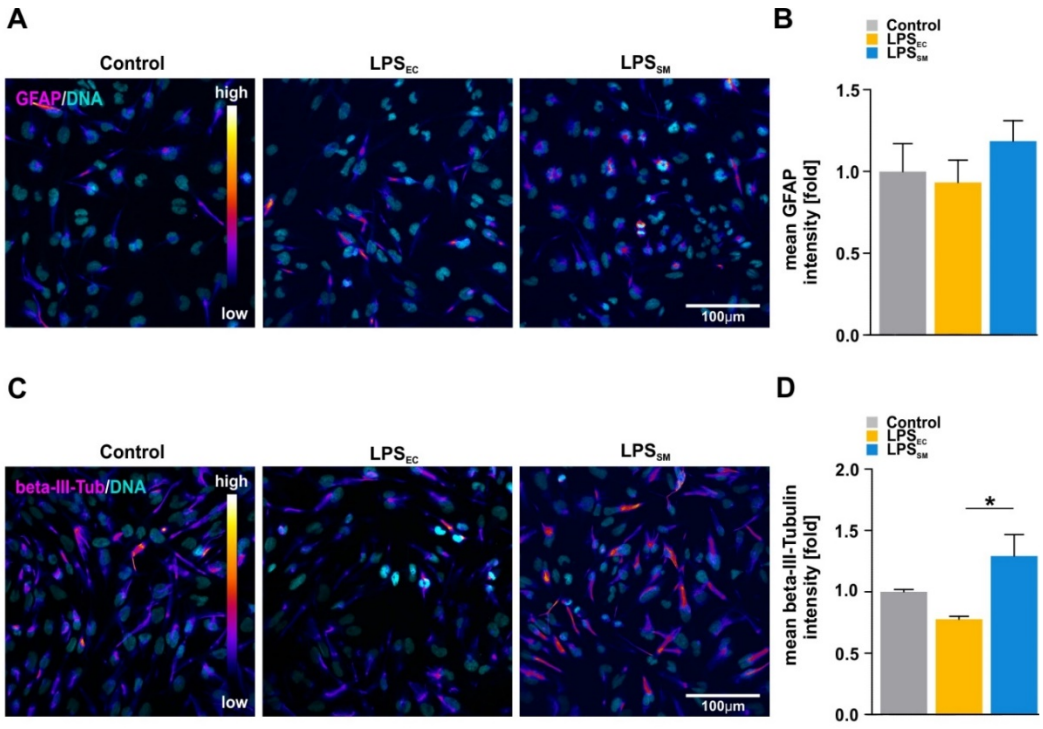

Figure 3.16. Only β-III-tubulin, not GFAP is increased at protein level when U251 cells were exposed to *S. minnesota* LPS. A. ICC of GFAP. **B.** Mean pixel intensity of GFAP. **C.** ICC of β-III –tubulin. **D.** mean pixel intensity of β-III –tubulin. Mean ± SEM from five independent experiments were analysed using ANOVA with Bonferroni correction (CI 95%) *p<0.05.

To study the impact of TRIF pathway and MyD88 pathway on cell differentiation, early passage U251 cells were transfected with vector pcDNA3.1 –IRF3 and vector pRosa-IKK2-ca separately, to constitutively express the IRF3 and to activate the NF-κB. To demonstrate the two down-stream pathways impaction to cell differentiation, ICC were used. U251 cells were cultured and stained with the differentiation marker β-III-tubulin and GFAP antibodies, β-III-tubulin and GFAP positive cells (cells have higher differentiation potential) were counted (Fig. 3.17). As shown in Fig. 3.17, there are more percentage of U251 cells showed β-III-tubulin and GFAP positive when transfected with pcDNA3.1 –IRF3. Therefore, it is clear that IRF3 activation would lead to higher differentiation potential of U251 cells. However, when transfected cells with pcDNA3.1 –IRF3, there is only significant percentage difference of β-III-tubulin positive cells (Fig. 3.17A), but not GFAP positive cells (Fig. 3.17B). Also, a decreasing trend of β-III-tubulin could be seen in the pRosa- IKK2-ca transfected cells comparing to the control group (Fig. 3.17A).

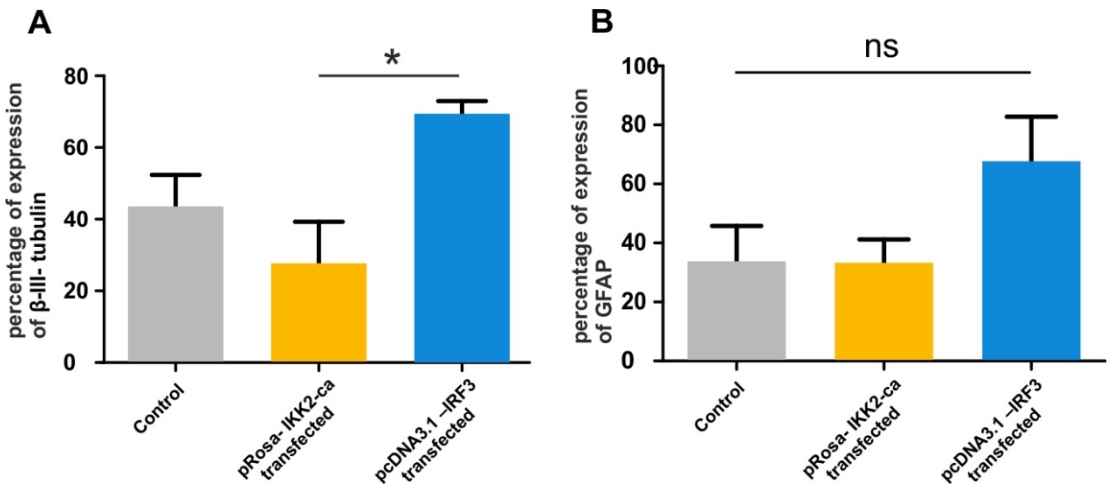

Figure 3.17. IRF3 activation significantly increased β-III-tubulin expressed cells, but had no significant impaction to GFAP expressed cells. A. pcDNA3.1 –IRF3 transfected cells has significant higher percentage of β-III-tubulin positive cells. **B.** There is no significant difference of GFAP positive cells among three groups. Mean ± SEM from a minimum of 5 biological repeats were analysed using ANOVA with Bonferroni correction (CI 95%) *p<0.05.

Inhibition of TLR4 and TLR4 mediated MyD88 pathway prevent the TLR4 ligand induced changes of stemness and differentiation.

In order to assess if the observed effects are mediated by TLR4 and are not influenced by other signalling events, MyD88-dependent signalling inhibitor IMD0354 and the TLR4 antagonist *Rhodobacter sphaeroides* LPS were applied. To assess the effectiveness of these inhibitors to abrogate NF-κB signalling, NF-κB-GFP-Luc U251 reporter cell line [204] was used. Briefly, GFP and luciferase are produced in response to NF-κB activation in these reporter cells. U251-NF-κB-GFP-Luc have been cultivated as spheres, followed by a 7 day treatment with *E. coli* or *S. minnesota* LPS (Fig. 3.18).

IMD0354 can significantly inhibited the TLR4 signalling, as the luciferase signals (NF-κB activity) of U251 + IMD0354 are significantly lower than the control group in all conditions. *R. sphaeroids* LPS treated U251 cells (control, *E.coli* LPS treated and *S. minnesota* LPS treated cells) showed similar NF-κB- dependent luciferase activity,

proved that the TLR4- mediated MyD88 pathway was suppressed by *R. sphaeroids* LPS (Fig. 3.18).

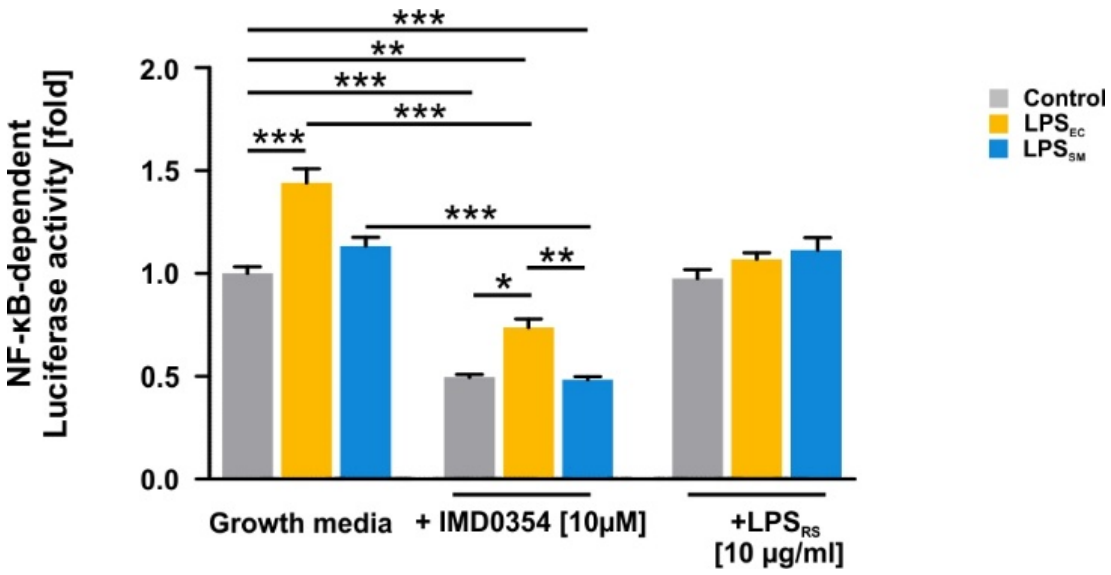

Figure 3.18. IMD0354 and LPS_{RS} significantly suppress the NF-κB activation. NF-κB-dependent luciferase activity in U251-NF-κB-GFP-LUC stable reporter cell line was measured after 7-day exposure to *S. minnesota* or *E. coli* LPS. Cells were simultaneously cultivated with either 10 μM of the MyD88-dependent inhibitor IMD0354 or 10μg/ml the TLR4-antagonist LPS_{RS}. Presence of IMD0354 significantly reduced NF-κB- dependent luciferase expression in all conditions, whereas *R. sphaeroides* blocked NF-κB- activation by *E. coli* LPS or *S. minnesota* LPS. Mean ± SEM from 3 independent experiments were analysed using ANOVA with Bonferroni correction (CI 95%); *p<0.05; **p<0.01; ***p<0.001. LPS_{RS}: LPS derived from *Rhodobacter sphaeroides.*

After assessing the functionality of the inhibitors, the expression of CD133 and β-III-tubulin using qPCR and ICC were analysed. With qPCR, when testing the mRNA level of CD133 and β-III-tubulin, there is no significant difference among control group, *E. coli* LPS treated group and *S. minnesota* LPS treated group (Fig. 3.19). In comparison to Fig. 3.7 and Fig. 15, when added IMD0354 or *R. sphaeroides* LPS to cells, there is no longer any increased folds of mRNA transcription. Suggested that inhibition of

TLR4 and TLR4 mediated MyD88 pathway prevent the increasing of stemness and differentiation in response to *E. coli* LPS and *S. minnesota* LPS at mRNA level.

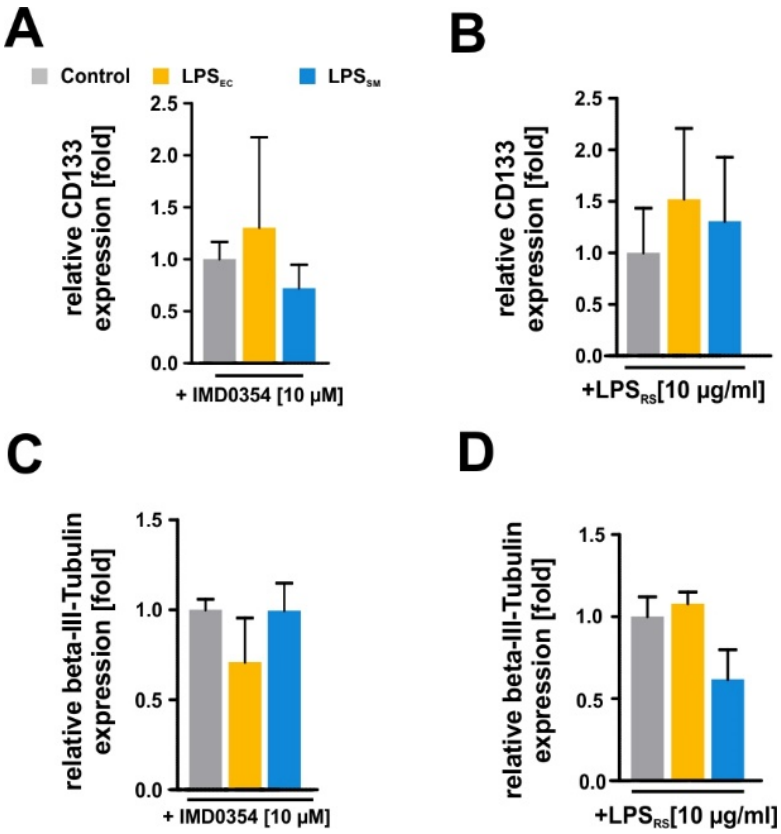

Figure 3.19. CD133 mRNA and β-III-tubulin mRNA expression relative to GAPDH and PPIA were not significantly different in all conditions tested. A &B. The inhibition of TLR4 and TLR4 mediated NF-κB biased signalling prevents the increase of CD133 in response to *E. coli* LPS. **C&D.** The inhibition of TLR4 and TLR4 mediated NF-κB biased signalling prevents the increase of β-III- tubulin in response to *S. minnesota* LPS. Mean ± SEM from three independent experiments were analysed using ANOVA with Bonferroni correction (CI 95%); *p<0.05; **p<0.01; ***p<0.001. LPS_{RS}: LPS derived from *Rhodobacter sphaeroides.*

The expression of CD133 and β-III-tubulin were tested using ICC. Pixel intensity of CD133 and β-III-tubulin were quantified in all conditions in the presence of IMD0354 or *R. sphaeroides* LPS (Figure 3.20). When inhibit the TLR4-mediated NF-κB biased signalling using IMD0354, there is a significant increase of CD133 protein expression in *S. minnesota* LPS stimulated cells, but not in *E. coli* LPS stimulated cells (Fig. 3.20A).

Suggested that the CD133 increase in *E. coli* LPS treated cells (Fig. 3.8B) are highly TLR4 – mediated NF-κB biased signalling dependent. However, with *R. sphaeroides* LPS added to the cell, there is no significant difference of CD133 among all conditions (Fig. 3.20B), suggested that the two downstream pathways of TLR4 are both involved in impacting the stemness of U251 cells. As for the protein level expression of β-III-tubulin, there is no significant difference of pixel intensity in all conditions. Suggested that the inhibition of TLR4 and TLR4 mediated NF-κB biased signalling can prevent the increase of the differentiation of U251 cells.

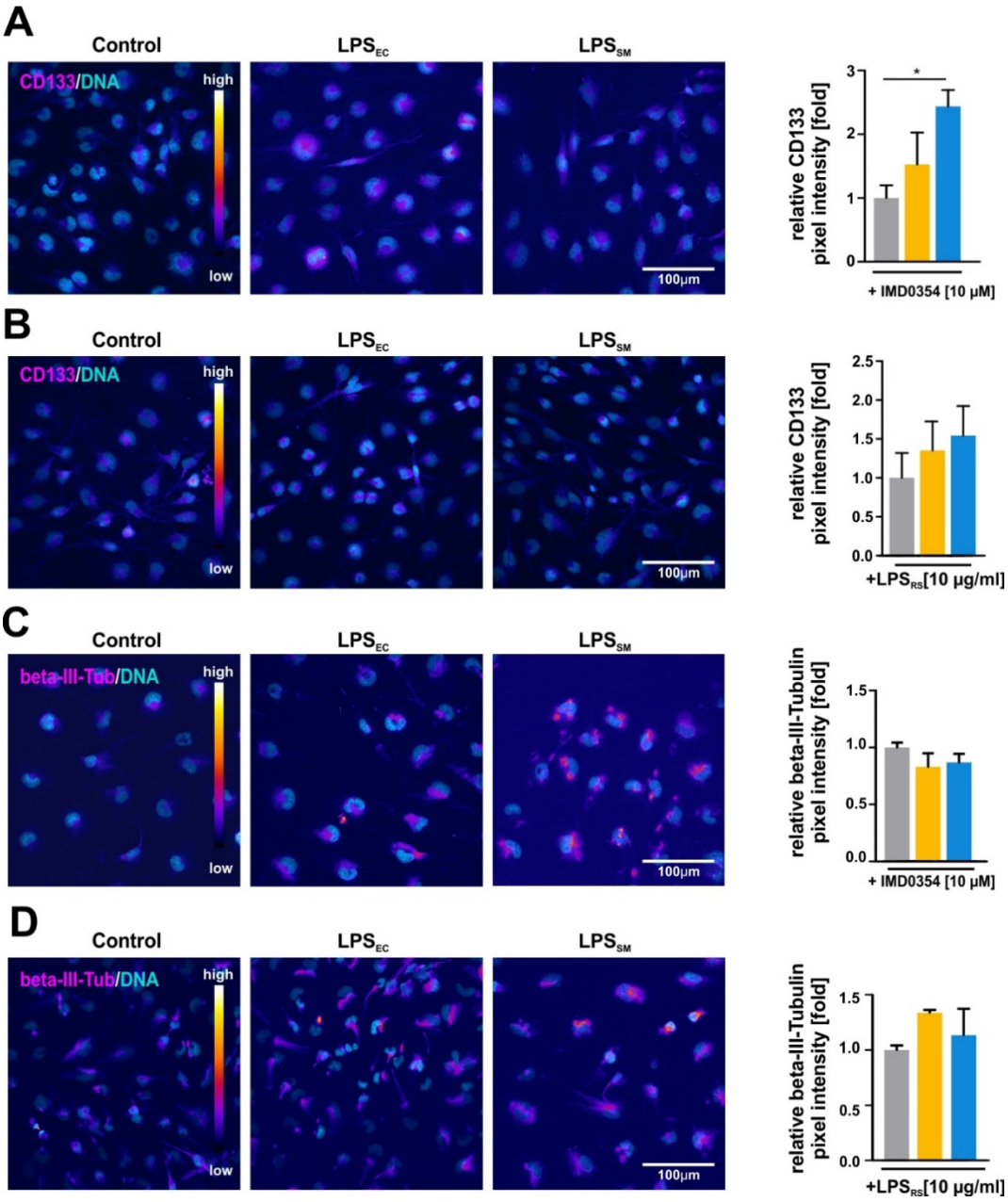

Figure 3.20. ICC and pixel intensity of U251 cells' CD133 and β-III-tubulin in the presence of IMD0354 or *R. sphaeroides* LPS. A. CD133 expression when add IMD0354 to U251 cells. Significant difference could be seen among *S. minnesota* LPS and control group. **B.** CD133 expression when add *R. sphaeroides* LPS to cells. No significant difference among all conditions. **C.** β-III-tubulin expression when add IMD0354 to cells. No significant difference among all conditions. **D.** β-III-tubulin expression when add *R. sphaeroides* LPS to cells. No significant difference among all conditions. Mean ± SEM from three independent experiments were analysed using ANOVA with Bonferroni correction (CI 95%); *p<0.05. LPS_{RS}: LPS derived from *Rhodobacter sphaeroides.*

3.3. Discussion

Tumour recurrence after glioblastoma treatment still remains poorly understood. Recent studies suggested that CSCs play key roles in glioblastoma initiation, progression, and therapeutic recurrence. In this chapter, I investigated the effects of TLR4-mediated biased signalling on the behaviour of CSCs. Specifically, tumorigenicity, stemness, migration, viability, proliferation, and differentiation.

I first demonstrated that the cell population studied contains a stem cell-like cells. This was shown by demonstrating their ability to form spheres in presence of FGF-2 and EGF, as well as their expression of CD133 and nestin, which are well known stemness markers of glioblastoma [106]. Apart from CD133 and nestin, other stemness related cell surface proteins are also suggested as CSC markers including the cell surface glycoprotein CD44, and the cytosolic enzyme aldehyde dehydrogenase 1 (ALDH1) [23, 260, 261]. Another study proposed that CD44 and CD15 are potential markers for glioblastoma [115], but these markers can label large number of somatic cells and increase the false positive rate [106]. $CD133^+$ cells, however, are known to have capability of initiating tumours [5]. Therefore, I chose CD133 and nestin to be the CSC markers to be assessed in this chapter. Using a sphere formation assay, I showed that U251 cells were able to form spheres. CD133 positive sub-populations were determined using MACS. Results suggested that in tumourispheres, the percentage of CD133 positive cells was 8.07%±1.48%, while adherent U251 cells had a less CSC percentage of 4.88 ± 0.37% (Fig. 1.1C). Similar research including an *in vivo* test of U87 and U251 cells carried out by Romaneko et al. showed 10%-11% of these populations were CSCs [262]. In primary xenografts this percentage has been reported to be higher, with CSCs comprising 19%-22% of the whole cell population in glioblastoma [5], and 17% -44% in breast tumour xenografts [263]. The increase of $CD133^+$ cell percentage difference between this study and the rest could be due to the cell line, the passage of the cells, the cytokines difference in different batches of FBS, the usage of B27 etc.

Using immunocytochemistry, I have also demonstrated that U251 cells express the CSC marker nestin. The presence of these two CSC markers suggested that the U251

cell line contains CSC-like cells. Due to the relatively high CSC percentage in this cell line, U251 cells have been used as a model for glioblastoma-initiating stem cells [193, 264]. This is the reason why U251 has been selected to be the experimental material in this chapter. In comparison to other glioblastoma cell types like U87MG, or A172, U251 has higher percentage of CSCs.[264].

In our previous study, Zeuner et al. demonstrated that *E. coli* LPS is the MyD88 dependent signalling biased ligand, and *S. minnesota* LPS is the biased ligand to activate TRIF pathway/ MyD88 independent pathway [79]. In this chapter, I used soft agar assay to study the anchorage-independent growth ability and thus tumourigenicity of CSCs [258]. It has been demonstrated that in the soft agar, only cells with tumorigenic properties could survive and develop into colonies[265]. Tumourigenic ability is known to be one of key CSCs properties [266]. In the soft agar assay I presented, it could be seen that *E. coli* LPS and TNFα are able to increase the number of colonies in comparison with control group and *S. minnesota* LPS treated group (Fig. 3.4). This suggested that *E. coli* LPS and TNFα induced NF-κB activation may play a very important role here. In addition, *E. coli* LPS treated U251 cells result to larger colonies compare to other groups, suggested that TLR4- mediated MyD88 dependent pathway can increase the tumourigenicity of U251 cells. Furthermore, *S. minnesota* LPS, as a TLR4 mediated MyD88 independent ligand, has an effect of reduce the size of the colonies [267]. In addition, Afify and Seno suggested that inflammation, especially the activation of NF-κB activation in cells are involved in the tumour initiation and promotion [268]. Afify and Seno set up a model of transmitting pluripotent stem cells into CSCs, and demonstrated several impact factors of the process. It was suggested that the pro-inflammatory cytokines, ROS, and some pro-inflammatory pathways including NF-κB pathway, STAT3 pathway, MAPK pathway, and Akt pathway were the positive impact factors to the tumour initiation and tumour progression [268]. All in all, activating NF-κB via TLR4 promotes the tumourigenesis and cancer progression.

U251 proliferation and viability were assessed after stimulating cells with *E. coli* LPS and *S. minnesota* LPS. The whole population of U251 cells was used in the assay, and no significant difference could be seen among different conditions (Fig. 3.5). However, even though there is no significant difference between the total cell numbers

in the unsorted population, the percentages of CSCs and non- CSCs may have changed after LPS stimulation. U251 cells were cultivated as spheres followed by *E. coli* LPS and *S. minnesota* LPS treatment for 7 days (Fig. 3.6), and CD133 $^{+}$ cells were counted after MACS separation. Treatment of U251 with *E. coli* LPS resulted in nearly two fold increase of CD133 $^{+}$ cells (compared to cells treated with *S. minnesota* LPS and control cells (Fig. 3.9). In other words, the level of CSCs of U251 cells stimulated by *E. coli* LPS showed a significant increase, and it could be a result of the activation of TLR4. Thus, I found that *E. coli* LPS could promote the transition of non-CSCs to CSCs and helped maintain the CSCs themselves. Non-CSCs (CD133^{-}) were collected and cultivated in medium containing different LPS chemotypes. After 7 days of *E. coli* LPS treatment, 7% of CD133^{+} were counted in cells previously negative for this marker (Fig. 3.10). In addition, *E. coli* LPS treated cells showed lowest percentage of CD133^{-} cells (Fig. 3.11). Based on these results (Fig. 1.1C and Fig. 3.10), I propose that the percentage of CSCs in U251 keeps a balanced percentage below 10% in this project model and showed transitions between CSCs and non- CSCs. In other words, if the percentage of CSCs is lower than the balanced percentage, the transition of non-CSCs to CSCs may happen, and vice versa. This transition progress keeps the CSC subpopulation in certain percentage among the tumour cells. Some studies suggested that microRNA (miRNAs) play a role in regulation of the CSC sub population in tumours [269], and therefore might cause the transition between CSCs and non-CSCs, but the exact mechanism is not yet fully understood. Cabrera et al. suggested that the shift from a non-CSC state to a CSC state may be due to latent plasticity of non-CSCs, and the transition between non-CSCs and CSCs may be regulated by some micro-environmental signals and cell-cell interactions in the tumour niche [57]. As the CSCs showed high transition in *E. coli* LPS treated group, I propose that TLR4- mediated MyD88 – NF-κB pathway might trigger the dynamic transition between CSC and non-CSCs and vice versa.

Notably, it has been reported that cultivation in presence of chemotherapeutic agents also increases the percentage of CSCs. Briefly, Auffinger demonstrated that exposure of unsorted U251 cells to Temozolomide (TMZ) increases the percentage of CSCs via boosting the transition from non-CSCs into CSCs [270]. Of cause, this may also because of the apoptosis of non-CSCs caused by the TMZ. Interestingly, Gao et al. suggested that high-mobility group box 1 (HMGB1) is responsible for TMZ resistance

in glioblastoma. In addition they claimed that TLR4, one of the main receptors of HMGB1, in cooperation with TLR2, TLR9, promotes the formation of CSCs [271]. All in all, the results presented above suggest that TLR4-mediated NF-κB activation promotes the stemness of glioblastoma cells, and might have a function of maintaining a balance between non-CSCs and CSCs in glioblastoma. IRF3, has been suggested to have inhibiting effects on glioma proliferation [217]. Tian et al. demonstrated that IRF3 could inhibiting cell proliferation in colorectal cancer by preventing the nuclear translocation of β-catenin, which is a cell cycle regulator [182, 272]. However, based on my results, there was no significant change of cell proliferation after cells were stimulated with anti-inflammatory pathway biased ligand *S. minnesota* LPS.

To further study the role of TLR4 signaling on stemness of U251 cells, the expression of stemness-related and CD133 and nestin in response to a 7-day LPS treatment was studied. These markers have been reported to have clinical relevance in glioblastoma pathology [273]. For nestin expression, I did not observe a significant difference between cells treated with *E. coli* LPS, *S. minnesota* LPS, and untreated cells at mRNA level (Fig. 3.7B). Moreover, there was no significant increase of nestin positive cells after activating IRF3 or NF-κB constitutively (Fig. 3.12). However, cells transfected with constitutively active IKK-2 showed a trend towards increase in percentage of nestin^{+} cells. This effect might be due to the cultivation period as adherent cells in presence of FCS, which has been previously shown to differentiate U251 cells [274]. However, U251 lack the expression of CD14, therefore presence of FCS for our experiments is crucial since it contains sCD14 as well as LBP to enable TLR4 signalling via MyD88-independent pathway [225]. However, Ferrandze et al. suggested that NF-κB activation through TLR4 signalling is able to promote the proliferation of glioblastoma CSCs and inhibit the terminal differentiation of them [275]. To my understanding, this suggested that the TLR4 mediated NF-κB activation can increase the stemness of Glioblastoma.

As for CD133 expression, an increase could be seen at mRNA level and protein level in *E. coli* LPS treated cells (Fig. 3.7A, Fig. 3.8B). CD133 protein was seen to have an increase at cytoplasm and nucleus area (Fig. 3.7A). According to Pietrus et al., the nucleus area expressed CD133 was linked to tumour angioinvasion property, and Huang et al. suggested that CD133 expression in nucleus was associated to poor

prognosis in non-small lung cancer [276, 277]. In my in vitro study, this CD133 increase in nucleus area suggested that those U251 cells has more stemness property. In actual tumour, the high stemness cells with high nucleus expression level might be the cause of poor prognosis in glioblastoma. I therefore hypothesized that this observed CD133 was upregulated due to NF-κB-activation. Studies showed that NF-κB-activation in glioblastoma cells has been associated with tumour invasiveness, proliferation, stemness and resistance to chemotherapy [227, 273, 278]. Moreover, constitutive NF-κB-activation has been reported to be sufficient to transform neural stem cells into gliome CSC-like cells [267]. In accordance with our findings, it has Rinkenbaugh and others shown that the activation of NF-κB also increases stemness in glioblastoma initiating cells [279]. In addition, Lai and colleagues showed that hepatocarcinoma stem cells maintain stemness and CD133 expression after stimulation with LPS. However, neither did they state the chemotype nor the purity of the used LPS. Insufficiently purified LPS triggers both TLR4- and TLR2- mediated NF-κB activation due to contaminations with bacterial cell wall components (lipopeptides) [280]. Consequently, this led to the suggestion that the effects observed by Lai and colleagues might not be mediated by TLR4. Indeed, signalling via TLR2/MyD88/NF-κB has also been demonstrated to enhance tumour recurrence, proliferation, as well as invasion in breast cancer stem cells [281]. Focusing back on stemness, the LPS I used in this project was ultrapure LPS, suggesting that stemness of glioblastoma is highly impacted by TLR4 mediated MyD88 dependent NF-κB activation. In particular, my results suggest that the TLR4 mediated MyD88 dependent pathway has might increase the stemness of U251 cells. Apart from the expression of stemness markers, our soft agar assay also indicated that TLR4-mediated MyD88-NF-κB signalling promotes stemness in U251 cells. Due to the contact inhibition, non-CSCs tend to progress to apoptosis in the soft agar and only the CSCs should survive [265]. In our results, after 21 days of cultivation, U251 cells treated with TNFα and *E. coli* LPS showed more and larger colonies in comparison to control group (Fig.3.3&3.4). Importantly, *E.coli* LPS, MyD88 biased ligand of TLR4 and TNFα are well known to activate the NF-κB signalling [79].

To address the impact of the TLR4 ligands *E. coli* LPS and *S. minnesota* LPS on the migration of U251 cells, a wound healing assay was performed. When U251 cells were stimulated with *E. coli* LPS or S. *minnesota* LPS, I did not see any significant difference

on cell migration compared to the control group. However, an increase of migration rate could be seen when U251 cells were stimulated with TNFα (Fig. 3.14 A). This might be because cells were only treated with LPS for 4 hours before scratching, as well as during the healing, and *E. coli* LPS mediated NF-κB activation requires longer time than TNFα induced NF-κB activation. Or, the change to the cells due to the TLR4 pathway activation was not at translational level of proteins. To further study this in more detail, U251 cells were transfected with pRosa- IKK2-ca to increase the activity of IKKβ and to constitutively activate the MyD88/NFκB pathway or pcDNA3.1 –IRF3 vector to increase the level of active IRF3. With IKK2-ca, the NF- κB activation was constitutively (tested using U251-NF- κB reporter cell line and luciferase assay as preliminary experiment, data not shown). Results indicated that cells with higher NF-κB activation level migrated significantly faster than the control group and cells with higher IRF3 level (Fig. 3.13 & 3.14 B). These results suggest that U251 cell migration is promoted by TLR4-mediated NF-κB activation. Similarly, Authier et al. demonstrated that the constitutive activation of NF-κB induced by IKKβ can promote the migration in fibroblast [282]. They also demonstrated that this is due to the induction of pro-migration gene expression, such as MM3, downstream of TNF receptor [282]. As for the anti-inflammatory transcription factor IRF3, Tarassinshin and Lee demonstrated that IRF3 is able to inhibit glioma migration and invasion [217]. They suggested the impact could only be observed when human glioma cells were stimulated with cytokine combination, IL-1/IFN, but not with LPS stimulation [217].

The level of differentiation of cancer cells in solid tumours is very important as it indicates the progression of the tumour. In general, more differentiated tumours are less aggressive than less differentiated tumours [229]. In this chapter, the impact of TLR4 biased signalling on U251 differentiation was evaluated. U251 cells were stimulated with *E. coli* or *S. minnesota* LPS. ICC and qPCR were used to assess the differentiation marker GFAP and β-III-tubulin at both protein and mRNA level. Results showed that both GFAP and β-III-tubulin were increased at mRNA level when U251 cells were treated with *S. minnesota* LPS, and showed no significant change under the *E. coli* stimulation (Fig. 3.15). At protein level, expression of β-III-tubulin per cell was significantly higher in *S. minnesota*- treated cells were compared with E. coli LPS-treated cells in our ICC results (Fig. 3.16). Those results suggest that when stimulating

U251 cells with TLR4 ligands that activate MyD88-independent pathway, CSCs differentiate. Other studies also suggested the anti-tumour effects of IRF3. Up regulation of IRF3 could inhibit gastric cancer growth and induces differentiation by modifying the gene expression of anti- tumour related genes [283, 284]. The soft agar assay also proved this. In soft agar assay, under same cultivation time, *S. minnesota* LPS treated cells formed significantly smaller colony size compared to other groups (Fig 3.3 & 3.4). This suggested a decrease of tumourigenicity in U251 cells. In accordance with my results, IRF3 has been shown to suppress tumour growth of prostate cancer. This has been suggested to occur through an immune-mediated anti-cancer mechanism, involving secretion of type I interferons [285]. Moreover, it has been suggested that IRF3 can mediate anti-cancer apoptosis in response to dsRNA and activate pro–apoptotic protein Bcl-2 family protein Bax [286, 287].

In order to further validate the finding on the impact of TLR4 signalling on differentiation of CSCs, I transfected cells with 'pcDNA3.1 –IRF3' to increase the expression of IRF3. A Significant increase in β-III-tubulin positive cells could be seen compared to the control group (transfected with pcDNA™5/FRT as control vector) and pRosa- IKK2-ca positive cells (Fig. 3.17). No significant changes of GFAP positive cells have been observed, but there was an increasing trend of GFAP positive cells in pcDNA3.1 –IRF3 transfected group. As for β-III-tubulin, results showed that higher percentage of cells in U251 expressed β-III-tubulin when IRF3 was activated. This further proves my previous view, that activating TRIF dependent pathway would lead to higher expression level of the neuron specific β-III-tubulin proteins, hence increase the level of differentiation in the U251 population. This would cause the IRF3 activated U251 cells to be in a less aggressive stage in comparison to control group and MyD88/NFκB pathway activated cells. All in all, the results suggested that *S. minnesota* LPS and TRIF pathway may have anti-tumour effect and promotes cell differentiation, suggested that more U251 cells tend to show the capacity of differentiation while TRIF pathway is activated. Similar experiments were demonstrated. pRosa- IKK2-ca vector was also used in a study carried by Swarnkar et al. to study the NF-κB activation [288]. The constitutive activation of NF-KB was demonstrated to show an inhibiting effects to the differentiation of osteoblasts, chondrocytes and stromal cells [288].

TLR4 expression is increased in glioblastoma [193], theoretically making it a suitable target for glioblastoma therapy. By applying the TLR4/NF-κB signalling inhibitor IMD0354 [204] and the TLR4-antagonist *R. sphaeroides* LPS to the cells, it can be assessed if the effect of LPS are TLR4 specific. By using a novel U251-NF-κB reporter cell line, I demonstrated that treatment with the inhibitor or antagonist reduced NF-κB or maintained basal NF-κB-activation when U251-reporter cells were cultivated with LPS from *E. coli* or *S. minnesota*, respectively (Fig. 3.18). When IMD0354 or *R. sphaeroides* LPS were applied, *S. minnesota* LPS no longer had impact on β-III-tubulin expression in U251 cells, both at mRNA and protein level (Fig. 3.19). When *R. sphaeroides* LPS was used, *E. coli* LPS no longer showed an impact on CD133 expression at both mRNA level and protein level, suggesting that TLR4-mediated NF-kB activation is the key to stemness. This is evidenced by my results showing that an inhibition of TLR4 and TLR4 mediated NF-κB biased signalling can prevent the increase of the stemness and differentiation of U251 cells.

It is worth to notice that when IMD0354 is applied and thus IKKβ was inhibited, there was still a significant CD133 expression in *S. minnesota* LPS treated cells (Fig. 3.20A). This is because there is a link between the two TLR4 downstream pathways: MyD88 – independent and MyD88 –dependent pathway (Fig. 3.21). When CD14 is present in the media, TRIF –mediated late phase NF-κB activation could occur leading to, production of IFN-β [169, 289]. In this case, NF-κB activation would lead to a moderate CD133 expression in *S. minnesota* LPS stimulated cells.

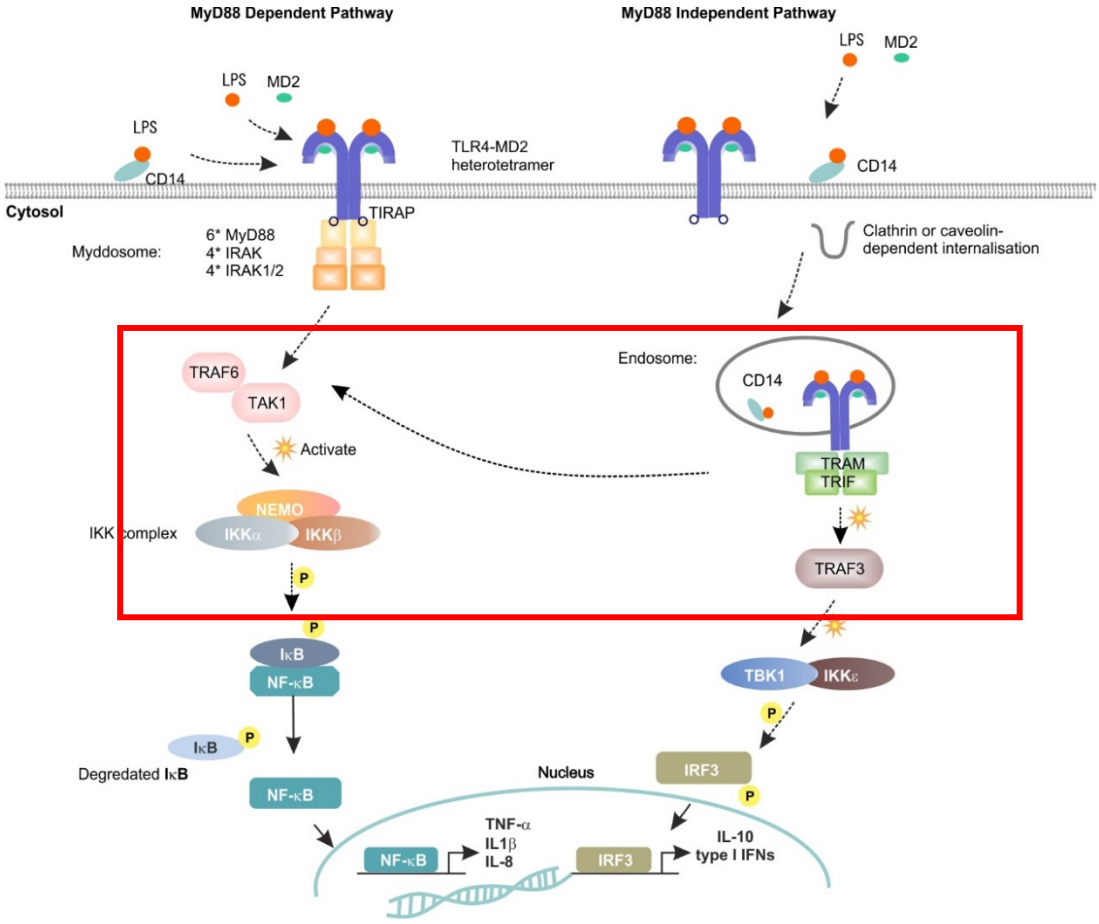

Figure 3. 21. TLR4 downstream pathways. Activation of MyD88 independent pathway could cause the later activation of NF-κB. Red box: Apart from MyD88 dependent pathway, the activation of NF-κB activation is also reported in MyD88-independent pathway, but the responses are delayed compared to IRF3 activation [124]. This NF-κB activation is recognized as late phase NF-κB activation compared to the early NF-κB activation in MyD88-dependent pathway. In this case, TRIF is essential for NF-κB activation, IFN-β production can be modulated by TRIF-mediated late phase NF-κB activation alone [124, 169]. Abbreviations: MD-2: myeloid differentiation factor 2. TIRAP: TIR domain-containing adaptor protein. TRAF: TNF receptor-associated factor. TAK1: TRAF-activated kinase 1. IRAK: Interleukin receptor-associated kinase. NEMO: NF-κB essential modulator. IKK: IκB kinase. TRIF: TIR domain-containing adaptor- inducing interferon- β. TRAM: TRIF – related adaptor molecule. TBK: TRAF family member-associated NF-κB activator- binding kinase.

3.4. Conclusion

To conclude, I demonstrated that stimulation of TLR4-mediated NF-κB activity increased the percentage of CSCs and promoted the transition of non-cancer stem cells to CSCs. In addition, both MyD88/ NF-κB and IRF3 pathways have opposing effects on U251 cell behaviour. The pro-inflammatory TLR4-mediated NF-κB activation promotes tumourigenicity of CSCs, increases their migration, and elevated the overall percentage of the CSCs. TLR4-mediated IRF3 pathway is able to increase the differentiation potential of U251 cells at both mRNA and protein level, and suppress the tumourigenicity of glioblastoma. My results suggest that the TLR4/ NF-κB signalling axis is a pro-tumourigenic pathway and TLR4/ IRF3 pathway is an anti-tumourigenic pathway. Importantly, the latter anti-inflammatory pathway might be able to shift the malignant tumour cells to early tumour stage by inducing their differentiation.

Within glioblastoma, a small population of CSC tend to stay quiescent in tumours [86]. This characteristic provides treatment resistance for the CSCs and make them difficult to be targeted in clinic. In my opinion, targeting TLR4 in future therapies might have two clinical aspects: 1). Targeting and promoting the IRF3 signalling pathway. The TLR4-mediated IRF3 could induce differentiation of CSCs so that it could be less difficult to target them or/and induce apoptosis; 2).Suppressing the TLR4-mediated NF-κB pathway and therefore decreasing the invasion and stemness of the cancer cells, at the same time, decreasing the disturbance of anti-tumour gene expression caused by NF-κB.

In sum, the results shown in this chapter provide new insights in how biased signalling mediated by TLR4 could affect cancer stem cell characteristics. These observations grant new insights in tumour development and tumour recurrence. By developing drugs to regulate TLR4 downstream pathways, it could offer new treatment options for glioblastoma either alone or in combination with conventional treatment options.

3.5. Limitations

In glioblastoma, the CSC markers were suggested to be CD133, CD44, CD15, SSEA-1 and nestin etc. (table 1.1). The rationale of using just CD133 in my study to

identify CSCs was based on the studies done by Singh et al.[5, 24]. In Singh's studies, only $CD133^+$ cells had tumourigenesis characteristics in glioblastoma, which suggested that $CD133^+$ cells are CSCs. However, it is still possible that some CSCs are not $CD133^+$, which may lead to some possible bias in this study.

The percentage increase of $CD133^+$ cells was not as high as some other studies using cell lines or xenografts. This may due to the cell line differences or cultivation condition differences. Alternative cultivation techniques could be considered, and more CSCs percentage increase could benefit on this study

The U251 monolayer cultivation followed the TLR4 ligand stimulation to the tumourispheres may or may not lead to the differentiation or de-differentiation of the CSCs, hence may affect the percentage of CSCs in the cell group. This could be studied more concisely by using another control group, which was monolayer cultivated U251 cells. In addition, using the 3D tumourisphroids as another group of control sould be considered.

U251 cells were mainly seeded in 2D monolayers. The characteristic of those monolayer cultured cells could be different from clinical tumours. It is worth to use 3D cell culturing to demonstrate some of the experiments, for example experiments to determine the stemness, the proliferation and differentiation of cells. Also, instead of only using LPS, more TLR4 ligands could be used. It has been suggested that IRF3 anti-inflammatory response might not able to be triggered via LPS stimulation [217]. Therefore, it is worth to try some other IRF3 biased stimulations, like Poly (I: C) or Monophosphoryl Lipid A (MPLA) to study the impact of IRF3 to the CSC behaviours [290].

In addition, because of the blood –brain barrier, LPS is very likely not going to be exist in human brain cancers. Instead, the inflammation microenvironment of GBM is sterile inflammation caused by multiple cytokines. It is worth to use the Damage-Associated Molecular Patterns and Pathogen-Associated Molecular Patterns as ligands of TLR4. Last, our study mainly used 2D cell culture technique and just used cell lines to demonstrate our results. How the CSCs behave in actual patient tumour is now remain unknown. It is worth to use primary tumour cells in 3D scaffold materials to study the TLR4 biased signalling in GBM.

3.6. Future work

Future work following on this project could include three phases. First, further studying the activation of the signalling pathways using different TLR4 ligands and study the activation level of the TLR4 downstream signalling pathway using protein analysis to understand the trigger mechanisms of the biased signalling. Damage-Associated Molecular Patterns and Pathogen-Associated Molecular Patterns they exist in GBM and could be used as ligands of TLR4 in the future study [291, 292]. Second, primary cells and 3D cell culturing could be used to study the biased signalling. Also, animal experiments could be introduced. By transplanting CSCs to immune deficiency animals after stimulating with TLR4 ligands, it will help us to understand how the TLR4 signalling is impacting the tumourigenesis, especially the anti-tumour effects of TLR4-mediated IRF3 pathway. Furthermore, the selective TLR4-mediated IRF3 pathway could be a potential drug target in clinics to go to clinical trial. Currently, The TLR4-IRF3 pathway agonist MPLA prepared from *S. minnesota* LPS has been shown to have clinical success as an vaccine adjuvant and has been suggested to inhibit inflammation in cells [293, 294]. For further research, this TLR4- IRF3 biased ligand or other ligands derived from *S.minnestota* LPS could be used as adjuvants with traditional cancer therapy. MPLA and other *S. minnesota* LPS derived ligands may able to induce differentiation to the tumour population, decrease the stemness of the tumour and hopefully decrease the therapy resistance of GBM. In combination with conventional cancer therapies, this kind of TLR4-IRF3 biased ligands may form more efficient cocktail treatments.

Chapter 4. 3D cell culture impacts stemness and drug resistance of U251 cells

4.1. Introduction

4.1.1 3D cell culture

In the process of development of anti-tumour drugs, 2D cell culture has been widely used in *in vitro* cancer research as one type of to identify the molecular mode of action of multiple chemical molecules. Comparing to *in vivo* animal models, conventional 2D cell culture are more standardized and is cheaper and simpler. However, it 2D cell culture lacks the effects of extracellular matrix (ECM) and tumour microenvironment (TME). Moreover, it is not capable of mimicking the complexity and heterogeneity of human tumours [295, 296]. Lastly, 2D cell culture induces a forced apical polarity potentially changing fundamental properties of the tumour cells.

To bridge up the *in vit*ro 2D cell culture and *in vivo* animal model study, 3D multicellular cell culture has been introduced to cancer research. Bissell et al. suggested that the microenvironments of cells influences the nature of the tissue context. The maintenance of the features of cells is essential for normal function of the tissue, including proliferation, differentiation, survival and secretion [61]. 3D cell culture has also been used to study cell migration, cell-cell interactions, cell-ECM interactions, drug penetration, drug response and drug resistance [295, 297-301]. Unlike conventional 2D cell culture study, because of the 3D shape due and more pathophysiological resemblance with primary tumour tissue, cancer cells can proliferate or quiescent or even necrotic to form a mixture of different cell stages just like clinical tumours [295]. Therefore, in comparison to in vivo animal models, 3D cell culture is able to provide more representative data for anti-cancer drug discovery research without being prohibitively expensive.

It has been shown that gene expression at transcriptional and translational level has been changed roughly 30% when cancer cells are cultivated in 2D [59]. 3D cell culture, however, has been shown to recover some critical characteristics of tumour cells absent in 2D (Table 4.1) [302]. Evidence showed that although cells lose many of their native *in vivo* features after being separated from the primary tumour and cultured in *in vitro* 2D methods, their differences in morphological changes, growth, and gene/protein expression are largely restored when the cells are placed back into an *in*

vivo environment (e.g. an animal model) or grown in an environment that resembles the ECM [59, 303, 304].

Therefore, 3D cell culture models are useful and cost effective tools allowing to study the tumour growth mechanisms including intracellular cell signalling, cancer plasticity, cancer heterogeneity and other fundamental properties of cancers [297]. It is also useful for developing new treatment options, by functions as promising drug test models before animal trials. For example, significant progress using 3D cell culture in recent years resulting in the development of targeted anti-cancer drugs, such as imatinib, trastuzumab, and crizotinib [297]. Those exemplifies the significance of 3D cell culturing in understanding cell biological circumstances and phenotypic heterogeneities during the tumour development [305].

	2D CELL CULTURE	3D CELL CULTURE
Cell-Cell	Limited cell-cell interaction	Surrounding cell-cell interaction
Cell-ECM	No cell-ECM interaction	Cell-ECM interaction
Cell adhesion	Restricted on 2D plate	Dispersed in 3D
Mobility	Uninhibited dispersion and migration	Sterically hindered dispersion and migration
Scaffold	Glass or polystyrene	Physical structure with matrix
Soluble gradient	Absent	Present in spheroids
Drug resistance	Non- representative	Sensitivity similar to in vivo
Cell cycle stage	Cells all at same stage	Cells at various stage in spheroids
Phenotypic diversity	Conforming	Diverse

Table 4. 1. Physiological differences between conventional 2D cell culture and 3D cell culture. In conventional 2D cell culture, cells grow as a 2D monolayer and has limited intercellular interaction, no cell-ECM interaction, no soluble gradient, non-

representative drug resistance, no phenotypic diversity and same cell cycle stage. 3D cell culture overcomes those problems and provide intercellular and cell-ECM interactions, nutrient/drug gradient, representative drug resistance data, various stages of cells and phenotypic diversity. Information provided by Law et al.[295].

4.1.2 3D cell culture models

There are multiple ways of creating spherically structured multicellular 3D cell culture models. 3D cell culture models in cancer research can be produced either scaffold-free or scaffold- based. Scaffold free assembly of 3D *in vitro* tumour models can be mainly divided into two types: 1) static technologies including hanging-drop and forced floating [306]; 2) agitation-based culture using dynamic flow technologies using microgravity bioreactors and stirring tank bioreactors [307, 308]. The nature of scaffold based 3D cell culture models to cancer cell culturing is to provide space (or pores) by either biological derived materials or synthetic materials for cells to assemble, to have intercellular adhesion and aggregation happen [304, 309]. It also provides necessary ECM compounds like collagen, growth factors, and mimicking the complexity of *in vivo* tumour associated matrix [307]. Notably both, scaffold-free and scaffold-based 3D cultivation methods have specific advantages and disadvantages (see below).

One of the first 3D cell culture models was soft agar assay. This assay was first designed in 1956 by Puck to cultivate HeLa cells and was further described in 1970s to grow cancer stem cells (CSC) [265, 310]. It has been widely used nowadays to evaluate cellular transformation *in vitro*. In Chapter 3, soft agar assay was introduced and was used to evaluate the impact of TLR4 ligands on CSC colony formation.

Hanging-drop and forced floating methods are also widely used in generating cancer cell spheroids. Cells are either cultivated in low adherent plates or cultivation media droplets to prevent adhesion to any surfaces [302]. With appropriate conditions (stimulations, nutrients or growth factors), cells are able to self-assemble and form round shaped spheroids (Fig .4.1). Those two methods have advantages. Comparing to other 3D cell culture models, they are simple, easy to process in any lab, and cost less. Spheroids can be formed and easily collected from the medium and used for further experiments. In some studies, spheroids were formed with those two methods

and then put into shake flasks/ bio reactors for long-term further growth to improve gas and mass transfer within the spheroids [308, 311] for further analyzation.

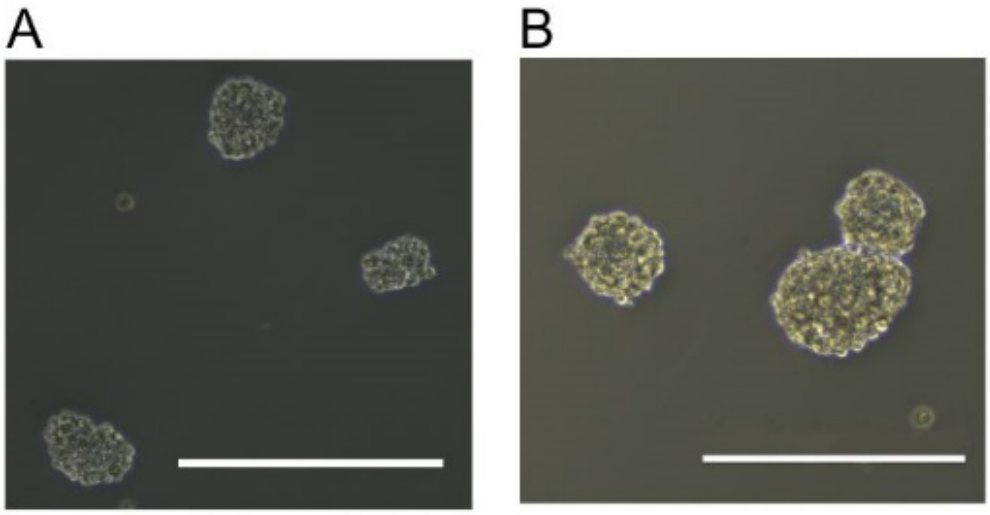

Figure 4.1. Forced floating method could be used to form glioblastoma cell line derived spheroids. A. U373 cell spheroids. **B.** U251 cell spheroids. Scale bar: 400μm.

The scaffold-based 3D cell culture uses acellular matrix to grow cells. The matrix hold the cells and provide the ECM environment for them. Current materials for 3D scaffold are diverse, including natural materials such as collagen based gels, hyaluronic acid/ hyaluronan (HA) based gel, biopolymers, or synthetic based materials (Table. 4.1). Matrigel™, an animal-derived ECM membrane, was discovered and is commercially available since 1984, and has been used widely for cellular applications ever since [312]. Applications of using Matrigel™ were tissue engineering [313], stem cell research [314], and cancer research [315, 316]. This mice-tumour derived ECM contains collagen, laminin, growth factors that can mimic the ECM and has benefits of studying cell differentiation and angiogenesis [317, 318]. However, this type of material is extracted from mice, hence it is difficult to stay consistent among batches or to be well defined [319]. Also, Matrigel™ may contain endogenous growth factors which do not exist in clinic human tumours [302]. To overcome this difficulty and to avoid the batch-to-batch variability of Matrigel, some other manufactured materials have been developed. For example, polymeric scaffolds using synthetic hydrogels, such as polyethylene glycol hydrogel (PEG hydrogel), polyvinyl alcohol hydrogel, and Poly (2-

hydroxyethly methacrylate) hydrogel have been used in 3D cell culture [302]. Those are polymers that forms hydrogel in aqueous solutions. Unlike Matrigel™, those materials gives higher reproducibility and co-culture ability [320]. Advantages of synthetic scaffolds are also clear. Compared to natural gels, synthetic scaffolds do not have batch-to-batch variation. Also, hydrogels is easier to transport soluble chemicals, nutrients, and oxygen to the cells [321]. Currently, there are different types of scaffolds used in cancer cell research, with different advantages and disadvantages (shown in Table. 4.1).

In this chapter, GrowDex® and GrowDex-T® were used as 3D cell culture scaffolds. GrowDex® and GrowDex-T® are natural material derived nanofibrillar cellulose polymers, but GrowDex-T® was coated with negatively charged ion and made into anionic manofibrillar cellulose. Those two materials are both biocompatible with human cells, and had been used on cancer cells, mesenchymal stromal cells, etc. [322, 323]. For many hydrogels, getting clear images of the in-cultured cells could be difficult. This could be affected by spatial gel inhomogeneity, which is known to reduce the optical clarity of several hydrogels including polystyrene, alginate hydrogels, etc. [324, 325]. GrowDex® and GrowDex-T®, however, do not have very high light absorbance or whole visible light spectrum and interferes with multiple microscopy-based methods, including immunocytochemistry and live cell imaging [322].

4.1.3 3D spheroid formation mechanism and microenvironment

In suspension, cells naturally tend to aggregate through self-assembly [326]. This process leads to the formation of multi-cellular spheroids. Mechanistically, this process involves joining ECM proteins, integrin, and E-cadherin [327]. A model with three steps has been suggested by Lin and Chang. In this model, dispersed cells first form loose cell aggregates through integrin and ECM binding, followed by upregulation and accumulation of E-cadherin. Then, E-cadherin forms tight hemophilic cadherin-cadherin bonds between cells and promotes the aggregation and spheroid compaction [328] (Fig. 4.2).

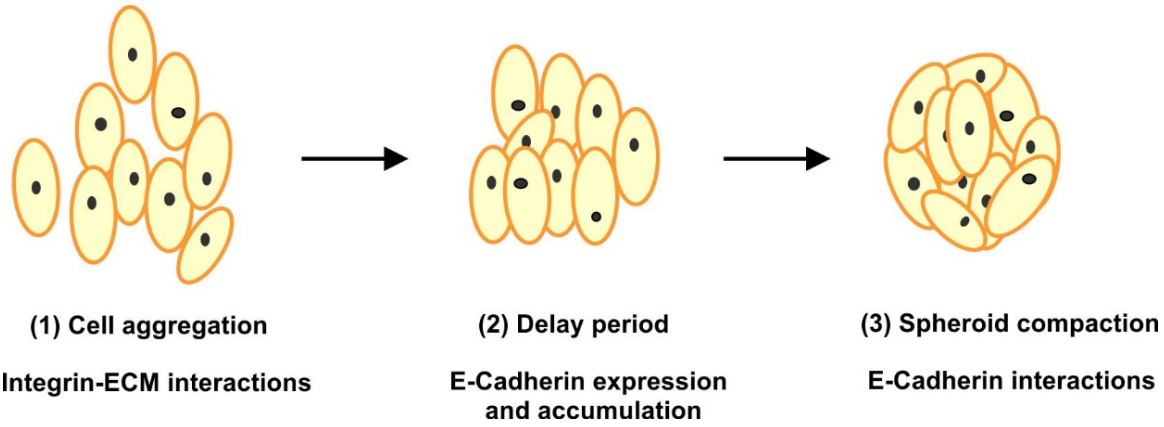

Figure 4.2. Schematic graph of Lin & Chang's model of spheroid formation mechanism. Spheroid formation can be divided into three steps. (1) Cell aggregation; (2) Delay period; (3) Spheroid compaction. Information provided by Lin & Chang [328].

Even though cells aggregate together and form round shaped structures, cells within the spheroids still obtain oxygen and nutrients in the growth medium through diffusion. Therefore, with the growth of the size of spheroids, gradients of oxygen, carbon dioxide, nutrients, growth factors etc. form[328]. Microelectrodes and pH-sensitive indicators were used to determine the diffusion limitation of O_2 and CO_2, suggested that 150-200μm is the maximum diffusion distance [329-331]. Spheroids with diameter > 300μm have been suggested to have varied microenvironment status (Fig. 4.3). Cells at the outside layer of spheroids tend to proliferate, as they can obtain adequate amount of oxygen and nutrient supply. Middle layer of cells are able to survive, but tend to stay quiescent, while the cells at the inner core of the spheroids are under cellular stress. Microenvironment of this inner core is necrotic and anoxic, metabolic waste accumulates in this area, pH value is low, and the cells are innutritious [328]. However, the spheres generated in chapter 3 and this chapter, by using the forced floating method were not big enough to have a necrotic core.

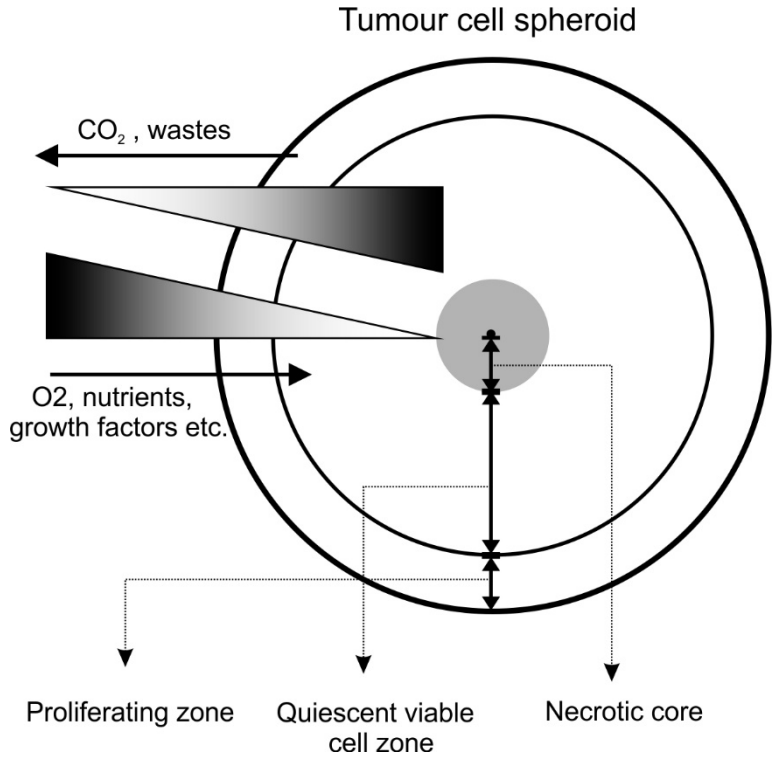

Figure 4.3. Schematic diagram of zones of cells in a 3D spheroid (spheroid diameter >300μm). Three zones of cells could be observed in 3D tumour spheroids, they are proliferating zone, quiescent viable cell zone and necrotic core. Gradient of CO_2 and wastes decreases from core to the outside layer of spheroids. Gradient of O_2, nutrients and growth factors etc. decreases from outside layer of spheroids to the core. Information provided by Lin & Chang [328].

4.1.4 3D culture of GBM

Many studies use 3D cell culture to study GBM and the advantages are clear. The cell response to different therapeutic agents of GBM shows differences between 2D and 3D cell culture models [304]. Compared to 2D cultured cells, 3D cultured glioblastoma cells may have different properties terms of morphology, proliferation, migration, stemness, viability etc. [332]. This may introduce bias in studying anti-cancer drug candidates in pre-clinical trials using *in vivo* animal model. In addition, based on CSC model, 3D spherical culture is able to enrich the CSC percentage in the cell population [106]. CSCs, however, are one of the key focuses of cancer research. They are known to possess specific characteristics such as relative high quiescence, resistance to

chemotherapy agents, radiotherapy resistance, apoptosis resistance, and high hypoxic stability [333, 334]. Therefore, using 3D cell culture to mimic the TME and to help identifying and eliminating CSCs could bring more comprehensive insights to anti-cancer research.

It is becoming increasingly clear that the limited success of GBM clinical trials is related to the molecular heterogeneity among and within GBM tumours [335, 336]. A patient –derived GBM organoid 3D model was described by Fadi et al. This 3D model has the benefits of maintaining many key clinical features of GBM tumours and can be used to discover patient-specific treatment strategies [337]. Yi et al. bio-printed reconstituted GBM tumours from patient-derived tumour cells to study the cell responses to chemo- and radio- therapy [338]. In this study, co-culturing of GBM cells, endothelial cells, and de-cellularized ECM from brain tissue was used. This model mimicked the TME of clinical tumours and was suggested to be an efficient way to identify the effective GBM treatments [338].

Scaffold-based 3D culturing was also used in GBM study. GBM cells were grown in collagen-hyaluronan composite hydrogels by Rao et al. to investigate cell morphology, cell migration and cell invasion in tumours [339]. Collagen and hyaluronan are important compounds in brain ECM, and collagen plays an important role in cell migration [339]. In this study, Rao et al. suggested that GBM migration has an inverse pattern of hyaluronan concentration [339]. Poly(ethylene glycol), another synthetic material was also used to culture GBM by Heffernan et al. U118 and U87 cells were used, and their results suggested that this type of scaffold is useful to generate artificial 3D TME [340].

In this chapter, a cellulose based hydrogen gel GrowDex® was used to grow GBM cell line U251. GrowDex® is a biocompatible material composed of nanofibrilar cellulose and is suitable for *in vitro* research. It mimics the ECM and supports cell growth of different cell types including mesenchymal stem cells and various tumour cells[332]. Compare to other hydrogels, this cellulose based hydrogel allowed me to recover spheroids using cellulose enzyme GrowDase™ to recover cells for further assays [341]. In this chapter, the structure of GrowDex® hydrogel was analysed, and the U251 cell viability, proliferation and Temozolomide resistance was tested.

4.1.5 Advantage of 3D cell culture for future cancer drug discovery

With more and more anti-cancer agents coming to our attention, it seems that 3D cell culture is a promising tool for cancer reseach. Though most 3D cell culture models can only mimic certain aspects of *in vivo* TME, they still provide a much better model for drug discovery. 3D models are suggested to be necessary for preliminary pharmaceutical drug screening, as it will give a more accurate response and more linear drug response compared to 2D drug screening platform [342]. Another benefit of 3D cell culture is to provide potential to produce co-culture of different cell types. Even though this technique was mostly used in tissue engineering, it can mimic and provide a more 'real' TME for cancer research [343]. Currently, great effort is being expended in attempts to recapitulate human TME, but there are many challenges to overcome. Unlike in *in vivo* studies, clinical tumours are located inside the human body, surrounded by ECM and stromal cells, with more complex niche and TME, which are very difficult to fully mimic. In detail, TME *in vivo* is always complex and dynamic, with great complexity of growth factors (FGF2, VEGF, EGF, etc.), cytokines (IL-1β, IL-6, IL-8, etc.), different types of cells (fibroblasts, immune cells, adipose cells, etc.) [344], complex blood vessel, nutrient and oxygen supply, etc.

Nevertheless, although there are limitations, *in vitro* 3D tumour models bridge the gap between 2D-culture systems and animal trials. Different ways have been demonstrated, and the pros and cons of those methods are been evaluated respectively (Table 4. 2). When these methods are being carried out in an actual lab, it is necessary to take into account various factors such as expense, the ease of chemical modification, reproducibility (recapitulation), biocompatibility, batch-to-batch variability, cellular adhesive property, and whether the material is enzymatically degradable, or whether they are recapitulating cells' ECM.

Type of gel	Distribution to oncology study	Advantage	Disadvantage	Examples
Matrigel ™: Reconstituted basement membrane from extracts of Engelbreth-Holm-Swam mouse tumours [345]	Used widely for cell-culturing model systems, particularly for evaluating angiogenesis [317] and cellular differentiation [318].	Able to introduce ECM-specific compounds, including collagen, laminin, fibronectin, growth factors etc. Provide MMP* biding sites, suitable for different cell lines to proliferate or stay stem-like phenotype [319].	Not consistent or well defined. Need to prepare in lab. Have batch-to-batch variability [319].	In tumourigenicity research of breast, ovarian cancer cell lines [315], xenografts [316], stem cell research [314] and tissue engineering [313].
Collagen-based gel	Establish *in vitro* models for evaluation of EMT and cellular behaviour.	Collagen gel mimics ECM, as collagen is the most abundant protein in ECM, and provides similar properties like ECM. Also, it is able to add different synthetic cross-linking agents, cytokines and growth factors to the gel.[346]	Low in collagen intensity, large percentage of fluid [347]	Fabrication of nano-and microstructure by plastic compression[347]
Hyaluronic acid/hyaluronan (HA) based gel	HA is associated to tumour progression and could also be used as 3D scaffold in oncology.	HA is chemical versatile, able to tailor the mechanical features. Able to add compounds like MMP between HA chains [348]. It is also found in ECM, can mimic the TME [349].	May have physicochemical effects to cells due to the high molecular weight (1000-8000kDa) and coiled chain [349].	HA-polyethylene glycol hydrogel used in tissue engineering [350]. Cross linking HA with divinyl sulfone for cell culturing [351]

Biopolymers: nanofibrillar cellulose	Could be used as good supports as scaffold material.	Low immunogenicity, good for biocompatibility [352].Easy for medium and metabolite exchange[353]. Very good control of the growth factors, cytokines and nutrient amounts. Easy to degrade and recruit cells for further analysation. Little absorbance of visible light, suitable for microscopy [323].	Need to add ECM components like growth factors and serum in the culture.	GrowDex® and GrowDex® -T[323]

Table 4. 2: Types of different 3D cell culture scaffolds, the applications and pros and cons of the materials. [307]

MMP: matrix metalloproteinases.

4.2. Results

GrowDex-T® aNFC hydrogel microarchitecture contain heterogeneous pore sizes.

0.5% aNFC hydrogel microarchitecture was scanned using electron microscopy (SEM). High- resolution SEM images showed a dense mesh-like network of nanofibers (Fig. 4.4). Mean fibre diameter was measured as 28.8± 0.6nm (Fig. 4.5A). For pore size, the average value was 10.5 ± 0.9 μm^2 (Fig. 4.5B). Among small sized pores (<10μm^2), 2/3 pores are having sizes less than 4 μm^2 (Fig. 4.5C).

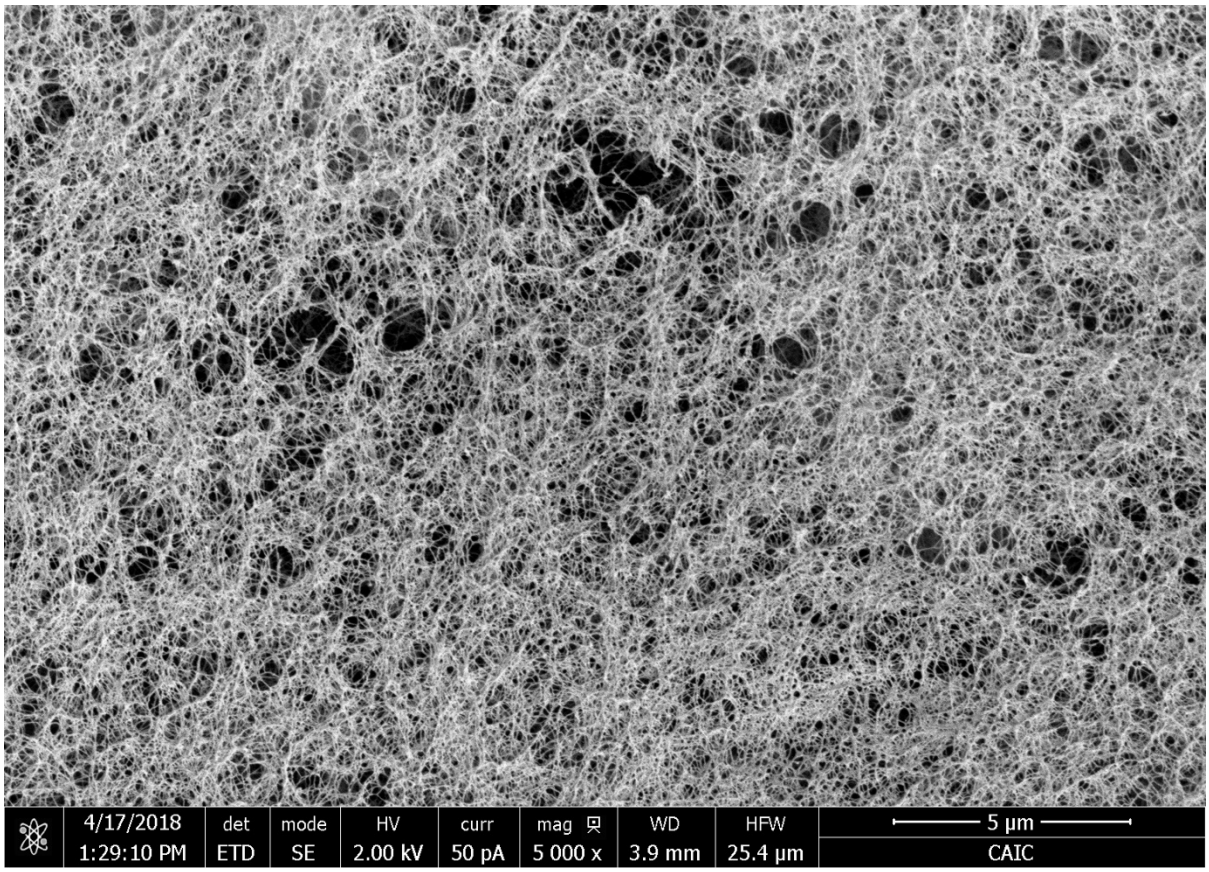

Figure 4.4. SEM imaging of 0.5% GrowDex® aNFC. Scale bar =5µm. Showed the dense-mash nanofiber structure of 0.5% aNFC, in which heterogeneous pores had been formed. Picture provided by J. Sheard et al. supplementary data [322].

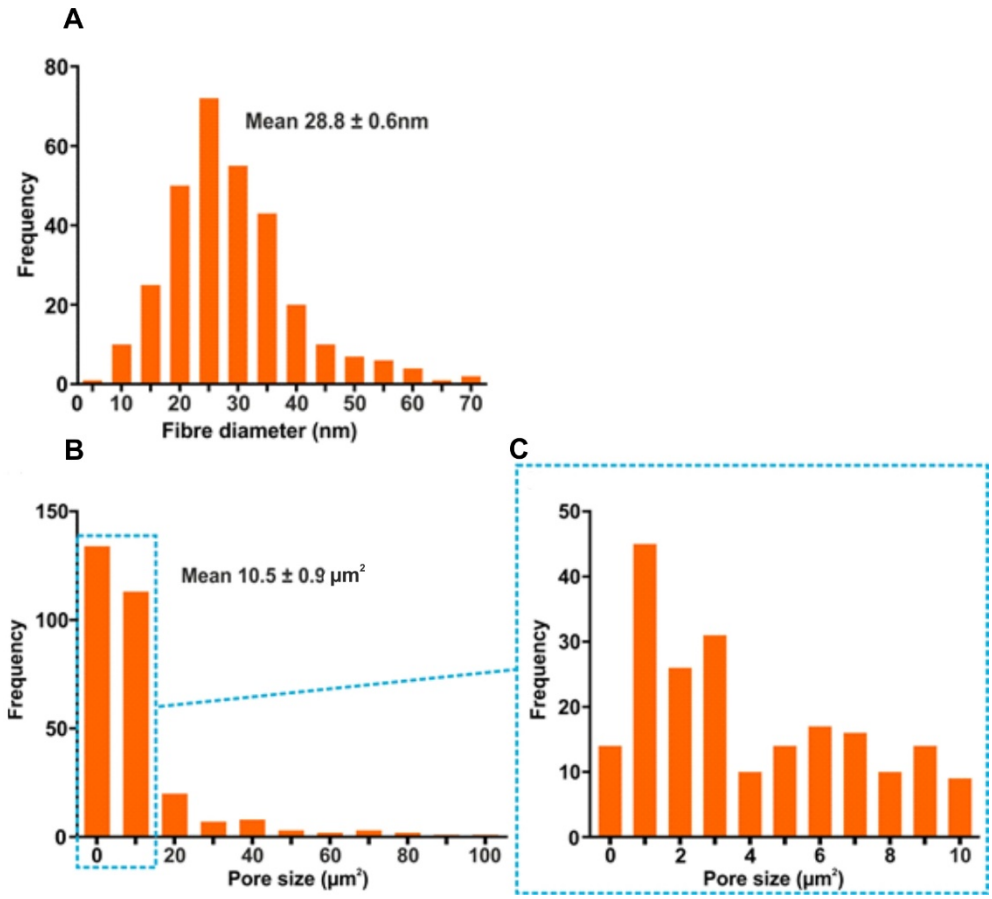

Figure 4.5. Distribution histogram of 0.5% 3D aNFC hydrogel fibre diameter and pore size ranging from 1-100μm². **A.** Distribution of fibre diameter, mean fibre diameter was 28.8± 0.6nm. **B**. Distribution of fibre pore size, mean area was 10.5 ± 0.9 μm². **C.** Distribution of fibre pore size <10 μm². [322]

U251 cells grown in different concentrations of NFC forms different sizes of spheroids.

U251 cells were seeded in 0.1%, 0.2% GrowDex® NFC hydrogel 1000 cells/μl, pictures were taken (Fig. 4.6A&4.6B). Circle area of all distinguishable spheroids were measured. There is significant difference of spheroid size between the two groups (Fig.4.6C). Mean circle area of spheroids in 0.1% aNFC was 1481.5 μm², and the mean circle area of spheroids in 0.2% NFC was 4627 μm². Diameter of 50 spheroids per picture was also measured. There was significant difference between the two conditions. Mean value of spheroids diameter was: 100.42μm

of spheroids in 0.1% NFC; 42.62μm of spheroids in 0.2% NFC. It is worth to mention that, when cultivate U251 cells in 0.1% NFC, there were several spheroids that were much bigger than the rest (Fig. 4.6A). Top 15 biggest spheroids in 0.1% NFC has an average diameter of 170.3 μm. The biggest oval-shaped spheroid 0.1%, has its transverse of 397 μm (pointed with arrow in Fig. 4.6A). Results suggested that spheroid size in the 0.1% NFC has higher variety compare to the spheroid size in 0.2% NFC, 0.1% NFC cultivated U251 can form much larger spheroids compare to 0.2% NFC cultivated U251.

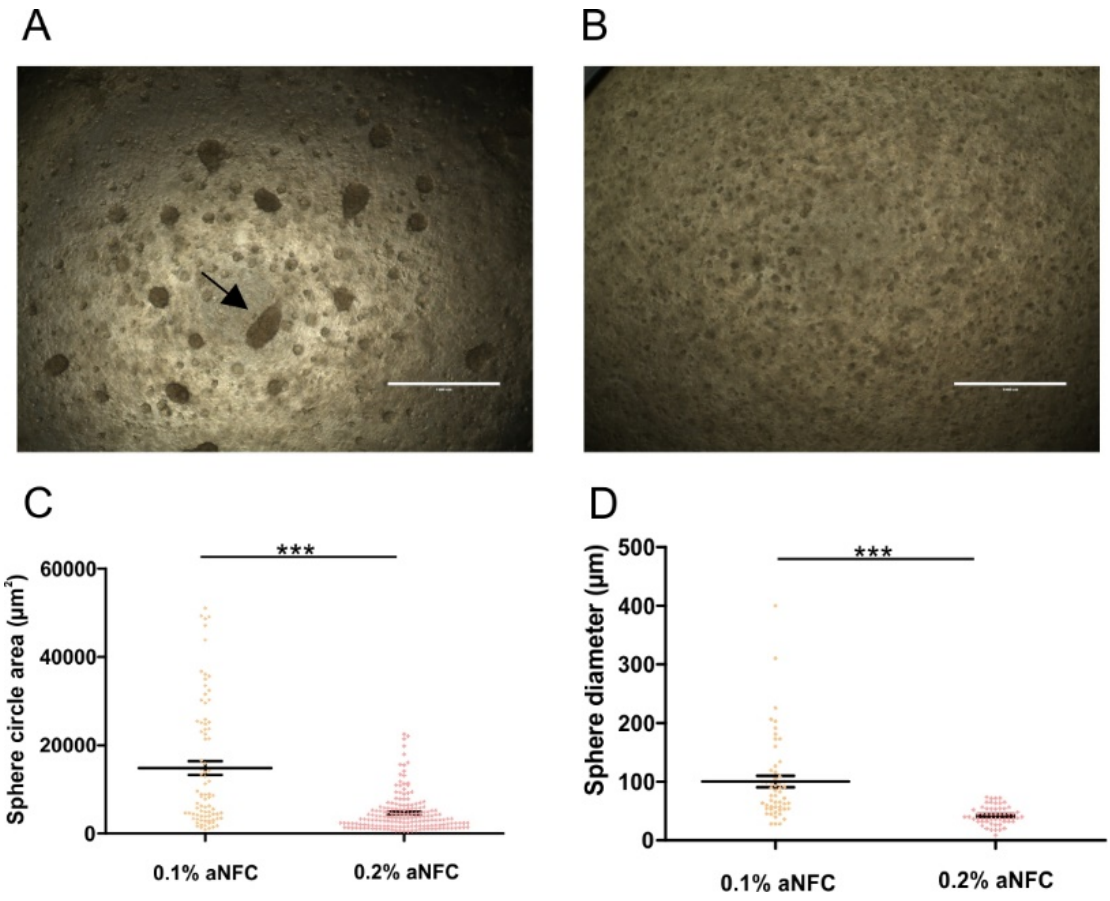

Figure 4.6. U251 cell spheroids pictures and sizes in 0.1% NFC and 0.2% NFC. A. U251 cells seeded in 0.1% NFC with 1000cells/μl. Arrow: the biggest spheroid formed in this well. **B.** U251 cells seeded in 0.2% NFC with 1000cells/μl. **C.** Spheroids' size measurement. There is significant difference of spheroid sizes. Scale bar= 1000μm. ***p<0.0001. n=3.

U251 cells cultivated in 0.1% NFC, 0.2% NFC showed no significant difference in cell viability.

U251 cells were seeded in 0.1% NFC, 0.2% NFC with 500 cells/μl and 1000 cells/μl respectively. After 7 days of cultivation, cell viability (total cell metabolic rate) was measured. There was no significant difference between the 500 cells/μl 0.1% NFC and 500 cells/μl 0.2% NFC group, or 1000 cells/μl 0.1% NFC and 1000 cells/μl 0.2% NFC group, indicated that the cell viability was not affected by the percentage of NFC hydrogel (Fig. 4.7). Due to the low cell numbers in 2D control, it is reasonable that the control group had lower viability/ metabolic rate than 3D cultivated cell groups.

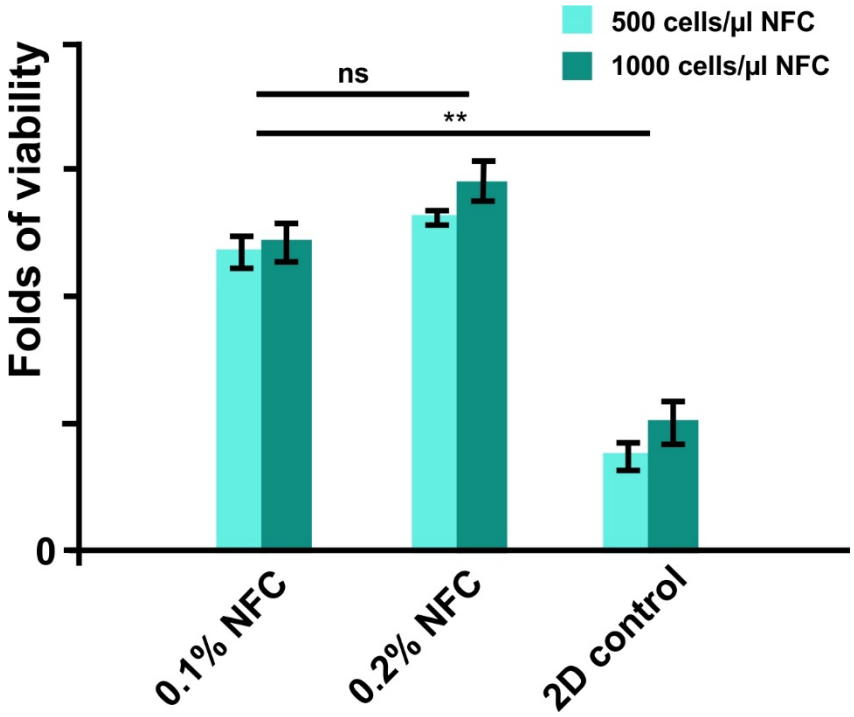

Figure 4.7. Viability of U251 cells measured by XTT assay was not impacted by the concentration of NFC. U251 cells were cultivated in 0.1% NFC and 0.2% NFC hydrogel, with 500 cells/μl and 1000 cells/μl. n=3. **p<0.01.

TNFα and *E. coli* LPS promote the spheroid formation in 0.2% NFC at both spheroids' number and size.

U251 cells were seeded in 0.2% NFC with 1000 cells/μl and treated with TNFα, *E. coli* LPS and *S. minnesota* LPS in the top layer of growth medium. Blank treatment was used as control. After 7 days of treatment, pictures of spheres were taken (Fig. 4.8). Spheroid number was determined. Under the stimulation of TNFα and *E. coli* LPS, there were significant increase of cell numbers in those two groups in comparison to control group and *S. minnesota* LPS treated group. However, there was no significant difference between the *S. minnesota* LPS and the control group. In addition, spheroids' diameter were measured. Significant sphere size increase could be observed in TNFα and *E. coli* LPS treated group in comparison with *S. minnesota* LPS treated group and control group. There is no significant difference between the *S. minnesota* LPS treated group and control group (Fig. 4.9). Results suggested that the TNFα and *E. coli* LPS are able to promote the spheroid growth.

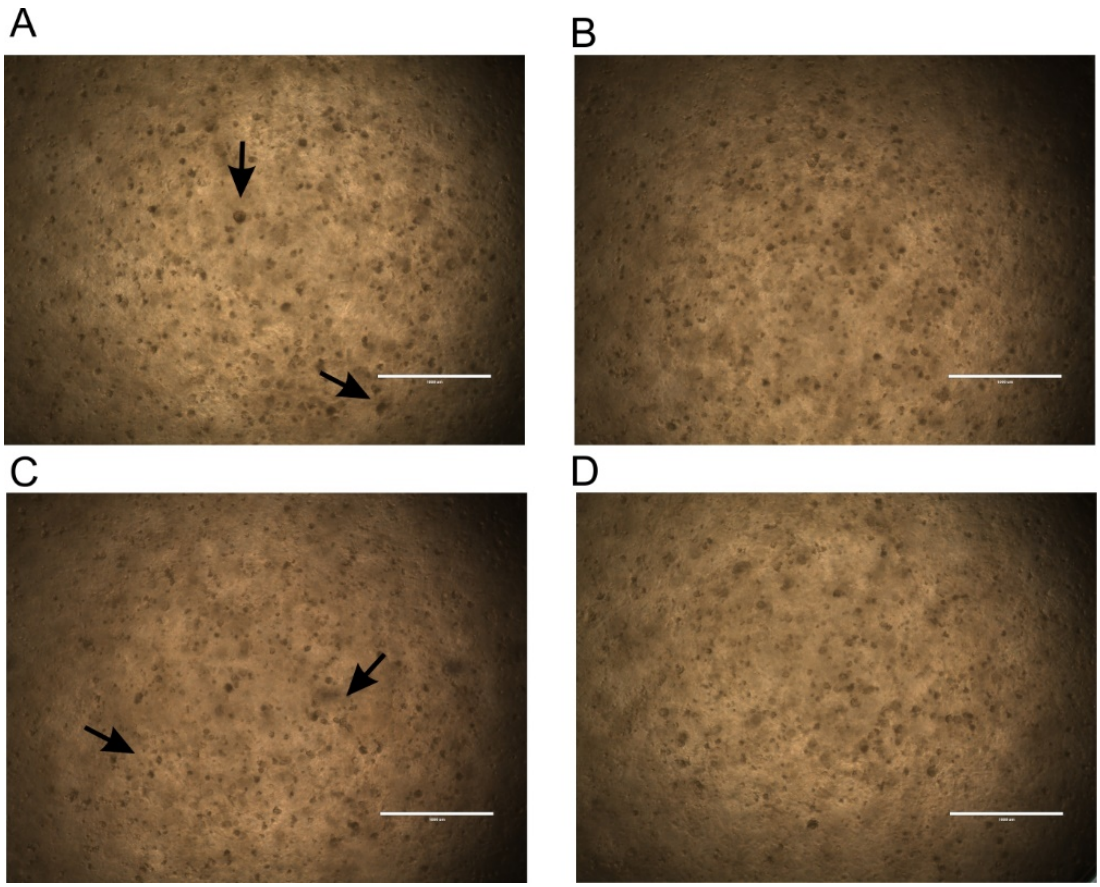

Figure 4.8. TNFα and *E.coli* LPS treated U251 formed larger spheroids than *S. minnesota* LPS treated U251 and untreated control. U251 cells were seeded in 0.2% aNFC for 7 days, treated with TNFα, *E. coli* LPS and *S. minnesota* LPS**. A.** TNFα treated spheroids. Arrows: some large spheroids was formed under the treatment of TNFα. **B.** *E. coli* LPS treated spheroids. **C**. S. minnesota LPS treated spheroids. Arrows: The size of spheroids formed under the treatment of *S. minnesota* LPS were relatively smaller than TNFα treated spheroids' size. **D.** Untreated spheroids. Scale bar=1000μm.

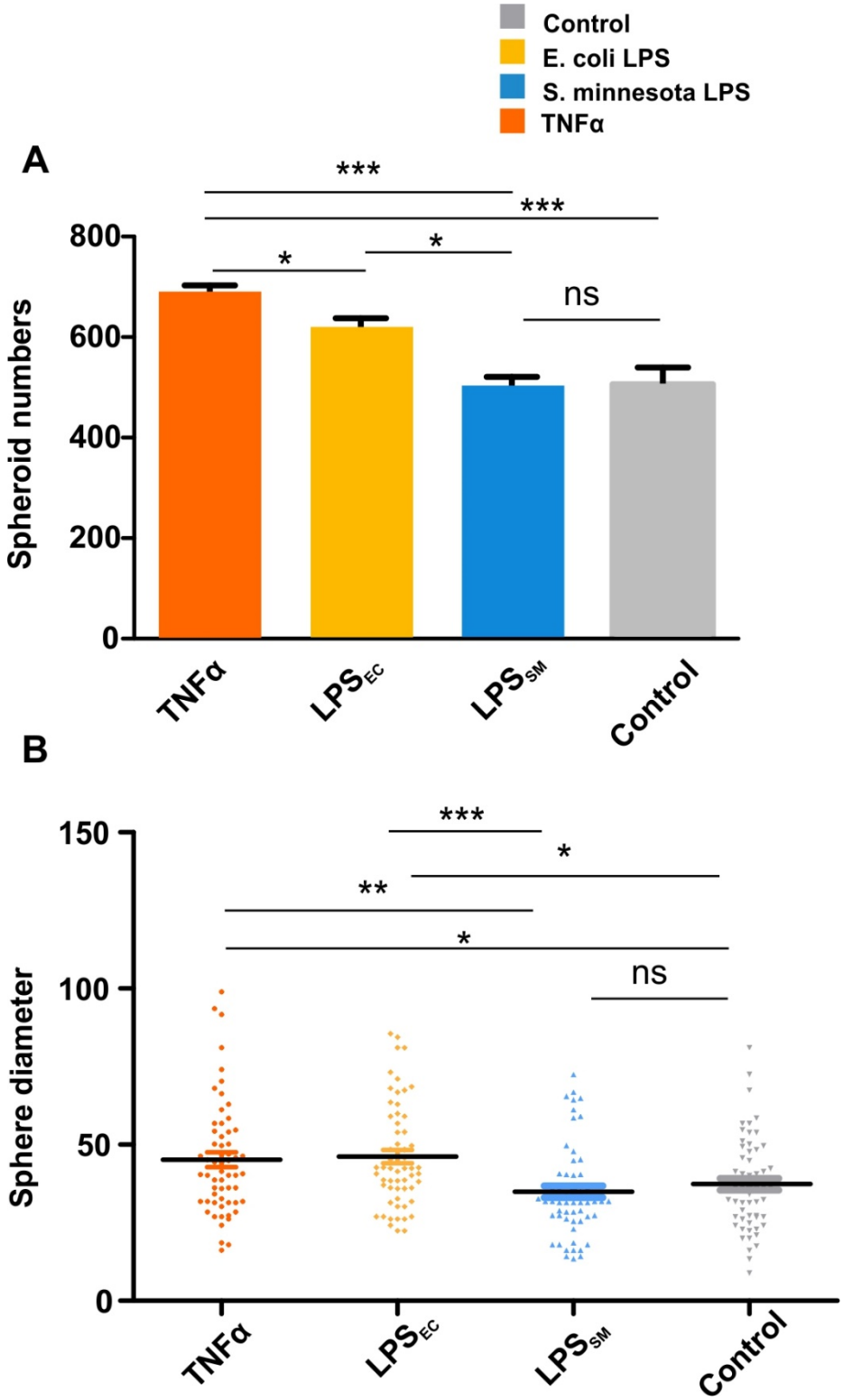

Figure 4.9. TNFα and *E. coli* LPS increased the number and diameter of spheroids in 0.2% aNFC. A. Spheroid number of four groups. Significant increase could be seen in TNFα, *E. coli* LPS treated U251 cells, no significant difference could be seen in *S. minnesota* LPS treated U251 cells. **B.** Spheroid diameter of four groups. Significant increase could be seen between in TNFα and

E.coli LPS treated group. No significant difference could be seen between *S. minnesota* LPS treated and control group. *p<0.5, **p<0.01, ***p<0.001. n=3.

Proliferation rate of U251 cells in 0.2% NFC hydrogel is higher than 2D culturing but is not effected by TNFα.

U251 cells were treated with TNFα for 72 hours in 0.2% aNFC hydrogel. GrowDase™, the cellulose digest enzyme for GrowDex® was used to recruit spheroids from the NFC hydrogel. Cells were seeded in 100µl 0.2% NFC in 96 well plates at 100 cells/µl density. In parallel, U251 cells were seeded in 2D with same amount of cell number. After 72 hours, it is significant that 0.2% NFC cultured cells proliferate significantly quicker than 2D cultured U251 cells (Fig.4. 10), which could due to the growth space difference for the cells. However, there is no significant difference of TNFα treated 0.2% aNFC cultured cells and non-treated 0.2% NFC cultured cells.

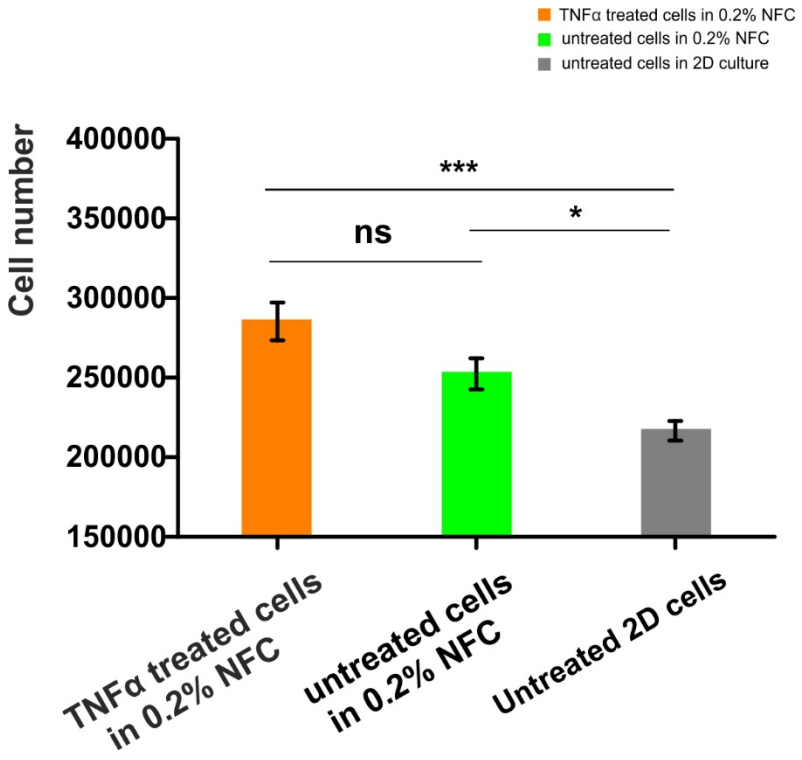

Figure 4.10. U251 cell number in 3 days of cultivation in 0.2% aNFC were significantly higher than in 2D cultivation. Significant increase of cell number could be seen in 0.2% aNFC cultivated cells in comparison to 2D cultivated cells.

TNFα increases the percentage of nestin positive cells.

Untreated spheroids in 0.2% aNFC were scanned using ICC. Spheroids were located 100-200 μm above the bottom of the well, formed different sizes of spheroids. TNFα treated, TNFα+ NF-κB inhibitor Bay11-7082 treated and untreated spheroids were shown in Fig. 4.11 A-F. Significantly increase percentage of nestin positive cells could be observed in TNFα treated and TNFα+ NF-κB inhibitor Bay11-7082 treated spheroids compare to untreated spheroids. (Fig.4.12) One spheroid from TNFα + Bay11-7082 was picked to deep analyse the percentage of nestin. This newly developed 3D volumetric analysis is able to analyse the spheroid volume, spheroid diameter, and process cell count. In this particular spheroid, (spheroid of Fig. 4.11C, Fig. 4.13 & 4.14). 25 out of 136 cells were marked as nestin positive cells, occupied 18% of the spheroid cell population, but nestin positive area only occupied 4.1% of the spheroid volume (Fig. 4.13, Table 4.3).

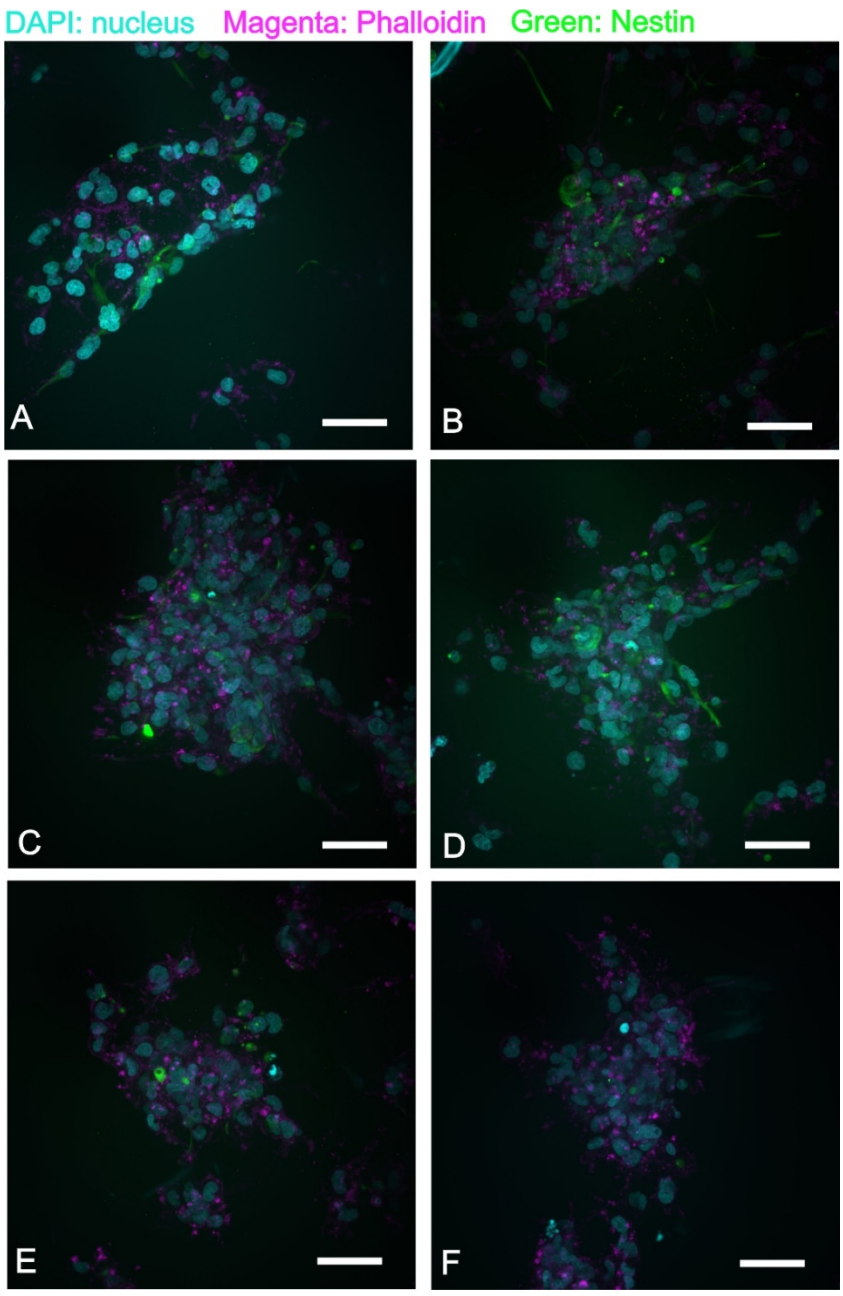

Figure 4.11. ICC of TNFα treated spheroids, TNFα + Bay11-7082 treated spheroids and untreated spheroids. A&B: TNFα treated spheroids. C&D: TNFα + Bay11-7082 treated spheroids. E&F: untreated spheroids. Spheroid A,B,C, and D contain more nestin positive cells than spheroid E&F. Cyan: DAPI. Magenta: Phalloidin. Green: nestin. Scale bar= 50μm.

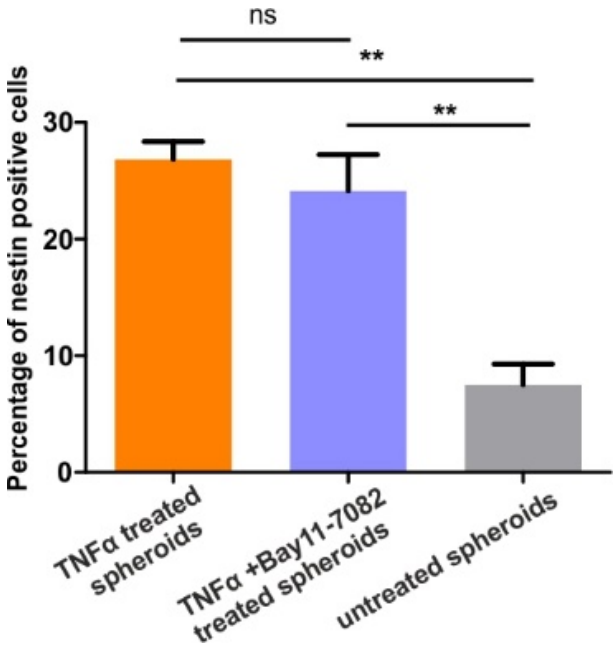

Figure 4. 12. TNFα and TNFα + Bay11-7082 treated spheroids contained higher percentage of nestin positive cells. Significant increase of nestin positive cells could be seen in TNFα treated spheroids, TNFα + Bay11-7082 treated spheroids in comparison to untreated cells. **p<0.01. n=3.

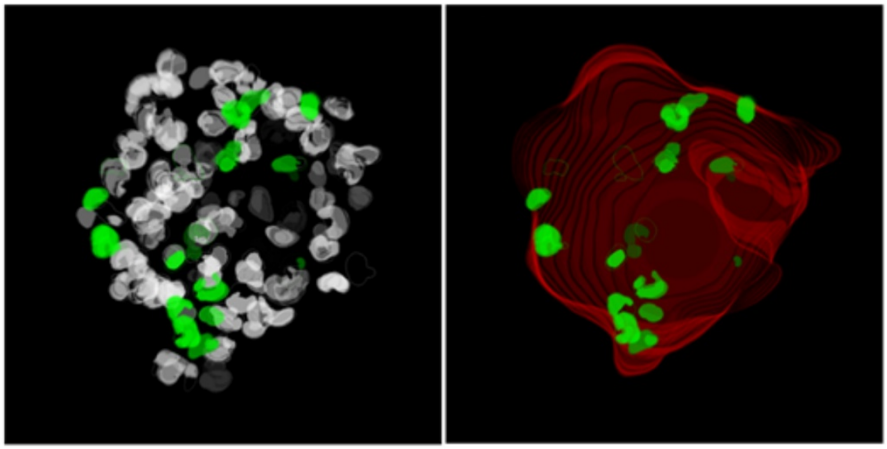

Figure 4. 13. Software image of 3D volumetric analysis of a TNFα + Bay11-7082 treated spheroids showed nestin positive cells exist in U251 spheroids. Nestin positive cells are distributed mainly in the middle layer of the spheroid. (My own work, published [323].)

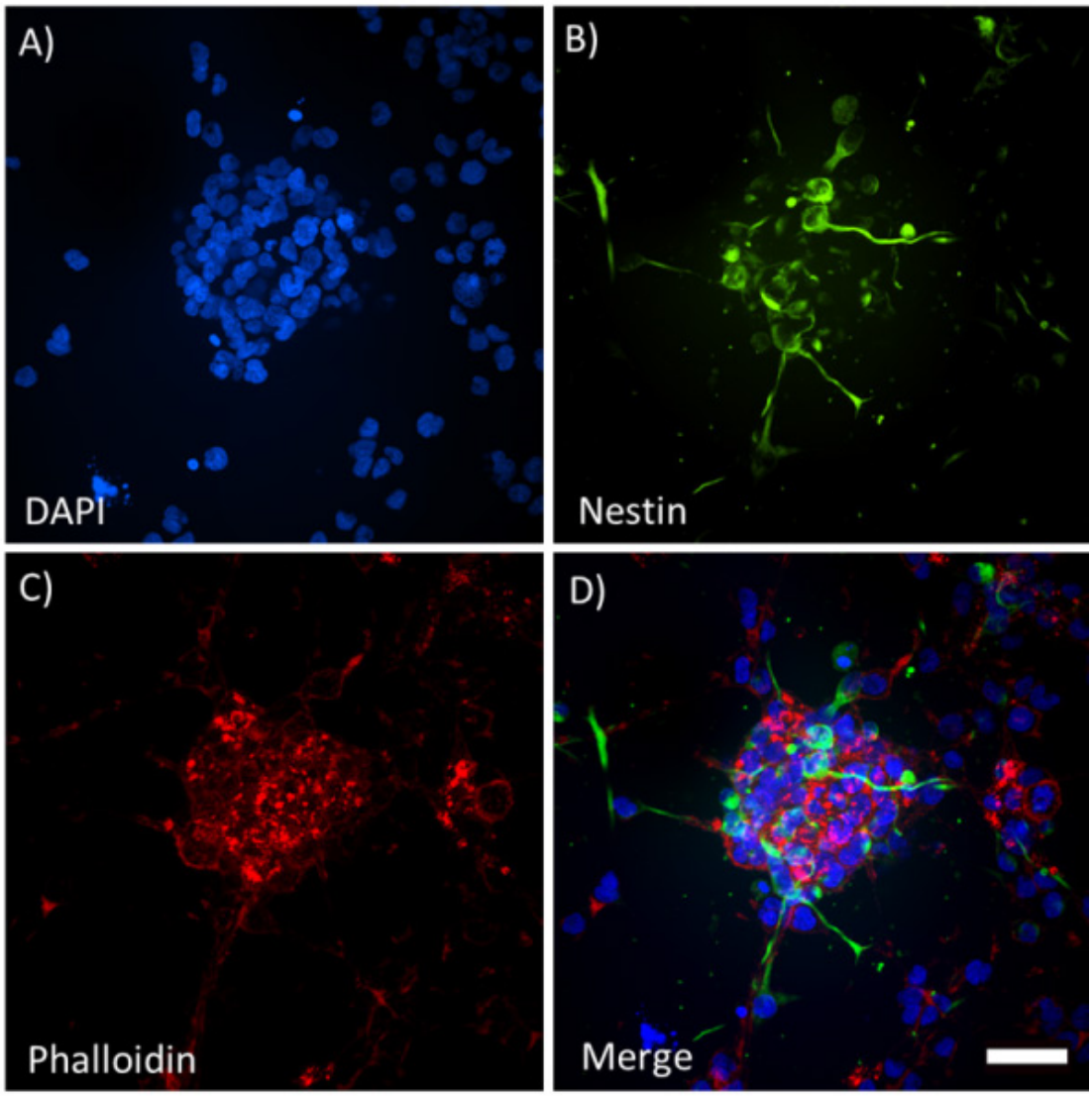

Figure 4.14. High clarity images of 3D volumetric analysis of a TNFα + Bay11-7082 treated spheroids grown in GrowDex-T®, showed that CSCs located at the ledge of spheroids. Higher nestin expression level could be observed in the surrounding cells of the spheroid. Maximum projection images of the U251 spheroids were acquired on the ImageXpress Micro Confocal system using the 40x Water Immersion CFI Apochromat LWD Lambda S. Z-stack of 120µm (20 x 5µm step size). Spheroid was hold by the scaffold and there were some single cells surrounded next to the spheroids. Clear nestin labeled cells could be observed.. Fixed spheroids were labelled for: **A.** DAPI. **B.** Nestin. **C**. Phalloidin. **D.** All channels merged. Scale bar = 50µm. (My own work, published [323].)

Measurement	Spheroid
Spheroid volume	612640 μm^3
Spheroid Diameter	135 μm
Spheroid Depth	85 μm
Total cell count per spheroid	136
Nestin-positive cell count	25
Percentage nestin-positive cell per spheroid	18%
Nestin-positive volume	25176 μm^3
Average distance between positive cells	15.9 μm

Table 4. 3. 3D volumetric analysis of one spheroids [323].

0.2% NFC cultured U251 cells has higher resistance to Temozolomide compare to 2D cultured U251 cells

TMZ, one of the traditional GBM chemotherapy reagent, was used to test if the 3D culture can increase the drug resistance of U251. Cells were cultivated for 3 days to allow cells to process at least one cell cycle. Using XTT assay, IC_{50} of TMZ was determined. Data was normalised using the average absorbance of XTT assay of untreated cells. Prism was used to analyse the curve. IC_{50} of U251 cells 2D cell culture was 109.6 μM, and the IC_{50} of which in 0.2% NFC was 162.7 μM. Results suggested the 3D cell culture in 0.2% NFC increased the *in vitro* TMZ resistance of U251 cells (Fig. 4.15).

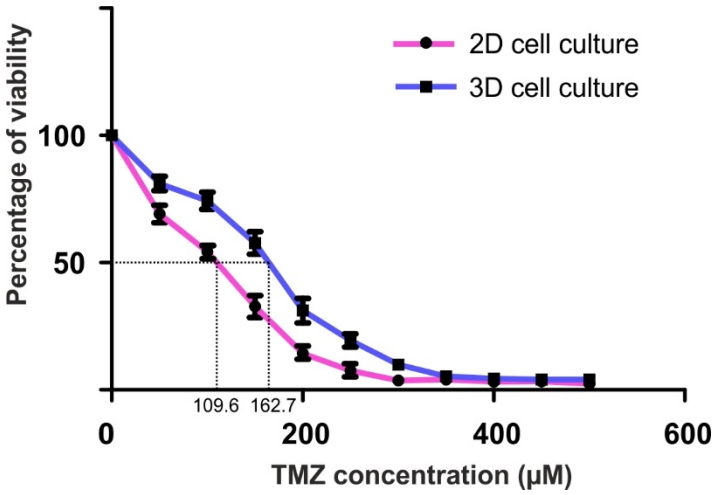

Figure 4.15. 0.2% NFC 3D cultured U251 cells had higher IC_{50} compare to 2D cultured U251 cells. IC_{50} of TMZ in 2D cell culture was 109.6 μM, and the IC_{50} of which in 0.2% NFC was 162.7 μM.

4.3. Discussion

In 3D cell culture models, many types of scaffold materials have been used. For 3D scaffold-based cell culture, it is always necessary to test if the material is biocompatible and to study the microstructure of the material. In this chapter, NFC and aNFC were used to grow GBM cells. A similar study was carried by Rao et al. using collagen- HA composite hydrogels. Compared to collagen-HA hydrogel (Fig. 4.15), the aNFC hydrogel I used had smaller and less variant pore size. The pore size of 0.5% aNFC had a mean value of 0.5 ± 0.9 μm^2, and 87.4% of the pores had sizes < 20 μm^2 (Fig. 4.5). Even though different concentrations of the hydrogel were expected to result in different pore sizes, the result with 0.5% aNFC showed that the material was steady and dense, formed a mash-like network for cells to grow (Fig. 4.5). In addition, the viability of U251 cells was not affected by the use of the NFC hydrogel (Fig. 4.7). Therefore, GrowDex® is a suitable material for 3D cell culturing in this project.

Hydrogel scaffold is very useful in studying the 3D cell behaviours, as it provides space for cells and has great penetration level for O_2 and nutrients. In this chapter, U251 cells were seeded in 0.2% NFC hydrogel. NF-κB biased TLR4 ligand *E. coli* LPS, and IRF3 biased TLR4 ligand *S. minnesota* LPS were

used to treat U251 cells. TNFα was used as positive control to activate NF-κB. Under the stimulation with TNFα and *E. coli* LPS, more and larger spheroids were formed in comparison to *S. minnesota* LPS treated group. This result could be explained by two different phenomena: faster spheroid assembly and cell proliferation. My hypothesis is that NF-κB activation first caused U251 cells to assemble with fewer cell numbers, then promoted proliferation of U251 CSCs after the formation of spheroids. Lin& Chang's model suggests that E-cadherin is one of the essential proteins during the spheroid assembly progress [328]. As cadherin-cadherin bonds are key in the spheroid formation process, more E-cadherin could lead to assembly of more cells and quicker assembly rate. Chua et al suggested that NF-κB can repress E-cadherin expression [354]. Therefore, when NF-κB was activated by the TNFα or NF-κB biased ligand *E. coli* LPS, those U251 cells expressed less E-cadherin. This could cause the cells to from smaller spheroids and more spheroids. Additionally, TNF had been proved to enhance the neuro stem cell aggregation [355]. In other words, due to the lack of E-cadherin, instead of forming less and bigger spheroids, those cells that were close to each other may tend to form smaller and more spheroids instead. After the spheroids formation, during the 7 days of cell cultivation, the CSCs proliferated. In chapter 3, my results of soft agar assay indicated that NF-κB activation increases the tumourigenicity of U251 cells. Also, Ferrandez et al. suggested that NF-κB activation is able to induce proliferation of glioblastoma CSCs [198]. Therefore, in 3D NFC hydrogel, TNFα and the NF-κB biased ligand *E. coli* LPS treated U251 CSCs may had higher proliferation rate and higher tumourigenicity. As result, after 7 days of cultivation, U251 treated with TNFα and NF-κB biased ligand *E. coli* LPS formed more spheroids and some larger spheroids compared to *S. minnesota* LPS treated untreated U251 cells (Fig. 4.9).

To further study the impact of NF-κB activation on U251 proliferation in 3D, U251 cells were seeded in 3D NFC and 2D in parallel. The results revealed that 3D cultivation increased the proliferation of U251 compared to the conventional 2D cultivation. However, there was no significant change but trend toward an increase of proliferation rate between the TNFα treated and untreated spheroids in 3D. This fit with my proliferation assay results in Chapter 3

(Chapter 3, Fig. 3.5). However, in Chapter 3, my results also showed that NF-κB biased TLR4 ligand *E. coli* LPS was able to increase the percentage of CSCs in U251. Therefore, NF-κB activation may not significantly affect the total proliferation rate of U251, but might have a positive effect to CSCs on cell proliferation, which has also been demonstrated by Ferrandez et al. [198]. Here, cell proliferation was evaluated using cell counting. GrowDase™, the enzyme that digests NFC was used to collect the spheroids from the 3D scaffold. This is one of the benefits of using GrowDex® hydrogel. In many 3D cell culturing models, recovering spheroids from the scaffold can be difficult. In those cases, the mechanisms of cell proliferation assay provided in market were mainly based on evaluating cell metabolism rate or the quantification of cell proliferation linked proteins, but not measuring the cell numbers directly [356-358]. By using the digestible scaffold GrowDex®, it was much easier to collect the cells after various treatments and determine the cell numbers and thus the proliferation rate of the total cell population. In contrast to other hydrogels, aNFC as a 3D scaffold allows simple light imaging [322]. U251 cells were seeded in aNFC and treated with TNFα. After 7 days of treatment, U251 spheroids were fixed in the aNFC for confocal imaging. Because of the optical properties of the scaffold, high clarity pictures of fixed spheroids could be taken. The images showed the exact distribution of the spheroids within the scaffolds (Fig. 4.14) [323]. U251 cells were stimulated with TNFα, and TNFα + NF-κB inhibitor Bay11-7082. In both conditions, there was an increase of Nestin expression, suggesting that TNFα could have increased the stemness of U251 cells (Fig. 4.12). In my 2D cultivation result in Chapter 3, the increase of nestin expression was not significant when cells were treated with TNFα. As 3D cell cultured cells could recover some critical characteristics of tumour cells absent in 2D [302], this result suggested that TNFα and NF-κB activation could increase the stemness in clinical GBM tumours.

Interestingly, TNFα + NF-κB inhibitor Bay11-7082 treatment still increased the nestin expression in the spheroids. Bay 11- 7082's inhibitory function was to inhibit the translocation of NF-κB by inhibiting the phosphorylation of IκB-α and the translocation of p65 [359]. Based on the results showed by Lee et al., the translocation of p65 could still be observed after 60 mins of the treatment of

Bay + LPS, meant that the p65 translocation still happened after adding the inhibitor[359]. In addition, Lee's results showed that with the 10μM of Bay11-7082 added to the cells, a significant increase of NF-κB in HEK293 cells could be tested using NF-κB luciferase assay [359]. Those results indicated that with 10μM of Bay and 10μM of TNFα added to the U251 cells, there might not be full inhibition of NF-κB activation, hence it is reasonable to see an increased expression of nestin in those cells (Fig. 4.12). It is worth to mention that, within the untreated spheroids cultured in 3D aNFC, the percentage of CSCs was 7.48± 2.5%, while in Chapter 3, the percentage of CSCs in spheroids produced using forced float method was 8.07± 1.48%. There was no significant difference of CSC percentage in spheroids cultivated between those two methods.

One spheroid treated with TNFα and Bay11-7082 was analyzed using 3D volumetric analysis. The nestin positive cells were labeled out (Fig. 4.13). Results showed that there was 18% of CSCs in this particular spheroid, which distributed mainly in the outside layers of the spheroid. Peng et al. studied the distribution of CSCs in human GBM using clinical GBM specimens. Peng's results showed that the percentage of $CD133^+$ cells and $SOX2^+$ cells (CD133 and SOX2 are the CSC markers chosen by Peng et al.) were significantly higher at the infiltrating tumour edges in comparison to other tumour areas. In addition, CSCs were also found to have high percentage in the peritumoural normal brain area [360]. Peng's results suggested that CSCs are responsible for the tumour invasion and progression. In some studies, CSCs have been found to locate near the core of the spheroids instead. Ham et al. demonstrated that the breast cancer spheroids core cells express CSC- linked genes [361], while in some other studies, CSCs have been found in both core region and edge regions. Gomez et al. suggested that in head and neck cancer spheroids, CSCs could be divided into non- invasive core region CSCs, and invasive edge region CSCs[362]. In my results, CSCs were also found in the outer layer of spheroids, indicated that 3D scaffold cell culture helped restoring the actual stemness features of the CSCs in the tumour spheroids, might related to invasiveness. By using 3D scaffold, in the future, CSCs behaviours could be better studied.

Due to the obvious advantages in providing more physiologically relevant information, and more predictive data for *in vivo* tests, 3D cell culture system have gained huge interest in drug discovery and pre-clinical tests [304]. As 3D cell culture helped mimicking the clinical tumour microenvironments, it is able to provide a simpler, faster and more cost-effective drug testing compared to using animal models. Compared to 2D cell culture, 3D cell culture could also give more reliable data about drug resistance. TMZ resistance was tested in 2D and 3D cultured U251 cells. A dramatic increase of TMZ resistance was shown in the 3D cultured cells using XTT assay (Fig. 4.15). By moving U251 cells to 3D cell culture from 2D cell culture, their IC_{50} of TMZ increased by 1/3. The IC_{50} of U251 in 3D cell culture was 162.7μM. In other studies, the suggested IC_{50} of TMZ of GBM cells varied. IC_{50} of U251 was tested around 100μM by Agnihotri et al. [363], 50μM by Ujifuku et al. [364], 50~100μM by Nifterik et al. [365]. In those studies, U251 were cultivated in 2D. However, in a 3D cell culture study demonstrated by Eroje and Waston, IC_{50} of U251 was 242.4 μM [366], and in a study using patient derived GMB cells, the IC_{50} could be vary from 94.3μM to 1049μM[367]. Those numbers showed that the drug resistance of cells in 3D cell culture is higher and closer to the clinical tumours. However, these differences in the IC_{50} values of TMZ could be caused by the different experimental conditions. The length of TMZ treatment, the cell passage number of cell lines, the sample variety of primary cells, and the hypoxic cell culture conditions could all o affect the IC_{50} of TMZ [367]. My results showed that 2D and 3D cultured U251 cells had different sensitivity to classical GBM chemotherapy drug TMZ exposure. As similar theory was also suggested when testing Trastuzumab in breast cancer. Trastuzumab is a monoclonal antibody that targets HER2 in breast cancer cells. Pickl and Ries demonstrated that Trastuzumab showed dramatically different effects on 2D cells as compared to those in 3D. They suggested that 3D cell culture had benefits in reflecting *in vivo* aspects of HER signaling, hence it should be a better model to test Trastuzumab [368]. However, 3D cell culture does not necessarily induce higher drug resistance of cells. Anti-cancer drug Tirapazamine, a hypoxia-activated cytotoxin, was demonstrated to have higher efficiency in 3D spheroids compared to the 2D monolayers of cells, as 3D spheroids had higher numbers of hypoxic cells than 2D [369]. When human epithelial carcinoma cell line was

treated with 72 hours 10μM Tirapazamine, the viability of 2D cells was around 75%, but the viability of 3D cells was lower than 40% [369]. Those results suggested that, different cell culture environment could be crucial when testing the drug responses of cells. In addition, the drug penetration in spheroids could also affect the drug efficiency [370].

4.4. Conclusion

In this Chapter, 3D cell culture was introduced and had shown great benefits on GBM in comparison to 2D monolayers. Currently, a variety of 3D cell culture models is being developed. One of the 3D scaffold cell culture models, GrowDex®, was used in this chapter for GBM cell line culture. U251 cells showed a significant increase of tumorigenesis and stemness when stimulated with TNFα in 3D cell culture. My results also demonstrated that U251 cells in 3D cell culture proliferated quicker than 2D and had higher resistance to TMZ.

3D cell culture can contribute a lot to drug discovery. Currently, standard procedures in drug discovery star with screening drug candidates in 2D cell culture-based analysis, followed by *in vivo* animal tests and then clinical trials. Evidence showed that many of the drug candidates failed during clinical trials, due to the lack of clinical efficiency or high toxicity [371]. Therefore, to improve the current drug development process, 3D cell culture could be an efficient method to bridge up the gap between 2D cell culture and pre-clinical trials.

4.5. Limitations

In this chapter, CSC distributions in 3D spheroids could be studied with more spheroids. Only one spheroid was analyzed in depth using the 3D volumetric analysis. This was due to time restrains resulting from the cooperation between our lab and the commercial partner Molecular Devices. If more spheroids could be analyzed using this method, more data could be collected, and the results could be more impactful. In addition, the inhibition of NF-κB activation was not efficient using Bay11-7082. According to Lee et al., a higher concentration of Bay11-7082 (up to 20μM) can be added to the cells before inducing cell death [359].

In addition, when checking the distribution of the CSCs in spheroids, nestin was used instead of CD133. To make the story complete, CD133 should be considered.

Some other NF-κB inhibitors could be used. For example, MLN4924 could be used to inhibit the TNF- induced activation of NF-κB. This compound has been suggested to have higher inhibiting efficacy and less cytotoxicity than Bay11-7082 [372].

4.6. Future work

U251 cell spheroids were cultured and fixed in the in 3D scaffold, by using ICC, the distribution of CSCs could be seen (Fig. 4.14). Future studies could use this as benefit. The mimicked ECM in 3D cell culturing could change the morphology and different protein expression level of cancer cells. In the future research of this project, it is worth to use 3D cell culturing to study the actual molecular mechanisms in primary GBM cancer cells and GBM CSCs. By labelling the live primary CSCs and using the 3D cell culture methods, the migration and proliferation pattern of CSCs could be studied. This might provide better understanding on the metastasis mechanisms. Last, 3D cell culturing could be used in pre-clinical trials. Primary GBM cells could be seeded in 3D and treated with *S. minnesota* LPS derived TLR4 ligands or other anti-cancer drugs. The efficacy and toxicity of the anti-cancer drug candidates could be evaluated. This evaluation would give more reliable results comparing to 2D cell cultivation. In addition, combination of the drug candidates or combination of radio- and chemo- therapy could be applied to the cells in 3D cell culture. Those cells could be recruited from the scaffold for further analyzation and give better understanding of the pathological or genomic effects of the drugs.

Chapter 5. Generation of an IRF3-dependent mCMV-mCherry-P2A-Renella luciferase reporter system.

5.1. Introduction

Activation of the MyD88-dependent and MyD88-independent signalling via TLR4 result in the activation of pro-inflammatory nuclear factor NF-κB and/or the anti-

inflammatory/anti-viral IRF3 [373]. A previous study from the Widera lab observed that different TLR4 agonists, for example LPS derived from various species of bacteria, result in differential activation levels of the two downstream pathways NF-κB and IRF3 [79]. It was noted that the signalling activation was biased and was ligand-dependent [79]. In cancer cells, the inflammatory microenvironment promoted by NF-κB contributes to cancer progression and is essential for the proliferation, migration and invasion of cancer cells [193, 374]. Furthermore, the activation of TLR4 via LPS stimulation also plays an important role in the cellular resistance of anti-tumour treatment of GBM cells [193]. To understand the ligand-dependent biased activation of TLR4 downstream pathways, new tools need to be developed. These novel tools should be able to visualise and quantify the activation level of the two downstream pathways of TLR4.

A dual NF-κB reporter cell line U251-NF-κB-GFP-luciferase (Luc) was generated and characterised previously [204]. Briefly, the reporter vector system was introduced using lentivirus into the U251-MG cell, containing GFP and *firefly* luciferase which allowed assessment of the levels of NF-κB activity using fluorescence microscopy, luminometry, and flow cytometry. The reporter cell line has proved to be a very useful tool in assessing the activation level of pro-inflammatory signalling via TLR4 when U251 cells were stimulated with different TLR4 ligands. In addition, it has been shown that the inflammatory response in U251 cells is heterogeneous, and that biased agonism can be detected in the U251-NF-κB-GFP-Luc similarly to unmodified U251 cells [79]. Ligand-dependent differences in NF-κB activation were also detected using U251-NF-κB-GFP-Luc. Briefly, stimulation with *E. coli* derived LPS activates NF-κB stronger than *S. minnesota* derived LPS [79], suggesting E. coli LPS is NF-κB biased TLR4 ligand. Although the U251-NF-κB-GFP-Luc reporter cell line has been a very useful tool to study chronic neuroinflammation, it still has limited potential to assess anti-inflammatory pharmaceutical compounds and the activity of IRF3. Therefore, to further study the activation level of the two downstream pathways, I developed a quadruple reporter cell line as a tool for the simultaneous investigation of pro-inflammatory and anti-inflammatory effects of the TLR4 agonists and potential drugs.

In order to study the anti-inflammatory axis of TLR4 signalling, I designed and generated a lentiviral vector that contains a tandem of mCherry and *Renilla* luciferase (RLuc) protein under the control of the IRF3 promotor. I aimed to generate an IRF3 mCMV promoter-mCherry-*Renilla* luciferase reporter system for integration into the U251-NF-κB-GFP-RLuc cells, which forms a quadruple detection system of both pro- and anti- inflammatory pathways, named 'Quad Fire' reporter system. This new quadruple reporter system should allow simultaneous monitoring of NF-κB and IRF3 activity via microscopy, and flow cytometry by assessing GFP and mCherry expression. Moreover, NF-κB-dependent bioluminescence of *Firefly* luciferase and IRF3-driven *Renilla* luminescence could be used to simultaneously study pro- and anti-inflammatory signalling via TLR4.

5.2. Results

Design of the IRF3mCMV-mCherry-RLuc dual reporter construct

A vector was designed as in Fig 5.1. Minimal cytomegalovirus (mCMV) promoter was chosen as it has a very low basal transcription level and upstream of this an IRF3 binding site was inserted. mCherry, a red fluorescent protein, was chosen as the fluorescence signal reporter protein. *Renilla* luciferase was chosen as the chemiluminescence signal reporter protein, which could be detected along with the firefly luciferase signal using Dual-Luciferase® Reporter Assay System (Promega). When an IRF3-containing complex binds to its promoter region, the transcription of the DNA sequence will start. As the result, mCherry and *Renilla* Luciferase will be transcribed and translated in the cell. To avoid any possible toxicity of mCherry, 2A self-cleaving peptides (P2A) was chosen as a cleavage protein to be transcribed and translated between mCherry and *Renilla* Luciferase, to help cleave the two proteins from each other. *mCherry* could slowly degrade in the cells [375], instead of accumulating with *Renilla* Luciferase. Blasticidin was the selective antibiotic for this system in mammalian cells.

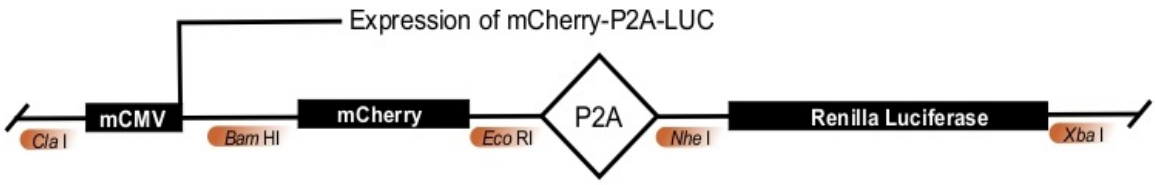

Figure. 5.1: Vector design of mCherry/Renilla luciferase reporter system of anti-inflammatory pathway. The fragments of DNA pieces are: IRF3mCMV promoter, mCherry, P2A and *Renilla* Luciferase. The restriction enzyme used are: *Cla* I, *Bam* HI, *Eco* RI, *Nhe* I and *Xba* I. After the binding of IRF3 to the IRF3mCMV promoter the expression of mCherry-P2A-*Renilla* Luciferase (RLuc) occurs.

Amplification, purification and cloning of the IRF3mCMV promoter

In order to generate a minimal CMV promoter with an upstream IRF3 binding site, a primer was designed to the 5' end of the minimal CMV promoter in pcDNA3.1 (+)-Blast and using BGH reverse as a 3' primer PCR was conducted using pcDNA3.1 (+)-Blast as template. The resulting PCR product was separated by agarose gel electrophoresis, excised and purified. The PCR product was then digested using the restriction enzymes *Cla* I and *Bam* HI and ligated into pBluescript KS (+) digested with the same enzymes. Colonies were screened by PCR using the flanking primers (-20) M13 forward and M13 reverse, and positive colonies expanded and plasmid DNA prepared and sent for DNA sequencing.

Amplification, purification and cloning of mCherry

Amplification of mCherry for the IRF3-senstive reporter construct was achieved by amplifying mCherry from the vector pmCherry2-N1 by PCR using the primers mCherryBamHIfor and mCherrynostopEcoRIrev. A PCR product of the expected size was excised, purified and digested with the restriction enzymes *Bam* HI and *Eco* RI. The digested DNA was gel purified and then ligated into pcDNA3.1-Blast digested with the same enzymes. Colonies were screened by PCR using the primers CMV forward and mCherrynostopEcoRIrev (Fig. 5.2) and positive colonies expanded and plasmid DNA sent for DNA sequencing.

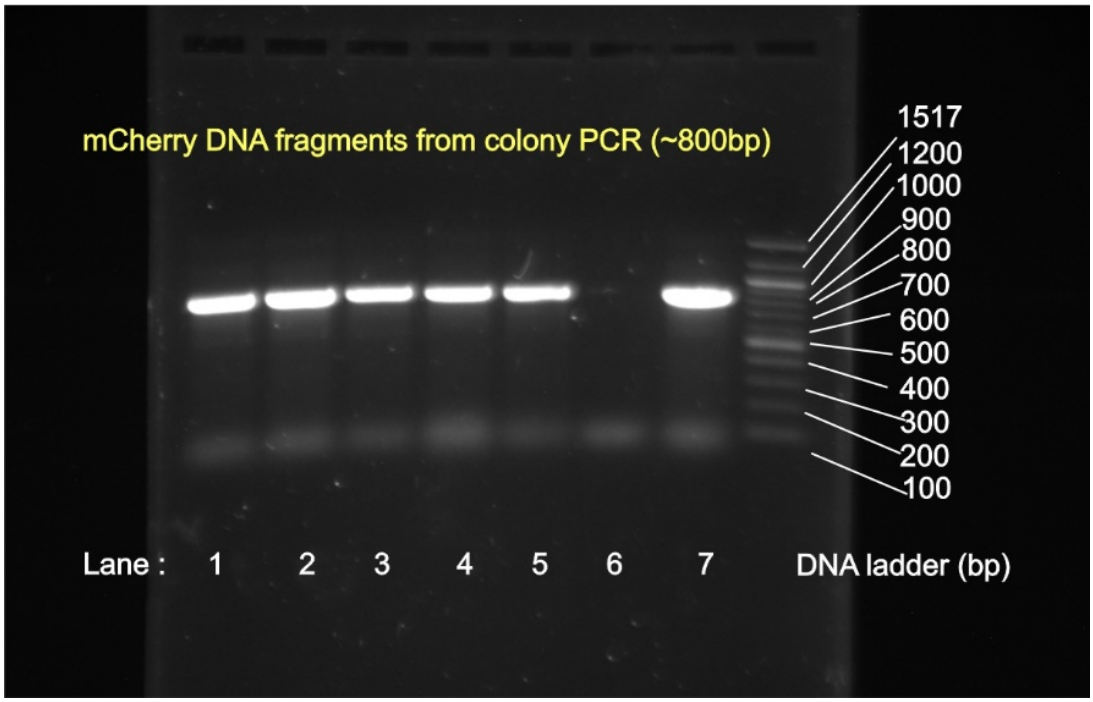

Figure 5.2. mCherry DNA fragments were successfully amplified and checked using colony PCR. Seven colonies from the transfected pcDNA3.1mCherry was tested using colony PCR. DNA ladder were loaded on the right. mCherry fragments length were around 800bps. All colonies except for colony in lane 6 were positive.

Amplification, purification and cloning of P2A self-cleaving peptide

Construction of the self-cleaving linker between the mCherry and *Renilla* luciferase was achieved by PCR. Two long primers (EcoRI-P2Alongfor and P2Along-NheI-rev) were designed with an overlap of 30 bp, which formed the

template for a PCR reaction. Amplification of the template was performed by PCR using 5' and 3' short primers (EcoRI-P2Ashortfor and P2Ashort-NheI-rev). The resulting PCR product was gel purified, digested with *Eco* RI and *Nhe* I and sub-cloned into the pcDNA3.1-Blast. Colonies that grew on the agar plate were screened by colony PCR using the flanking primers CMV forward and BGH reverse (Fig. 5.3A). Plasmid DNA was prepared for two of the positive colonies and digested with an enzyme that cut only the plasmid (*Nde* I) and an enzyme that cut only the P2A insert (*Bmg* BI) (Fig. 5.3B). The positive plasmid (colony 2) was then sent for sequencing to ensure the integrity of the sequence.

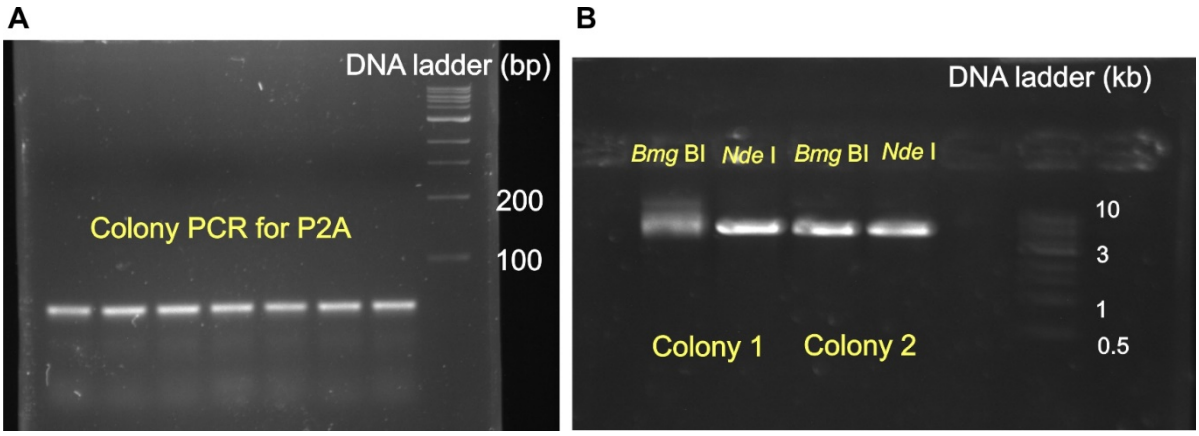

Figure 5.3. P2A DNA were successfully amplified and checked using colony PCR and single digest. A. Colony PCR of seven *E. coli* colonies, all of them were positive for a DNA fragment of the expected size for P2A. **B.** Colony 2 showed single bands when digested by *Bmg* BI and *Nde* I, suggested that colony 2 had correct DNA sequence.

Construction of the dual reporter for IRF3 in pBluescript KS (+)

To generate the IRF3 reporter cassette in pBluescript KS (+), a 4-way ligation was performed. The vector pBluescript KS (+)-IRF3mCMV was digested with *Bam* HI and *Xba* I, the mCherry insert was released from pcDNA3.1-Blast-mCherry using Bam HI and *Eco* RI and P2A was released from pcDNA3.1-Blast-P2A using *Eco* RI and *Nhe* I. Finally, the coding region for *Renilla* luciferase was obtained by digesting the plasmid pRL-cmv (E2261, promega) using the restriction enzymes *Nhe* I and *Xba* I. All DNA fragments were gel purified and ligated in a single reaction. Competent *E. coli* were transformed and plated onto agar plates containing ampicillin. Colonies of bacteria were then screened by

PCR using the flanking primers for pBluescript KS (+) [(-20) M13 forward and M13 reverse] (Fig. 5.4A). The three positive colonies were grown up and plasmid DNA prepared and analysed by restriction digest using *Bam* HI and *Xba* I (Fig. 5.4B).

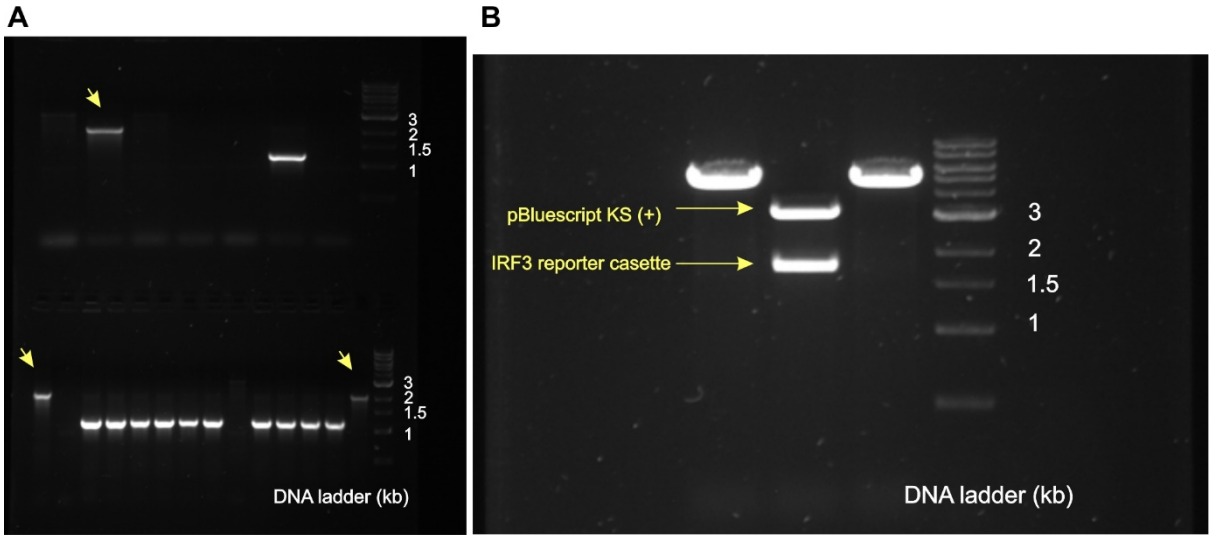

Figure 5.4. IRF3 reporter cassette was generated in pBluescript KS (+), checked by colony PCR and restriction digest. A. Colony PCR of twenty one *E. coli* colonies, only three of them showed the IRF3 reporter cassette band (~1800 bp, indicated by arrows). **B.** Plasmid DNA from the three positive colonies was digested using *Bam* HI and *Xba* I. Only one colony showed IRF3 reporter cassette (indicated by arrows).

Sub-cloning of the IRF3 reporter cassette into the lentiviral vector, pLenti6.3 blast

pLenti6.3 blast vector (Invitrogen) was transformed into the GM2163 competent cells. The vector was prepared using a Plasmid Mini-prep, purified and digested with *Cla* I and *Xba* I. The IRF3 reporter cassette (IRF3-mCMV-mCherry-P2A-RLuc) was sub-cloned into the pLenti 6.3 blast by releasing from the pBluescript KS (+) IRF3-mCMV-P2A-mCherry using *Cla* I and *Xba* I, followed by ligation. Colonies from the transformation were screened by PCR using the primers CMVfor and mCherrynostopEcoRIrev. Positive colonies were selected and grown overnight to prepare plasmid DNA which was then screened by restriction digest using *Bam* HI and *Xba* I and separately *Afl* II. The *Bam* HI and *Xba* I digest released an insert of the expected size and the *Afl* II digest confirmed the

presence of the long terminal repeats. DNA from a positive clone was then used to transform competent Stbl3 *E. coli* and a maxi prep DNA prepared. The DNA was then checked thoroughly by restriction digest using all the enzymes using to generate the construct (single digests) and also a combination of Afl II and *Eco* RI, and *Afl* II and *Nhe* I to confirm the integrity of the long terminal repeats (Fig .5.5).

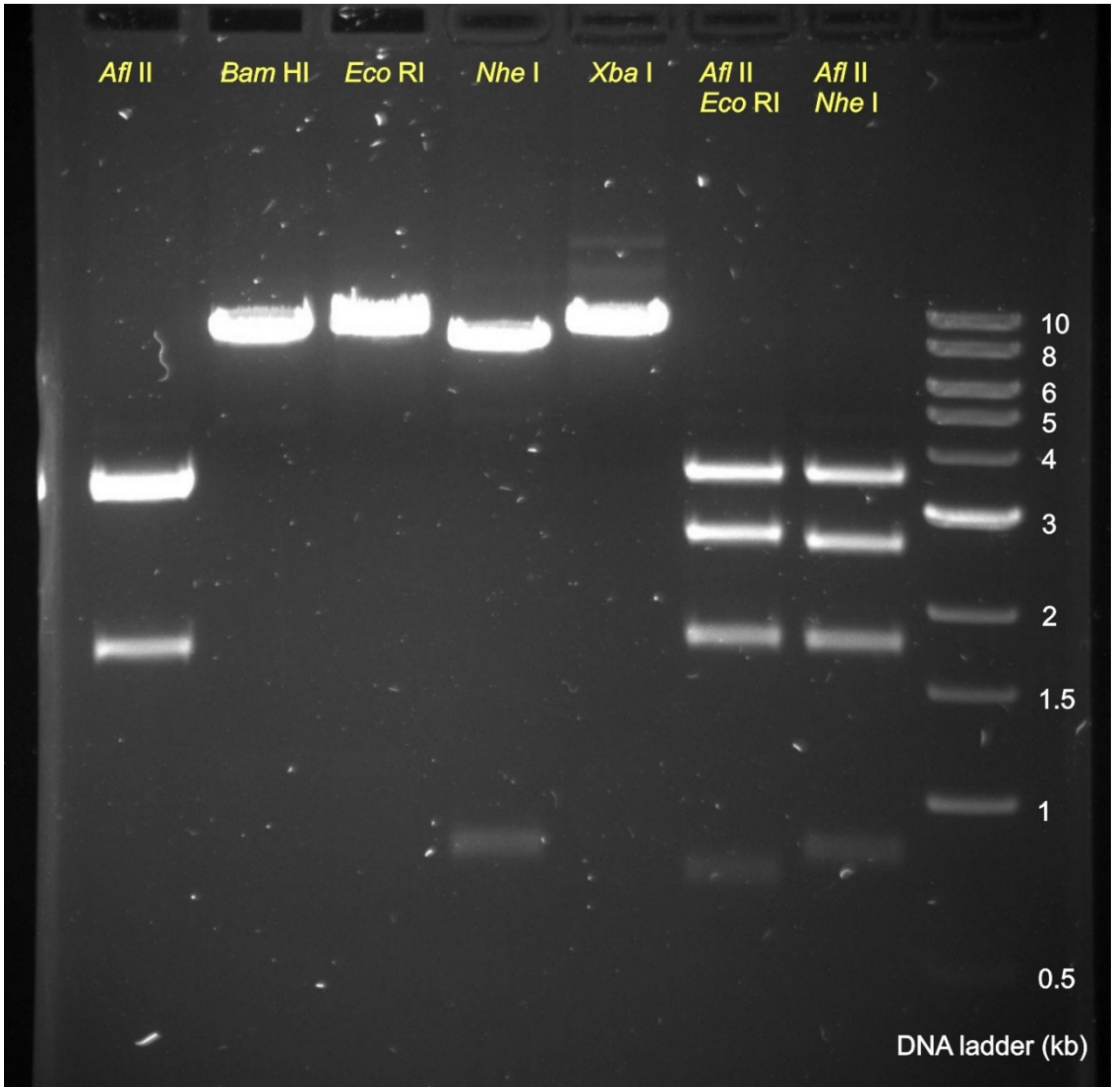

Fig. 5.5. Single and combination restriction digest of complete pLenti6.3-IRF3mCMV-mCherry-P2A-RLuc vector showed the sub-cloning of IRF3 cassette to pLenti 6.3 vector was successful. Single digests of the vector showed the vector contain those key restriction sites; *Afl* II digestion showed the integrity of long terminal repeats.

Immunocytochemistry of ICC showed mCherry was successfully expressed when U251 cells were transfected by constructed vectors.

The mCherry-P2A-RLuc was sub-cloned into the CMV promoter vector pcDNA3.1 by releasing from the pBluescript KS (+) IRF3-mCMV-P2A-mCherry using *Bam* HI and *Xba* I followed by ligation. The sub-cloned vector was checked using restriction digests and colony PCR. U251 cells were transfected with either pcDNA3.1-mCherry-P2A-RLuc or pLenti6.3-IRF3mCMV-mCherry-P2A-RLuc to observe the basal expression of each of the constructs. The pcDNA3.1-mcherry-P2A-RLuc has a strong CMV promoter that constitutively expresses mCherry. After transfection cells were fixed and mCherry localised using direct immunofluorescence and using an anti-mCherry antibody. In cells transfected with the constitutively expressing construct mCherry expression was detected using both direct fluorescence and using the mCherry antibody. The signals for these overlapped indicating that both methods detected the same protein. In cells expressing the IRF3-dependent construct, a similar staining pattern was observed albeit at a lower expression level. Also, in those pLenti6.3-IRF3mCMV-mcherry-P2A-RLuc transfected U251, there was still a basal expression level of mCherry.

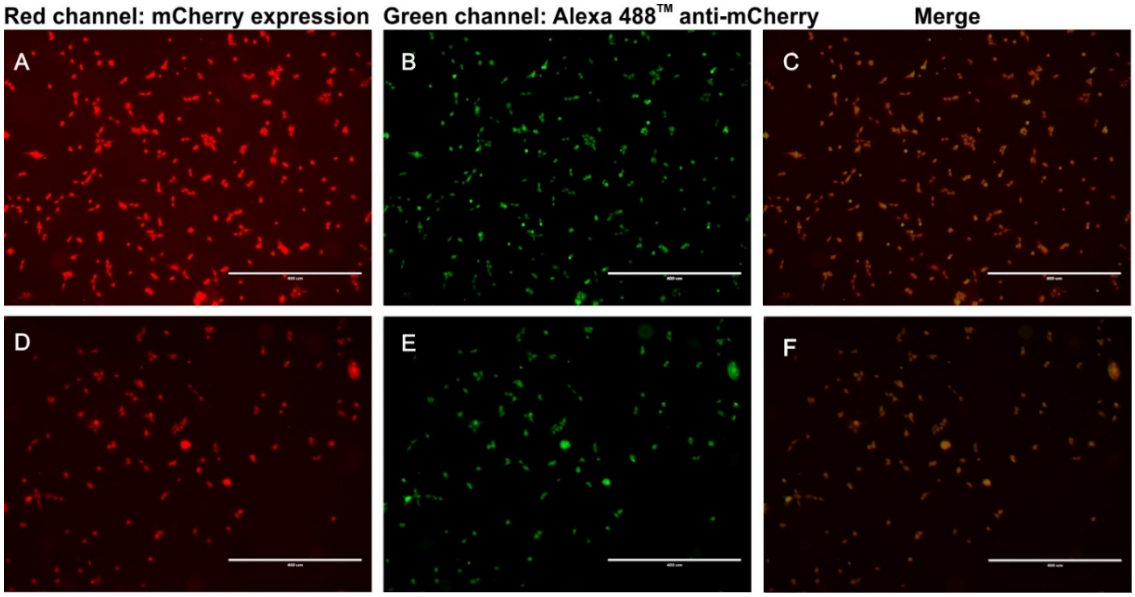

Figure 5.5. mCherry in 'mCherry P2A Renilla Luciferase' DNA strand was successfully translated and showed red signal. Immunocytochemistry was used to double check the protein. **A.** pLenti6.3-mIRF3-CMV-mCherry-P2A-RLuc transfected U251 expressed mCherry which was directed observed using the red channel of immunofluorescence microscope. **B.**pLenti6.3-IRF3-CMV-mCherry-P2A-RLuc transfected U251 expressed mCherry was labelled with anti-mCherry antibody as well as Alexa Fluor™ 488 and observed under the green channel of immunofluorescence microscope. **C.** Merged figure of A&B. **D.** pcDNA3.1-mcherry-P2A-RLuc transfected U251 expressed mCherry which was directly detected using the red signal of immunofluorescence microscope. **E.** pcDNA3.1-mcherry-P2A-RLuc transfected U251 expressed mCherry was labelled with anti-mCherry antibody as well as Alexa fluor ™ 488 and observed under the green channel of immunofluorescence microscope. **F.** Merged figure of D&E. Scale bar=400μm.

***Renilla* luciferase was successfully expressed and cleaved from mCherry.**
In order to determine if the mCherry and *Renilla* Luciferase are cleaved from each other after expression in cells, U251 cells were left transfected with pcDNA5/FRT (control), pcDNA3.1-mcherry-P2A-RLuc+pcDNA5/FRT (constitutive vector), pLenti6.3-IRF3mCMV-mCherry-RLuc + pcDNA5/FRT, pLenti6.3-IRF3mCMV-mCherry-RLuc+pcDNA3.1-IRF3, or untransfected. The pLenti6.3-IRF3mCMV-mCherry-RLuc transfected U251 cells were co-transfected with pcDNA3.1-IRF3. This provided constitutive expressed IRF3 in the cell which could bind to the IRF3 binding site of the IRF3mCMV promoter and promote the expression of the downstream genes.

After 48 h, cell lysates were prepared and analysed by western blotting using an antibody to *Renilla* luciferase and β-actin, as loading control. For *Renilla* luciferase, no immunoreactive bands were detected in untransfected cells and control vector transfected cells (Fig.5.6.A, lane 1&5). In cells transfected with the constitutively expressing construct an immuoreactive band of the expected size for RLuc (~36 kDa) was clearly visible. In cells transfected the constitutive IRF3 expressing construct, a distinct but clearly fainter immunoreactive band was

detected (Fig.5.6.A, lane 2&4). In cells transfected with the IRF3mCMV-mCherry-P2A-RLuc construct no immunoreaction band was clearly visible (Fig. 5.6.A, lane 3). β-actin (42kDa) was detected at similar levels in all samples (Fig. 5.6.B). As the RLuc was detected at the expected molecular mass, it is clear that mCherry and RLuc are cleaved from each other after expression in U251 cells.

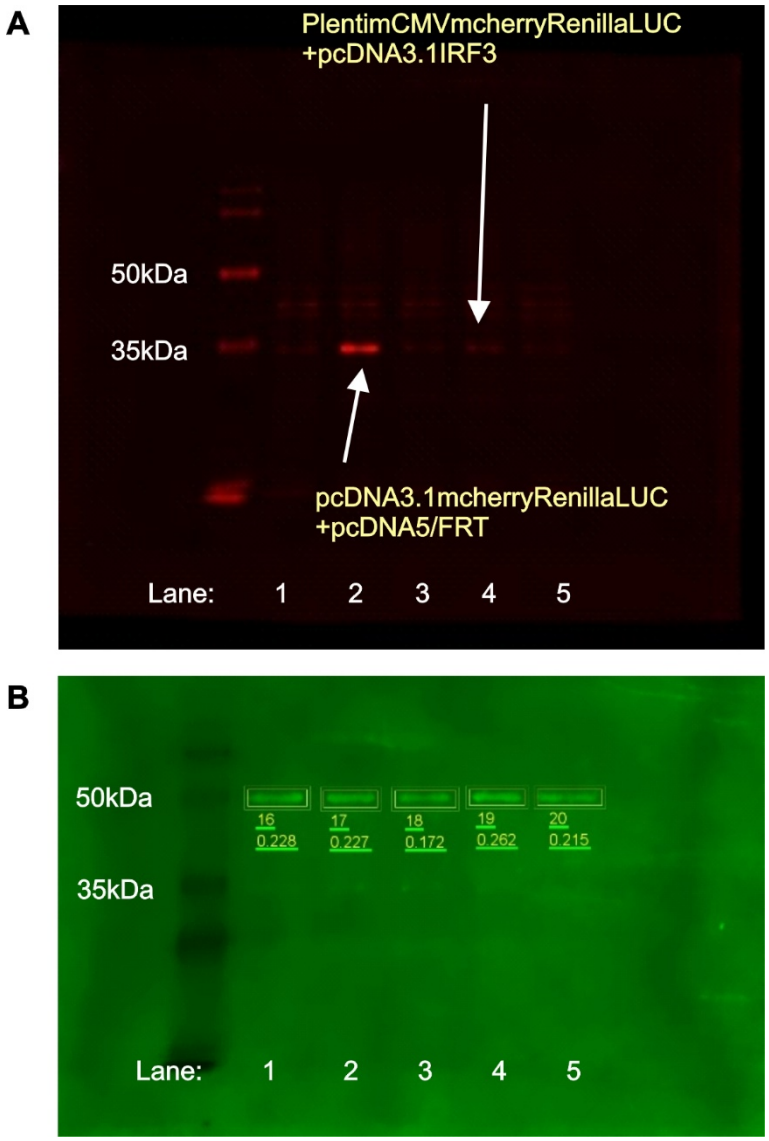

Figure 5.6. Renilla luciferase (36kDa) was successfully expressed and cleaved from mCherry protein in U251 cells. Lanes: (U251 transfected with) 1. pcDNA5/FRT (control vector), 2. pcDNA3.1-mcherry-P2A-RLuc+pcDNA5/FRT (constitutive vector), 3. pLenti6.3-mCMV-mCherry-P2A-RLuc + pcDNA5/FRT, 4. pLenti6.3-mCMV-mCherry-RLuc+pcDNA3.1-IRF3, 5. Remained untransfected (control). **A**. *Renilla* luciferase labelled with rabbit anti-*Renilla* luciferase primary

antibody and Alexa Flour™ 680 conjugated donkey-anti-rabbit secondary antibody. Lane 2 showed clear 36kDa band and lane 4 showed a weaker 36kDa band. There were no bands the size of uncleaved mCherry-*Renilla* luciferase protein (roughly 65kDa) in this channel. **B.** Housekeeping protein β-actin was labelled with mouse-anti β-actin primary antibody and donkey anti-mouse 800 secondary antibody. All groups showed β-actin bands at 42kDa at similar brightness.

IFR3-dependent activation of the IRF3mCMV-mCherry-P2A-RLuc construct increases *Renilla* Luciferase activity in U251 cells

U251 cells were transfected as above and cultivated for 3 days before processing for a luciferase assay. Significant increase of the *Renilla* luciferase activity could be detected in pcDNA3.1-mcherry-P2A-Rluc transfected cells and pLenti6.3-mCMV-mCherry-P2A-RLuc+ pcDNA3.1 IRF3 co-transfected U251 cells in comparison to un-transfected or empty vector transfected cells (Fig. 5.7).

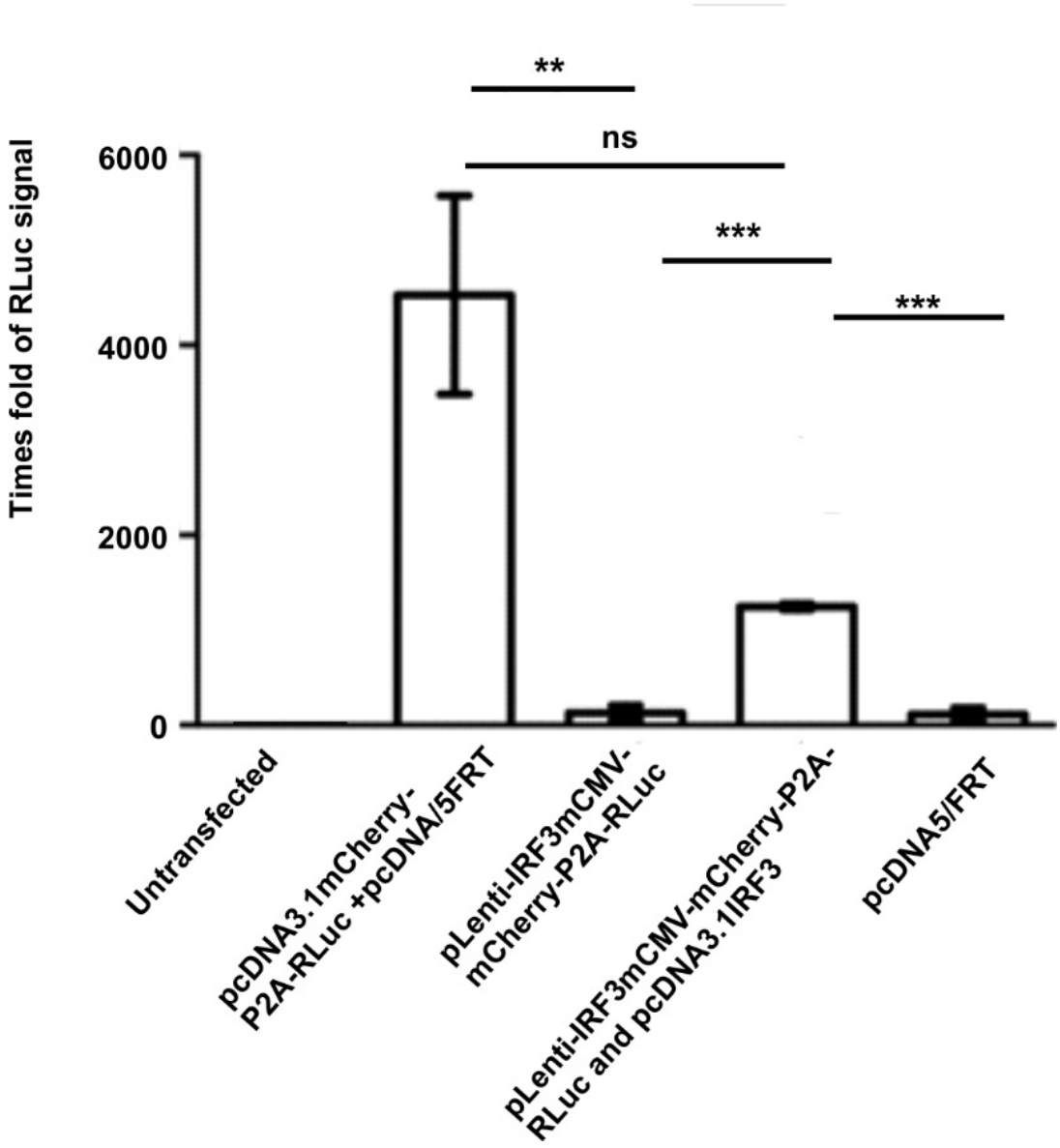

Figure 5.7. pcDNA3.1-mcherry-P2A-RLuc and pLent6.3-IRF3-mCMV-mCherry-P2A-RLuc+pcDNA3.1 IRF3 transfected U251 cells showed significantly higher *Renilla* luciferase signals than the control groups and pLenti6.3-IRF3-mCMV-mCherry-P2A-RLuc transfected cells. Data normalised to untransfected U251 cells. Mean ± SEM from three different experiments were analysed using ANOVA with Bonferroni correction (CI 95%); p<0.01, ***p<0.001.

‘Quad Fire’ reporter system effectively generates ligand-dependent luciferase activity

U251-NF-κB-GFP-Luc reporter cells were transfected with pLenti6.3-IRF3-mCMV-mCherry-P2A-RLuc to generate a ‘Quad Fire’ reporter system. The transfected cells were seeded in 12 well plates and treated with TLR4 ligands separately. Significant difference could be observed when stimulating the U251 ‘Quad Fire’ reporter system. TNFα and *E. coli* LPS gave significantly high signals via pro-inflammatory pathway (Fig. 5.8A), while *S. minnesota* LPS and TLR3 agonist Poly (I: C) gave significantly high activation levels of the IRF3 dependent pathway (Fig. 5.8B). The results showed that the ‘Quad Fire’ reporter system could be used as a screening system for the activation level of the ligand-biased TLR4 signalling pathways.

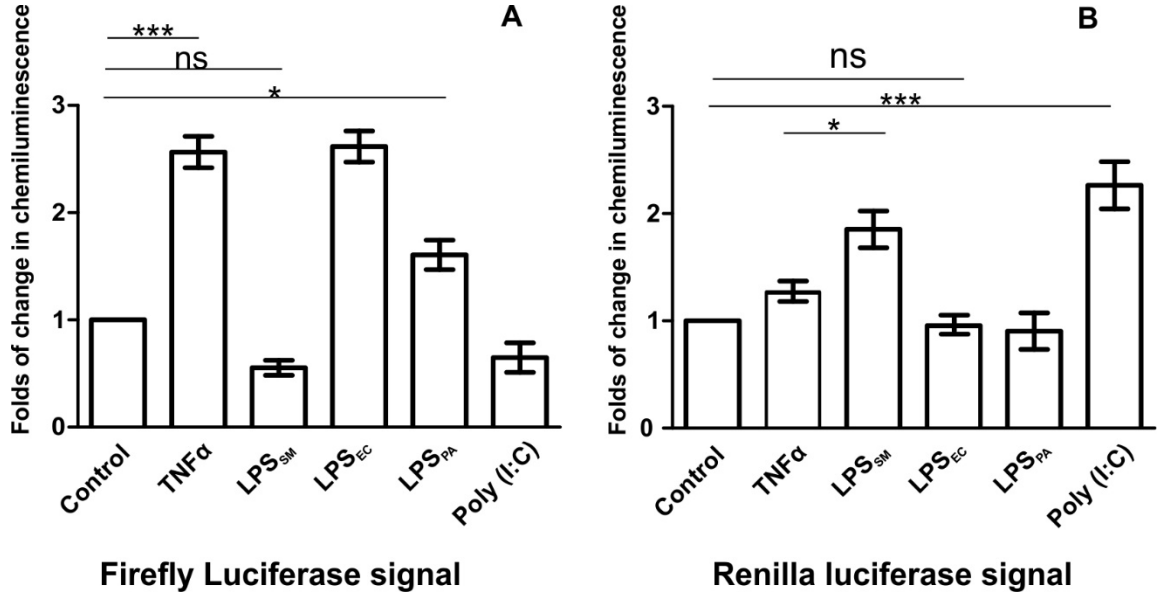

Figure 5.8. Dual luciferase results showed that ‘Quad Fire’ reporter system was able to show the different activation level of NF-κB and IRF3 in cells. **A**. *E. coli* LPS and TNFα had a significantly high Firefly luciferase signal**. B**. S. minnesota LPS, and poly (I:C) had a significantly high *Renilla* luciferase signal in comparison to other groups. However, the signal was not as strong as the Firefly luciferase signal generated by *E. coli* LPS and TNFα stimulation. Mean ± SEM from a minimum of three different experiments were analysed using ANOVA with Bonferroni correction (CI 95%); *p<0.05,**p<0.01,***p<0.001.

5.3. Discussion

In GBM cells, TLR4-mediated inflammation plays an important role in TME, and NF-κB has been reported to be involved in multiple inflammatory pathways in GBM cells and GBM CSCs [376]. TLR4, as a very important pattern recognition receptor, has been found on many types of cells including dendritic cells, epithelial cells, megakaryocytes, cancer cells etc. [377-380]. The NF-κB signalling triggered by the activation of TLR4 contributes to inflammation pathways of the cells and also give rise to the tumour development in TME [381]. However, the IRF3, transcription factors of anti-inflammatory cytokines like IFNβ, could also be activated by TLR4 activation, but though MyD88-independent pathway [382]. The aim of this chapter was to generate the stable 'Quad Fire' reporter system to use as a robust tool for assessing the pro- and anti-inflammatory pathway activation levels under the stimulation of different TLR4 ligands in GBM and GBM CSCs. To achieve this, the IRF3mCMV-mCherry-P2A-Renilla luciferase cassette had to be integrated into the genome of U251-NF-κB-GFP-Luc reporter cells. To react to the IRF3 transcription factor, IRF3mCMV-mCherry-P2A-Renilla luciferase had to have a binding site for IRF3, to trigger the downstream transcription of the gene. In addition, mCherry and *Renilla* luciferase had to be cleaved from each other to give accurate *Renilla* luciferase signals as well as to maintain the health of U251 cells. This is to make sure mCherry could slowly degrade in the cells as fluorescent proteins may have potential toxicity to cells [383]. The Luciferase reporter system was widely used in many studies for studying cellular pathways and inflammation [379, 384, 385].

In this chapter, to test the IRF3 binding site, I used pcDNA3.1-IRF3-FL to co-transfect U251 cells with the construct vector pLenti6.3 IRF3Mcmv-mCherry-P2A-RLuc. The constitutive expressed IRF3 in the cell should bind to the IRF3 binding site and the downstream open reading frame of mCherry-P2A-RLuc thus, be expressed. In fact co-transfection of the IRF3-expressing plasmid with the reporter plasmid did indeed promote expression of mCherry and *Renilla* luciferase.

I also demonstrated that mCherry could be expressed successfully in the constructed vector transfected cells. The direct immunofluorescence of mCherry

was checked for pcDNA3.1 mCherry-P2A-RLuc transfected U251 cells pLenti6.3-IRF3mCMV-mCherry-P2A-RLuc transfected U251 cells. Both cells were also labelled with mCherry antibody and Alexa Fluor 488™ (Fig. 5.5). The positive results of immunocytochemistry suggested mCherry was correctly translated into proteins in those cells. To test the basal level of the mCherry expression under normal cell cultivation condition, the U251 cells used in this experiment was not serum starved and not stimulated. Presumably due to a basal activation of IRF3 in U251 cells, the pLenti6.3-IRF3mCMV-mCherry-P2A-RLuc transfected cells still showed mCherry signal. Therefore, for screening the anti-inflammatory pathway activation level under the stimulation of particular ligands in the future, it is suggested to serum-starve the cells for a short period of time prior to the stimulation to alleviate the influence of the growth factors and the existed transcription factors and to give more accurate reporter responses of the tested ligands.

To demonstrate that *Renilla* luciferase protein was expressed correctly and to test if mCherry and *Renilla* luciferase protein was cleaved from each other, western blotting was used (Fig. 5.6). *Renilla* luciferase protein was labelled by the mouse-anti-*Renilla* and Alexa Fluor™ 680 (Fig. 5.6A). 36kDa *Renilla* luciferase bands could be seen in this channel. A bright band could be seen from the protein from constitutive pcDNA3.1-mCherry-P2A-RLuc transfected cells, and a fainter band could be seen from the protein from pLenti6.3-IRF3mCMV-mCherry-P2A-RLuc + pcDNA3.1IRF3 transfected cells. Also, no band could be seen in other groups. This suggested that the *Renilla* luciferase could be expressed successfully, and the level *Renilla* luciferase expression of IRF3-mCherry-P2A-RLuc reporter system was IRF3 dependent. However, the band signal of *Renilla* luciferase in pLenti6.3-IRFmCMV-mCherry-P2A-RLuc and pcDNA3.1 IRF3 co-transfected U251 cells in (Fig. 5.6A, lane 4) was not as bright as lane 2. This might be due to the low Renilla luciferase level in the sample, which might be cause by the not high-enough transfection efficiency of the vectors to U251 cells. Moreover, the RLuc activation level was tested using *Renilla* Luciferase assay. U251 cells were left transfected with constructed vectors and in combination of constructed vectors and IRF3 constitutive expression vectors. Compared to control groups, it was clear that the constitutive

constructed vector pcDNA3.1 mcherry-P2A-RLuc transfected U251 cells and constructed vector pLenti6.3-IRF3mCMV-P2A-RLuc + pcDNA3.1 IRF co-transfected cells showed significantly higher *Renilla* luciferase signal than the other three groups, and there was no significant difference between the described two groups.

Finally, a dual luciferase assay was used to test the 'Quad Fire' reporter system. U251-NF-κB-GFP-Luc reporter cells were transfected with the pLenti6.3IRFmCMV-mCherry-P2A- Renilla luciferase vector for the establishment of a transient 'Quad Fire' system. TNFα, poly (I:C) and different TLR4 ligands were used to stimulate the transfected cells to test the 'Quad Fire' system. Here, TNFα was used as the positive control of the activation of NF-κB. When TNFα binds to TNF receptors, the receptor interact to adaptor protein TNF receptor associated factor (TRAF) and triggers the downstream pathways similar to the TLR4-mediated MyD88-dependent pathway, activates the NF-κB and drives the expression of pro-inflammatory cytokines [386]. For the activation of IRF3, poly (I:C) was used as the positive control. Unlike TLR4, TLR3 only activates the adaptor protein TIRF to mediate the induction of IFN-inducible genes through the activation of IRF3 [387], and poly (I:C) was known as one of the TLR3 agonist [388]. Both TLR4 and TLR3 had been proved to express in U251 cells [79, 389], the IRF3 regulation could be influenced by both TLRs. In the dual luciferase assay, 'Quad Fire' reporter cells stimulated with *E. coli* LPS and TNFα showed a significantly high *Firefly* luciferase signal; *S. minnesota* LPS, poly (I:C) stimulated 'Quad Fire' reporter cells showed significantly higher *Renilla* luciferase signal, in comparison to other groups. Very importantly, it has been demonstrated by Zeuner et al. that *E. coli* LPS is a pro-inflammatory biased ligand that can promote the activation of NF-κB, and *S. minnesota* LPS is an anti-inflammatory biased ligand that activates IRF3. In combination with my results, this suggested that 'Quad Fire' could effectively generates ligand-dependent responses and could be used as a tool to quantify the activation level of the NF-κB and IRF3.

There is great application potential of this 'Quad Fire' system. From chapter 3 and 4, I demonstrated that those two downstream pathways of TLR4 were able to impact the tumourigenesis, stemness, proliferation, migration, and

differentiation of U251 cells and its' CSCs. However, up until now, the mechanism of this biased activation pattern was not fully understood. It has been suggested that the chemo-type of the TLR4 ligand was the key regulatory factor of the TLR4 biased signalling activation [390]. Quad Fire, therefore, could be used to quantify the activation level of both downstream pathways under the stimulation of TLR4 ligands and help to study the mechanism of the biased signalling.

In addition, this 'Quad Fire' reporter system could be used in multiple cell lines to overcome the difficulties of acquiring the quantification of the inflammatory response linked with NF-κB activation and anti-inflammatory response triggered by IRF3. The NF-κB-GFP-Luc reporter system were successfully integrated into the megakaryocytes by me and my colleagues [379]. Luciferase assay showed that the inflammatory molecules stimulated by NF-κB activation could be successfully and easily quantified. Those molecules included Pam3CSK4, TNFα, and ultrapure *E. coli* LPS etc. Also, this NF-κB activation could be inhibited by using IMD0354 in a dose-dependent manner[379]. This research brought direct results of the inflammation level in the megakaryocytes triggered by different PAMPs, which was poorly studied previously.

Current reporter systems that provide signals for both pro- and anti- inflammatory signalling pathways are quite limited in the market. The current ones are mostly dual reporter cell lines which only provide limited methods for signalling detection. For example, commercially available human THP-1 monocytes NF-κB-SEAP and IRF-lucia Reporter cells (Invivogen) and Human T Lymphocytes - NF-κB/IRF reporter cells (Invivogen).The signals of those could only be detected via chemiluminescence assays. The 'Quad Fire' reporter system developed here would allow the pro- and anti- inflammatory signals to be observed and quantified using different ways. Microscopy, flow-cytometry and bioluminescence could all be used on evaluating the signals produced by 'Quad Fire'.

5.4. Conclusion

'Quad Fire' reporter system was designed, generated and tested. Multiple methods could be used to test the ligand- biased signals given from 'Quad Fire' reporter system. This robust quadruple reporter system should be able to give response to a range of PAMPs and DAMPs, and their pathway inhibitors. It will

be a very useful tool to understand the inflammation of cells linked to NF-κB, and the anti-inflammation reactions of cells linked to IRF3. The quadruple reporter system could be applied to a broad range of inflammatory molecules that act via NF-κB and anti-inflammatory molecules that act via IRF3 in various types of cells. More importantly, it could help to deeply understand the mechanism of TLR4 biased signalling which plays a very important role in inflammation responses and anti-cancer treatment.

5.5. Limitations

Transfection was used to generate temporary 'Quad Fire reporter system' cells. Even though the transfection rate of the U251 cells was quite high, there was still a large percentage of un-transfected U251-NF-κB-GFP-Luc reporter cells (28.7%) that could cause the luciferase assay results to shift. Also, more TLR4 ligands should be tested in this chapter, so that the ligand-dependent biased signalling could be better understood.

5.6. Future Work

'Quad Fire' reporter system is a robust tool to study the TLR4 mediated NF-κB and IRF3 activation. Future work should include: 1. Full generation of the 'Quad Fire' reporter cell lines. For stable cell line generation, GMB cell line U251 could be used. To achieve this, lentivirus contain IRF3mCMV-mCherry-P2A-RLuc should be made to transduce in to the U251-NF-κB-GFP-Luc reporter cells. Selective antibiotic blasticidin and puromycin should be used to select positive clones. Positive clones need to be analysed in activity assays. Also, the 'Quad Fire' reporter system could be used on other cell lines for stable reporter cell line generation. 2. Once the 'Quad Fire' reporter cell line is generated, more TLR4 ligands could be used on targeting the cell to study the mechanism of the biased TLR4 biased signalling. In addition, 'Quad Fire' reporter system could also be used to screen pro- and anti-inflammatory molecules that act via NF-κB and IRF3 in multiple cells, and more importantly, in CSCs. By shifting the pro-inflammatory TME of the CSC niche, it could bring new insight the anti-cancer treatments.

Chapter 6. Microemulsion formulation of curcumin have increased stability and anti-inflammatory activity compared to native CUR.

6.1. Introduction

The tumour microenvironment, which is predominantly regulated by inflammatory cells, is now recognised as an essential participant in the neoplastic process, supporting cancer proliferation, survival, and migration. Tumour cells also use selectins and chemokines released by the immune system. Those signalling pathway activators interact with the receptors on tumour cells and promote cancer cell migration and metastasis [199].

The use and efficacy of medicinal plants in the treatment of various diseases has attracted considerable interest in recent years. Herbal compounds have been extracted and their qualities investigated in relation to the treatment of various diseases including cancers. Providing specific mechanisms of therapeutic performance of these compounds has been the focus of extensive research. Curcumin (CUR), [1,7-bis-(4-hydroxy-3-methoxyphenyl)-1,6-heptadiene-3,5-dione], a pharmacologically active herbal component that comprises 2-8% of turmeric [391], is one of the potential plant-derived drugs suggested to prevent the development of cancer and neuro-inflammatory conditions such as Alzheimer's disease [392]. Apart from this, because of the high biding affinity of CUR to amyloid-β, CUR has also been developed into early diagnostic probe to Alzheimer's disease. CUR, on the other hand, has low intrinsic toxicity and a variety of characteristics that have huge potential for anti-inflammatory applications in pharmacology. Many pre-clinical and clinical studies have suggested that curcumin has anti-cancer effects *in vitro*, including inhibiting tumour growth by interfering with the cancer cell proliferation cycle and inducing cell apoptosis [393, 394], and inhibiting cell proliferation [395] thereby inhibiting carcinogenesis [396]. Some studies also indicated that CUR has antioxidant, anti-inflammatory (especially inhibition of NF-κB activation), and antibacterial properties [395, 397-399].

CUR has multi-targeting property (shown in Table 6.1). CUR is able to target varieties of inflammatory signalling pathways. In many chronic diseases, including in the tumour microenvironment, the oxidative stress and an accumulation of oxygen reactive species (ROS) can be found [239]. ROS, however, plays important roles in NF-κB and TNF-α pathways and creates ROS-NF-κB-TNF-α positive feedforward loop. CUR has been suggested to alleviate oxidative stress via suppressing the pro-inflammatory pathways related to ROS and TNF-α [400]. One signalling pathway that CUR could trigger is the nuclear factor erythroid-2 (NRF2) – KEAP1 signalling pathway which decreases the ROS level in cells [400]. Youn et al. demonstrated that CUR inhibits IKKβ kinase activity [401], leading to inhibition of the TLR4-MyD88 dependent pathway and the reduction of the NF-κB activation directly triggered by the MyD88-dependent pathway and the late NF-κB activation triggered by the MyD88-independent pathway. As a result, the pro-inflammatory cytokines IL-1β, IL-6, MCP-1, and MMP-9 expression could be decreased [402]. In addition, EKR1/2 and p38 signalling pathways have been shown to be inhibited by CUR [403]. Those are the signalling pathways that could be activated by TAK1, which can then stimulate the transcription factor AP-1, and AP-1 is known as playing important roles in cancer development by promoting inflammation [404], maintaining cell proliferation and survival [405], activating cell invasion [406] and avoiding immune destruction [407]. Also, Epstein et al. found that CUR is able not only to suppress the cell expression of inflammatory cytokines but also to promote the anti-inflammatory cytokine IL-8 [408]. All in all, CUR has very strong anti-inflammatory effects and provides great insights to anti-inflammatory drug development in chronic diseases and cancer research.

Targets	Effects	Reference
Protein kinase: MAPK, JNK, PKC, IκBα kinase, growth factor receptor protein tyrosine kinases	Inhibition and downregulation of the protein kinases	[391] [409]
Anti-apoptotic proteins	Induction of cytochrome-*c* release, activation of caspase -3 and caspase -9, down regulation of Bcl-2	[410, 411] [412] [413]
Pro-inflammatory proteins	Downregulation of COX-2, 5-LOX	[414] [415]
Cytokines/growth factors	Downregulation of TNF, IL-6, IL-8, IL-12, and fibroblast growth factor-2	[416] [417, 418]
Transcription factors	Suppression of NF-κB, STAT3, AP-1, Egr-1. Activation of β-catenin	[419] [420] [421]
Oxidant systems	Upregulation of heam oxygenase, downregulation of xanthine oxidase, clearing reactive oxygen/superoxide	[422-424]
Metalloproteinases	Attenuation of MMP-9 activity and amelioration of MMP-2 activity	[425]

Table 6.1. CUR has multiple targets and multiple effects [391]. Abbreviations: Bcl-2: B-cell lymphoma 2. COX-2: Cyclooxygenase-2. 5-LOX: 5-Lipoxygenae. TNF: tumour necrosis factor. IL: Interleukin. NF-κB: Nuclear factor kappa B. STAT3: signal transducer and activator of transcription 3. AP-1: activator protein 1. Egr-1: early growth response 1. MMP-9: matrix metallopeptidase 9.

However, one of the barriers of using CUR is that CUR has negligible solubility in water and a very rapid degradation rate. Therefore, the main problem to solve prior to its clinical use is to increase its drug delivery efficiency. CUR is a 'di-feruloyl-methane', a hydrophobic polyphenol, with the chemical formula $C_{21}H_{20}O_6$ (as shown in Fig. 6.1). Its low aqueous solubility and poor penetration through the intestinal wall make it a classed IV molecule within the biopharmaceutical

classification system [426-428]. In general, CUR degrades rapidly under physiological settings (0.1M phosphate buffer, serum free medium, 37ºC and pH7.2), with just 10% compound remaining after 30 mins [429]. Apart from that, the low solubility and low penetration through the intestinal wall lead to the accumulation of CUR in the intestine [430]. Therefore, it is very important to develop a better drug delivery system for CUR. Sanduk, Hisham and I proposed as potential formulation for CUR delivery a synergistic microemulsion system of triglyceride (oil phase) encapsulating curcumin-ferulic acid eutectic nanocrystals and stabilised by Brij® O10 (Fig. 6.2). The nanocrystals were filled with triglyceride oil and are stable in aqueous phase. Ferulic acid (FA) is one of the products of the photodegradation of CUR. In this study, FA was used to form CUR-FA eutectic nanocrystals inside the surfactant polyoxyethylene or sodium deoxycholate [430].

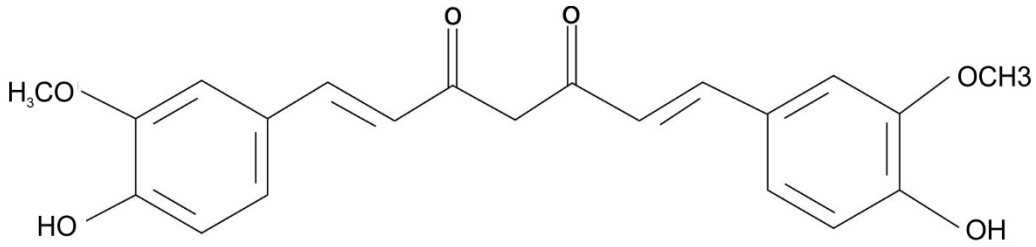

Fig. 6.1 Chemical formula of CUR it is a hydrophobic polyphenol [396]. It has two aromatic rings containing o-methoxy phenolic groups. The two rings are connected by a seven-carbon chain. The crystal state of CUR exists in cis-form [431].

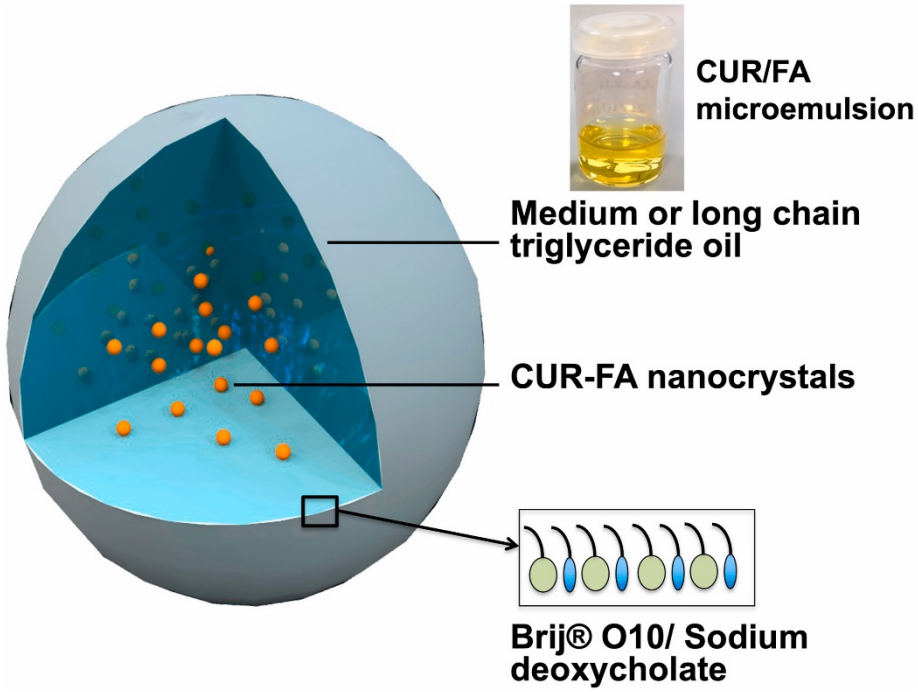

Figure. 6.2 Schematic figure of microemulsions encapsulating CUR/FA mixtures. Polyoxyethylene or sodium deoxycholate are used as the surface of nanocrystal to wrap up CUR and ferulic acid (FA), which are dissolved in triglycerides- based oil. The nanocrystals were stabilized using Brij® O10/ Sodium deoxycholate in aqueous continuous phase [430].

Different types of triglycerides were used in this chapter to compare the main differences between them and the improvement of modified drug delivery system in comparison to the non-modified oil dissolved curcumin was measured. CUR dissolved in liquid glyceryl tricaprate, with and without FA and CUR dissolved in solid glyceryl tricaprate, with and without FA were tested. The four types of CUR condition are shown in the table below (Table. 6.2).

Initiates of CUR condition	CUR condition
CUR + DMSO	CUR simply dissolve in DMSO
CUR1	7% C18:1E10, 1% liquid glycerl trioleate
CUR2	7% C18:1E10, 1% liquid glycerl trioleate, CUR:FA (1:1)
CUR3	7% C18:1E10, 1% solid glyceryl tricaprate
CUR4	7% C18:1E10, 1% solid glyceryl tricaprate, CUR:FA (1:1)

Table 6.2. Formulations of CUR used in this chapter. DMSO: dimethyl sulfoxide.

6.2. Results

IC_{50} of CUR1 was between 50-100μM.

Modified CUR delivery system, CUR1, synergistic micro emulsion system of triglyceride (oil phase) encapsulating curcumin showed IC_{50} at the concentration between 50-100μM (Fig. 6.3B), while CUR+DMSO showed very low toxicity and did not reach its IC_{50} even up to a concentration of 400μM (Fig. 6.3A).

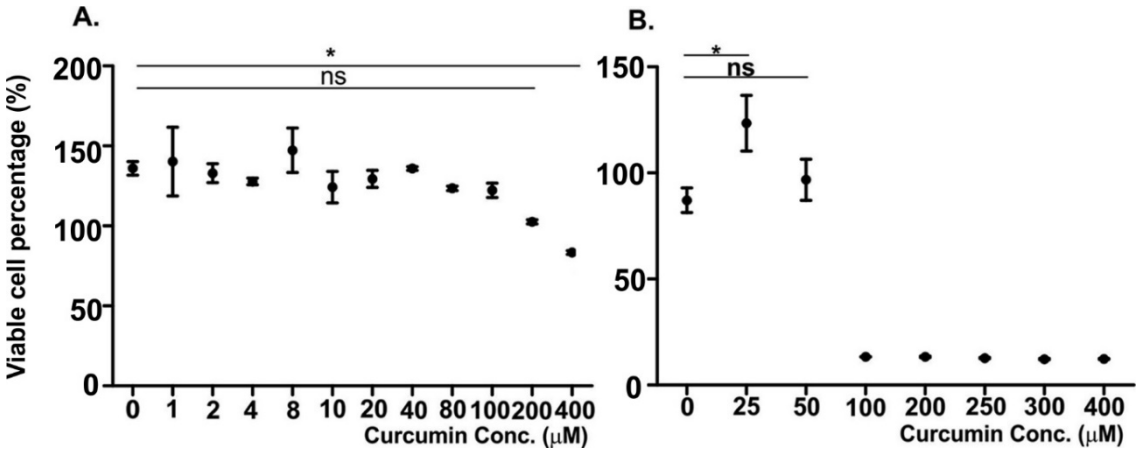

Figure 6.3. U251 cell viability decreases when treated with CUR+DMSO and modified CUR microemulsion delivery system, the IC50 CUR microemulsion delivery system was between 50-100μM. U251 cells were treated with CUR+ DMSO and delivery system packed CUR. **A.** Original format

of CUR dissolved in DMSO showed very low cell toxicity. **B.** CUR packed in microemulsion showed no cytotoxicity under 50μM. The IC_{50} of CUR 1 was 50-100 μM. Data were normalised to the mean value of the untreated U251 cells (Control group). Data is presented from at least three independent experiments.*$p<0.05$.

As the CUR1 showed no cytotoxicity to U251 cells at concentrations lower than 50μM, we decided to use 10μM of CUR and CUR1 for U251 cell treatment. With 10μM of CUR and CUR1 in presence, U251 cells grew and did not show any morphological difference when compared to untreated cells (Fig. 6.4).

Pictures of U251 cells were taken on the day when cells reached 50% confluency (Fig. 6.4A & 6.4C). Fig 6.4A & 6.4B showed U251 cells treated with CUR +DMSO on Day 0 (the day cells reach 50% confluency) of CUR treatment and Day 2, 48 hours after CUR treatment. Fig 6.4C & 6.4D showed U251 cells treated with CUR1 on Day 0 and Day 2. I compared the left to the right, the cell number of the two groups increased due to the cell proliferation. However, there was no difference on cell morphology between the two treatments (A&B verses C&D).

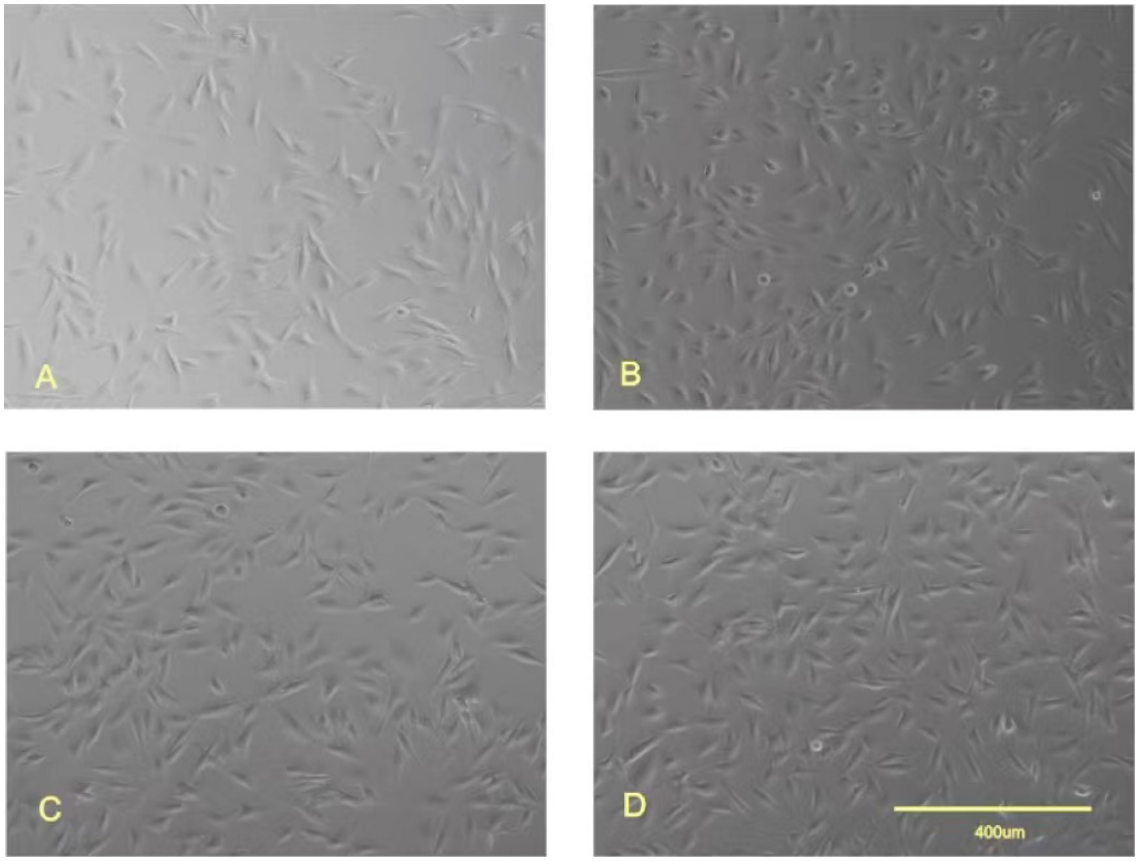

Fig. 6.4 U251 cell showed no morphology difference after the treatment of CUR+ DMSO and CUR1. A. CUR+DMSO day0; **B.** CUR+DMSO day2; **C.** CUR1 day 0; **D.** CUR1 day2. Pictures were taken using EVOS XL CORE (Thermofisher), Scale bar= 400μm.

Formulated CUR showed significantly stronger anti-inflammatory effect than original format of CUR.

By using Luciferase assay, I demonstrated that the new CUR formulations had significantly higher anti-inflammatory effects in U251 cells exposed to TNF-α than the native form of CUR. U251 cells were exposed to pro-inflammatory molecules TNF-α and *E.coli* LPS and treated with CUR + DMSO, CUR1, CUR2, CUR3, and CUR4 [79]. The IKK inhibitor Bay-11-7072 was used as a positive control [359]. In comparison to the control group (U251 cells grow in growth media, without any treatment), TNFα and *E. coli* LPS significantly promoted inflammation level. However, when treated with CUR, the inflammation level was significantly suppressed. In addition, the CUR1, CUR2, CUR3 and CUR4 treatments showed stronger anti-inflammatory effects compared to CUR+DMSO (native CUR control). The anti-inflammatory effects of the newly developed CUR formulations

are around 2 to 2.5 times stronger than native CUR+DMSO (Fig. 6.5). This suggested that microemulsions are a promising formulation to deliver CUR to cells, so that the anti-inflammatory effects of CUR acts more efficiently on cells. Furthermore, in both treatment groups, there was no significant difference in the anti-inflammatory effects among CUR1, CUR2 and CUR3, CUR4 suggesting that the types of triglycerides are not impacting the anti-inflammatory function of CUR.

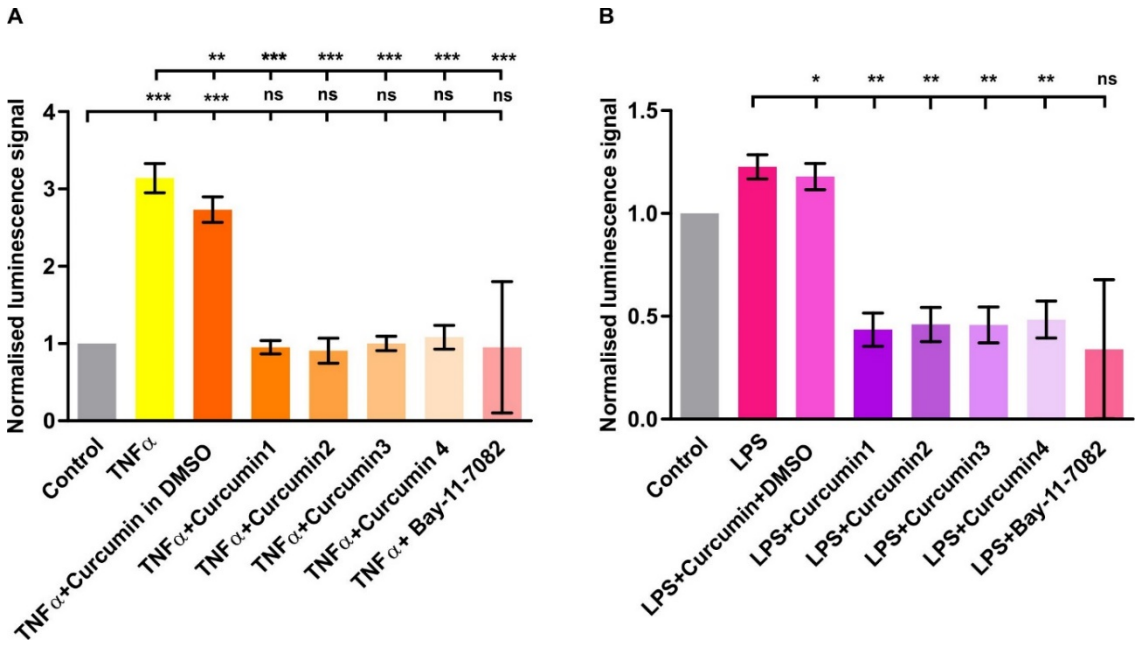

Figure 6.5. CUR1, CUR2, CUR3, and CUR4 showed higher anti-inflmmatory effect to U251 cells compared to native CUR+DMSO U251–NF-κB-GFP-Luc cells were exposed to TNF-α or LPS followed by a subsequent assessment of NF-κB-dependent luciferase activity. **A.** U251–NF-κB-GFP-Luc co-exposed to TNF-α and microemulsion of CUR/FA show significantly lower levels of NF-κB activity when compared to cells exposed either to TNF-α alone or to a combination of TNF-α and CUR. **B.** Microemulsion of CUR/FA decrease *the E. coli* LPS-induced activity of NF-κB compared to LPS alone or a combination of CUR and LPS. Data is presented as mean ± standard deviation from five independent experiments. *$p < 0.05$, **$p < 0.01$, and ***$p < 0.001$ were considered significant (ANOVA with Bonferroni correction, CI 95%).

Stability of formulated CUR showed significantly stronger anti-inflammatory effect than original format of CUR at 24-hours' time point.

CUR samples' concentration were determined using photometer. UV spectrophotometer was used to monitor CUR peak at wavelength of 429 nm. Within this region there are no overlapping peaks with degradation products nor from FA [430]. Figure 6.6 showed the degradation of CUR samples in liquid oil based and solid oil based microemulsions (Fig. 6.6A & 6.6B). There was a slight trend that CUR in liquid based solution (blue line in Fig. 6.6A) degraded faster than those in solid oil based solution (blue line in Fig. 6.6B). More importantly, native CUR+DMSO degraded significantly faster than CUR microemulsions. After 24 hours, there was only less than 45% of native CUR+DMSO left in the sample.

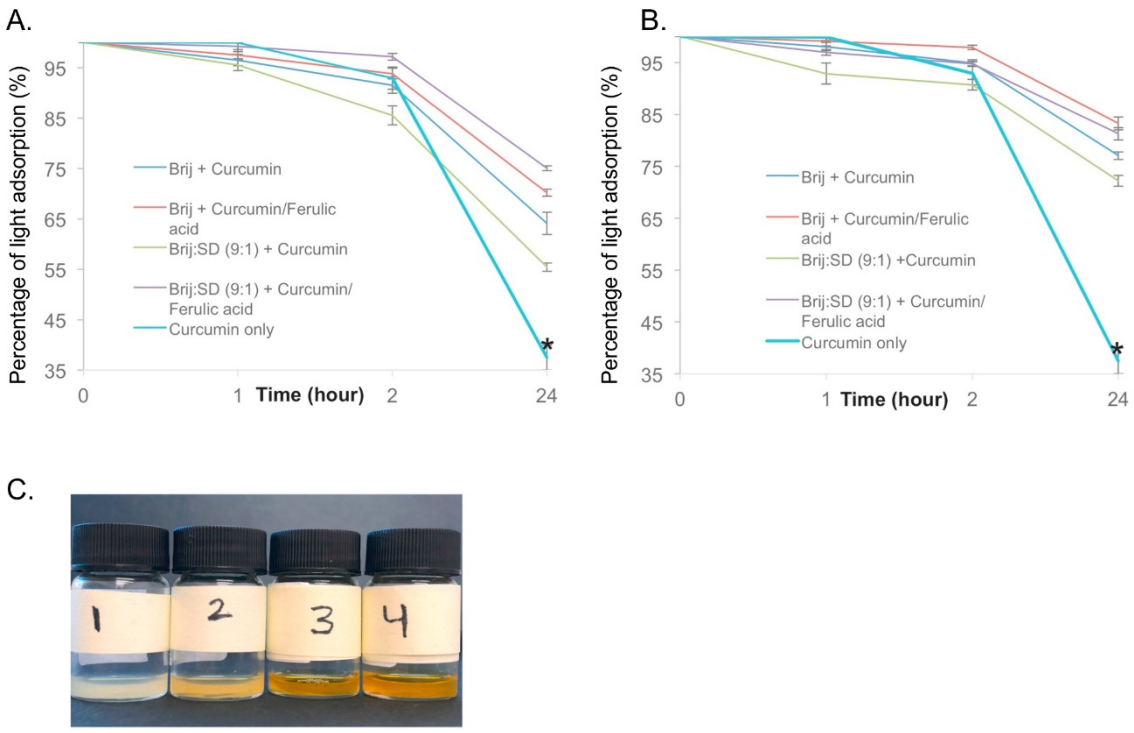

Figure 6.6. Native CUR+DMSO degraded significantly faster than CUR microemulsions. Degradation of CUR measured at wavelength of 429 nm using photospectroscopy after exposure to methanol and phosphate buffer (pH 7.5) in microemulsions prepared with 5% oil and 20% surfactant compared to CUR alone using **A**. Liquid oil glyceryl trioleate. **B.** Solid oil glyceryl tricaprate. (*$p < 0.05$: All microemulsions with the addition of either CUR or CUR/FA are significantly different to CUR alone without incorporation into the microemulsions)

C. Native CUR+DMSO degraded faster than CUR emulsions and had lighten colour compared to CUR microemulsions. Sample 1 was native CUR in DMSO. Sample 2-4 were CUR/FA microemulsions after storage for 12 months at ambient conditions. All CUR/FA samples contained similar concentration of CUR and had similar colour intensity when were freshly prepared.

6.3. Discussion

In this study, the anti-inflammatory potential of newly prepared CUR formulations was tested using a previously developed U251-NF-κB-GFP-LUC reporter cell line [204]. Although there are many studies indicating similar anti-inflammatory effects of the compound CUR, drug delivery problems still present barriers to clinical use of CUR. In general, the degradation rates of CUR in microemulsions samples were significantly slower than the native CUR+DMSO, suggested that the CUR in microemulsions was much more stable in comparison to native CUR in DMSO (Fig. 6.6). Furthermore, the newly designed CUR microemulsions had higher anti-inflammatory potential and did not have noticeable toxicity at their efficient concentration of 10μM. Through luciferase assay, CUR was proved to have anti-inflammatory effects on its own. The TNF-α and *E. coli* LPS stimulated cells with CUR dissolved in DMSO significantly decreased NF-κB activation (Fig. 6.5), potentially because CUR blocked the TNF-α signalling pathway by inhibiting IKK. However, this reduction was not as prominent as when using CUR microemulsions. The modified formulations of CUR were 2-2.5 times stronger in anti-inflammatory effect than CUR dissolved in DMSO. In addition, FA was packed 1:1 ratio with CUR in CUR2 and CUR4. In those two groups, the CUR concentration was half of the CUR1 and CUR3, but there was no significant difference of anti-inflammatory effects among the four groups. This suggested that FA might have a positive effect on the anti-inflammatory function of CUR. Another possible reason for the non-significant difference between those groups is that the CUR concentration in CUR2 and CUR4 (both with CUR and FA) might already be higher than the efficient concentration. The inhibition might have reached saturation in all four groups, so that inhibition levels of the four groups were being same. In addition, Farah demonstrated that FA helped stabilise the

CUR and helped decrease the degradation rate of the CUR molecule [430], while in CUR1 and CUR3 without FA, some CUR molecules might degrade. Those may lead to the final concentration of activated CUR in those four groups being similar. However, FA has been suggested to have antioxidant and anti-inflammatory capacity, just like CUR. Yin et al. demonstrated that FA is able to induce intracellular antioxidant enzyme activity, and at the same time decrease the pro-inflammatory cytokine TNF-α and IL-6 [432].

This study suggested that CUR has a strong effect in suppressing the pro-inflammatory NF-κB signalling pathway U251 cancer cells. In some other studies, CUR has been shown to negatively affect TLR4- NF-κB signalling pathways in lung cancer cells, breast cancer cells, liver cancer cells, neurons, macrophages etc. [433-437]. As *E. coli* LPS is one of the MyD88-dependent pathway biased TLR4 ligands, this study also suggested that CUR inhibits LPS –induced inflammation in U251 cells. In chapters 3 & 4, I demonstrated that TLR4-mediated MyD88-dependent pathway increases the migration and stemness of the glioblastoma cells, and promotes the tumourigenicity and proliferation of GBM CSCs. The TLR4-mediated MyD88 –independent pathway, however, is able to increase the differentiation potential of U251 cells, decrease the migration ability, and suppress the tumourigenicity of glioblastoma. CUR has been proved to strongly inhibit IKK and NF-κB activation. Unlike MyD88-independent biased TLR4 ligands, which can still drive the late activation of NF-κB, CUR molecule promises to ‘switch off’ all the TLR4 downstream NF-κB activation and induce anti-inflammatory cytokines in cells.

In glioblastoma, it has been suggested that CUR is able to decrease the proliferation, migration and invasion of glioma cells [202]. Senft et al. demonstrated that CUR was able to decrease the level of biologically active phospho-STAT3, the cell cycle regulating gene c-Myc, and proliferation marker Ki67 in glioma cells *in vitro* [202]. Also, CUR has been proved to induce G2/M cell cycle arrest in glioma cells by Klinger and Mittal [438]. Glioma CSCs are known to stay quiescent; the function of CUR to trap cells in G2/M will strongly increase the efficiency of anti-glioma drugs.

Most clinical trials involving CUR focus on chronic diseases and different types of cancer. Up to now, there were 293 clinical trials involving CUR listed on the clinicaltrials.gov. [439]. Those studies mainly focus on gastrointestinal diseases (inflammatory bowel disease, Cohn's disease etc.), cognitive disorders (Alzheimer's disease, cognitive impairment), chronic diseases in organs or tissues (kidney disease, chronic pulmonary disease etc.) and cancer (lymphoblastic leukaemia, melanoma, prostate cancer and breast cancer etc.) However, only one clinical trial about CUR in glioblastoma could be found in the literature, with the ClinicalTrials.gov identifier number NCT01712542. It studied the concentration of CUR in glioblastoma, but data have not been published yet. However, there has been some scientific discussion about the delivery efficiency of CUR through the blood brain barrier (BBB) [440, 441]. Askarizadeh et al. claimed that the BBB is the major obstacle of CUR's delivery to the brain, and nanoparticle delivery system should be one of the options to solve this [441]. Tsai et al. demonstrated that poly (lactic-co-glycolic acid) capsulated CUR was able to cross rat BBB. The nanoparticle, poly (lactic-co-glycolic acid) CUR capsule was not only highly lipid soluble but also small enough to enter BBB (163 ± 8.1 nm) [440]. Those nanoparticles were up-taken by brain microglia after 15 mins of injection and there was a significant increase of CUR in the brain areas comparing to unwrapped CUR [440]. Our nanoparticle size generated by Farah varied from 12.0 ± 0.04 nm to 23.9 ± 0.1 nm, which was a lot smaller than the poly(lactic-co-glycolic acid) CUR capsule [430]. It is very likely that this microemulsion particle will be able to pass through the BBB.

6.4. Conclusion

CUR has a strong anti-inflammatory effect in glioma cancer cells. It not only suppresses the NF-κB activation, but also increases the level of anti-inflammatory cytokines. Our newly developed microemulsion CUR delivery system overcame the problem of inefficient CUR delivery and provided the possibility of efficient anti-inflammatory effects to human cells. The newly designed CUR microemulsion also had advantages as having slow degradation rate. This delivery system could be used in many inflammatory diseases, and also brought insight to the glioma CSC targeting. As CUR is strongly anti-

inflammatory to cancer cells, and might have an ability to decrease the stemness, proliferation and migration of CSCs, it could be used as potential anti-cancer adjuvant in clinics.

6.5. limitation

In this study, the control for formulated CUR is not provided, apart from the original format of CUR, the 7% C18:1E10, 1% liquid glycerl trioleate alone should be tested in U251 cells as another control group.

6.6. Future work

Future work should focus on the delivery efficiency of the nanoparticle though BBB and to the organs. CUR could be used with traditional anti-cancer therapies to study the proliferation, migration and differentiation of CSCs, either *in vitro* or *in vivo*. In addition, 3D cell culture could be used to demonstrate the CUR microemulsion toxicity and transporting efficiency.

Moreover, *In vivo* work using rat or mouse could be included. *In vivo* work should include injecting animals with CUR in microemulsion with multiple working concentrations followed by determination of the distribution of CUR in brain and multiple organs. In parallel, *In vivo* work should include combination of CUR and traditional anti-glioblastoma therapy to determine the effect of CUR to glioblastoma cells and glioblastoma CSCs.

Chapter 7. General conclusion

GBM is a highly aggressive brain cancer that is characterized by a high rate of recurrence and resistance to conventional therapies. The existence of glioblastoma CSCs has been proposed as a potential explanation for these features, as those CSCs possess self-renewal and differentiation capacities that allow them to maintain and propagate the tumour [24]. My research has shown that TLR4 plays an important role in the maintenance and progression of GBM, particularly through its interaction with the GBM CSCs.

This study investigated how TLR4 biased signaling impacts glioma cell behavior. Both 2D and 3D cell culture techniques were used to address the impact of TLR4-mediated biased signaling on the stemness, proliferation, migration, differentiation, and survival of GBM CSCs. I demonstrated that that different chemotypes of LPS differentially impact the behavior of CSCs in glioblastoma, while 3D cell culture should bring changes to cell behavior in comparison to 2D.

In chapter 3, *E. coli* LPS and *S. minnesota* LPS was used as NF-κB and IRF3 biased TLR4 ligands, showed different impacts to the GBM CSCs. U251 cells were cultured using tumourispheroids formation in suspension medium to increase the percentage of $CD133^{+}$ cells. In comparison to monolayer culturing system. The two downstream pathways of TLR4 signaling, showed different impacts to the CD133+ cells (which were considered as CSCs) in the U251 cells. It was demonstrated that the stimulation of TLR4-mediated NF-κB activity increased the percentage of CSCs and promoted the transition of non-cancer stem cells to CSCs. This pro-inflammatory TLR4-mediated NF-κB activation promotes tumourigenicity of CSCs, increases their migration, and elevated the overall percentage of the CSCs. The other pathway, TLR4-mediated IRF3 pathway, however, is able to increase the differentiation of U251 cells at both mRNA and protein level and suppress the tumourigenicity of glioblastoma. These transcription factors are known to be important in the regulation of immune and inflammatory responses, my study showed that they are also involved in the regulation of CSC properties.

In chapter 4, I addressed the different impacts of biased signaling on GBM cells in 2D and 3D. The research sought to understand how 3D cell culture changes the CSC behaviors. By using 0.2% NFC and aNFC hydrogel as scaffold, I further demonstrated that NF-κB activation increased the tumourigenesis of U251 cells, and the peripheral distribution of the CSCs in U251 tumourispheres. However, there was no significant change but a trend toward an increase in the proliferation rate between the TNFα treated and untreated spheroids in 3D. This suggests that NF-κB activation may not significantly affect the total proliferation rate of U251, but might have a positive effect on CSCs' cell proliferation or the stemness of the whole U251 population. As for drug resistance of cells, I demonstrated that U251 cells in 3D cell culture proliferated quicker than 2D and had higher resistance to TMZ.

A novel quadruple reporter system ‘Quad-fire’ was successfully generated in chapter 5. This could be a robust tool for quantifying the activation level of the two downstream pathways of TLR4. A dual luciferase assay was used to test the quadruple reporter system, suggesting the successful establishment of the ‘Quad Fire’. Overall, the ‘Quad Fire’ system could be used to screen both TLR4 mediated pro- and anti-inflammatory pathway activation levels under the stimulation of TLR4 ligands in the future, which would be a great help in understanding the mechanism of the biased signaling of TLR4 in cancer cells as well as CSCs.

Lastly, the study used curcumin, the most pharmacologically active component in turmeric, as a TLR4-NF-κB inhibitor. An efficient curcumin delivery system was proposed, and it was suggested to have great potential in GMB treatment.

Targeting the TLR4 biased signaling in CSCs is meaningful. The implications of these findings are significant for the treatment of GBM. By suppressing the TLR4 mediated NF-κB activation, and activating the TLR4 mediated IRF3 activation, a new balance of the signaling might reduce the CSCs’ stemness, tumourigenesis and the proliferation level of the whole GBM population. Furthermore, the IRF3 pathway is able to introduce differentiation of the glioma CSCs, which may lead to better results of traditional cancer therapies. For further research, this TLR4- IRF3 biased ligand or other ligands derived from *S.*

minnestota LPS could be used as adjuvants with traditional cancer therapy. MPLA and other *S. minnesota* LPS derived ligands may able to induce differentiation to the tumour population, decrease the stemness of the tumour and hopefully decrease the therapy resistance of GBM [290].

In conclusion, this study provides valuable insights into the mechanisms of TLR4 biased signaling in GBM CSC behavior. TLR4 and its biased downstream pathways could be essential to the maintenance and progression of GBM. Targeting TLR4 signalling in GBM CSCs has emerged as a promising therapeutic strategy for the treatment. This study demonstrated the importance of understanding TLR4 biased signaling in cancer biology and provides insights into developing targeted therapies.

Reference

1. Liao, W.T., et al., *Metastatic cancer stem cells: from the concept to therapeutics.* Am J Stem Cells, 2014. **3**(2): p. 46-62.
2. Dick, D.B.J.E., *Human acute myeloid leukemia is organized as a hierarchy that originates from a primitive hematopoietic cell.* Nature, 1997. **3**: p. 18.
3. Yu, Z., et al., *Cancer stem cells.* Int J Biochem Cell Biol, 2012. **44**(12): p. 2144-51.
4. Pardal, R., M.F. Clarke, and S.J. Morrison, *Applying the principles of stem-cell biology to cancer.* Nat Rev Cancer, 2003. **3**(12): p. 895-902.
5. Singh, S.K., et al., *Identification of human brain tumour initiating cells.* Nature, 2004. **432**(7015): p. 396-401.
6. Ayob, A.Z. and T.S. Ramasamy, *Cancer stem cells as key drivers of tumour progression.* J Biomed Sci, 2018. **25**(1): p. 20.
7. Fisher, R., L. Pusztai, and C. Swanton, *Cancer heterogeneity: implications for targeted therapeutics.* Br J Cancer, 2013. **108**(3): p. 479-85.
8. GM., C., *The cell: A Molecular Approach*, in *The cell: A Molecular Approach*. 2000.
9. Nowell, P.C., *The clonal evolution of tumor cell populations.* Science, 1976. **194**(4260): p. 23-8.
10. Secker-Walker, L.M., *The meaning of a clone.* Cancer Genet Cytogenet, 1985. **16**(2): p. 187-8.
11. Seifert, M., R. Scholtysik, and R. Kuppers, *Origin and Pathogenesis of B Cell Lymphomas.* Methods Mol Biol, 2019. **1956**: p. 1-33.
12. Lan, Y., et al., *Revealing clonality and subclonality of driver genes for clinical survival benefits in breast cancer.* Breast Cancer Res Treat, 2019.
13. Rustad, E.H., et al., *Baseline identification of clonal V(D)J sequences for DNA-based minimal residual disease detection in multiple myeloma.* PLoS One, 2019. **14**(3): p. e0211600.
14. Kneppers, J., et al., *Frequent clonal relations between metastases and non-index prostate cancer lesions.* JCI Insight, 2019. **4**(2).
15. Mueller, W., et al., *Clonal analysis in glioblastoma with epithelial differentiation.* Brain Pathol, 2001. **11**(1): p. 39-43.
16. Fialkow, P.J., et al., *Evidence for a clonal origin of head and neck tumors.* Int J Cancer, 1972. **9**(1): p. 133-42.
17. Maley, C.C., et al., *Genetic clonal diversity predicts progression to esophageal adenocarcinoma.* Nat Genet, 2006. **38**(4): p. 468-73.
18. Greaves, M. and C.C. Maley, *Clonal evolution in cancer.* Nature, 2012. **481**(7381): p. 306-13.
19. Heppner, G.H., *Tumor heterogeneity.* Cancer Res, 1984. **44**(6): p. 2259-65.
20. Nobusawa, S., et al., *Intratumoral patterns of genomic imbalance in glioblastomas.* Brain Pathol, 2010. **20**(5): p. 936-44.
21. Castor, A., et al., *Distinct patterns of hematopoietic stem cell involvement in acute lymphoblastic leukemia.* Nat Med, 2005. **11**(6): p. 630-7.
22. Cox, C.V., et al., *Characterization of acute lymphoblastic leukemia progenitor cells.* Blood, 2004. **104**(9): p. 2919-25.
23. Al-Hajj, M., et al., *Prospective identification of tumorigenic breast cancer cells.* Proc Natl Acad Sci U S A, 2003. **100**(7): p. 3983-8.
24. Singh, S.K., et al., *Identification of a cancer stem cell in human brain tumors.* Cancer Res, 2003. **63**(18): p. 5821-8.
25. Li, Z., *CD133: a stem cell biomarker and beyond.* Exp Hematol Oncol, 2013. **2**(1): p. 17.
26. Luo, Y., et al., *Single-cell transcriptome analyses reveal signals to activate dormant neural stem cells.* Cell, 2015. **161**(5): p. 1175-1186.
27. Wolfien, M., et al., *Hematopoietic stem-cell senescence and myocardial repair - Coronary*

artery disease genotype/phenotype analysis of post-MI myocardial regeneration response induced by CABG/CD133+ bone marrow hematopoietic stem cell treatment in RCT PERFECT Phase 3. EBioMedicine, 2020. **57**: p. 102862.
28. Hristov, M. and C. Weber, *Endothelial progenitor cells in vascular repair and remodeling.* Pharmacol Res, 2008. **58**(2): p. 148-51.
29. Arndt, K., et al., *CD133 is a modifier of hematopoietic progenitor frequencies but is dispensable for the maintenance of mouse hematopoietic stem cells.* Proc Natl Acad Sci U S A, 2013. **110**(14): p. 5582-7.
30. Hemmati, H.D., et al., *Cancerous stem cells can arise from pediatric brain tumors.* Proc Natl Acad Sci U S A, 2003. **100**(25): p. 15178-83.
31. Neradil, J. and R. Veselska, *Nestin as a marker of cancer stem cells.* Cancer Sci, 2015. **106**(7): p. 803-11.
32. Zbinden, M., et al., *NANOG regulates glioma stem cells and is essential in vivo acting in a cross-functional network with GLI1 and p53.* EMBO J, 2010. **29**(15): p. 2659-74.
33. Dick, J.E., *Breast cancer stem cells revealed.* Proc Natl Acad Sci U S A, 2003. **100**(7): p. 3547-9.
34. Cariati, M., et al., *Alpha-6 integrin is necessary for the tumourigenicity of a stem cell-like subpopulation within the MCF7 breast cancer cell line.* Int J Cancer, 2008. **122**(2): p. 298-304.
35. Bonnet, D. and J.E. Dick, *Human acute myeloid leukemia is organized as a hierarchy that originates from a primitive hematopoietic cell.* Nat Med, 1997. **3**(7): p. 730-7.
36. Ricci-Vitiani, L., et al., *Identification and expansion of human colon-cancer-initiating cells.* Nature, 2007. **445**(7123): p. 111-5.
37. O'Brien, C.A., et al., *A human colon cancer cell capable of initiating tumour growth in immunodeficient mice.* Nature, 2007. **445**(7123): p. 106-10.
38. Yeung, T.M., et al., *Cancer stem cells from colorectal cancer-derived cell lines.* Proc Natl Acad Sci U S A, 2010. **107**(8): p. 3722-7.
39. Hermann, P.C., et al., *Distinct populations of cancer stem cells determine tumor growth and metastatic activity in human pancreatic cancer.* Cell Stem Cell, 2007. **1**(3): p. 313-23.
40. Li, C., et al., *Identification of pancreatic cancer stem cells.* Cancer Res, 2007. **67**(3): p. 1030-7.
41. Matsuda, Y., S. Kure, and T. Ishiwata, *Nestin and other putative cancer stem cell markers in pancreatic cancer.* Med Mol Morphol, 2012. **45**(2): p. 59-65.
42. Collins, A.T., et al., *Prospective identification of tumorigenic prostate cancer stem cells.* Cancer Res, 2005. **65**(23): p. 10946-51.
43. Son, M.J., et al., *SSEA-1 is an enrichment marker for tumor-initiating cells in human glioblastoma.* Cell Stem Cell, 2009. **4**(5): p. 440-52.
44. Fang, D., et al., *A tumorigenic subpopulation with stem cell properties in melanomas.* Cancer Res, 2005. **65**(20): p. 9328-37.
45. Civenni, G., et al., *Human CD271-positive melanoma stem cells associated with metastasis establish tumor heterogeneity and long-term growth.* Cancer Res, 2011. **71**(8): p. 3098-109.
46. Klemba, A., et al., *Surface markers of cancer stem-like cells of ovarian cancer and their clinical relevance.* Contemp Oncol (Pozn), 2018. **22**(1A): p. 48-55.
47. Parte, S.C., S.K. Batra, and S.S. Kakar, *Characterization of stem cell and cancer stem cell populations in ovary and ovarian tumors.* J Ovarian Res, 2018. **11**(1): p. 69.
48. Yang, Z.F., et al., *Significance of CD90+ cancer stem cells in human liver cancer.* Cancer Cell, 2008. **13**(2): p. 153-66.
49. Rountree, C.B., et al., *Expansion of liver cancer stem cells during aging in methionine adenosyltransferase 1A-deficient mice.* Hepatology, 2008. **47**(4): p. 1288-97.
50. Ma, S., et al., *Identification and characterization of tumorigenic liver cancer*

stem/progenitor cells. Gastroenterology, 2007. **132**(7): p. 2542-56.
51. Sullivan, J.P., J.D. Minna, and J.W. Shay, *Evidence for self-renewing lung cancer stem cells and their implications in tumor initiation, progression, and targeted therapy.* Cancer Metastasis Rev, 2010. **29**(1): p. 61-72.
52. Yan, X., et al., *Identification of CD90 as a marker for lung cancer stem cells in A549 and H446 cell lines.* Oncol Rep, 2013. **30**(6): p. 2733-40.
53. Prince, M.E., et al., *Identification of a subpopulation of cells with cancer stem cell properties in head and neck squamous cell carcinoma.* Proc Natl Acad Sci U S A, 2007. **104**(3): p. 973-8.
54. Krishnamurthy, S. and J.E. Nor, *Head and neck cancer stem cells.* J Dent Res, 2012. **91**(4): p. 334-40.
55. Peitzsch, C., et al., *Cancer Stem Cells in Head and Neck Squamous Cell Carcinoma: Identification, Characterization and Clinical Implications.* Cancers (Basel), 2019. **11**(5).
56. Fiedorowicz, M., et al., *Renal carcinoma CD105-/CD44- cells display stem-like properties in vitro and form aggressive tumors in vivo.* Sci Rep, 2020. **10**(1): p. 5379.
57. Cabrera, M.C., R.E. Hollingsworth, and E.M. Hurt, *Cancer stem cell plasticity and tumor hierarchy.* World J Stem Cells, 2015. **7**(1): p. 27-36.
58. Korkaya, H., S. Liu, and M.S. Wicha, *Breast cancer stem cells, cytokine networks, and the tumor microenvironment.* J Clin Invest, 2011. **121**(10): p. 3804-9.
59. Birgersdotter, A., R. Sandberg, and I. Ernberg, *Gene expression perturbation in vitro--a growing case for three-dimensional (3D) culture systems.* Semin Cancer Biol, 2005. **15**(5): p. 405-12.
60. Benya, P.D. and J.D. Shaffer, *Dedifferentiated chondrocytes reexpress the differentiated collagen phenotype when cultured in agarose gels.* Cell, 1982. **30**(1): p. 215-24.
61. Bissell, M.J., et al., *The organizing principle: microenvironmental influences in the normal and malignant breast.* Differentiation, 2002. **70**(9-10): p. 537-46.
62. Chang, W.H., R.A. Cerione, and M.A. Antonyak, *Extracellular Vesicles and Their Roles in Cancer Progression.* Methods Mol Biol, 2021. **2174**: p. 143-170.
63. Ibanez, F., et al., *TLR4 participates in the transmission of ethanol-induced neuroinflammation via astrocyte-derived extracellular vesicles.* J Neuroinflammation, 2019. **16**(1): p. 136.
64. Jabalee, J., R. Towle, and C. Garnis, *The Role of Extracellular Vesicles in Cancer: Cargo, Function, and Therapeutic Implications.* Cells, 2018. **7**(8).
65. Taraboletti, G., et al., *Bioavailability of VEGF in tumor-shed vesicles depends on vesicle burst induced by acidic pH.* Neoplasia, 2006. **8**(2): p. 96-103.
66. Montecalvo, A., et al., *Mechanism of transfer of functional microRNAs between mouse dendritic cells via exosomes.* Blood, 2012. **119**(3): p. 756-66.
67. Tian, T., et al., *Exosome uptake through clathrin-mediated endocytosis and macropinocytosis and mediating miR-21 delivery.* J Biol Chem, 2014. **289**(32): p. 22258-67.
68. Mills, J., et al., *Cancer-Derived Extracellular Vesicle-Associated MicroRNAs in Intercellular Communication: One Cell's Trash Is Another Cell's Treasure.* Int J Mol Sci, 2019. **20**(24).
69. Vitale, S.R., et al., *Detection of tumor-derived extracellular vesicles in plasma from patients with solid cancer.* BMC Cancer, 2021. **21**(1): p. 315.
70. Reddy, K.B., *MicroRNA (miRNA) in cancer.* Cancer Cell Int, 2015. **15**: p. 38.
71. Izumchenko, E., et al., *The TGFbeta-miR200-MIG6 pathway orchestrates the EMT-associated kinase switch that induces resistance to EGFR inhibitors.* Cancer Res, 2014. **74**(14): p. 3995-4005.
72. Si, W., et al., *The role and mechanisms of action of microRNAs in cancer drug resistance.* Clin Epigenetics, 2019. **11**(1): p. 25.

73. Al-Nedawi, K., et al., *Intercellular transfer of the oncogenic receptor EGFRvIII by microvesicles derived from tumour cells.* Nat Cell Biol, 2008. **10**(5): p. 619-24.
74. Chen, K., Y.H. Huang, and J.L. Chen, *Understanding and targeting cancer stem cells: therapeutic implications and challenges.* Acta Pharmacol Sin, 2013. **34**(6): p. 732-40.
75. Takebe, N., et al., *Targeting Notch, Hedgehog, and Wnt pathways in cancer stem cells: clinical update.* Nat Rev Clin Oncol, 2015. **12**(8): p. 445-64.
76. Zhang, T., et al., *NF-kappaB signaling in inflammation and cancer.* MedComm (2020), 2021. **2**(4): p. 618-653.
77. Duan, S., et al., *PTEN deficiency reprogrammes human neural stem cells towards a glioblastoma stem cell-like phenotype.* Nat Commun, 2015. **6**: p. 10068.
78. Pradhan, A., Q.T. Lambert, and G.W. Reuther, *Transformation of hematopoietic cells and activation of JAK2-V617F by IL-27R, a component of a heterodimeric type I cytokine receptor.* Proc Natl Acad Sci U S A, 2007. **104**(47): p. 18502-7.
79. Zeuner, M.T., et al., *Biased signalling is an essential feature of TLR4 in glioma cells.* Biochim Biophys Acta, 2016. **1863**(12): p. 3084-3095.
80. Matsui, W.H., *Cancer stem cell signaling pathways.* Medicine (Baltimore), 2016. **95**(1 Suppl 1): p. S8-S19.
81. Loh, C.Y., et al., *Signal Transducer and Activator of Transcription (STATs) Proteins in Cancer and Inflammation: Functions and Therapeutic Implication.* Front Oncol, 2019. **9**: p. 48.
82. Catarina Fernandes, A.C., Lígia Osório, Rita Costa Lago, Paulo Linhares, Bruno Carvalho, and Cláudia Caeiro., *Chapter 11Current Standards of Care in Glioblastoma Therapy*, in *Glioblastoma*, De Vleeschouwer S, Editor. 2017.
83. Alves, A.L.V., et al., *Role of glioblastoma stem cells in cancer therapeutic resistance: a perspective on antineoplastic agents from natural sources and chemical derivatives.* Stem Cell Res Ther, 2021. **12**(1): p. 206.
84. Chen, K., et al., *The metabolic flexibility of quiescent CSC: implications for chemotherapy resistance.* Cell Death Dis, 2021. **12**(9): p. 835.
85. Mannino, M. and A.J. Chalmers, *Radioresistance of glioma stem cells: intrinsic characteristic or property of the 'microenvironment-stem cell unit'?* Mol Oncol, 2011. **5**(4): p. 374-86.
86. Bao, S., et al., *Glioma stem cells promote radioresistance by preferential activation of the DNA damage response.* Nature, 2006. **444**(7120): p. 756-60.
87. Chen, W., et al., *Cancer Stem Cell Quiescence and Plasticity as Major Challenges in Cancer Therapy.* Stem Cells Int, 2016. **2016**: p. 1740936.
88. Doan, P., et al., *Glioblastoma Multiforme Stem Cell Cycle Arrest by Alkylaminophenol Through the Modulation of EGFR and CSC Signaling Pathways.* Cells, 2020. **9**(3).
89. Begicevic, R.R. and M. Falasca, *ABC Transporters in Cancer Stem Cells: Beyond Chemoresistance.* Int J Mol Sci, 2017. **18**(11).
90. Ma, S., et al., *CD133+ HCC cancer stem cells confer chemoresistance by preferential expression of the Akt/PKB survival pathway.* Oncogene, 2008. **27**(12): p. 1749-58.
91. Phillips, T.M., W.H. McBride, and F. Pajonk, *The response of CD24(-/low)/CD44+ breast cancer-initiating cells to radiation.* J Natl Cancer Inst, 2006. **98**(24): p. 1777-85.
92. Muller, M., et al., *EblacZ tumor dormancy in bone marrow and lymph nodes: active control of proliferating tumor cells by CD8+ immune T cells.* Cancer Res, 1998. **58**(23): p. 5439-46.
93. Sagar, J., et al., *Role of stem cells in cancer therapy and cancer stem cells: a review.* Cancer Cell Int, 2007. **7**: p. 9.
94. Yoon, S.K., *The biology of cancer stem cells and its clinical implication in hepatocellular carcinoma.* Gut Liver, 2012. **6**(1): p. 29-40.
95. Hanif, F., et al., *Glioblastoma Multiforme: A Review of its Epidemiology and Pathogenesis*

through Clinical Presentation and Treatment. Asian Pac J Cancer Prev, 2017. **18**(1): p. 3-9.
96. Louis, D.N., et al., *The 2021 WHO Classification of Tumors of the Central Nervous System: a summary.* Neuro Oncol, 2021. **23**(8): p. 1231-1251.
97. Rock, K., et al., *A clinical review of treatment outcomes in glioblastoma multiforme--the validation in a non-trial population of the results of a randomised Phase III clinical trial: has a more radical approach improved survival?* Br J Radiol, 2012. **85**(1017): p. e729-33.
98. Ohka, F., A. Natsume, and T. Wakabayashi, *Current trends in targeted therapies for glioblastoma multiforme.* Neurol Res Int, 2012. **2012**: p. 878425.
99. Walid, M.S., *Prognostic factors for long-term survival after glioblastoma.* Perm J, 2008. **12**(4): p. 45-8.
100. Bruce JN, C.K., Waziri A, et al., *Glioblastoma multiforme [monograph on the Internet].* https://emedicine.medscape.com/article/283252-overview, Last updated: Jun 28, 2018.
101. Cloughesy, T.F., W.K. Cavenee, and P.S. Mischel, *Glioblastoma: from molecular pathology to targeted treatment.* Annu Rev Pathol, 2014. **9**: p. 1-25.
102. Puliyappadamba, V.T., et al., *The role of NF-kappaB in the pathogenesis of glioma.* Mol Cell Oncol, 2014. **1**(3): p. e963478.
103. Uchida, N., et al., *Direct isolation of human central nervous system stem cells.* Proc Natl Acad Sci U S A, 2000. **97**(26): p. 14720-5.
104. Du, Z., et al., *Oct4 is expressed in human gliomas and promotes colony formation in glioma cells.* Glia, 2009. **57**(7): p. 724-33.
105. Zhang, L., et al., *The expression of SALL4 in patients with gliomas: high level of SALL4 expression is correlated with poor outcome.* J Neurooncol, 2015. **121**(2): p. 261-8.
106. Lathia, J.D., et al., *Cancer stem cells in glioblastoma.* Genes Dev, 2015. **29**(12): p. 1203-17.
107. Day, B.W., et al., *EphA3 maintains tumorigenicity and is a therapeutic target in glioblastoma multiforme.* Cancer Cell, 2013. **23**(2): p. 238-48.
108. Rheinbay, E., et al., *An aberrant transcription factor network essential for Wnt signaling and stem cell maintenance in glioblastoma.* Cell Rep, 2013. **3**(5): p. 1567-79.
109. Li, Z., et al., *Turning cancer stem cells inside out: an exploration of glioma stem cell signaling pathways.* J Biol Chem, 2009. **284**(25): p. 16705-16709.
110. Zheng, H., et al., *PLAGL2 regulates Wnt signaling to impede differentiation in neural stem cells and gliomas.* Cancer Cell, 2010. **17**(5): p. 497-509.
111. Jeon, H.M., et al., *Inhibitor of differentiation 4 drives brain tumor-initiating cell genesis through cyclin E and notch signaling.* Genes Dev, 2008. **22**(15): p. 2028-33.
112. Jacobs, J.J., et al., *The oncogene and Polycomb-group gene bmi-1 regulates cell proliferation and senescence through the ink4a locus.* Nature, 1999. **397**(6715): p. 164-8.
113. Gregorieff, A. and H. Clevers, *Wnt signaling in the intestinal epithelium: from endoderm to cancer.* Genes Dev, 2005. **19**(8): p. 877-90.
114. Borah, A., et al., *Targeting self-renewal pathways in cancer stem cells: clinical implications for cancer therapy.* Oncogenesis, 2015. **4**: p. e177.
115. Bhat, K.P.L., et al., *Mesenchymal differentiation mediated by NF-kappaB promotes radiation resistance in glioblastoma.* Cancer Cell, 2013. **24**(3): p. 331-46.
116. Luo, M., et al., *Stem cell quiescence and its clinical relevance.* World J Stem Cells, 2020. **12**(11): p. 1307-1326.
117. Cooper, J. and F.G. Giancotti, *Integrin Signaling in Cancer: Mechanotransduction, Stemness, Epithelial Plasticity, and Therapeutic Resistance.* Cancer Cell, 2019. **35**(3): p. 347-367.
118. Holland, E.C., *Glioblastoma multiforme: the terminator.* Proc Natl Acad Sci U S A, 2000. **97**(12): p. 6242-4.

119. Loeffler, J.S., et al., *Clinical patterns of failure following stereotactic interstitial irradiation for malignant gliomas.* Int J Radiat Oncol Biol Phys, 1990. **19**(6): p. 1455-62.
120. Anderson, K.V., G. Jurgens, and C. Nusslein-Volhard, *Establishment of dorsal-ventral polarity in the Drosophila embryo: genetic studies on the role of the Toll gene product.* Cell, 1985. **42**(3): p. 779-89.
121. Lemaitre, B., et al., *The dorsoventral regulatory gene cassette spatzle/Toll/cactus controls the potent antifungal response in Drosophila adults.* Cell, 1996. **86**(6): p. 973-83.
122. Bell, J.K., et al., *Leucine-rich repeats and pathogen recognition in Toll-like receptors.* Trends Immunol, 2003. **24**(10): p. 528-33.
123. Botos, I., D.M. Segal, and D.R. Davies, *The structural biology of Toll-like receptors.* Structure, 2011. **19**(4): p. 447-59.
124. Akira, S. and K. Takeda, *Toll-like receptor signalling.* Nat Rev Immunol, 2004. **4**(7): p. 499-511.
125. Tsan, M.F. and B. Gao, *Endogenous ligands of Toll-like receptors.* J Leukoc Biol, 2004. **76**(3): p. 514-9.
126. Medzhitov, R., *Toll-like receptors and innate immunity.* Nat Rev Immunol, 2001. **1**(2): p. 135-45.
127. Nagai, Y., et al., *Essential role of MD-2 in LPS responsiveness and TLR4 distribution.* Nat Immunol, 2002. **3**(7): p. 667-72.
128. Takeuchi, O., et al., *Cutting edge: role of Toll-like receptor 1 in mediating immune response to microbial lipoproteins.* J Immunol, 2002. **169**(1): p. 10-4.
129. Nakata, T., et al., *CD14 directly binds to triacylated lipopeptides and facilitates recognition of the lipopeptides by the receptor complex of Toll-like receptors 2 and 1 without binding to the complex.* Cell Microbiol, 2006. **8**(12): p. 1899-909.
130. Aliprantis, A.O., et al., *Cell activation and apoptosis by bacterial lipoproteins through toll-like receptor-2.* Science, 1999. **285**(5428): p. 736-9.
131. Takeuchi, O., et al., *Differential roles of TLR2 and TLR4 in recognition of gram-negative and gram-positive bacterial cell wall components.* Immunity, 1999. **11**(4): p. 443-51.
132. Ozinsky, A., et al., *The repertoire for pattern recognition of pathogens by the innate immune system is defined by cooperation between toll-like receptors.* Proc Natl Acad Sci U S A, 2000. **97**(25): p. 13766-71.
133. Alexopoulou, L., et al., *Recognition of double-stranded RNA and activation of NF-kappaB by Toll-like receptor 3.* Nature, 2001. **413**(6857): p. 732-8.
134. Ohashi, K., et al., *Cutting edge: heat shock protein 60 is a putative endogenous ligand of the toll-like receptor-4 complex.* J Immunol, 2000. **164**(2): p. 558-61.
135. Vabulas, R.M., et al., *HSP70 as endogenous stimulus of the Toll/interleukin-1 receptor signal pathway.* J Biol Chem, 2002. **277**(17): p. 15107-12.
136. Yu, L., L. Wang, and S. Chen, *Endogenous toll-like receptor ligands and their biological significance.* J Cell Mol Med, 2010. **14**(11): p. 2592-603.
137. Hayashi, F., et al., *The innate immune response to bacterial flagellin is mediated by Toll-like receptor 5.* Nature, 2001. **410**(6832): p. 1099-103.
138. Takeuchi, O., et al., *Discrimination of bacterial lipoproteins by Toll-like receptor 6.* Int Immunol, 2001. **13**(7): p. 933-40.
139. Schwandner, R., et al., *Peptidoglycan- and lipoteichoic acid-induced cell activation is mediated by toll-like receptor 2.* J Biol Chem, 1999. **274**(25): p. 17406-9.
140. Heil, F., et al., *Species-specific recognition of single-stranded RNA via toll-like receptor 7 and 8.* Science, 2004. **303**(5663): p. 1526-9.
141. Baumann, C.L., et al., *CD14 is a coreceptor of Toll-like receptors 7 and 9.* J Exp Med, 2010. **207**(12): p. 2689-701.
142. Hemmi, H., et al., *A Toll-like receptor recognizes bacterial DNA.* Nature, 2000. **408**(6813):

p. 740-5.
143. Guan, Y., et al., *Human TLRs 10 and 1 share common mechanisms of innate immune sensing but not signaling.* J Immunol, 2010. **184**(9): p. 5094-103.
144. Lee, S.M., et al., *Toll-like receptor 10 is involved in induction of innate immune responses to influenza virus infection.* Proc Natl Acad Sci U S A, 2014. **111**(10): p. 3793-8.
145. Fore, F., et al., *TLR10 and Its Unique Anti-Inflammatory Properties and Potential Use as a Target in Therapeutics.* Immune Netw, 2020. **20**(3): p. e21.
146. Park, B.S., et al., *The structural basis of lipopolysaccharide recognition by the TLR4-MD-2 complex.* Nature, 2009. **458**(7242): p. 1191-5.
147. Rajaiah, R., et al., *CD14 dependence of TLR4 endocytosis and TRIF signaling displays ligand specificity and is dissociable in endotoxin tolerance.* Proc Natl Acad Sci U S A, 2015. **112**(27): p. 8391-6.
148. Vallance, T.M., et al., *Toll-Like Receptor 4 Signalling and Its Impact on Platelet Function, Thrombosis, and Haemostasis.* Mediators Inflamm, 2017. **2017**: p. 9605894.
149. Schaefer, L., et al., *The matrix component biglycan is proinflammatory and signals through Toll-like receptors 4 and 2 in macrophages.* J Clin Invest, 2005. **115**(8): p. 2223-33.
150. Chiron, D., et al., *Toll-like receptors: lessons to learn from normal and malignant human B cells.* Blood, 2008. **112**(6): p. 2205-13.
151. Smiley, S.T., J.A. King, and W.W. Hancock, *Fibrinogen stimulates macrophage chemokine secretion through toll-like receptor 4.* J Immunol, 2001. **167**(5): p. 2887-94.
152. Okamura, Y., et al., *The extra domain A of fibronectin activates Toll-like receptor 4.* J Biol Chem, 2001. **276**(13): p. 10229-33.
153. Kroger, N., et al., *A fludarabine-based dose-reduced conditioning regimen followed by allogeneic stem cell transplantation from related or unrelated donors in patients with myelodysplastic syndrome.* Bone Marrow Transplant, 2001. **28**(7): p. 643-7.
154. Vabulas, R.M., et al., *The endoplasmic reticulum-resident heat shock protein Gp96 activates dendritic cells via the Toll-like receptor 2/4 pathway.* J Biol Chem, 2002. **277**(23): p. 20847-53.
155. Roelofs, M.F., et al., *Identification of small heat shock protein B8 (HSP22) as a novel TLR4 ligand and potential involvement in the pathogenesis of rheumatoid arthritis.* J Immunol, 2006. **176**(11): p. 7021-7.
156. Dybdahl, B., et al., *Inflammatory response after open heart surgery: release of heat-shock protein 70 and signaling through toll-like receptor-4.* Circulation, 2002. **105**(6): p. 685-90.
157. Jiang, D., et al., *Regulation of lung injury and repair by Toll-like receptors and hyaluronan.* Nat Med, 2005. **11**(11): p. 1173-9.
158. Guillot, L., et al., *Cutting edge: the immunostimulatory activity of the lung surfactant protein-A involves Toll-like receptor 4.* J Immunol, 2002. **168**(12): p. 5989-92.
159. Molteni, M., S. Gemma, and C. Rossetti, *The Role of Toll-Like Receptor 4 in Infectious and Noninfectious Inflammation.* Mediators Inflamm, 2016. **2016**: p. 6978936.
160. Frantz, S., et al., *Toll4 (TLR4) expression in cardiac myocytes in normal and failing myocardium.* J Clin Invest, 1999. **104**(3): p. 271-80.
161. Marie-Theres Zeuner, G.S.C.a.D.W., *Biased signalling via TLR4 affects the stemness of glioma cancer stem cells.*
162. Bertani, B. and N. Ruiz, *Function and Biogenesis of Lipopolysaccharides.* EcoSal Plus, 2018. **8**(1).
163. Steimle, A., I.B. Autenrieth, and J.S. Frick, *Structure and function: Lipid A modifications in commensals and pathogens.* Int J Med Microbiol, 2016. **306**(5): p. 290-301.
164. Zeuner, M., K. Bieback, and D. Widera, *Controversial Role of Toll-like Receptor 4 in Adult Stem Cells.* Stem Cell Rev, 2015. **11**(4): p. 621-34.

165. Oeckinghaus, A. and S. Ghosh, *The NF-kappaB family of transcription factors and its regulation.* Cold Spring Harb Perspect Biol, 2009. **1**(4): p. a000034.
166. Lin, S.C., Y.C. Lo, and H. Wu, *Helical assembly in the MyD88-IRAK4-IRAK2 complex in TLR/IL-1R signalling.* Nature, 2010. **465**(7300): p. 885-90.
167. Tanimura, N., et al., *Roles for LPS-dependent interaction and relocation of TLR4 and TRAM in TRIF-signaling.* Biochem Biophys Res Commun, 2008. **368**(1): p. 94-9.
168. Pascual-Lucas, M., et al., *LPS or ethanol triggers clathrin- and rafts/caveolae-dependent endocytosis of TLR4 in cortical astrocytes.* J Neurochem, 2014. **129**(3): p. 448-62.
169. Yamamoto, M., et al., *Role of adaptor TRIF in the MyD88-independent toll-like receptor signaling pathway.* Science, 2003. **301**(5633): p. 640-3.
170. Hayden, M.S. and S. Ghosh, *Signaling to NF-kappaB.* Genes Dev, 2004. **18**(18): p. 2195-224.
171. Chen, F.E., et al., *Crystal structure of p50/p65 heterodimer of transcription factor NF-kappaB bound to DNA.* Nature, 1998. **391**(6665): p. 410-3.
172. Yang, C.C., et al., *Bcl-xL mediates a survival mechanism independent of the phosphoinositide 3-kinase/Akt pathway in prostate cancer cells.* J Biol Chem, 2003. **278**(28): p. 25872-8.
173. Widera, D., et al., *Neural stem cells, inflammation and NF-kappaB: basic principle of maintenance and repair or origin of brain tumours?* J Cell Mol Med, 2008. **12**(2): p. 459-70.
174. Widera, D., et al., *Potential role of NF-kappaB in adult neural stem cells: the underrated steersman?* Int J Dev Neurosci, 2006. **24**(2-3): p. 91-102.
175. Hayashi, S., et al., *Expression of nuclear factor-kappa B, tumor necrosis factor receptor type 1, and c-Myc in human astrocytomas.* Neurol Med Chir (Tokyo), 2001. **41**(4): p. 187-95.
176. Hinz, M., et al., *NF-kappaB function in growth control: regulation of cyclin D1 expression and G0/G1-to-S-phase transition.* Mol Cell Biol, 1999. **19**(4): p. 2690-8.
177. Ling, J. and R. Kumar, *Crosstalk between NFkB and glucocorticoid signaling: a potential target of breast cancer therapy.* Cancer Lett, 2012. **322**(2): p. 119-26.
178. Taniguchi, K. and M. Karin, *NF-kappaB, inflammation, immunity and cancer: coming of age.* Nat Rev Immunol, 2018. **18**(5): p. 309-324.
179. Miyamoto, M., et al., *Regulated expression of a gene encoding a nuclear factor, IRF-1, that specifically binds to IFN-beta gene regulatory elements.* Cell, 1988. **54**(6): p. 903-13.
180. Yanai, H., et al., *Revisiting the role of IRF3 in inflammation and immunity by conditional and specifically targeted gene ablation in mice.* Proc Natl Acad Sci U S A, 2018. **115**(20): p. 5253-5258.
181. Doyle, S., et al., *IRF3 mediates a TLR3/TLR4-specific antiviral gene program.* Immunity, 2002. **17**(3): p. 251-63.
182. Tian, M., et al., *IRF3 prevents colorectal tumorigenesis via inhibiting the nuclear translocation of beta-catenin.* Nat Commun, 2020. **11**(1): p. 5762.
183. Pattwell, S.S. and E.C. Holland, *Putting Glioblastoma in Its Place: IRF3 Inhibits Invasion.* Trends Mol Med, 2017. **23**(9): p. 773-776.
184. Banchereau, J. and V. Pascual, *Type I interferon in systemic lupus erythematosus and other autoimmune diseases.* Immunity, 2006. **25**(3): p. 383-92.
185. Lin, W.W. and M. Karin, *A cytokine-mediated link between innate immunity, inflammation, and cancer.* J Clin Invest, 2007. **117**(5): p. 1175-83.
186. Tseng, P.H., et al., *Different modes of ubiquitination of the adaptor TRAF3 selectively activate the expression of type I interferons and proinflammatory cytokines.* Nat Immunol, 2010. **11**(1): p. 70-5.
187. Hu, J., et al., *Targeting TRAF3 signaling protects against hepatic ischemia/reperfusions injury.* J Hepatol, 2016. **64**(1): p. 146-59.

188. Wang, C., et al., *The E3 ubiquitin ligase Nrdp1 'preferentially' promotes TLR-mediated production of type I interferon.* Nature Immunology, 2009. **10**: p. 744.
189. Fang, H., et al., *TLR4 is essential for dendritic cell activation and anti-tumor T-cell response enhancement by DAMPs released from chemically stressed cancer cells.* Cell Mol Immunol, 2014. **11**(2): p. 150-9.
190. Goto, Y., et al., *Activation of Toll-like receptors 2, 3, and 4 on human melanoma cells induces inflammatory factors.* Mol Cancer Ther, 2008. **7**(11): p. 3642-53.
191. He, W., et al., *TLR4 signaling promotes immune escape of human lung cancer cells by inducing immunosuppressive cytokines and apoptosis resistance.* Mol Immunol, 2007. **44**(11): p. 2850-9.
192. Kelly, M.G., et al., *TLR-4 signaling promotes tumor growth and paclitaxel chemoresistance in ovarian cancer.* Cancer Res, 2006. **66**(7): p. 3859-68.
193. Che, F., et al., *TLR4 interaction with LPS in glioma CD133+ cancer stem cells induces cell proliferation, resistance to chemotherapy and evasion from cytotoxic T lymphocyte-induced cytolysis.* Oncotarget, 2017. **8**(32): p. 53495-53507.
194. Lai, F.B., et al., *Lipopolysaccharide supports maintaining the stemness of CD133(+) hepatoma cells through activation of the NF-kappaB/HIF-1alpha pathway.* Cancer Lett, 2016. **378**(2): p. 131-41.
195. Haghparast, A., M. Heidari Kharaji, and A.M. Malvandi, *Down-regulation of CD14 transcripts in human glioblastoma cell line U87 MG.* Iran J Immunol, 2011. **8**(2): p. 111-9.
196. Tewari, R., et al., *Involvement of TNFalpha-induced TLR4-NF-kappaB and TLR4-HIF-1alpha feed-forward loops in the regulation of inflammatory responses in glioma.* J Mol Med (Berl), 2012. **90**(1): p. 67-80.
197. Alvarado, A.G., et al., *Glioblastoma Cancer Stem Cells Evade Innate Immune Suppression of Self-Renewal through Reduced TLR4 Expression.* Cell Stem Cell, 2017. **20**(4): p. 450-461 e4.
198. Ferrandez, E., et al., *NFκB activation in differentiating glioblastoma stem-like cells is promoted by hyaluronic acid signaling through TLR4.* Scientific Reports, 2018. **8**(1): p. 6341.
199. Coussens, L.M. and Z. Werb, *Inflammation and cancer.* Nature, 2002. **420**(6917): p. 860-7.
200. Liu, J., P.C. Lin, and B.P. Zhou, *Inflammation fuels tumor progress and metastasis.* Curr Pharm Des, 2015. **21**(21): p. 3032-40.
201. Thuringer, D., et al., *Transactivation of the epidermal growth factor receptor by heat shock protein 90 via Toll-like receptor 4 contributes to the migration of glioblastoma cells.* J Biol Chem, 2011. **286**(5): p. 3418-28.
202. Senft, C., et al., *The nontoxic natural compound Curcumin exerts anti-proliferative, anti-migratory, and anti-invasive properties against malignant gliomas.* BMC Cancer, 2010. **10**: p. 491.
203. (ECACC), E.C.o.A.C.C. *ECACC General Cell Collection: U-251 MG (formerly known as U-373 MG)*. Available from: https://www.culturecollections.org.uk/products/celllines/generalcell/detail.jsp?refId=09063001&collection=ecacc_gc.
204. Zeuner, M.T., et al., *Development and Characterisation of a Novel NF-kappaB Reporter Cell Line for Investigation of Neuroinflammation.* Mediators Inflamm, 2017. **2017**: p. 6209865.
205. Schindelin, J., et al., *Fiji: an open-source platform for biological-image analysis.* Nat Methods, 2012. **9**(7): p. 676-82.
206. Thermofisher scientific , I. *Mach1 T1R competent cells*. Available from: https://www.thermofisher.com/uk/en/home/life-science/cloning/competent-cells-for-

transformation/competent-cells-strains/mach1-competent-cells.html.
207. Thermofisher scientific , I. *One Shot™ Stbl3™ Chemically Competent E. coli*. Available from: https://www.thermofisher.com/order/catalog/product/C737303.
208. Kawasaki, T. and T. Kawai, *Toll-like receptor signaling pathways.* Front Immunol, 2014. **5**: p. 461.
209. Stewart, W.C. and E.A. Anderson, *Effect of a cholinesterase inhibitor when injected into the medulla of the rabbit.* J Pharmacol Exp Ther, 1968. **162**(2): p. 309-18.
210. Garay, R.P., et al., *Cancer relapse under chemotherapy: why TLR2/4 receptor agonists can help.* Eur J Pharmacol, 2007. **563**(1-3): p. 1-17.
211. Uehori, J., et al., *Dendritic cell maturation induced by muramyl dipeptide (MDP) derivatives: monoacylated MDP confers TLR2/TLR4 activation.* J Immunol, 2005. **174**(11): p. 7096-103.
212. Hua, D., et al., *Small interfering RNA-directed targeting of Toll-like receptor 4 inhibits human prostate cancer cell invasion, survival, and tumorigenicity.* Mol Immunol, 2009. **46**(15): p. 2876-84.
213. Ran, S., *The Role of TLR4 in Chemotherapy-Driven Metastasis.* Cancer Res, 2015. **75**(12): p. 2405-10.
214. Pusztai, L., et al., *Changes in plasma levels of inflammatory cytokines in response to paclitaxel chemotherapy.* Cytokine, 2004. **25**(3): p. 94-102.
215. Byrd-Leifer, C.A., et al., *The role of MyD88 and TLR4 in the LPS-mimetic activity of Taxol.* Eur J Immunol, 2001. **31**(8): p. 2448-57.
216. Duan, Z., et al., *Discovery of differentially expressed genes associated with paclitaxel resistance using cDNA array technology: analysis of interleukin (IL) 6, IL-8, and monocyte chemotactic protein 1 in the paclitaxel-resistant phenotype.* Clin Cancer Res, 1999. **5**(11): p. 3445-53.
217. Tarassishin, L. and S.C. Lee, *Interferon regulatory factor 3 alters glioma inflammatory and invasive properties.* J Neurooncol, 2013. **113**(2): p. 185-94.
218. Takazawa, Y., et al., *Toll-like receptor 4 signaling promotes the migration of human melanoma cells.* Tohoku J Exp Med, 2014. **234**(1): p. 57-65.
219. Wu, K., et al., *TLR4/MyD88 signaling determines the metastatic potential of breast cancer cells.* Mol Med Rep, 2018. **18**(3): p. 3411-3420.
220. Wang, W. and J. Wang, *Toll-Like Receptor 4 (TLR4)/Cyclooxygenase-2 (COX-2) Regulates Prostate Cancer Cell Proliferation, Migration, and Invasion by NF-kappaB Activation.* Med Sci Monit, 2018. **24**: p. 5588-5597.
221. Friedl, P. and K. Wolf, *Tumour-cell invasion and migration: diversity and escape mechanisms.* Nat Rev Cancer, 2003. **3**(5): p. 362-74.
222. Su, Y.J., et al., *Polarized cell migration induces cancer type-specific CD133/integrin/Src/Akt/GSK3beta/beta-catenin signaling required for maintenance of cancer stem cell properties.* Oncotarget, 2015. **6**(35): p. 38029-45.
223. Vicente-Manzanares, M. and A.R. Horwitz, *Cell migration: an overview.* Methods Mol Biol, 2011. **769**: p. 1-24.
224. Sever, R. and J.S. Brugge, *Signal transduction in cancer.* Cold Spring Harb Perspect Med, 2015. **5**(4).
225. Yang, Z., et al., *Soluble CD14 and lipopolysaccharide-binding protein from bovine serum enable bacterial lipopolysaccharide-mediated cytotoxicity and activation of bovine vascular endothelial cells in vitro.* J Leukoc Biol, 1996. **59**(2): p. 241-7.
226. Briukhovetska, D., et al., *Interleukins in cancer: from biology to therapy.* Nat Rev Cancer, 2021. **21**(8): p. 481-499.
227. Webb, A.H., et al., *Inhibition of MMP-2 and MMP-9 decreases cellular migration, and angiogenesis in in vitro models of retinoblastoma.* BMC Cancer, 2017. **17**(1): p. 434.
228. Zakaria, N., et al., *Inhibition of NF-kappaB Signaling Reduces the Stemness*

Characteristics of Lung Cancer Stem Cells. Front Oncol, 2018. **8**: p. 166.
229. Jogi, A., et al., *Cancer cell differentiation heterogeneity and aggressive behavior in solid tumors.* Ups J Med Sci, 2012. **117**(2): p. 217-24.
230. Sidell, N., *Retinoic acid-induced growth inhibition and morphologic differentiation of human neuroblastoma cells in vitro.* J Natl Cancer Inst, 1982. **68**(4): p. 589-96.
231. Spinella, M.J., et al., *Retinoic acid promotes ubiquitination and proteolysis of cyclin D1 during induced tumor cell differentiation.* J Biol Chem, 1999. **274**(31): p. 22013-8.
232. Guttridge, D.C., et al., *NF-kappaB controls cell growth and differentiation through transcriptional regulation of cyclin D1.* Mol Cell Biol, 1999. **19**(8): p. 5785-99.
233. Tang, P., et al., *Regulation of adipogenic differentiation and adipose tissue inflammation by interferon regulatory factor 3.* Cell Death Differ, 2021. **28**(11): p. 3022-3035.
234. Pencheva, N., et al., *Identification of a Druggable Pathway Controlling Glioblastoma Invasiveness.* Cell Rep, 2017. **20**(1): p. 48-60.
235. Kitamura, S., et al., *Establishment and characterization of renal progenitor like cells from S3 segment of nephron in rat adult kidney.* FASEB J, 2005. **19**(13): p. 1789-97.
236. Aponte, P.M. and A. Caicedo, *Stemness in Cancer: Stem Cells, Cancer Stem Cells, and Their Microenvironment.* Stem Cells Int, 2017. **2017**: p. 5619472.
237. Zhao, W., Y. Li, and X. Zhang, *Stemness-Related Markers in Cancer.* Cancer Transl Med, 2017. **3**(3): p. 87-95.
238. Suzuki, S., et al., *The neural stem/progenitor cell marker nestin is expressed in proliferative endothelial cells, but not in mature vasculature.* J Histochem Cytochem, 2010. **58**(8): p. 721-30.
239. Moloney, J.N. and T.G. Cotter, *ROS signalling in the biology of cancer.* Semin Cell Dev Biol, 2018. **80**: p. 50-64.
240. Pelicano, H., D. Carney, and P. Huang, *ROS stress in cancer cells and therapeutic implications.* Drug Resist Updat, 2004. **7**(2): p. 97-110.
241. Karin, M., et al., *NF-kappaB in cancer: from innocent bystander to major culprit.* Nat Rev Cancer, 2002. **2**(4): p. 301-10.
242. Baldwin, A.S., *Control of oncogenesis and cancer therapy resistance by the transcription factor NF-kappaB.* J Clin Invest, 2001. **107**(3): p. 241-6.
243. Duffey, D.C., et al., *Inhibition of transcription factor nuclear factor-kappaB by a mutant inhibitor-kappaBalpha attenuates resistance of human head and neck squamous cell carcinoma to TNF-alpha caspase-mediated cell death.* Br J Cancer, 2000. **83**(10): p. 1367-74.
244. Inoue, J., et al., *NF-kappaB activation in development and progression of cancer.* Cancer Sci, 2007. **98**(3): p. 268-74.
245. Huang, S., et al., *Nuclear factor-kappaB activity correlates with growth, angiogenesis, and metastasis of human melanoma cells in nude mice.* Clin Cancer Res, 2000. **6**(6): p. 2573-81.
246. Sizemore, N., S. Leung, and G.R. Stark, *Activation of phosphatidylinositol 3-kinase in response to interleukin-1 leads to phosphorylation and activation of the NF-kappaB p65/RelA subunit.* Mol Cell Biol, 1999. **19**(7): p. 4798-805.
247. Kaisho, T. and S. Akira, *Toll-like receptor function and signaling.* J Allergy Clin Immunol, 2006. **117**(5): p. 979-87; quiz 988.
248. Liou, G.Y., et al., *Mutant KRas-Induced Mitochondrial Oxidative Stress in Acinar Cells Upregulates EGFR Signaling to Drive Formation of Pancreatic Precancerous Lesions.* Cell Rep, 2016. **14**(10): p. 2325-36.
249. Singh, R. and M.J. Czaja, *Regulation of hepatocyte apoptosis by oxidative stress.* J Gastroenterol Hepatol, 2007. **22 Suppl 1**: p. S45-8.
250. Wang, Y., et al., *Hepatocyte resistance to oxidative stress is dependent on protein kinase C-mediated down-regulation of c-Jun/AP-1.* J Biol Chem, 2004. **279**(30): p. 31089-97.

251. Roberts, P.J. and C.J. Der, *Targeting the Raf-MEK-ERK mitogen-activated protein kinase cascade for the treatment of cancer.* Oncogene, 2007. **26**(22): p. 3291-310.
252. McCubrey, J.A., et al., *Roles of the Raf/MEK/ERK pathway in cell growth, malignant transformation and drug resistance.* Biochim Biophys Acta, 2007. **1773**(8): p. 1263-84.
253. Steelman, L.S., et al., *Contributions of the Raf/MEK/ERK, PI3K/PTEN/Akt/mTOR and Jak/STAT pathways to leukemia.* Leukemia, 2008. **22**(4): p. 686-707.
254. Su, Z., et al., *DNA Polymerase Iota Promotes Esophageal Squamous Cell Carcinoma Proliferation Through Erk-OGT-Induced G6PD Overactivation.* Front Oncol, 2021. **11**: p. 706337.
255. Azoitei, N., et al., *Protein kinase D2 is a novel regulator of glioblastoma growth and tumor formation.* Neuro Oncol, 2011. **13**(7): p. 710-24.
256. Mihailovic, T., et al., *Protein kinase D2 mediates activation of nuclear factor kappaB by Bcr-Abl in Bcr-Abl+ human myeloid leukemia cells.* Cancer Res, 2004. **64**(24): p. 8939-44.
257. Horibata, S., et al., *Utilization of the Soft Agar Colony Formation Assay to Identify Inhibitors of Tumorigenicity in Breast Cancer Cells.* J Vis Exp, 2015(99): p. e52727.
258. Borowicz, S., et al., *The soft agar colony formation assay.* J Vis Exp, 2014(92): p. e51998.
259. Seluanov, A., et al., *Hypersensitivity to contact inhibition provides a clue to cancer resistance of naked mole-rat.* Proc Natl Acad Sci U S A, 2009. **106**(46): p. 19352-7.
260. Shaikh, M.V., M. Kala, and M. Nivsarkar, *CD90 a potential cancer stem cell marker and a therapeutic target.* Cancer Biomark, 2016. **16**(3): p. 301-7.
261. Huang, R., et al., *The expression of aldehyde dehydrogenase 1 (ALDH1) in ovarian carcinomas and its clinicopathological associations: a retrospective study.* BMC Cancer, 2015. **15**: p. 502.
262. Romanenko, M.V., et al., *Oncolytic Effect of Adenoviruses Serotypes 5 and 6 Against U87 Glioblastoma Cancer Stem Cells.* Anticancer Res, 2019. **39**(11): p. 6073-6086.
263. Eyre, R., et al., *Patient-derived Mammosphere and Xenograft Tumour Initiation Correlates with Progression to Metastasis.* J Mammary Gland Biol Neoplasia, 2016. **21**(3-4): p. 99-109.
264. Qiang, L., et al., *Isolation and characterization of cancer stem like cells in human glioblastoma cell lines.* Cancer Lett, 2009. **279**(1): p. 13-21.
265. Puck, T.T., P.I. Marcus, and S.J. Cieciura, *Clonal growth of mammalian cells in vitro; growth characteristics of colonies from single HeLa cells with and without a feeder layer.* J Exp Med, 1956. **103**(2): p. 273-83.
266. Uchida, Y., et al., *Analogy between sphere forming ability and stemness of human hepatoma cells.* Oncol Rep, 2010. **24**(5): p. 1147-51.
267. Kaus, A., et al., *Neural stem cells adopt tumorigenic properties by constitutively activated NF-kappaB and subsequent VEGF up-regulation.* Stem Cells Dev, 2010. **19**(7): p. 999-1015.
268. Afify, S.M. and M. Seno, *Conversion of Stem Cells to Cancer Stem Cells: Undercurrent of Cancer Initiation.* Cancers (Basel), 2019. **11**(3).
269. Bao, B., et al., *Overview of cancer stem cells (CSCs) and mechanisms of their regulation: implications for cancer therapy.* Curr Protoc Pharmacol, 2013. **Chapter 14**: p. Unit 14 25.
270. Auffinger, B., et al., *Conversion of differentiated cancer cells into cancer stem-like cells in a glioblastoma model after primary chemotherapy.* Cell Death Differ, 2014. **21**(7): p. 1119-31.
271. Gao, X.Y., et al., *Temozolomide Treatment Induces HMGB1 to Promote the Formation of Glioma Stem Cells via the TLR2/NEAT1/Wnt Pathway in Glioblastoma.* Front Cell Dev Biol, 2021. **9**: p. 620883.
272. Olmeda, D., et al., *Beta-catenin regulation during the cell cycle: implications in G2/M and apoptosis.* Mol Biol Cell, 2003. **14**(7): p. 2844-60.
273. Li, B., et al., *CD133 in brain tumor: the prognostic factor.* Oncotarget, 2017. **8**(7): p.

11144-11159.
274. Zhang, S., et al., *Identification of U251 glioma stem cells and their heterogeneous stem-like phenotypes.* Oncol Lett, 2013. **6**(6): p. 1649-1655.
275. Ferrandez, E., et al., *NFkappaB activation in differentiating glioblastoma stem-like cells is promoted by hyaluronic acid signaling through TLR4.* Sci Rep, 2018. **8**(1): p. 6341.
276. Pietrus, M., et al., *CD133 Expression in the Nucleus Is Associated with Endometrial Carcinoma Staging and Tumor Angioinvasion.* J Clin Med, 2021. **10**(10).
277. Huang, M., et al., *High CD133 expression in the nucleus and cytoplasm predicts poor prognosis in non-small cell lung cancer.* Dis Markers, 2015. **2015**: p. 986095.
278. Sun, X. and P.D. Kaufman, *Ki-67: more than a proliferation marker.* Chromosoma, 2018. **127**(2): p. 175-186.
279. Rinkenbaugh, A.L. and A.S. Baldwin, *The NF-kappaB Pathway and Cancer Stem Cells.* Cells, 2016. **5**(2).
280. Hirschfeld, M., et al., *Cutting edge: repurification of lipopolysaccharide eliminates signaling through both human and murine toll-like receptor 2.* J Immunol, 2000. **165**(2): p. 618-22.
281. Wang, W., S.A. Nag, and R. Zhang, *Targeting the NFkappaB signaling pathways for breast cancer prevention and therapy.* Curr Med Chem, 2015. **22**(2): p. 264-89.
282. Authier, H., et al., *IKK phosphorylates RelB to modulate its promoter specificity and promote fibroblast migration downstream of TNF receptors.* Proc Natl Acad Sci U S A, 2014. **111**(41): p. 14794-9.
283. Jiao, S., et al., *Targeting IRF3 as a YAP agonist therapy against gastric cancer.* J Exp Med, 2018. **215**(2): p. 699-718.
284. Brown, M.C., et al., *Viral infection of cells within the tumor microenvironment mediates antitumor immunotherapy via selective TBK1-IRF3 signaling.* Nat Commun, 2021. **12**(1): p. 1858.
285. Gambara, G., et al., *TLR3 engagement induces IRF-3-dependent apoptosis in androgen-sensitive prostate cancer cells and inhibits tumour growth in vivo.* J Cell Mol Med, 2015. **19**(2): p. 327-39.
286. Vince, J.E. and J. Tschopp, *IRF-3 partners Bax in a viral-induced dance macabre.* EMBO J, 2010. **29**(10): p. 1627-8.
287. Chipuk, J.E., et al., *Direct activation of Bax by p53 mediates mitochondrial membrane permeabilization and apoptosis.* Science, 2004. **303**(5660): p. 1010-4.
288. Swarnkar, G., et al., *Constitutive activation of IKK2/NF-kappaB impairs osteogenesis and skeletal development.* PLoS One, 2014. **9**(3): p. e91421.
289. Takeda, K., T. Kaisho, and S. Akira, *Toll-like receptors.* Annu Rev Immunol, 2003. **21**: p. 335-76.
290. Albert Vega, C., et al., *Differential response induced by LPS and MPLA in immunocompetent and septic individuals.* Clin Immunol, 2021. **226**: p. 108714.
291. Hernandez, C., P. Huebener, and R.F. Schwabe, *Damage-associated molecular patterns in cancer: a double-edged sword.* Oncogene, 2016. **35**(46): p. 5931-5941.
292. Pearson, J.R.D., et al., *Immune Escape in Glioblastoma Multiforme and the Adaptation of Immunotherapies for Treatment.* Front Immunol, 2020. **11**: p. 582106.
293. Wang, Y.Q., et al., *MPL Adjuvant Contains Competitive Antagonists of Human TLR4.* Front Immunol, 2020. **11**: p. 577823.
294. Stark, R., et al., *Monophosphoryl lipid A inhibits the cytokine response of endothelial cells challenged with LPS.* Innate Immun, 2015. **21**(6): p. 565-74.
295. Law, A.M.K., et al., *Advancements in 3D Cell Culture Systems for Personalizing Anti-Cancer Therapies.* Front Oncol, 2021. **11**: p. 782766.
296. Zanoni, M., et al., *3D tumor spheroid models for in vitro therapeutic screening: a systematic approach to enhance the biological relevance of data obtained.* Sci Rep, 2016.

6: p. 19103.
297. Thoma, C.R., et al., *3D cell culture systems modeling tumor growth determinants in cancer target discovery.* Adv Drug Deliv Rev, 2014. **69-70**: p. 29-41.
298. Baker, B.M. and C.S. Chen, *Deconstructing the third dimension: how 3D culture microenvironments alter cellular cues.* J Cell Sci, 2012. **125**(Pt 13): p. 3015-24.
299. Kimlin, L.C., G. Casagrande, and V.M. Virador, *In vitro three-dimensional (3D) models in cancer research: an update.* Mol Carcinog, 2013. **52**(3): p. 167-82.
300. Wartenberg, M., et al., *Regulation of the multidrug resistance transporter P-glycoprotein in multicellular tumor spheroids by hypoxia-inducible factor (HIF-1) and reactive oxygen species.* FASEB J, 2003. **17**(3): p. 503-5.
301. Minchinton, A.I. and I.F. Tannock, *Drug penetration in solid tumours.* Nat Rev Cancer, 2006. **6**(8): p. 583-92.
302. Amaral, R.L.F., et al., *Comparative Analysis of 3D Bladder Tumor Spheroids Obtained by Forced Floating and Hanging Drop Methods for Drug Screening.* Front Physiol, 2017. **8**: p. 605.
303. Kenny, P.A., et al., *The morphologies of breast cancer cell lines in three-dimensional assays correlate with their profiles of gene expression.* Mol Oncol, 2007. **1**(1): p. 84-96.
304. Edmondson, R., et al., *Three-dimensional cell culture systems and their applications in drug discovery and cell-based biosensors.* Assay Drug Dev Technol, 2014. **12**(4): p. 207-18.
305. Bates, S.E., L. Amiri-Kordestani, and G. Giaccone, *Drug development: portals of discovery.* Clin Cancer Res, 2012. **18**(1): p. 23-32.
306. Breslin, S. and L. O'Driscoll, *Three-dimensional cell culture: the missing link in drug discovery.* Drug Discov Today, 2013. **18**(5-6): p. 240-9.
307. Ferreira, L.P., V.M. Gaspar, and J.F. Mano, *Design of spherically structured 3D in vitro tumor models -Advances and prospects.* Acta Biomater, 2018. **75**: p. 11-34.
308. Franchi-Mendes, T., N. Lopes, and C. Brito, *Heterotypic Tumor Spheroids in Agitation-Based Cultures: A Scaffold-Free Cell Model That Sustains Long-Term Survival of Endothelial Cells.* Front Bioeng Biotechnol, 2021. **9**: p. 649949.
309. Sutherland, R.M., J.A. McCredie, and W.R. Inch, *Growth of multicell spheroids in tissue culture as a model of nodular carcinomas.* J Natl Cancer Inst, 1971. **46**(1): p. 113-20.
310. Hamburger, A.W. and S.E. Salmon, *Primary bioassay of human tumor stem cells.* Science, 1977. **197**(4302): p. 461-3.
311. Schmelzer, E., et al., *Long-term three-dimensional perfusion culture of human adult bone marrow mononuclear cells in bioreactors.* Biotechnol Bioeng, 2015. **112**(4): p. 801-10.
312. Gomillion, C.T. and K.J.L. Burg, *6.22 Adipose Tissue Engineering*, in *Comprehensive Biomaterials II*, P. Ducheyne, Editor. 2017, Elsevier: Oxford. p. 403-415.
313. Kawaguchi, N., et al., *De novo adipogenesis in mice at the site of injection of basement membrane and basic fibroblast growth factor.* Proc Natl Acad Sci U S A, 1998. **95**(3): p. 1062-6.
314. Patel, R. and A.J. Alahmad, *Growth-factor reduced Matrigel source influences stem cell derived brain microvascular endothelial cell barrier properties.* Fluids Barriers CNS, 2016. **13**: p. 6.
315. Mullen, P., et al., *Effect of Matrigel on the tumorigenicity of human breast and ovarian carcinoma cell lines.* Int J Cancer, 1996. **67**(6): p. 816-20.
316. Benton, G., et al., *Matrigel: from discovery and ECM mimicry to assays and models for cancer research.* Adv Drug Deliv Rev, 2014. **79-80**: p. 3-18.
317. Ponce, M.L., *Tube formation: an in vitro matrigel angiogenesis assay.* Methods Mol Biol, 2009. **467**: p. 183-8.
318. Hocevar, S.E., L. Liu, and R.K. Duncan, *Matrigel is required for efficient differentiation of isolated, stem cell-derived otic vesicles into inner ear organoids.* Stem Cell Res, 2021. **53**:

p. 102295.
319. Badylak, S.F., D.O. Freytes, and T.W. Gilbert, *Extracellular matrix as a biological scaffold material: Structure and function.* Acta Biomater, 2009. **5**(1): p. 1-13.
320. Fang, Y. and R.M. Eglen, *Three-Dimensional Cell Cultures in Drug Discovery and Development.* SLAS Discov, 2017. **22**(5): p. 456-472.
321. Nguyen, K.T. and J.L. West, *Photopolymerizable hydrogels for tissue engineering applications.* Biomaterials, 2002. **23**(22): p. 4307-14.
322. Sheard, J.J., et al., *Optically Transparent Anionic Nanofibrillar Cellulose Is Cytocompatible with Human Adipose Tissue-Derived Stem Cells and Allows Simple Imaging in 3D.* Stem Cells Int, 2019. **2019**: p. 3106929.
323. Yiming Meng, J.S., Andy Bashford. *High-content quantitation of cancer stem cells from a glioblastoma cell line cultured in 3D using GrowDex®-T hydrogel*. 2021 [cited 2022 05/03/2022]; Available from: https://www.upmbiomedicals.com/resource-center/application-notes/high-content-quantitation-of-cancer-stem-cells-from-a-glioblastoma-cell-line-cultured-in-3d-using-growdex-t-hydrogel/.
324. Ruigang Liu, W.O., *Spatial Inhomogeneities of Polystrene Gels Prepared from Semidilute Solutions.* Macromolecules, 2006. **39**(12): p. 9.
325. Thu, B., et al., *Inhomogeneous alginate gel spheres: an assessment of the polymer gradients by synchrotron radiation-induced X-ray emission, magnetic resonance microimaging, and mathematical modeling.* Biopolymers, 2000. **53**(1): p. 60-71.
326. Ryu, N.E., S.H. Lee, and H. Park, *Spheroid Culture System Methods and Applications for Mesenchymal Stem Cells.* Cells, 2019. **8**(12).
327. Cui, X., Y. Hartanto, and H. Zhang, *Advances in multicellular spheroids formation.* J R Soc Interface, 2017. **14**(127).
328. Lin, R.Z. and H.Y. Chang, *Recent advances in three-dimensional multicellular spheroid culture for biomedical research.* Biotechnol J, 2008. **3**(9-10): p. 1172-84.
329. Mueller-Klieser, W., *Method for the determination of oxygen consumption rates and diffusion coefficients in multicellular spheroids.* Biophys J, 1984. **46**(3): p. 343-8.
330. Carlsson, J. and H. Acker, *Relations between pH, oxygen partial pressure and growth in cultured cell spheroids.* Int J Cancer, 1988. **42**(5): p. 715-20.
331. Curcio, E., et al., *Mass transfer and metabolic reactions in hepatocyte spheroids cultured in rotating wall gas-permeable membrane system.* Biomaterials, 2007. **28**(36): p. 5487-97.
332. Knowlton, S., et al., *Bioprinting for cancer research.* Trends Biotechnol, 2015. **33**(9): p. 504-13.
333. Settleman, J., *Cancer: Bet on drug resistance.* Nature, 2016. **529**(7586): p. 289-90.
334. Dean, M., T. Fojo, and S. Bates, *Tumour stem cells and drug resistance.* Nat Rev Cancer, 2005. **5**(4): p. 275-84.
335. Neftel, C., et al., *An Integrative Model of Cellular States, Plasticity, and Genetics for Glioblastoma.* Cell, 2019. **178**(4): p. 835-849 e21.
336. Mandel, J.J., et al., *Inability of positive phase II clinical trials of investigational treatments to subsequently predict positive phase III clinical trials in glioblastoma.* Neuro Oncol, 2018. **20**(1): p. 113-122.
337. Ahuja, K., et al., *High resolution melting based method for rapid discriminatory diagnosis of co-infecting Leptomonas seymouri in Leishmania donovani-induced leishmaniasis.* Parasitol Int, 2020. **75**: p. 102047.
338. Yi, H.G., et al., *A bioprinted human-glioblastoma-on-a-chip for the identification of patient-specific responses to chemoradiotherapy.* Nat Biomed Eng, 2019. **3**(7): p. 509-519.
339. Rao, S.S., et al., *Glioblastoma behaviors in three-dimensional collagen-hyaluronan composite hydrogels.* ACS Appl Mater Interfaces, 2013. **5**(19): p. 9276-84.

340. Heffernan, J.M., et al., *Bioengineered Scaffolds for 3D Analysis of Glioblastoma Proliferation and Invasion.* Ann Biomed Eng, 2015. **43**(8): p. 1965-77.
341. biomedicals, U., *GrowDex Guide*. 2022.
342. joanne ossai, J.S., Darius Widera, *Human glioblastoma (U251): 3D model demonstrates increased cell viability and linear drug response over 2D*. 2018.
343. Kawaguchi, N., K. Hatta, and T. Nakanishi, *3D-culture system for heart regeneration and cardiac medicine.* Biomed Res Int, 2013. **2013**: p. 895967.
344. Wang, M., et al., *Role of tumor microenvironment in tumorigenesis.* J Cancer, 2017. **8**(5): p. 761-773.
345. Benton, G., et al., *Multiple uses of basement membrane-like matrix (BME/Matrigel) in vitro and in vivo with cancer cells.* Int J Cancer, 2011. **128**(8): p. 1751-7.
346. Yuan, Z., et al., *Development of a 3D Collagen Model for the In Vitro Evaluation of Magnetic-assisted Osteogenesis.* Sci Rep, 2018. **8**(1): p. 16270.
347. R. A. Brown, M.W., C.-B. Chuo,U. Cheema,S. N. Nazhat, *Ultrarapid Engineering of Biomimetic Materials and Tissues: Fabrication of Nano- and Microstructures by Plastic Compression.* Advanced Functional Materials. **15**(11): p. 9.
348. Chen, W.J., et al., *Ki-67 is a valuable prognostic factor in gliomas: evidence from a systematic review and meta-analysis.* Asian Pac J Cancer Prev, 2015. **16**(2): p. 411-20.
349. Cowman, M.K., et al., *The Content and Size of Hyaluronan in Biological Fluids and Tissues.* Front Immunol, 2015. **6**: p. 261.
350. Leach, J.B. and C.E. Schmidt, *Characterization of protein release from photocrosslinkable hyaluronic acid-polyethylene glycol hydrogel tissue engineering scaffolds.* Biomaterials, 2005. **26**(2): p. 125-35.
351. Hahn, S.K., et al., *Anti-inflammatory drug delivery from hyaluronic acid hydrogels.* J Biomater Sci Polym Ed, 2004. **15**(9): p. 1111-9.
352. Liu, Z. and G. Vunjak-Novakovic, *Modeling tumor microenvironments using custom-designed biomaterial scaffolds.* Curr Opin Chem Eng, 2016. **11**: p. 94-105.
353. Xu, X.X., et al., *Encapsulated human hepatocellular carcinoma cells by alginate gel beads as an in vitro metastasis model.* Exp Cell Res, 2013. **319**(14): p. 2135-44.
354. Chua, H.L., et al., *NF-kappaB represses E-cadherin expression and enhances epithelial to mesenchymal transition of mammary epithelial cells: potential involvement of ZEB-1 and ZEB-2.* Oncogene, 2007. **26**(5): p. 711-24.
355. Widera, D., et al., *Nuclear Factor-kappaB controls the reaggregation of 3D neurosphere cultures in vitro.* Eur Cell Mater, 2006. **11**: p. 76-84; discussion 85.
356. biology, R. *3D Tumor Spheroid Assay Service*. 2022 02/09/2022]; Available from: https://www.reactionbiology.com/services/cell-based-assays/3d-tumor-spheroid-assay?gclid=CjwKCAjwsMGYBhAEEiwAGUXJaaS0pjSQ2Bl4Vme3L2hiDYKcUFubb_ZsQMg0gcQXJ6hw6l-ULXPgGRoCXoUQAvD_BwE.
357. biocompany, V.A. *Cell Proliferation Assay*. 2022 08/09/2022]; Available from: https://visikol.com/services/in-vitro/cell-proliferation/.
358. Thermofisher scientific , I. *Cell Proliferation 8-Plex Human ProcartaPlex™ Panel*. 2022; Available from: https://www.thermofisher.com/order/catalog/product/EPX080-15844-901?gclid=CjwKCAjwsMGYBhAEEiwAGUXJadA0-702bFFQ8VQ08PLC37LEGUqyPbNrD3RqC7vrDMO3-BwBGghxJRoC9FUQAvD_BwE&ef_id=CjwKCAjwsMGYBhAEEiwAGUXJadA0-702bFFQ8VQ08PLC37LEGUqyPbNrD3RqC7vrDMO3-BwBGghxJRoC9FUQAvD_BwE:G:s&s_kwcid=AL!3652!3!550207172865!p!!g!!cell%20proliferation%20assay&cid=bid_pca_ilu_r01_co_cp1359_pjt0000_bid00000_0se_gaw_nt_pur_con.
359. Lee, J., et al., *BAY 11-7082 is a broad-spectrum inhibitor with anti-inflammatory activity against multiple targets.* Mediators Inflamm, 2012. **2012**: p. 416036.

360. Peng, L., et al., *Distribution of cancer stem cells in two human brain gliomas.* Oncol Lett, 2019. **17**(2): p. 2123-2130.
361. Ham, S.L., et al., *Engineered Breast Cancer Cell Spheroids Reproduce Biologic Properties of Solid Tumors.* Adv Healthc Mater, 2016. **5**(21): p. 2788-2798.
362. Gomez, K.E., et al., *Cancer Cell CD44 Mediates Macrophage/Monocyte-Driven Regulation of Head and Neck Cancer Stem Cells.* Cancer Res, 2020. **80**(19): p. 4185-4198.
363. Agnihotri, S., et al., *Alkylpurine-DNA-N-glycosylase confers resistance to temozolomide in xenograft models of glioblastoma multiforme and is associated with poor survival in patients.* J Clin Invest, 2012. **122**(1): p. 253-66.
364. Ujifuku, K., et al., *miR-195, miR-455-3p and miR-10a(*) are implicated in acquired temozolomide resistance in glioblastoma multiforme cells.* Cancer Lett, 2010. **296**(2): p. 241-8.
365. van Nifterik, K.A., et al., *Absence of the MGMT protein as well as methylation of the MGMT promoter predict the sensitivity for temozolomide.* Br J Cancer, 2010. **103**(1): p. 29-35.
366. Musah-Eroje, A. and S. Watson, *A novel 3D in vitro model of glioblastoma reveals resistance to temozolomide which was potentiated by hypoxia.* J Neurooncol, 2019. **142**(2): p. 231-240.
367. Poon, M.T.C., et al., *Temozolomide sensitivity of malignant glioma cell lines - a systematic review assessing consistencies between in vitro studies.* BMC Cancer, 2021. **21**(1): p. 1240.
368. Pickl, M. and C.H. Ries, *Comparison of 3D and 2D tumor models reveals enhanced HER2 activation in 3D associated with an increased response to trastuzumab.* Oncogene, 2009. **28**(3): p. 461-8.
369. Tung, Y.C., et al., *High-throughput 3D spheroid culture and drug testing using a 384 hanging drop array.* Analyst, 2011. **136**(3): p. 473-8.
370. Smalley, K.S., M. Lioni, and M. Herlyn, *Life isn't flat: taking cancer biology to the next dimension.* In Vitro Cell Dev Biol Anim, 2006. **42**(8-9): p. 242-7.
371. Hopkins, A.L., *Network pharmacology: the next paradigm in drug discovery.* Nat Chem Biol, 2008. **4**(11): p. 682-90.
372. Rauert-Wunderlich, H., et al., *The IKK inhibitor Bay 11-7082 induces cell death independent from inhibition of activation of NFkappaB transcription factors.* PLoS One, 2013. **8**(3): p. e59292.
373. Buchanan, M.M., et al., *Toll-like receptor 4 in CNS pathologies.* J Neurochem, 2010. **114**(1): p. 13-27.
374. Chen, W., et al., *Human astrocytes secrete IL-6 to promote glioma migration and invasion through upregulation of cytomembrane MMP14.* Oncotarget, 2016. **7**(38): p. 62425-62438.
375. Khmelinskii, A., et al., *Incomplete proteasomal degradation of green fluorescent proteins in the context of tandem fluorescent protein timers.* Mol Biol Cell, 2016. **27**(2): p. 360-70.
376. Soubannier, V. and S. Stifani, *NF-kappaB Signalling in Glioblastoma.* Biomedicines, 2017. **5**(2).
377. Uronen-Hansson, H., et al., *Toll-like receptor 2 (TLR2) and TLR4 are present inside human dendritic cells, associated with microtubules and the Golgi apparatus but are not detectable on the cell surface: integrity of microtubules is required for interleukin-12 production in response to internalized bacteria.* Immunology, 2004. **111**(2): p. 173-8.
378. Hornef, M.W., et al., *Toll-like receptor 4 resides in the Golgi apparatus and colocalizes with internalized lipopolysaccharide in intestinal epithelial cells.* J Exp Med, 2002. **195**(5): p. 559-70.
379. Vallance, T.M., et al., *Development and characterization of a novel, megakaryocyte NF-*

kappaB reporter cell line for investigating inflammatory responses. J Thromb Haemost, 2021. **19**(1): p. 107-120.
380. Li, J., et al., *The role of toll-like receptor 4 in tumor microenvironment.* Oncotarget, 2017. **8**(39): p. 66656-66667.
381. Aggarwal, B.B., *Nuclear factor-kappaB: the enemy within.* Cancer Cell, 2004. **6**(3): p. 203-8.
382. Fitzgerald, K.A., et al., *LPS-TLR4 signaling to IRF-3/7 and NF-kappaB involves the toll adapters TRAM and TRIF.* J Exp Med, 2003. **198**(7): p. 1043-55.
383. Jensen, E.C., *Use of fluorescent probes: their effect on cell biology and limitations.* Anat Rec (Hoboken), 2012. **295**(12): p. 2031-6.
384. Lai, C., X. Jiang, and X. Li, *Development of luciferase reporter-based cell assays.* Assay Drug Dev Technol, 2006. **4**(3): p. 307-15.
385. Sarrion-Perdigones, A., et al., *Simultaneous Examination of Cellular Pathways using Multiplex Hextuple Luciferase Assaying.* Curr Protoc Mol Biol, 2020. **131**(1): p. e122.
386. Hayden, M.S. and S. Ghosh, *Regulation of NF-kappaB by TNF family cytokines.* Semin Immunol, 2014. **26**(3): p. 253-66.
387. Kawai, T. and S. Akira, *Toll-like receptor downstream signaling.* Arthritis Res Ther, 2005. **7**(1): p. 12-9.
388. Kumar, A., J. Zhang, and F.S. Yu, *Toll-like receptor 3 agonist poly(I:C)-induced antiviral response in human corneal epithelial cells.* Immunology, 2006. **117**(1): p. 11-21.
389. Qin, Z., et al., *TLR3 regulates PD-L1 expression in human cytomegalovirus infected glioblastoma.* Int J Clin Exp Pathol, 2018. **11**(11): p. 5318-5326.
390. Kruger, C.L., et al., *Quantitative single-molecule imaging of TLR4 reveals ligand-specific receptor dimerization.* Sci Signal, 2017. **10**(503).
391. Sharma, R.A., W.P. Steward, and A.J. Gescher, *Pharmacokinetics and pharmacodynamics of curcumin.* Adv Exp Med Biol, 2007. **595**: p. 453-70.
392. Chen, M., et al., *Use of curcumin in diagnosis, prevention, and treatment of Alzheimer's disease.* Neural Regen Res, 2018. **13**(4): p. 742-752.
393. Prasad, S., et al., *Curcumin, a component of golden spice: from bedside to bench and back.* Biotechnol Adv, 2014. **32**(6): p. 1053-64.
394. Duvoix, A., et al., *Chemopreventive and therapeutic effects of curcumin.* Cancer Lett, 2005. **223**(2): p. 181-90.
395. Ranjan, D., et al., *Curcumin inhibits mitogen stimulated lymphocyte proliferation, NFkappaB activation, and IL-2 signaling.* J Surg Res, 2004. **121**(2): p. 171-7.
396. Mansouri, K., et al., *Clinical effects of curcumin in enhancing cancer therapy: A systematic review.* BMC Cancer, 2020. **20**(1): p. 791.
397. Sharifi-Rad, J., et al., *Turmeric and Its Major Compound Curcumin on Health: Bioactive Effects and Safety Profiles for Food, Pharmaceutical, Biotechnological and Medicinal Applications.* Front Pharmacol, 2020. **11**: p. 01021.
398. Ono, K., et al., *Curcumin has potent anti-amyloidogenic effects for Alzheimer's beta-amyloid fibrils in vitro.* J Neurosci Res, 2004. **75**(6): p. 742-50.
399. Sun, C., et al., *Curcumin Promoted miR-34a Expression and Suppressed Proliferation of Gastric Cancer Cells.* Cancer Biother Radiopharm, 2019. **34**(10): p. 634-641.
400. He, Y., et al., *Curcumin, inflammation, and chronic diseases: how are they linked?* Molecules, 2015. **20**(5): p. 9183-213.
401. Youn, H.S., et al., *Inhibition of homodimerization of Toll-like receptor 4 by curcumin.* Biochem Pharmacol, 2006. **72**(1): p. 62-9.
402. Parodi, F.E., et al., *Oral administration of diferuloylmethane (curcumin) suppresses proinflammatory cytokines and destructive connective tissue remodeling in experimental abdominal aortic aneurysms.* Ann Vasc Surg, 2006. **20**(3): p. 360-8.
403. Shi, X., et al., *Curcumin inhibits Abeta-induced microglial inflammatory responses in vitro:*

Involvement of ERK1/2 and p38 signaling pathways. Neurosci Lett, 2015. **594**: p. 105-10.
404. Ji, Z., et al., *Inflammatory regulatory network mediated by the joint action of NF-kB, STAT3, and AP-1 factors is involved in many human cancers.* Proc Natl Acad Sci U S A, 2019. **116**(19): p. 9453-9462.
405. Shaulian, E. and M. Karin, *AP-1 in cell proliferation and survival.* Oncogene, 2001. **20**(19): p. 2390-400.
406. Ozanne, B.W., et al., *Transcription factors control invasion: AP-1 the first among equals.* Oncogene, 2007. **26**(1): p. 1-10.
407. Atsaves, V., et al., *AP-1 Transcription Factors as Regulators of Immune Responses in Cancer.* Cancers (Basel), 2019. **11**(7).
408. Epstein, J., et al., *Curcumin suppresses p38 mitogen-activated protein kinase activation, reduces IL-1beta and matrix metalloproteinase-3 and enhances IL-10 in the mucosa of children and adults with inflammatory bowel disease.* Br J Nutr, 2010. **103**(6): p. 824-32.
409. Collett, G.P. and F.C. Campbell, *Curcumin induces c-jun N-terminal kinase-dependent apoptosis in HCT116 human colon cancer cells.* Carcinogenesis, 2004. **25**(11): p. 2183-9.
410. Jiang, M.C., et al., *Curcumin induces apoptosis in immortalized NIH 3T3 and malignant cancer cell lines.* Nutr Cancer, 1996. **26**(1): p. 111-20.
411. Yan, C., et al., *Gene expression profiling identifies activating transcription factor 3 as a novel contributor to the proapoptotic effect of curcumin.* Mol Cancer Ther, 2005. **4**(2): p. 233-41.
412. Kuo, M.L., T.S. Huang, and J.K. Lin, *Curcumin, an antioxidant and anti-tumor promoter, induces apoptosis in human leukemia cells.* Biochim Biophys Acta, 1996. **1317**(2): p. 95-100.
413. Rao, J., et al., *Curcumin reduces expression of Bcl-2, leading to apoptosis in daunorubicin-insensitive CD34+ acute myeloid leukemia cell lines and primary sorted CD34+ acute myeloid leukemia cells.* J Transl Med, 2011. **9**: p. 71.
414. Goel, A., C.R. Boland, and D.P. Chauhan, *Specific inhibition of cyclooxygenase-2 (COX-2) expression by dietary curcumin in HT-29 human colon cancer cells.* Cancer Lett, 2001. **172**(2): p. 111-8.
415. Rao, C.V., *Regulation of COX and LOX by curcumin.* Adv Exp Med Biol, 2007. **595**: p. 213-26.
416. Chan, M.M., *Inhibition of tumor necrosis factor by curcumin, a phytochemical.* Biochem Pharmacol, 1995. **49**(11): p. 1551-6.
417. Abe, Y., S. Hashimoto, and T. Horie, *Curcumin inhibition of inflammatory cytokine production by human peripheral blood monocytes and alveolar macrophages.* Pharmacol Res, 1999. **39**(1): p. 41-7.
418. Gupta, B. and B. Ghosh, *Curcuma longa inhibits TNF-alpha induced expression of adhesion molecules on human umbilical vein endothelial cells.* Int J Immunopharmacol, 1999. **21**(11): p. 745-57.
419. Bharti, A.C., N. Donato, and B.B. Aggarwal, *Curcumin (diferuloylmethane) inhibits constitutive and IL-6-inducible STAT3 phosphorylation in human multiple myeloma cells.* J Immunol, 2003. **171**(7): p. 3863-71.
420. Sugimoto, K., et al., *Curcumin prevents and ameliorates trinitrobenzene sulfonic acid-induced colitis in mice.* Gastroenterology, 2002. **123**(6): p. 1912-22.
421. Moon, Y., W.C. Glasgow, and T.E. Eling, *Curcumin suppresses interleukin 1beta-mediated microsomal prostaglandin E synthase 1 by altering early growth response gene 1 and other signaling pathways.* J Pharmacol Exp Ther, 2005. **315**(2): p. 788-95.
422. Balogun, E., et al., *Curcumin activates the haem oxygenase-1 gene via regulation of Nrf2 and the antioxidant-responsive element.* Biochem J, 2003. **371**(Pt 3): p. 887-95.
423. Shen, L. and H.F. Ji, *Insights into the inhibition of xanthine oxidase by curcumin.* Bioorg Med Chem Lett, 2009. **19**(21): p. 5990-3.

424. Nakamae, I., et al., *Curcumin Derivatives Verify the Essentiality of ROS Upregulation in Tumor Suppression.* Molecules, 2019. **24**(22).
425. Swarnakar, S., et al., *Curcumin regulates expression and activity of matrix metalloproteinases 9 and 2 during prevention and healing of indomethacin-induced gastric ulcer.* J Biol Chem, 2005. **280**(10): p. 9409-15.
426. John, M.K., et al., *Development and pharmacokinetic evaluation of a curcumin co-solvent formulation.* Anticancer Res, 2013. **33**(10): p. 4285-91.
427. Wahlang, B., Y.B. Pawar, and A.K. Bansal, *Identification of permeability-related hurdles in oral delivery of curcumin using the Caco-2 cell model.* Eur J Pharm Biopharm, 2011. **77**(2): p. 275-82.
428. Tonnesen, H.H., M. Masson, and T. Loftsson, *Studies of curcumin and curcuminoids. XXVII. Cyclodextrin complexation: solubility, chemical and photochemical stability.* Int J Pharm, 2002. **244**(1-2): p. 127-35.
429. Wang, Y.J., et al., *Stability of curcumin in buffer solutions and characterization of its degradation products.* J Pharm Biomed Anal, 1997. **15**(12): p. 1867-76.
430. Farah Sanduk, Y.M., Darius Widera, Radoslaw M. Kowalczyk, Nicholas Michael, Amanpreet Kaur, Vivian Yip, Sandra Zulu, Irene Zavrou, Lulu Hana, Muhammad Yaqoob, Hisham Al-Obaidi *Enhanced anti-inflammatory potential of degradation resistant curcumin/ferulic acid eutectics embedded in triglyceride-based microemulsions.* Journal of drug delivery science and technology, 2020. **60**.
431. Priyadarsini, K.I., *The chemistry of curcumin: from extraction to therapeutic agent.* Molecules, 2014. **19**(12): p. 20091-112.
432. Yin, Z.N., et al., *Antioxidant and Anti-inflammatory Capacity of Ferulic Acid Released from Wheat Bran by Solid-state Fermentation of Aspergillus niger.* Biomed Environ Sci, 2019. **32**(1): p. 11-21.
433. Ailioaie, L.M. and G. Litscher, *Curcumin and Photobiomodulation in Chronic Viral Hepatitis and Hepatocellular Carcinoma.* Int J Mol Sci, 2020. **21**(19).
434. Guney Eskiler, G., et al., *Inhibition of TLR4/TRIF/IRF3 Signaling Pathway by Curcumin in Breast Cancer Cells.* J Pharm Pharm Sci, 2019. **22**(1): p. 281-291.
435. Panaro, M.A., et al., *The Emerging Role of Curcumin in the Modulation of TLR-4 Signaling Pathway: Focus on Neuroprotective and Anti-Rheumatic Properties.* Int J Mol Sci, 2020. **21**(7).
436. Zhang, L., et al., *Curcumin inhibits cell proliferation and migration in NSCLC through a synergistic effect on the TLR4/MyD88 and EGFR pathways.* Oncol Rep, 2019. **42**(5): p. 1843-1855.
437. Ni, H., et al., *Curcumin modulates TLR4/NF-kappaB inflammatory signaling pathway following traumatic spinal cord injury in rats.* J Spinal Cord Med, 2015. **38**(2): p. 199-206.
438. Klinger, N.V. and S. Mittal, *Therapeutic Potential of Curcumin for the Treatment of Brain Tumors.* Oxid Med Cell Longev, 2016. **2016**: p. 9324085.
439. *Curcumin search result* 2022 11/09/2022]; Available from: https://clinicaltrials.gov/ct2/results?term=curcumin&Search=Apply&age_v=&gndr=&type=&rslt=.
440. Tsai, Y.M., et al., *Curcumin and its nano-formulation: the kinetics of tissue distribution and blood-brain barrier penetration.* Int J Pharm, 2011. **416**(1): p. 331-8.
441. Askarizadeh, A., et al., *Neuroprotection by curcumin: A review on brain delivery strategies.* Int J Pharm, 2020. **585**: p. 119476.